IDENTIFICATION OF A NOVEL REGULATOR OF EXTRACELLULAR MATRIX DEGRADATION IN CHONDROCYTES

Isabella Collins

Lincoln College

Supervisors:

Dr Angus Wann

Dr Linda Troeberg

Professor Tonia Vincent

Thesis submitted to the University of Oxford

for the degree of Doctor of Philosophy

Abstract

There are currently no drugs that modify the progression of the degenerative joint disease osteoarthritis, which is characterised by protease-mediated degradation of the cartilage extracellular matrix. Identification of molecules that regulate protease activity could therefore lead to the development of new therapies for osteoarthritis. The Wann group previously showed that mutation of Intraflagellar transport protein 88 (IFT88) increased degradation of the cartilage matrix component aggrecan by proteases *in vitro*. As IFT88 is required for the assembly of a cell surface organelle called the primary cilium, the aim of my thesis was to investigate whether the primary cilium is involved in the regulation of protease activity. Based on the Wann group's finding that mutation of IFT88 impaired Low-density lipoprotein receptor-related protein 1 (LRP-1)-mediated endocytosis of extracellular proteases, I hypothesised that the primary cilium is a region of efficient endocytosis and thus regulates the extracellular activity of proteases.

To address this aim, I measured protease activity when four genes encoding proteins involved in cilia assembly were knocked down with siRNAs in a chondrocyte cell line. Generation of the AGEG aggrecan neoepitope was used as an indicator of protease activity. I showed that protease activity was not affected by knockdown of three of the ciliary genes tested. However, knockdown of the gene encoding Tau-tubulin kinase 2 (TTBK2) increased the activity of the protease A disintegrin and metalloproteinase with thrombospondin motifs 5 (ADAMTS-5). This increase was not associated with changes in ADAMTS-5 RNA levels during my experiments, constitutive activation of cilia-dependent hedgehog signalling, or reduced levels of the physiological ADAMTS-5 inhibitor, Tissue inhibitor of metalloproteinase 3 (TIMP-3). The effect of knockdown of the TTBK2 gene on ADAMTS-5 endocytosis could not be definitively determined.

Together, these results showed that whilst the primary cilium itself may not be required for protease activity regulation, TTBK2 is a novel regulator of ADAMTS-5 activity. Further investigation of the molecular mechanism of ADAMTS-5 regulation by TTBK2 may help to identify new therapeutic targets in osteoarthritis.

Declaration

I declare that this thesis is the result of my own work. All sources were acknowledged and cited in the References section of this thesis. This thesis has not been submitted before for examination at the University of Oxford or elsewhere.

Isabella Collins

Acknowledgements

I would like to thank my great supervisor, Dr Angus Wann, for his support, guidance and enthusiasm during my PhD. I would also like to thank my co-supervisor Dr Linda Troeberg for her expert advice, and Professor Tonia Vincent for her valuable insight. I would also like to express my thanks to the current and past members of the Centre for Osteoarthritis Pathogenesis Versus Arthritis for their help, particularly Dr Heba Ismail and Dr Kazuhiro Yamamoto.

Hefyd, diolch yn fawr i fy teulu a fy ffrindiau yn Rhydychen a Cymru am eu cefnogaeth. Yn olaf, diolch o galon i fy mam a fy chwaer, Nicola a Calista Collins, am eu cefnogaeth.

Table of contents

List of figures

List of tables

List of abbreviations

ADAM	Adamalysin
ADAMTS	A disintegrin and metalloproteinase with thrombospondin motifs
ADPKD	Autosomal dominant polycystic kidney disease
ANOVA	Analysis of variance
AP-2	Adaptor protein 2
AP2A1	Alpha-1 subunit of the AP-2 complex
ARL13B	ADP-ribosylation factor-like GTPase 13B
ATDC5	AT805 mouse teratocarcinoma chondrogenic cell line
BBS	Bardet-Biedl syndrome
BCA	Bicinchoninic acid
BSA	Bovine serum albumin
Ca^{2+}	Calcium ion
CALM	Clathrin assembly lymphoid myeloid leukaemia
CAV-1	Caveolin-1
CEP164	Centrosomal protein 164
CLTC	Clathrin heavy chain 1
CCM	Cerebral cavernous malformations
CP110	Centriolar coiled-coil protein of 110 kDa
CRISPR	Clustered regularly interspaced short palindromic repeats
CS	Chondroitin sulfate
C_T	Cycle threshold
CTGF	Connective tissue growth factor
DAPI	4',6-Diamidino-2-phenylindole
DMEM	Dulbecco's modified Eagle's medium
DMM	Destabilisation of the medial meniscus
DMMB	1,9-dimethylmethylene blue
DMOAD	Disease-modifying osteoarthritis drug
DMSO	Dimethyl sulfoxide
dNTP	2'-deoxynucloside 5'-triphosphate
ECL	Electrochemiluminescence
ECM	Extracellular matrix
EDTA	Ethylenediaminetetraacetic acid
EGTA	Ethylene glycol-bis(β-aminoethyl ether)-N,N,N',N'-tetraacetic acid
EEA1	Early endosomal antigen 1
EHD1	EPS15-homology domain-containing protein
ELISA	Enzyme-linked immunosorbent assay
FBS	Fetal bovine serum
FGF	Fibroblast growth factor
(s)GAG	(Sulfated) Glycosaminoglycan
GAPDH	Glyceraldehyde 3-phosphate dehydrogenase
GLI	Glioblastoma-associated oncogene homolog
GPR161	G protein-coupled receptor 161
HEK293	Human embryonic kidney 293 cells

Hh	Hedgehog
HTB94	Human chondrosarcoma cell line
IFN	Interferon
IFT	Intraflagellar transport
IgG	Immunoglobulin G
Ihh	Indian hedgehog
IL-1	Interleukin-1
IMCD3	Inner medullary collecting duct mouse cell line
INPP5E	Inositol Polyphosphate-5-Phosphatase E
Insig1/2	Insulin-induced gene 1 protein
IQR	Interquartile range
JNK2	c-Jun N-terminal kinase 2
kDa	Kilodalton
KIF	Kinesin
LDL	Low-density lipoprotein
LRP-1	Low-density lipoprotein receptor-related protein 1
MAPK	Mitogen-activated protein kinase
MDM2	Mouse double minute 2 homolog
MMP	Matrix metalloproteinase
MT1-MMP	Membrane-type 1 matrix metalloproteinase
NFkB	Nuclear factor kappa-light-chain-enhancer of activated B cells transcription factor
NIR	Near-infrared
NPHP4	Nephronophthisis 4
ORPK	Oak Ridge polycystic kidney mouse
PACE4	Paired basic amino acid cleaving enzyme 4
PAGE	Polyacrylamide gel electrophoresis
PBS	Phosphate-buffered saline
PC1	Polycystin-1
PC2	Polycystin-2
PC5/6	Proprotein convertase 5/6
PFA	Paraformaldehyde
PI(4)P	Phosphatidylinositol 4-phosphate
PI(4,5)P2	Phosphatidylinositol 4,5-bisphosphate
PIPES	Piperazine-N,N'-bis(2-ethanesulfonic acid)
PKA	Protein kinase A
PTCH1	Patched1
PTHrP	Parathyroid hormone-related protein
PVDF	Polyvinylidene fluoride
qPCR	Quantitative polymerase chain reaction
RAB	Ras-associated binding protein
RAP	Receptor-associated protein
RelA	V-rel avian reticuloendotheliosis viral oncogene homolog A (also known as p65)
RISC	RNA-induced silencing complex
RPM	Revolutions per minute
RUNX2	Runt-related transcription factor 2
SAG	Smoothened agonist

SCA11	Spinocerebellar ataxia 11
SD	Standard deviation
SDS	Sodium dodecyl sulfate
Shh	Sonic hedgehog
siRNA	Small interfering ribonucleic acid
SMO	Smoothened
SNX17	Sorting nexin 17
SUFU	Suppressor of Fused
TAg	Large T antigen
TBS	Tris-buffered saline
TCA	Trichloroacetic acid
TGF-β	Transforming growth factor beta
TIMP	Tissue inhibitor of metalloproteinase
TTBK2	Tau-tubulin kinase 2
uPARAP	Urokinase plasminogen activator receptor-associated protein
Wnt	Wingless-related integration site
WT	Wild type

CHAPTER 1

Introduction

1.1 Cartilage destruction in osteoarthritis

Articular cartilage is the tissue that lines the articulating surface of synovial joints and has important functions in lubrication and transfer of mechanical load. Destruction of articular cartilage is characteristic of osteoarthritis, a chronic degenerative joint disease associated with joint pain and loss of mobility. Osteoarthritis has a large impact on the lives of people with the disease: in 2010, knee and hip osteoarthritis was the 11th highest contributor to global disability out of 261 conditions studied[1], and knee osteoarthritis has been associated with increased risk of mortality in women[2]. Osteoarthritis is a growing health issue, as both the global prevalence of osteoarthritis and years lived with disability due to the disease have increased by 9.3 and 9.7% respectively between 1990 and 2017, which is likely due to population ageing[3]. Osteoarthritis with no known cause is called idiopathic osteoarthritis, and factors such as ageing, genetics and obesity confer increased risk of developing this type of osteoarthritis. Secondary osteoarthritis is caused by a pre-existing condition or joint injury, as with post-traumatic osteoarthritis.

Despite the high impact of osteoarthritis globally, there are currently no treatments beyond symptomatic relief and surgical joint replacement. Investigation of the molecular mechanisms regulating cartilage breakdown could lead to the development of new disease-modifying therapies to slow the progression of osteoarthritis.

1.1.1 Cartilage extracellular matrix structure and function

Articular cartilage is aneural and avascular, and consists of a single cell type, the chondrocyte. Chondrocytes secrete a highly specialised extracellular matrix (ECM) that has been estimated to occupy around 98% of the total tissue volume of cartilage from human knee joints[4]. Articular cartilage has three layers[5]. In the superficial zone, chondrocytes have a flattened morphology[6] and the main ECM components are tightly packed, fibrillar proteins, such as type II collagen fibres that are aligned parallel to the articular surface[7] (Figure 1.1A). The middle zone contains highly glycosylated proteins called proteoglycans and obliquely oriented collagen fibres. The

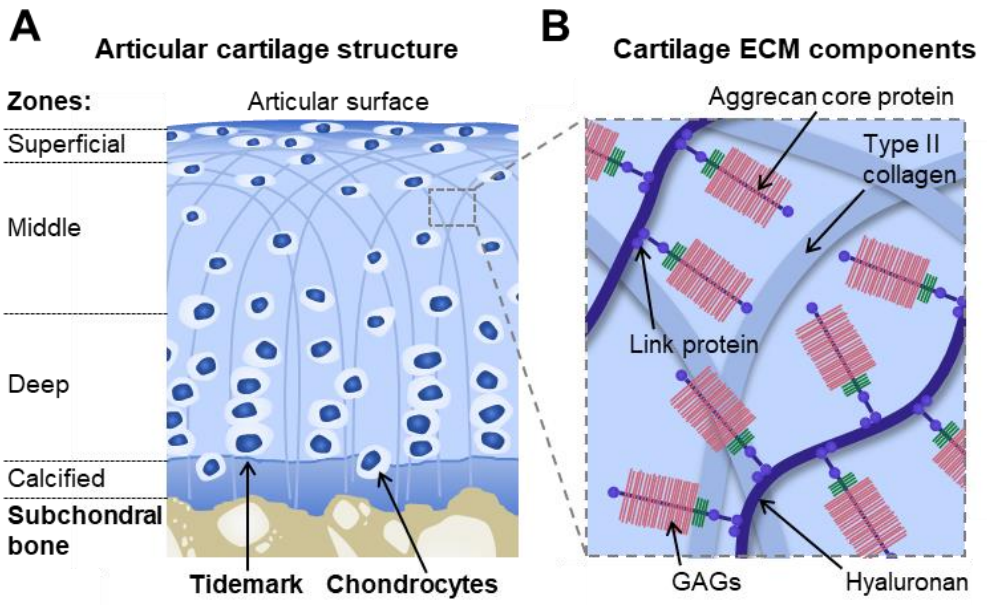

Figure 1.1 Structure of the articular cartilage and its extracellular matrix. ***A***) Articular cartilage is organised into three zones: the superficial zone closest to the articular surface, the middle zone and the deep zone, which is separated from the underlying subchondral bone by calcified cartilage. The morphology of chondrocytes varies between zones. ***B***) The main components of cartilage are type II collagen fibres, which provide tensile strength and restrain large aggregates of proteoglycans, principally aggrecan molecules, which are attached to hyaluronan via the link protein. Aggrecan consists of a core protein, to which the sulfated glycosaminoglycans (GAGs) chondroitin sulfate and keratan sulfate are attached. These GAGs confer a high negative charge that generates an osmotic gradient to draw water into cartilage, thus providing resistance to compressive forces. Adapted from Buckwalter et al., 1994.

deep zone contains rounded chondrocytes arranged in columns[6], high levels of proteoglycans, and large-diameter collagen fibres running perpendicular to the articular surface[8]. Below the deep zone is calcified cartilage that forms an interface with the underlying (subchondral) bone.

The mechanical properties of cartilage are determined by the composition and organisation of the extracellular matrix. One of main components of cartilage is type II collagen, which consists of a triple helix of three collagen alpha-1 polypeptide chains. Type II collagen confers high levels of tensile strength, as illustrated by the correlation observed between degradation of collagen and reduced resistance to deformation in human cartilage[9]. The other major component is the proteoglycan aggrecan, which, through interactions with hyaluronan and link protein, forms

large protein aggregates amongst the collagen network (Figure 1.1B). Chains of the sulphated glycosaminoglycans (GAGs) chondroitin sulfate and keratan sulfate are attached to the aggrecan core protein. By conferring a large, fixed negative charge to cartilage[10], the presence of these GAGs generates a strong osmotic pressure that in turn enables cartilage to reversibly deform under mechanical loading. Supporting this role for GAGs in cartilage, resistance to compression was reduced upon enzymatic removal of chondroitin sulfate in bovine cartilage explants[11], and correlated strongly with water content in human cartilage[12]. Maintaining the integrity of the cartilage extracellular matrix is therefore essential for its function in load bearing.

1.1.2 Osteoarthritis

The chronic degenerative joint disease osteoarthritis is characterised by destruction of cartilage and therefore loss of cartilage function[13], which leads to symptoms such as pain, joint stiffness and loss of joint mobility[14]. The cartilage damage in osteoarthritis is associated with increased degradation of cartilage matrix components (Figure 1.2). For example, total type II collagen content was reduced and levels of degraded collagen increased in osteoarthritic human cartilage relative to non-osteoarthritic cartilage[15]. Osteoarthritic cartilage also had reduced levels of chondroitin sulfate and keratan sulfate, which correlated with a reduction in the fixed charge density required for resistance to compression[10]. In addition to these matrix changes, chondrocytes in osteoarthritic cartilage exhibited elevated levels of proliferation and matrix synthesis[16], which results in formation of chondrocyte clusters[6] (Figure 1.2) and is thought to represent a failed attempt at cartilage repair.

Structural changes in other joint tissues are also observed in osteoarthritis[17] (Figure 1.2), such as subchondral bone sclerosis and cyst formation, and the development of bony projections called osteophytes. These bone changes lead to mechanical changes such as reduced bone stiffness[18] and are used for the radiographic diagnosis of osteoarthritis, alongside joint space narrowing due to cartilage loss[19]. Hyperplasia and infiltration of immune cells into the tissue that

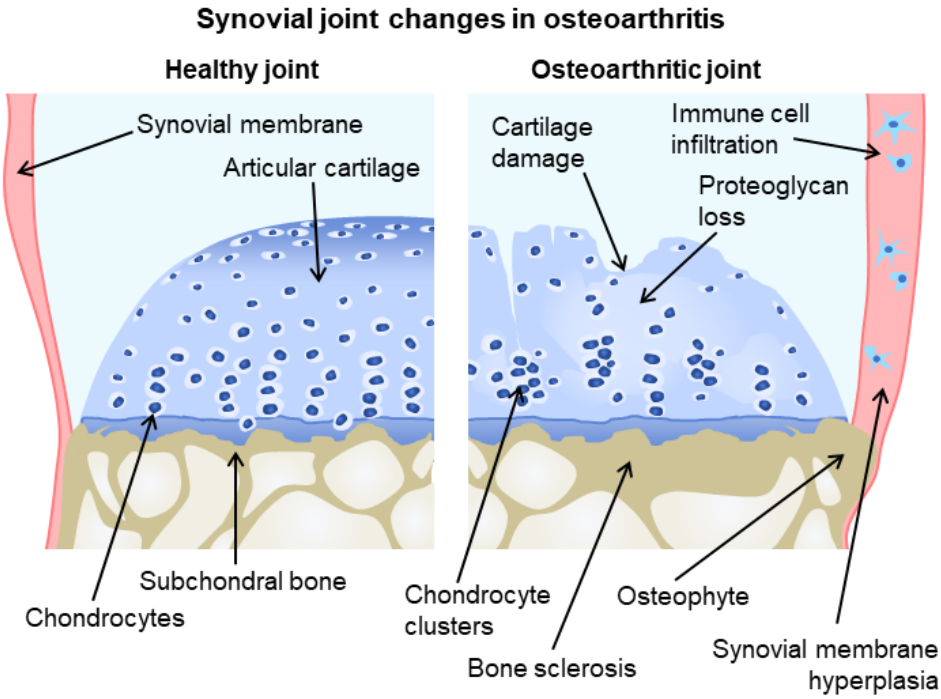

Figure 1.2 Structural changes in osteoarthritic joints. In osteoarthritis, the increased activity of extracellular matrix-proteases leads to proteoglycan loss and eventually cartilage damage. Chondrocyte clusters form due to increased proliferation during attempted repair. Bone changes also occur, such as sclerosis and the development of bony projections called osteophytes. In the synovial membrane, which is the tissue that lines the joint capsule and produces synovial fluid important for joint lubrication, hyperplasia and infiltration of immune cells are observed. Adapted from Glyn-Jones et al., 2015.

lines the joint capsule, the synovial membrane (Figure 1.2), have also been observed in early and late osteoarthritic tissue[20], and are associated with reduced joint-lubricating proteins in the synovial fluid[21].

In many individuals, the exact cause of osteoarthritis is unknown (idiopathic osteoarthritis), although several risk factors have been identified. One of the main risk factors is age[22], which has been proposed to contribute to the development of osteoarthritis via a number of mechanisms. These mechanisms include ageing resulting in the non-enzymatic production of advanced glycation end products. These abnormally glycated molecules have been shown to increase the release of cytokines that stimulate cartilage matrix catabolism, such as interleukin-6 and interleukin-8, in human osteoarthritic chondrocytes[23]. The production of advanced

glycated end products also correlated with an increase in collagen stiffness in human cartilage explants and thus a reduced resistance to mechanical loading[24]. Ageing may also reduce the anabolic capacity of chondrocytes, as proteoglycan synthesis in response to growth factors such as Insulin growth factor 1 (IGF-1) reduced with increasing age in isolated rat chondrocytes[25]. Other risk factors for osteoarthritis include genetics, as a recent genome-wide association study found that 65 genetic variants were associated with osteoarthritis[26], and obesity, which was consistently associated with knee osteoarthritis in a systematic review of osteoarthritis risk factors[27].

In some individuals, the development of osteoarthritis is due to previous injury or a pre-existing condition: this is classified as secondary osteoarthritis[28]. One type of secondary osteoarthritis is post-traumatic osteoarthritis, which is caused by joint injury. Evidence for this came from Lohmander et al. (2004), whose analysis of radiographic and patient-reported knee health in female athletes showed that the prevalence of symptomatic osteoarthritis was significantly increased in athletes with previous knee injuries[29].

There are currently no disease-modifying drugs that slow or prevent the development of the pathological features of osteoarthritis. Surgical replacement of joints is used to treat severe osteoarthritis and has been reported to improve the health-related quality of life[30]. However, there is some risk of revision of surgery, particularly in younger people[31]. The current non-surgical methods for treating osteoarthritis are limited to the management of symptoms. For example, non-steroidal anti-inflammatory drugs are recommended for pain relief, but cannot be used in individuals with some of the common comorbidities in osteoarthritis such as gastrointestinal and cardiovascular conditions[32].

Considering these limitations of current treatment methods, the development of disease-modifying osteoarthritis drugs (DMOADs) is clinically important, although no DMOADs have been successful in clinical trials so far. For example, recombinant human Fibroblast growth

factor 18 (FGF18), known as sprifermin, has been shown to increase matrix anabolism and promote cartilage repair in a rat model of osteoarthritis[33] and in bovine cartilage explants[34]. However, in a double-blind, placebo-controlled, randomised clinical trial, sprifermin treatment of individuals with knee osteoarthritis had no effect on pain, despite improving cartilage thickness[35]. Similarly, whilst targeting the subchondral bone changes in osteoarthritis with anti-bone resorptive drugs reduced bone and cartilage loss *in vivo*[36], these drugs had no effect on pain or radiographic disease progression[37].

1.1.3 Protease-mediated matrix degradation in osteoarthritis

Due to the importance of cartilage loss in the pathogenesis of osteoarthritis, many studies have focused on identifying the catabolic enzymes responsible for cartilage matrix degradation and investigating their potential as therapeutic targets.

Proteolysis of type II collagen is mainly mediated by enzymes of the matrix metalloproteinase (MMP) family. MMP-13 was primarily responsible for type II collagen degradation in numerous experimental systems, such as collagen cleavage by purified enzymes *in vitro*. Using this system, Knäuper et al. (1996) found that purified human MMP-13 preferentially cleaved type II collagen over type I and III[38]. Billinghurst et al. (1997) also found that MMP-13 cleavage of collagen was faster than MMP-1 or MMP-8 through the use of antibodies recognising the N- and C-terminal sequences (known as neoepitopes) of type II collagen fragments[39]. MMP-13 has also been linked to type II collagen degradation in humans, as an MMP-13-selective inhibitor reduced collagen neoepitope generation in human osteoarthritic cartilage[40]. Furthermore, immunohistochemical staining of MMP-13 and other MMPs was increased in osteoarthritic versus non-osteoarthritic cartilage[41], and the MMP-13 gene (*MMP13)* was the most statistically significantly upregulated MMP-encoding gene in osteoarthritis[42].

The role of MMP-13 in collagen degradation during osteoarthritis has been directly shown *in vivo*. Using a tetracycline-inducible expression system under the control of the type II collagen

gene promoter, Neuhold et al. (2001) found that post-natal, cartilage-specific expression of constitutively active MMP-13 in mice increased cartilage lesion formation and collagen neoepitope generation relative to wild-type (WT) mice[43]. Little et al. (2009) also found that histological cartilage damage caused by destabilisation of the medial meniscus of the knee joint (the DMM model of osteoarthritis) was reduced upon MMP-13 deletion relative to WT mice[44]. The cysteine protease cathepsin K, which cleaved purified type II collagen *in vitro*[45] and type II collagen within human cartilage explants[46], has also been shown to have a role in collagen degradation in animal models of osteoarthritis. For example, Hayami et al. (2012) found that treatments of rabbits with a cathepsin K-selective inhibitor reduced levels of degraded type II collagen fragments relative to WT rabbits upon surgical induction of osteoarthritis via transection of the anterior cruciate ligament[47].

Much effort has also been invested into the characterisation of the proteases that degrade the other major cartilage matrix component, aggrecan. Members of the multidomain ADAMTS (A disintegrin and metalloproteinase with thrombospondin motifs) family, and specifically ADAMTS-4 and ADAMTS-5 (Figure 1.3A), have been shown to be the principal aggrecan-degrading proteases. These proteases, known as aggrecanases, are defined by their ability to cleave aggrecan at the bond between amino acid residues 373 and 374 (glutamine and alanine, known as the Glu^{373}-^{374}Ala bond) within the interglobular domain (Figure 1.3B). Sandy et al. (1991) found that aggrecan fragments generated by cleavage at this site in bovine cartilage explants contained the N-terminal neoepitope ARGS[48]. This neoepitope has been detected in knee synovial fluid and cartilage[49] and was elevated in osteoarthritic cartilage relative to healthy controls[50].

ADAMTS-4 was first identified as an aggrecanase by Tortorella et al. (1999). This group showed that ADAMTS-4 purified from bovine cartilage that was stimulated with the cytokine interleukin-1 (IL-1), which has a pro-catabolic effect in cartilage and has frequently been used to induce

cartilage matrix degradation[51], generated aggrecan fragments containing the ARGS neoepitope *in vitro*[52]. Purified ADAMTS-4 also cleaved aggrecan at sites within the chondroitin sulfate-rich (CS) region (Figure 1.3B), such as its preferred cleavage site at the Glu[1667]-[1668]Gly bond[53]. The levels of neoepitopes generated by CS region cleavage, such as the N-terminal sequences GLGS and AGEG, and the C-terminal sequences KEEE and SELE, were also increased in osteoarthritic cartilage relative to healthy human cartilage[50].

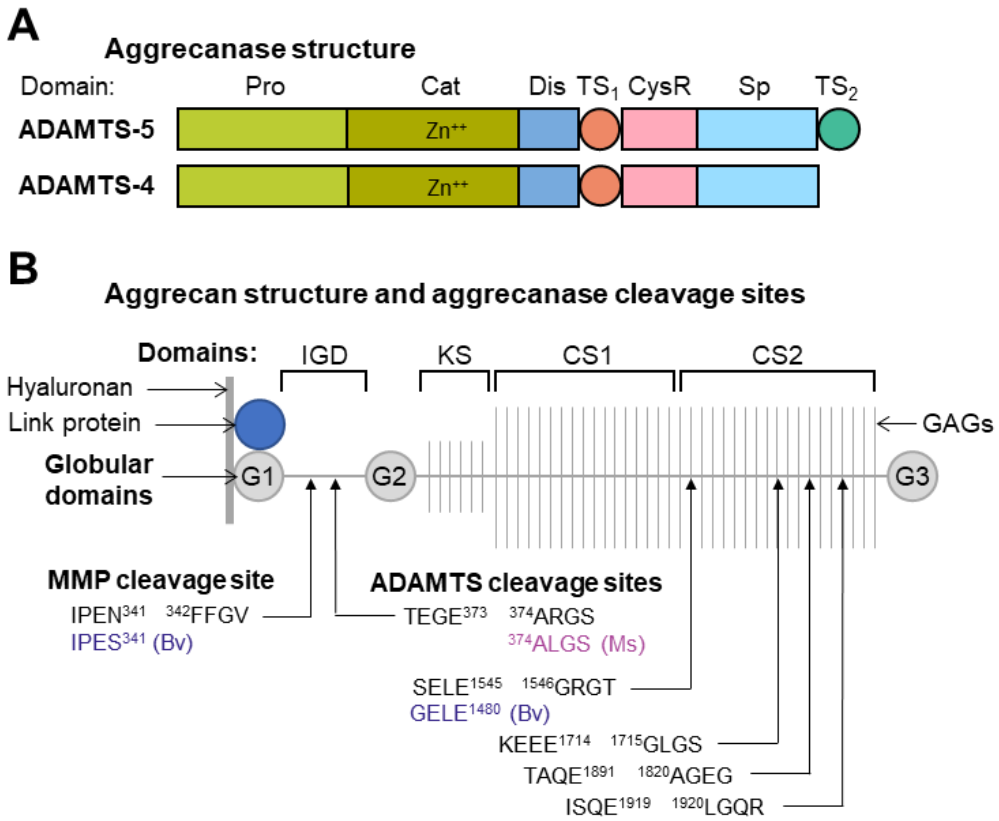

Figure 1.3 Aggrecanase structure and cleavage sites in the aggrecan core protein. ***A***) The principal aggrecanases, ADAMTS-5 and ADAMTS-4, consist of multiple domains: a prodomain (Pro) which is cleaved upon activation of the protease; a zinc catalytic domain (Cat); a disintegrin domain (Dis); a thrombospondin type I domain (TS); a cysteine-rich domain (Cys); and a spacer domain (Sp). Adapted from Gendron et al., 2007. ***B***) ADAMTSs or MMPs cleave aggrecan at specific sites within the core protein, which contains the interglobular domain (IGD), keratan sulfate domain (KS), and chondroitin sulfate domains (CS1 and CS2). This cleavage results in formation of aggrecan fragments, which are detected by antibodies targeting the N- and C-terminal amino acid sequences of the fragments, known as neoepitopes. Cleavage of bovine (Bv) or mouse (Ms) aggrecan results in small differences in the neoepitope sequences. Adapted from Malfait et al., 2002.

ADAMTS-5 has also been shown to cleave at the aggrecanase-defining Glu^{373}-^{374}Ala bond in the interglobular domain of aggrecan, and at the other sites in the chondroitin sulfate-rich region[54]. The relative contributions of ADAMTS-4 and ADAMTS-5 to overall aggrecan degradation have been investigated in a number of experimental systems. For example, Gendron et al. (2007) compared the aggrecan-degrading activities of ADAMTS-4 and ADAMTS-5 domain deletion mutants *in vitro*[55]. They found that Glu^{373}-^{374}Ala cleavage and Glu^{1480}-^{1481}Ala cleavage by full-length ADAMTS-5 was around 600-times and 200-times greater respectively than the most active ADAMTS-4 mutant, and thus proposed that ADAMTS-5 was the major aggrecanase in cartilage.

Transgenic mice have also been used to investigate the roles of aggrecanases in aggrecan degradation *in vivo*. Glasson et al. (2004) found that, when osteoarthritis was surgically induced in mice using the DMM model, deletion of the ADAMTS-4 catalytic domain in mice had no effect on histological cartilage damage or immunohistochemical staining of the NVTEGE aggrecan interglobular domain neoepitope (Figure 1.3B), relative to WT mice[56]. In contrast, they subsequently found that deletion of the ADAMTS-5 catalytic domain resulted in reduced cartilage loss and NVTEGE neoepitope staining relative to WT mice using the same model of osteoarthritis, as well as reduced proteoglycan loss from cartilage explants *ex vivo*[57]. Stanton et al. (2005) also showed that cartilage damage was reduced upon deletion of active ADAMTS-5 in a mouse model of inflammatory arthritis[58]. Together, these results support the proposal that ADAMTS-5 is the major aggrecanase and has an important role in osteoarthritis disease progression.

Further support for the central role of ADAMTS-5 in cartilage degradation has come from studies using human samples. For example, Larkin et al. (2015) found that inhibition of ADAMTS-5 with monoclonal antibodies in osteoarthritic cartilage blocked production of the ARGS aggrecan neoepitope much more effectively than ADAMTS-4 inhibition[59]. Ismail et al. (2015) also found

that small interfering RNA (siRNA)-mediated knockdown of the gene encoding ADAMTS-5 (*ADAMTS5)* in normal human chondrocytes reduced ARGS and AGEG neoepitope production relative to siRNA control chondrocytes, whereas knockdown of the ADAMTS-4 gene (*ADAMTS4)* had no effect[60].

Other groups have provided evidence that ADAMTS-4 may have a greater role in human osteoarthritis than these results indicate. For example, Song et al. (2007) found that *ADAMTS5* or *ADAMTS4* knockdown in osteoarthritic or cytokine-treated healthy human cartilage similarly reduced proteoglycan release and aggrecan neoepitope generation, relative to cartilage treated with non-targeting control siRNA[61]. Furthermore, Naito et al. (2007) showed that *ADAMTS4* expression was upregulated upon IL-1 treatment of human chondrocytes, and in osteoarthritic relative to healthy human cartilage, but no changes in *ADAMTS5* expression were detected[62]. Upregulation of *ADAMTS4* expression was also seen in human cartilage samples by Bau et al (2002).[63] and in IL-1-treated primary human chondrocytes by Fan et al. (2005)[64].

However, these increases in *ADAMTS4* expression have not been consistently observed, as Kevorkian et al. (2004) reported that the expression of both *ADAMTS5* and *ADAMTS4* was downregulated in osteoarthritis[42]. Also, increased protease expression at RNA level may not contribute to the increased aggrecanase activity in osteoarthritis as much as changes in the extracellular levels of proteases. Such changes at protein level may arise from disruption of the post-transcriptional mechanisms that have been shown to regulate the extracellular abundance of aggrecanases and thus their ECM-degrading activity (discussed below in Section 1.2). However, levels of ADAMTS-4 and ADAMTS-5 protein in cartilage have not been quantitatively measured, and only a few studies have used qualitative methods to examine changes at protein level in osteoarthritis. For example, Plaas et al. (2007) showed that immunohistochemical staining of both ADAMTS-5 and ADAMTS-4 was increased in osteoarthritic cartilage[65].

Other proteases are known to cleave aggrecan *in vitro*, but do not appear to have roles in pathophysiological cartilage degradation. For example, Fosang et al. (1996) found that MMP-13 cleaved the aggrecan interglobular domain at the Asn^{341}-^{342}Phe bond (Figure 1.3B)[66], but an MMP-selective inhibitor did not affect aggrecan neoepitope generation or overall proteoglycan release in human osteoarthritic cartilage[50]. Another enzyme of the ADAMTS family, ADAMTS-1, was identified as an aggrecanase[67], albeit with a higher substrate-to-enzyme ratio than ADAMTS-4 or ADAMTS-5[68]. However, deletion of ADAMTS-1 had no effect on proteoglycan degradation in osteoarthritic cartilage explants[61] or in a mouse model of inflammatory arthritis[69]. Cathepsin K has also been shown to cleave aggrecan[70], and histological cartilage damage was reduced upon surgical induction of osteoarthritis in rabbits treated with a cathepsin K inhibitor or in cathepsin K knockout mice[47]. However, the contribution of cathepsin K to aggrecan degradation *in vitro* and *in vivo* relative to ADAMTS-4 and ADAMTS-5 has not been addressed.

In summary, whilst the relative contributions of ADAMTS-4 and ADAMTS-5 to aggrecan degradation in humans is unclear, many studies have shown that these aggrecanases have an essential role in osteoarthritis pathogenesis. ADAMTS-4 and ADAMTS-5 are therefore important therapeutic targets, particularly as aggrecan may protect against proteolytic collagen degradation in addition to its function in maintaining the mechanical properties of cartilage. This wider chondroprotective role of aggrecan was proposed by Pratta et al. (2003), who found that aggrecan degradation occurred earlier than type II collagen degradation in bovine cartilage explants treated with IL-1[71]. They also found that MMP-selective inhibitors had no effect on IL-1-induced aggrecan degradation, whereas aggrecanase-selective inhibitors reduced collagen degradation, and suggested that the preservation of aggrecan might also prevent later matrix changes in osteoarthritis.

1.2 Mechanisms of regulation of protease activity

After the identification of cartilage matrix-degrading proteases such as MMP-13 and ADAMTS-5, many studies have focused on determining how these proteases are regulated in cartilage and dysregulated in osteoarthritis.

1.2.1 Transcriptional regulation of protease activity

Given that changes in *MMP13*, *ADAMTS4* and *ADAMTS5* expression have been observed in osteoarthritis, many studies have focused on identifying the transcription factors that modulate protease gene expression and the signalling pathways that induce them (Figure 1.4).

One such transcription factor is Runt-related transcription factor 2 (RUNX2). RUNX2 has been shown to regulate *MMP13* gene expression during chondrocyte differentiation in development[72] and activated the *ADAMTS5* gene promoter in chondrocytic cell lines and bovine articular chondrocytes[73]. RUNX2 may have a role in regulating proteolytic matrix degradation at transcriptional levels *in vivo*. Kamekura et al. (2006) found that constitutive, heterozygous deletion of RUNX-2 resulted in less severe cartilage damage relative to WT mice upon surgical induction of osteoarthritis via transection of the medial collateral ligament and removal of the medial meniscus, as well as reduced *Mmp13* expression in cartilage[74].

Multiple signal transduction pathways have been shown to induce RUNX2-mediated protease expression in response to different stimuli. These pathways include the hedgehog (Hh) signalling pathway, as siRNA-mediated depletion of RUNX2 in human chondrocytes inhibited the upregulation of *ADAMTS5* observed upon pathway activation by the Hh ligand Indian hedgehog (Ihh)[75]. Also, Fibroblast growth factor 2 (FGF2), which is released from cartilage in response to mechanical injury, increased *MMP13* and *ADAMTS5* expression and proteoglycan release in human articular chondrocytes via mitogen activated protein kinase (MAPK) signalling[76]. In addition to FGF2, mechanical load has also been shown to activate MAPK signalling and downstream RUNX-2 dependent protease expression. Tetsunaga et al. (2011) showed that cyclic

tensile strain increased *MMP13* and *ADAMTS5* expression in chondrocytic cell lines, which was abolished upon knockdown of RUNX2 with siRNAs or an inhibitor of p38 MAPK[77]. Burleigh et al. (2012) found that *Adamts5* expression was also sensitive to mechanical stimuli *in vivo*, as the upregulation of *Adamts5* expression observed after surgical induction of osteoarthritis in mice was not observed when joints were immobilised and thus mechanical load was reduced[78]. Altered mechanical load is therefore thought to be one of the main drivers of osteoarthritis pathogenesis[79].

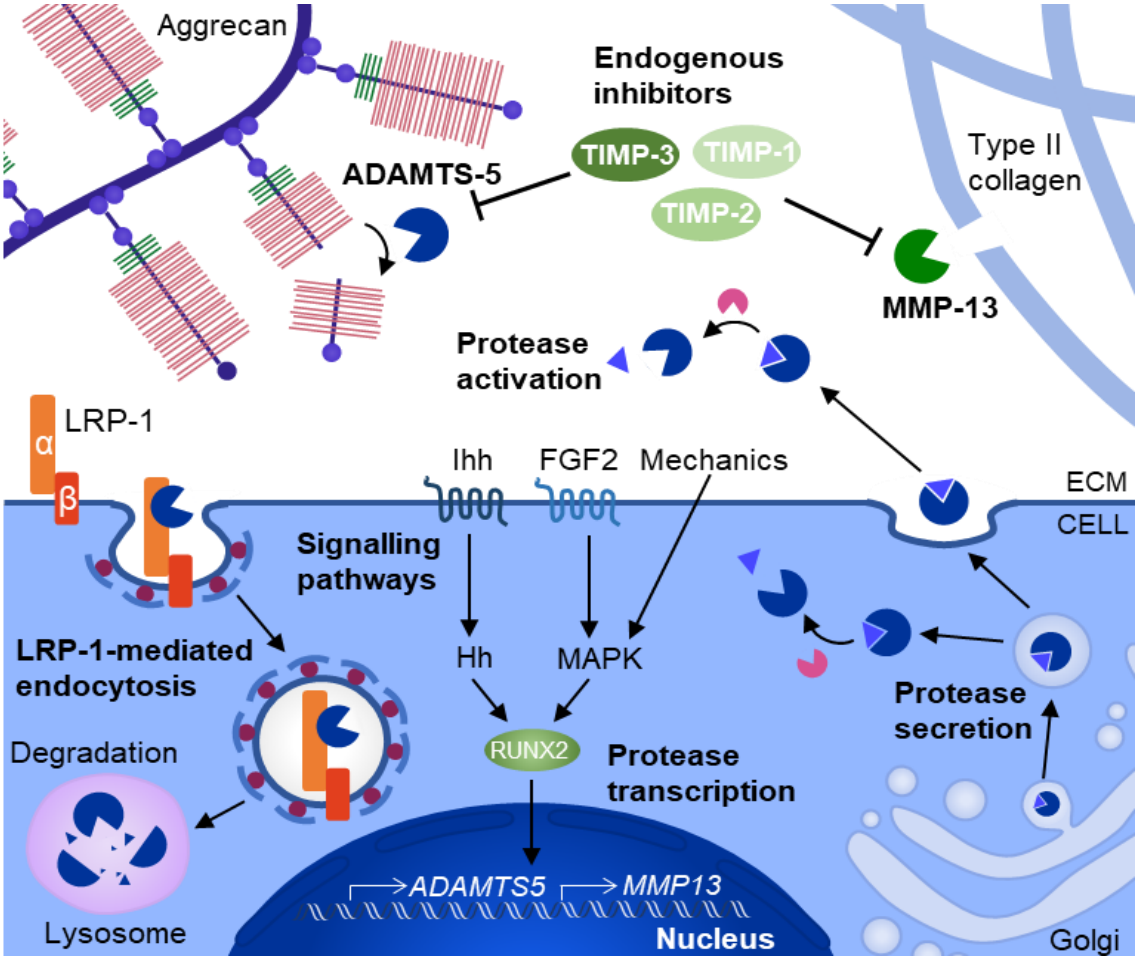

Figure 1.4 Mechanisms of protease activity regulation. Transcriptional regulation of protease expression has been linked to transcription factors such as RUNX2, which is activated by signalling pathways such as the hedgehog pathway, and FGF2- and mechanics-induced MAPK signalling. After transcription and translation, newly synthesised proteins are activated intracellularly or in the extracellular space after secretion. Protease activation involves proteolytic cleavage of an N-terminal prodomain. The extracellular activity of proteases is also regulated by endogenous inhibitors of the TIMP family and by clearance from the extracellular space by LRP-1-mediated endocytosis of proteases, leading to lysosomal degradation.

Inflammation in the joint has also been proposed to contribute to the development of osteoarthritis[80]. Specifically, inflammation of the synovium is observed in osteoarthritis, and involves infiltration of inflammatory cells and release of inflammatory cytokines[20], which are also released from chondrocytes upon mechanical injury during a process known as "mechanoflammation"[79]. These cytokines, such as IL-1, are then thought to stimulate cartilage matrix catabolism, as IL-1 has been shown to induce protease expression and matrix degradation *in vitro* and in cartilage explants[51,81].

However, there is little evidence for a role for IL-1 in osteoarthritis pathogenesis *in vivo*. For example, Clements et al. (2003) found that deletion of the IL-1 family member IL-1β in mice had no effect on cartilage damage and collagen or aggrecan neoepitope generation relative to WT mice upon surgical induction of osteoarthritis[82]. Nevertheless, other inflammatory cytokines may be involved in the development of osteoarthritis, such as IL-6. Supporting this, Ryu et al. (2011) found that deletion of IL-6 in mice reduced histological cartilage damage and immunohistochemical staining of MMP-3 and MMP-13 in cartilage[83], and IL-6 levels were increased in synovial fluid from osteoarthritic joints relative to non-osteoarthritic joints[84]. IL-18 has also been shown to induce a pro-catabolic phenotype *in vitro* by stimulating MMP-1, MMP-3 and MMP-13 RNA expression in human osteoarthritic chondrocytes[85] and reducing aggrecan synthesis in mouse chondrocytes[86]. Furthermore, treatment of mice with an IL-18-neutralising antibody was shown to reduce cartilage damage and synovial inflammation in collagen-induced arthritis[87].

Despite the lack of evidence for IL-1-mediated cartilage matrix catabolism *in vivo*, the study of the cellular response to IL-1 has led to the identification of other protease-regulating transcription factors. For example, IL-1 induced *MMP13* expression via the NFκB transcription factor complex in primary osteoarthritic chondrocytes[88]. Furthermore, Kobayashi et al. (2005) found that the NFκB subunit RelA was the *Adamts5* promoter-binding transcription factor that

induced the strongest *Adamts5* promoter activation in a mouse chondrogenic cell line, and that *RelA* knockdown in primary mouse chondrocytes inhibited IL-1-induced *Adamts5* expression[89].

In contrast to these studies, Ismail et al. (2015) found that treatment of primary human chondrocytes with IL-1 increased ADAMTS-5 aggrecan degradation without affecting *ADAMTS5* RNA expression[60]. These results, together with the lack of A*DAMTS5* upregulation in osteoarthritic cartilage in studies discussed in Section 1.1.3, imply that aggrecanase activity in cartilage may be regulated primarily at protein levels via post-transcriptional mechanisms, which are discussed in the following sections.

1.2.2 Regulation of protease activation by proprotein convertases

After transcription and translation, many proteases are synthesised as inactive zymogens containing a N-terminal prodomain, thus preventing inappropriate degradation of protease substrates during transport of the protease through the secretory pathway (Figure 1.4). Cleavage of the prodomain activates the protease, and the enzymes responsible for this cleavage are called proprotein convertases. One well-characterised proprotein convertase is Membrane-type 1 matrix metalloproteinase (MT1-MMP) on the cell surface, which, together with MMP-2, activated MMP-13 *in vitro*[90].

The identity of proprotein convertases that activate aggrecanases is less clear. Gao et al. (2002) found that processing of pro-ADAMTS-4 and subsequent aggrecan degradation was reduced by an inhibitor of the enzyme furin[91], which was expressed at higher levels in osteoarthritic cartilage relative to non-osteoarthritic cartilage[92]. Wang et al. (2004) also saw that mutation of furin recognition sites in the pro-domain of ADAMTS-4 or siRNA-mediated knockdown of furin reduced the levels of active ADAMTS-4 *in vitro*[93], further indicating that furin has a role in ADAMTS-4 activation. However, this group observed ADAMTS-4 processing in furin-deficient cell lines, and hypothesised that other convertases may also activate ADAMTS-4. Consistent with this hypothesis, Tortorella et al. (2005) showed that the proprotein convertases Paired basic

amino acid cleaving enzyme 4 (PACE4) or Proprotein convertase 5/6 (PC5/6) increased ADAMTS-4 activity *in vitro* to a greater extent than furin[94].

PACE4 has also been proposed to activate ADAMTS-5, but the evidence for this is not conclusive. Malfait et al. (2008) found that depletion of PACE4 from bovine cartilage extracts resulted in reduced cleavage of a fluorescent peptide containing the ADAMTS-5 pro-domain cleavage site, although the effect of depleting other proprotein convertases was not investigated[95]. PACE4 knockdown in primary human chondrocytes reduced IL-1-induced proteoglycan release, but the authors did not directly demonstrate that PACE4 could generate active ADAMTS-5 from pro-ADAMTS-5. In contrast, Longpré et al. (2009) showed that furin overexpression increased pro-ADAMTS-5 processing directly by western blot, but only in cell lines[96]. Therefore, the exact enzymes that activate ADAMTS-5 *in vivo,* and whether ADAMTS-5 activation is increased in osteoarthritis, are not yet known.

1.2.3 Endogenous inhibitors of proteases

The physiological inhibitors of MMPs and some ADAMTSs are members of the tissue inhibitors of metalloproteinases (TIMP) family (Figure 1.4). All four known TIMPs inhibit MMPs to varying extents[97], but only TIMP-3 was able to inhibit production of the ARGS aggrecan neoepitope by purified ADAMTS-4 and ADAMTS-5 *in vitro*[98], and sulfated GAG release in IL-1-stimulated porcine cartilage explants[99]. TIMP-3 has also been shown to inhibit cartilage matrix degradation *in vivo*, as constitutive deletion of TIMP-3 in mice reduced proteoglycan staining and increased aggrecan and collagen neoepitope generation in the adult knee joint[100]. Furthermore, cartilage-specific overexpression of mutant TIMP-3 with greater selectivity for aggrecanases over MMPs reduced cartilage damage and NVTEGE aggrecan neoepitope levels in the STR/ort mouse model of spontaneous osteoarthritis[101] and in the DMM surgical model of osteoarthritis[102]. Morris et al. (2010) also showed that protein levels of TIMP-3 were reduced in more severely damaged

cartilage relative to areas of lower-grade damage in osteoarthritic cartilage[103], indicating that TIMP-3 function may be lost during osteoarthritis.

Levels of extracellular TIMP-3, and thus its capacity to inhibit matrix-degrading proteases, are regulated by endocytosis. Troeberg et al. (2008) found that the polysaccharide calcium pentosan polysulfate inhibited proteoglycan release and aggrecan neoepitope production in porcine cartilage explants through increasing the extracellular levels of TIMP-3[104]. They also showed that extracellular TIMP-3 levels were increased when endocytosis was inhibited with cytochalasin D. In identifying the endocytic receptor required for TIMP-3 endocytosis, Scilabra et al. (2013) found that TIMP-3 uptake was impaired in mouse embryonic fibroblasts deficient in the endocytic receptor Low-density lipoprotein receptor-related protein 1 (LRP-1)[105]. The physiological importance of LRP-1 was demonstrated by Herz et al. (1992), who showed that deletion of LRP-1 in mice was lethal during the early stages of embryogenesis[106]. They proposed that this was due to impaired LRP-1-mediated endocytic uptake of a protease involved in embryo implantation, called urokinase, and its inhibitor. Subsequent studies have shown that LRP-1 mediates the endocytosis of a wide variety of ligands with diverse functions, and therefore has an important role in regulating tissue homeostasis[107]. Consistent with the role of LRP-1 in TIMP-3 endocytosis, Scilabra et al. also showed that TIMP-3 clearance was inhibited by treatment of a human chondrosarcoma cell line with receptor associated protein (RAP). RAP is a physiological competitive antagonist of the Low-density lipoprotein (LDL) receptor family, including LRP-1[108], and thus acts as a molecular chaperone during trafficking of the receptors to the cell surface[109]. Due to this ability to inhibit the ligand-binding ability of LRP-1, RAP has frequently been used experimentally to inhibit LRP-1-mediated endocytosis. Glycosaminoglycans of the extracellular matrix, such as heparin, have also been shown to bind to TIMP-3 and inhibit its endocytosis[110].

Subsequent studies have investigated how extracellular levels of TIMP-3 could be therapeutically increased in osteoarthritis. Chanalaris et al. (2017) found that the antiparasitic drug suramin inhibited the binding of TIMP-3 to LRP-1 *in vitro*, and increased extracellular TIMP-3 levels through inhibition of LRP-1-mediated endocytosis in human osteoarthritic chondrocytes[111]. Suramin also reduced cytokine-induced proteoglycan release and aggrecan neoepitope generation in human osteoarthritic cartilage explants, and in a subsequent study, protected against cartilage damage induced by papain injection in the knee joints of mice[112]. However, Scilabra et al. (2018) later found that increasing extracellular TIMP-3 levels through overexpression in a human embryonic kidney cell line (HEK293 cells) altered the composition of secreted[113] and cell surface-associated proteins[114]. For example, extracellular TIMP-1 levels were increased upon TIMP-3 overexpression, which was possibly due to increased competition for LRP-1 binding, and therefore any therapeutic enhancement of extracellular TIMP-3 could have multiple side effects.

1.2.4 Endocytosis of proteases

In addition to TIMP-3, LRP-1-mediated endocytosis has also been shown to regulate the extracellular levels of proteases, and is therefore an important regulator of protease activity (Figure 1.4). Studies have indicated that the internalisation of various MMPs is LRP-1-dependent *in vitro*: Emonard et al. (2004) showed that MMP-2 alone or in a complex with TIMP-2 interacted with LRP-1, and RAP inhibited the uptake of the pro-MMP-2-TIMP-2 complex in human fibrosarcoma cells[115]. Barmina et al. (1999) also saw that endocytosis of radiolabelled MMP-13 was impaired in LRP-1-deficient or RAP-treated mouse embryonic fibroblasts relative to WT or untreated cells[116].

More recently, Yamamoto et al. (2013) studied the role of aggrecanase endocytosis in cartilage. They found that clearance of extracellular ADAMTS-5 in porcine cartilage explants was inhibited by the small molecule dynasore, which inhibits the two main endocytic pathways, clathrin- and

caveolae-dependent endocytosis[117]. However, inhibition of caveolae-dependent endocytosis alone had no effect on clearance, suggesting that ADAMTS-5 endocytosis is mediated by clathrin-dependent pathways. They also found that ADAMTS-5 endocytosis is predominantly mediated by LRP-1, as treatment of explants with RAP inhibited ADAMTS-5 endocytosis and also resulted in increased ARGS neoepitope production and proteoglycan release. siRNA-mediated knockdown of LRP-1 also reduced ADAMTS-5 endocytosis in human chondrocytes. Subsequent work by this group showed that the activity of ADAMTS-4 was regulated by LRP-1-mediated endocytosis in porcine cartilage and primary human chondrocytes, although the affinity of ADAMTS-4 for LRP-1 was lower than that of ADAMTS-5[118]. Treatment of human chondrocytes with RAP also inhibited uptake of pro-MMP-13, which co-endocytosed with ADAMTS-5 or TIMP-3[119].

Yamamoto et al. (2013) also investigated whether the increased matrix degradation in osteoarthritis is related to impaired LRP-1-mediated endocytosis of proteases. They found that ADAMTS-5 endocytosis was reduced in osteoarthritic human cartilage relative to healthy controls, which was associated with a reduction in cell-associated levels of LRP-1 and an increase in soluble LRP-1 released from the explants[117,120]. The authors therefore hypothesised that impaired ADAMTS-5 endocytosis in osteoarthritic tissue was due to increased shedding of the LRP-1 receptor from the chondrocyte surface, which prevented the binding and subsequent uptake of LRP-1 ligands such as ADAMTS-5. LRP-1 receptor shedding involves proteolytic cleavage of the transmembrane LRP-1 β-chain[121], and various "sheddase" enzymes that mediate LRP-1 cleavage have been identified. One example is ADAM-12, which has been shown to inhibit the uptake of MMP-2 and MMP-9 and thus increase gelatinase activity *in vitro*[122]. Excessive shedding may also be involved in the pathogenesis of other conditions: in lung fluid from individuals with acute respiratory distress syndrome, levels of MMP-2 and MMP-9 were increased relative to healthy control samples and correlated with shed LRP-1 levels[123].

Consistent with their hypothesis, Yamamoto et al. (2017) found that inhibition of the sheddases, ADAM-17 and MMP-14 (also known as MT1-MMP), in osteoarthritic cartilage resulted in increased ADAMTS-5 uptake and reduced ARGS neoepitope production[120]. Ismail et al. (2015) also reported a link between shedding and cartilage matrix catabolism, as ADAMTS-5-mediated aggrecan degradation in human chondrocytes induced by IL-1 was associated with increased JNK signalling-dependent LRP-1 shedding[60]. Therapeutic targeting of protease endocytosis could therefore be a way to restore normal levels of protease activity in osteoarthritis.

1.2.5 Therapeutic targeting of cartilage matrix-degrading proteases

Drugs targeting proteases have been tested as potential treatments for osteoarthritis due to the importance of proteolytic matrix degradation in the development of the disease. For example, aggrecanase inhibitors have been developed, but only one clinical trial has been conducted beyond phase II. The ADAMTS-5 inhibitor used in this trial, which has recently been completed, was shown by Brebion et al. (2021) to inhibit IL-1-induced GAG release from mouse cartilage explants[124].

Broad-spectrum MMP inhibitors have also been investigated as potential disease-modifying osteoarthritis drugs due to their ability to reduce disease progression in animal models. Janusz et al. (2002) found that, after induction of osteoarthritis in rats through intra-articular injection of the metabolic inhibitor mono-iodoacetate, three broad-spectrum MMP inhibitors reduced the severity of cartilage and subchondral bone lesions[125]. However, oral administration of another MMP inhibitor in people with osteoarthritis during a randomised, double-blind clinical trial had no effect on radiographic joint space narrowing or pain scores relative to placebo-treated individuals[126]. Furthermore, use of this drug was associated with a number of adverse effects in musculoskeletal and connective tissues such as Dupuytren's contracture and other fibrosis-related conditions.

Therapeutic targeting of molecules shown to regulate protease activity *in vitro* has also been unsuccessful. Pharmacological inhibition of IL-1, which has been shown to induce proteolytic matrix catabolism via transcriptional (Section 1.2.1) and post-transcriptional mechanisms (Section 1.2.4), did not improve structural changes or symptoms in individuals with osteoarthritis. For example, an anti-IL-1α and IL-1β antibody had no effect on pain or synovitis in people with knee osteoarthritis relative to the placebo group in a phase II, randomised, double-blind clinical trial[127]. Inhibition of Wnt signalling has been tested as an anti-catabolic drug, given that overexpression of Wnt proteins in the synovium *in vivo* resulted in increased cartilage damage and aggrecan neoepitope production[128]. However, a placebo-controlled, randomised, double-blind trial of intra-articular injection of a Wnt pathway modulator in osteoarthritis did not meet its primary end-point, which was improvement in pain scores[129]. Further characterisation of the molecular mechanisms of protease activity regulation could help to identify new, more selective therapeutic targets, which in turn could lead to the development of drugs that effectively reduce cartilage damage and thus slow the progression of osteoarthritis without causing multiple side effects.

1.3 Role of the primary cilium in cartilage matrix homeostasis

To identify novel regulators of protease activity in chondrocytes, the Wann group has focused on proteins required for the formation and function of the primary cilium, which is an organelle with a pivotal role in cellular signalling. The primary cilium has been shown to be involved in cartilage development and has been associated with regulation of extracellular matrix composition and secretion in cartilage[130], but until recently, its role in matrix degradation in chondrocytes had not been studied.

1.3.1 Structure and function of the primary cilium

Primary cilia are non-motile organelles that regulate multiple cellular processes through sensing and transducing different signals. Primary cilia are assembled by most mammalian cell types[131], including chondrocytes[132]. The primary cilium consists of a central microtubule core called the axoneme, which is enclosed by the ciliary membrane (Figure 1.5). The axoneme grows out from a modified form of the older ("mother") centriole of the cell, which is known as the basal body. Primary cilia are assembled in the G_0/G_1 phase of the cell cycle, when centrioles are not engaged in formation of the mitotic spindle or duplicating, and disassembled upon cell cycle re-entry[133].

The molecular events required for cilia assembly (also referred to as ciliogenesis) have been characterised in recent years. In the early stages of ciliogenesis, the mother centriole is converted to a basal body through the acquisition of distal appendages, which are protein complexes recruited to the distal end of the mother centriole and are required for docking of the basal body to pre-ciliary membranes[134]. During cilia assembly via the extracellular pathway proposed by Sorokin[135], this membrane is the plasma membrane, resulting in formation of primary cilia on the cell surface that project into the extracellular environment (Figure 1.5). In the intracellular pathway generally used by non-apically polarised cells, distal appendages dock at the ciliary vesicle, which is formed through fusion of pre-ciliary vesicles mediated by EPS15-homology domain-containing protein (EHD1)[136]. The primary cilium then develops in the

cytoplasm and the ciliary vesicle eventually fuses with the plasma membrane, exposing the cilium to the cell surface whilst also creating an invagination of the plasma membrane called the ciliary pocket[137,138].

After membrane docking, removal of Centriolar coiled-coil protein of 110 kDa (CP110) from the distal end of the mother centriole enables the extension of centriolar microtubules to form the axoneme[139]. CP110 removal is mediated by Tau-tubulin kinase 2 (TTBK2)[140], which is recruited to centrioles by Centrosomal protein 164 (CEP164) at the onset of ciliogenesis[141]. Proteins involved in the ciliary trafficking process intraflagellar transport (IFT, Figure 1.6) are also

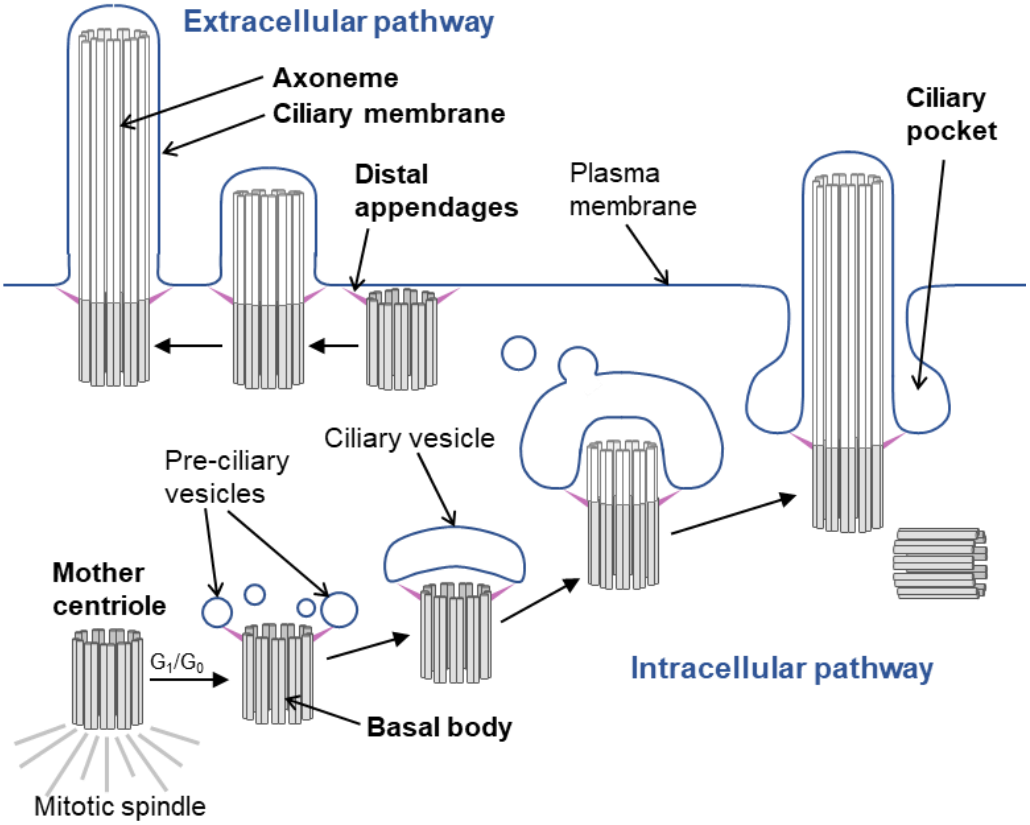

Figure 1.5 Intracellular and extracellular pathways of cilia assembly. During the G_1/G_0 phase of the cell cycle, when the mother centriole is not engaged in formation of the mitotic spindle, the mother centriole acquires distal appendages and becomes the basal body. In the extracellular pathway of ciliogenesis, the basal body docks at the plasma membrane directly via its distal appendages. Subsequent axoneme elongation forms a primary cilium that projects into the extracellular space. In the intracellular pathway, the distal appendages bind to pre-ciliary vesicles which develop into the ciliary vesicle. The axoneme elongates in the cytoplasm, and eventually the ciliary vesicle fuses with the plasma membrane, forming the ciliary pocket. Adapted from Benmerah, 2013.

recruited to the mother centriole. IFT enables the delivery of cargo required for assembly and maintenance of the cilium from the cytoplasm to the ciliary compartment[142], which lacks the machinery for protein synthesis. Transport from the base to the tip of the cilium (anterograde IFT) is performed by the IFT-B complex of proteins such as IFT81 and IFT74, which have been shown to carry the tubulin subunits used for construction of the axoneme[143]. Depletion of IFT-B complex proteins such as IFT88 is therefore characterised by shortened or absent cilia, as demonstrated in the kidneys of mice with a mutation in Intraflagellar protein 88 (IFT88)[144] and upon siRNA-mediated knockdown of IFT88 in a chondrogenic mouse cell line[145]. Similar disruption of cilia assembly has been observed upon knockout of subunits of the kinesin-2 motor protein complex, such as KIF3A[146], that transports IFT-B from the base to the tip of the cilium. Retrograde IFT from the tip to the base of the cilium is carried out by the IFT-A protein complex and the motor protein cytoplasmic dynein 2, mutation of which resulted in accumulation of proteins at the ciliary tip[147].

As the axoneme elongates, extension of the ciliary membrane occurs through the transport of Golgi-derived vesicles to the cilium by the trafficking proteins Ras-associated binding protein (Rab) 8 and 11[148,149]. Between the developing axoneme and the ciliary membrane, the transition zone forms (Figure 1.6). This is a region at the base of the cilium that separates the ciliary membrane from the contiguous plasma membrane by creating a barrier to the diffusion of proteins into the ciliary compartment[150]. Disruption of proteins that form the transition zone therefore alters the protein composition of the ciliary membrane: Awata et al. (2014) found that mutation of the transition zone protein Nephronophthisis 4 (NPHP4) in the green algae *Chlamydomonas reinhardti*, which assemble a structure analogous to the primary cilium called the flagellum, resulted in reduced flagellar membrane proteins and increased cytoplasmic proteins in the flagellum[151].

Receptors and other molecules involved in various signalling pathways are enriched at the primary cilium, and therefore disruption of cilia assembly or maintenance results in altered

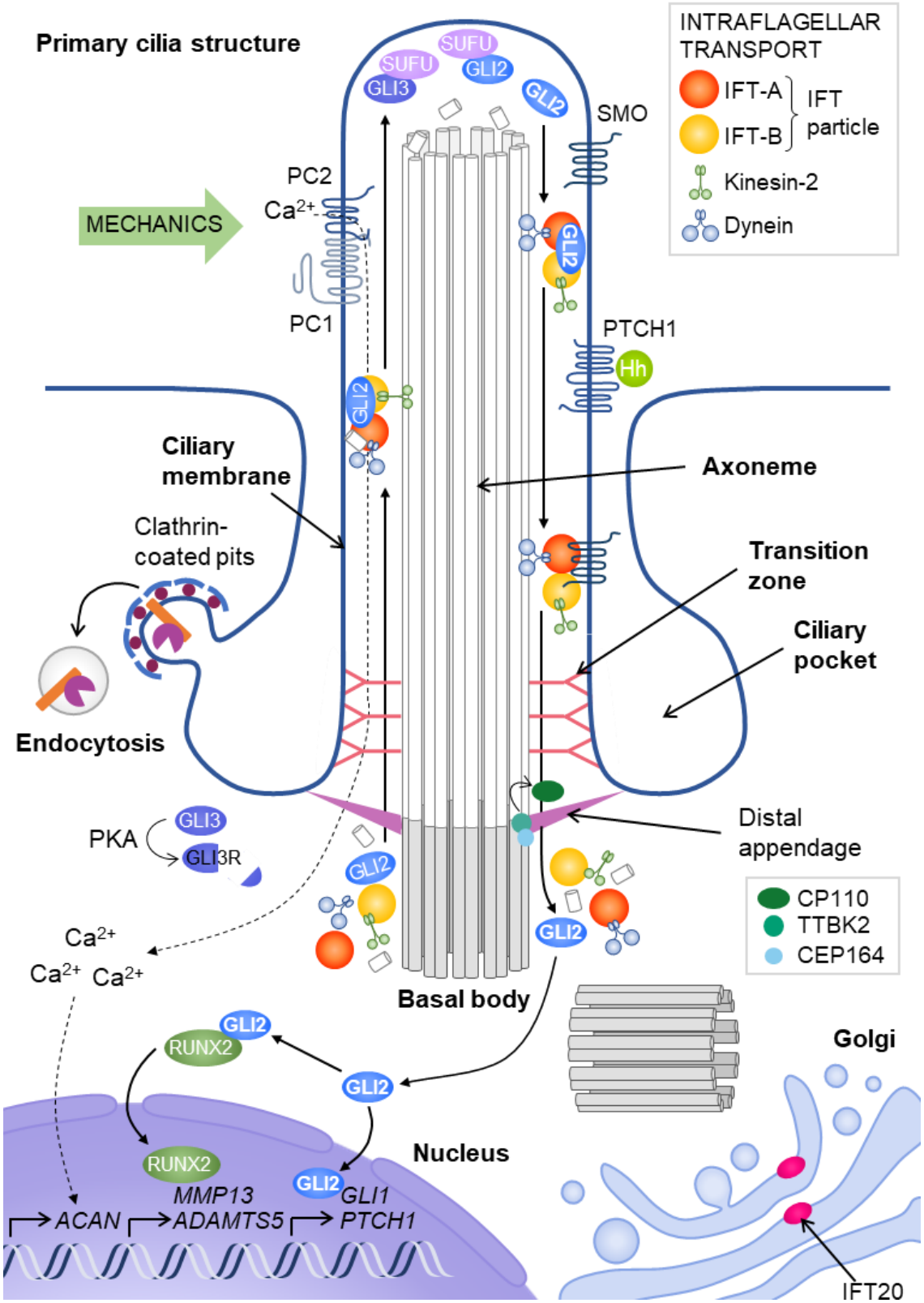

Figure 1.6 Structure of the primary cilium. Figure legend continued on following page.

Figure 1.6 Structure of the primary cilium continued. The primary cilium is assembled and maintained via intraflagellar transport (IFT) of cargo along the central microtubule core of the cilium, the axoneme. The axoneme elongates from the basal body, which develops from the mother centriole upon removal of the protein CP110 from the distal centriole by TTBK2. Ciliary entry is regulated by the transition zone. The ciliary membrane is enriched in proteins involved in cell signalling, such as the polycystins (PC1 and PC2) involved in mechanically-induced calcium signalling, and the key Hh pathway positive and negative regulators, Smoothened (SMO) and Patched1 (PTCH1). Events of the Hh signalling pathway occur at the cilium, such as proteolytic processing of the GLI3 transcription factor by protein kinase A (PKA) at the base of the cilium, and dissociation of GLI2 and GLI3 from Suppressor of Fused (SUFU) upon IFT-mediated transport to the ciliary tip. Clathrin-mediated endocytosis occurs at the ciliary pocket membrane, and the cilium is closely associated with the Golgi. Adapted from Collins and Wann, 2020.

cellular signalling. A pathway that is critically dependent on the primary cilium is the Hh signalling pathway. This was illustrated by Huangfu et al. (2003), who found that mice with mutations affecting three proteins involved in IFT and thus required for cilia assembly, IFT88, IFT172 and KIF3A, had developmental patterning defects[152], which were the same as defects observed upon mutation of the Hh pathway ligand Sonic hedgehog (Shh)[153]. The Hh signal transduction events that occur at the cilium have been characterised[154] (Figure 1.6). In the absence of Hh ligands, the Hh pathway inhibitor Patched1 (PTCH1) is present in the ciliary membrane[155], and inhibits Hh signalling by preventing entry of the Hh pathway activator Smoothened (SMO) into the cilium via an unknown mechanism[156]. Hh pathway target gene expression mediated by the Glioblastoma-associated oncogene homolog (GLI) transcription factors is inhibited by proteolytic processing of full-length GLI3 to a truncated repressor form by protein kinase A (PKA) at the base of the cilium[157], and through binding of GLI2 and GLI3 to their repressor Suppressor of Fused (SUFU)[158]. Binding of Hh ligands to PTCH1 results in SMO accumulation in the ciliary membrane and subsequent activation of Hh target gene expression, which occurs via inhibition of GLI proteolysis and subsequent dissociation of the GLI-SUFU complexes at the ciliary tip.

Ciliary processes such as IFT are essential for the coordination of these Hh pathway signalling events. Mutation of IFT25 resulted in altered trafficking of PTCH1 out of the cilium and reduced GLI2 accumulation at the ciliary tip upon pathway activation *in vitro*, as well as developmental defects characteristic of altered Hh signalling, such as polydactyly (formation of extra digits), *in vivo*[159]. Mutation of IFT proteins and other ciliary proteins in humans results in diseases known as ciliopathies[160], the phenotype of which is often attributed to altered Hh signalling. For example, Beales et al. (2007) found that *IFT80* was mutated in individuals with asphyxiating thoracic dystrophy (also known as Jeune syndrome), which was characterised by shortened rib bones and polydactyly, and that mutation of *ift80* in zebrafish resulted in similar defects to *shh*-null embryos[161].

In addition to soluble ligands such as Shh, primary cilia are also thought to initiate cellular signalling in response to mechanical stimuli. Praetorius and Spring showed that bending of the primary cilium in response to fluid flow increased intracellular calcium ion (Ca^{2+}) levels in a kidney epithelial cell line[162]. Nauli et al. (2003) subsequently showed that this mechanically-induced Ca^{2+} level increase was reduced by deletion or inhibition of the proteins Polycystin-1 (PC1) and Polycystin-2 (PC2)[163], which localise to the ciliary membrane[164] (Figure 1.6) and are mutated in individuals with autosomal-dominant polycystic kidney disease[165]. These results led to the hypothesis that fluid flow is sensed by the cilium, leading to an influx of Ca^{2+} ions into the cilium via the Ca^{2+}-permeable cation channel PC2. This results in the activation of calcium signalling and subsequent regulation of cellular processes, such as cell proliferation, that is disrupted in polycystic kidney disease and leads to cyst formation. Whilst Delling et al. (2016) found that fluid flow did not directly alter ciliary Ca^{2+} concentration in primary mouse kidney cells[166], the results of other studies have supported this hypothesised role for the cilium in maintaining cellular homeostasis in the kidney. For example, Moyer et al. (1994) found that mutation of IFT88, which reduced cilia assembly[144], caused polycystic kidney disease in mice (known as Oak Ridge Polycystic Kidney (ORPK) mice)[167]. More recently, Walker et al. (2019)

showed that mice expressing a mutant form of PC2 that did not localise to the cilium exhibited kidney cyst formation[168].

In summary, processes involved in assembly and maintenance of the structure of the primary cilium are essential for its function in coordinating the cellular response to various biochemical and mechanical signals. This important role in cellular signalling is exemplified by ciliopathies, which cause a variety of defects across many tissues of the body.

1.3.2 Roles of the primary cilium in cartilage extracellular matrix anabolism

The primary cilium has been shown to have an important role in the skeletal system, including in the regulation of cartilage matrix homeostasis, through its functions in cellular signalling and other processes. The role of ciliary signalling in skeletal development is illustrated by the developmental patterning defects present in ciliopathies; for example, polydactyly is caused by altered Shh signalling at the developing limb bud[169]. Furthermore, signalling via another Hh ligand, Ihh, regulates chondrocyte proliferation and differentiation during endochondral ossification[170]. This is the process by which bone is formed from cartilaginous templates, which consist of proliferating chondrocytes that secrete the type II collagen-rich cartilage matrix. At the centre of the template, proliferating chondrocytes differentiate into prehypertrophic and then hypertrophic chondrocytes, which secrete a matrix containing type X collagen that is remodelled to ultimately form bone, before undergoing apoptosis[171]. Eventually, the entire cartilage template is converted to bone, except at the articular surface and a region called the growth plate, which enables postnatal bone elongation.

Ihh regulates hypertrophic differentiation via a negative feedback loop with Parathyroid hormone-related protein (PTHrP) and also stimulates chondrocyte proliferation, as demonstrated by the reduction in bromodeoxyuridine-labelled proliferating chondrocytes in developing long bones upon deletion of Ihh in mice[172]. Deletion of Ihh in postnatal cartilage also resulted in loss of columns of proliferating chondrocytes in the tibial growth plate, which was

instead composed of type X-collagen-expressing hypertrophic chondrocytes, indicative of accelerated chondrocyte differentiation[173]. Consistent with the role of the cilium in regulating the Hh pathway, similar growth plate phenotypes have been observed upon disruption of ciliary proteins. For example, Yuan et al. (2015) found that postnatal deletion of IFT80 in mouse cartilage was associated with shortened and less organised growth plates and expanded regions of type X collagen expression, as well as reduced Hh signalling[174]. Therefore, the primary cilium regulates cartilage matrix composition during development as a function of its role in regulating chondrocyte differentiation.

Primary cilia might also regulate chondrocyte differentiation, and thus the cartilage matrix composition, via other cellular processes in addition to Hh signalling. Song et al. (2007) found that constitutive deletion of another IFT-B complex protein, KIF3A, in cartilage also resulted in loss of chondrocyte columns and ultimately loss of the growth plate[175]. In contrast to Yuan et al. (2003), no changes in Hh signalling were observed. Instead, Song et al. (2007) suggested that cell shape changes caused by disorganisation of the actin cytoskeleton upon KIF3A deletion, and impaired cell adhesion driven by altered localisation of focal adhesion kinase, disrupted the process by which dividing chondrocytes are arranged in columns (known as chondrocyte rotation). Re-organisation of F-actin into stress fibres was also associated with formation of shorter growth plates, reduced chondrocyte column linearity and failed chondrocyte hypertrophy when IFT88 was mutated in ORPK mice[176]. Such changes may be related to altered Wnt signalling, as mutation of the Wnt receptor Frizzled in chick embryos also resulted in loss of oriented chondrocyte division in the growth plate and formation of shortened limbs[177]. Yuan et al. (2003) also found that Wnt signalling was activated upon IFT80 deletion[174].

In addition to these studies reporting changes in the cartilage growth plate upon ciliary protein knockdown, members of the Wann group have recently found that postnatal, cartilage-specific deletion of *Ift88* reduced articular cartilage thickness, specifically in the calcified region of

cartilage adjacent to the subchondral bone[178]. This was possibly caused by accelerated chondrocyte hypertrophy driven by increased Hh signalling, as *Ift88* deletion also resulted in increased expression of the Hh target *Gli1*. As both cartilage thickness and Hh signalling were rescued by increased mechanical loading of joints, Coveney et al. (2021) proposed that IFT88 is required for regulating mechanically-induced Hh signalling and thus cartilage homeostasis. Disruption of IFT88 in chondrocytes *in vitro* has also been shown to impair the mechanosensitive signalling events that lead to the expression of cartilage matrix components. Wann et al. (2012) found that chondrocytes derived from ORPK mice had reduced compression-induced aggrecan expression and GAG synthesis relative to WT chondrocytes, which was likely due to reduced purinergic calcium signalling and expression of full-length PC1[179]. Further support for the role of ciliary polycystins in mechanotransduction in chondrocytes came from Thompson et al. (2021), who showed that knockdown of PC1 or PC2 abolished the upregulation of aggrecan and type II collagen expression induced by cyclic tensile strain, which also increased trafficking of PC2 to the ciliary membrane[180]. Rais et al. (2015) also found that reduced cilia assembly caused by KIF3A knockdown in the chondrogenic ATDC5 cell line was associated with reduced mechanically-induced aggrecan and type X collagen expression[181]. These studies therefore indicate that ciliary proteins regulate cartilage matrix synthesis in response to mechanical load.

Chondrocyte primary cilia have also been proposed to have a role in the secretion of the cartilage matrix. After observing a close spatial relationship between the primary cilium and the Golgi in various cells, including chondrocytes, Poole et al. (1985) hypothesised that the primary cilium links the matrix with the secretory machinery to facilitate adaptation of the matrix to mechanical load[132]. In this so-called "matrix-cilia-Golgi continuum", cilia sense mechanical signals, which are then relayed to the Golgi via mechanotransduction events at the cilium, and lead to changes in matrix production. Subsequent studies have identified proteins that could be involved in establishing such a connection between the cilium, Golgi and matrix secretion in chondrocytes. The main candidate for this is IFT20, which has been shown to be required for

cilia assembly and localised to the Golgi in chondrogenic cell lines[182]. Deletion of IFT20 in neural crest cells *in vivo* resulted in delayed secretion of type I collagen during development, which possibly contributed to abnormal bone mineralisation[183]. Furthermore, Kitami et al. (2019) proposed that the reduced proteoglycan staining in mouse cartilage upon postnatal deletion of IFT20, was due to impaired secretion of matrix by the Golgi, which was smaller in these mice relative to WT mice[182]. However, the exact mechanism by which IFT20 might traffic between the cilium and Golgi, and regulate matrix secretion, is unknown.

1.3.3 Role of the primary cilium in cartilage extracellular matrix catabolism

Primary cilia have also been linked to the regulation of matrix catabolism. The principal mechanism by which the cilium has been proposed to regulate cartilage matrix degradation is via activation of the Hh signalling pathway, which is thought to induce protease expression via the transcription factor RUNX2, as discussed in Section 1.2.1.

Evidence for the role of Hh signalling in cartilage degradation has come from the study of osteoarthritic human cartilage. For example, Lin et al. (2009) found that expression of the Hh target genes *PTCH1* and *GLI1*, as well *ADAMTS5* and *MMP13*, were increased in the most severely histologically damaged areas of osteoarthritic cartilage relative to the less damaged regions[75]. Furthermore, Wei et al. (2012) found that immunohistochemical staining of Ihh correlated with disease severity in osteoarthritic tissue, whereas negligible Ihh staining was observed in cartilage from healthy controls[184].

Modulation of Hh signalling *in vivo* has also provided evidence supporting a link between activation of the Hh pathway and cartilage catabolism. Lin et al. (2009) showed that activation of the pathway via deletion of one *Ihh* allele, constitutive deletion of *Gli2* in cartilage, or postnatal expression of active SMO, resulted in reduced cartilage proteoglycan staining, increased *Adamts5* expression and increased aggrecan and collagen neoepitope generation[75]. After surgical induction of osteoarthritis via removal of the medial meniscus, pharmacological

Hh blockade or inactivating SMO mutations increased proteoglycan staining and reduced neoepitope production relative to untreated or WT mice respectively. By imaging protease activity *in vivo* with fluorescent protease substrate probes, Zhou et al. (2014) also showed that cartilage-specific deletion of *Ihh* in adult mice reduced the activity of cathepsins and MMPs, including MMP-13, and reduced histological cartilage damage upon induction of osteoarthritis by partial removal of the medial meniscus[185].

Other *in vivo* studies have provided further insight into RUNX2-indpendent mechanisms by which Hh signalling might elicit proteolytic cartilage damage. Ali et al. (2016) saw that genes related to the cholesterol biosynthetic pathway were most affected by pharmacological modulation of the Hh pathway in osteoarthritic cartilage[186]. They subsequently found that deletion of the main negative regulators of cholesterol homeostasis, Insig1 and Insig2, resulted in increased *Mmp13* and *Adamts5* expression and spontaneous cartilage damage in adult mice, which was reversed upon cholesterol inhibition with statins. Rockel et al. (2016) proposed that Hh activation also causes cartilage damage by repressing expression of Wnt pathway target genes, such as the chondroprotective growth factor FGF18, given that constitutive activation of β-catenin-mediated Wnt signalling reduced cartilage damage and increased FGF18 expression when Smo was mutated in adult mice[187].

Increased articular cartilage matrix catabolism has also been observed upon direct disruption of ciliary proteins. For example, Kaushik et al. (2009) found that constitutive deletion or mutation of the BBSome complex proteins BBS1, BBS2 and BB6 reduced articular cartilage thickness and proteoglycan staining in adult mice[188]. Such changes may be indicative of the onset of osteoarthritic cartilage degradation in adulthood. However, as suggested by the authors, these changes may instead be related to failed production of normal cartilage during development, given the important role of the primary cilium in regulating chondrocyte differentiation. Consistent with the latter hypothesis, subsequent analysis of these mice showed that cartilage

damage was present at even earlier time points[189]. Changes in matrix deposition during cartilage development may also explain the observations of Chang et al. (2012). This group found that adult mice in which IFT88 was constitutively deleted in cartilage exhibited increased protease expression but also increased cartilage thickness[190]. The authors proposed that these results were indicative of attempted cartilage repair during the early stages of osteoarthritis caused by the increased Hh signalling also observed in these mice, but IFT88 deletion was later shown by the same group to cause growth plate disorganisation[191].

One way to avoid any developmental defects caused by disruption of ciliary proteins is to induce deletion at later postnatal time points. As described in Section 1.3.2, members of the Wann group deleted *Ift88* in adolescent mice at 8 weeks of age[178]. These mice exhibited reduced cartilage thickness two weeks after deletion relative to control mice at the same time point, spontaneous histological cartilage damage in adulthood, and also more severe disease after surgical induction of osteoarthritis. The reduction in cartilage thickness was associated with increased Hh signalling, but the absence of elevated aggrecan neoepitope generation in these mice indicated that this was not due to increased protease activity. Activation of Hh signalling has also been shown to have no effect on cartilage matrix degradation *in vitro*. Specifically, Thompson et al. (2015) found that treatment of bovine or human cartilage explants with recombinant Ihh increased *Ptch1* and *Gli1* expression, but did not affect *ADAMTS5* and *MMP13* expression or sulfated GAG release[192].

To more directly determine the mechanism by which ciliary proteins might regulate protease activity, the Wann group measured proteolytic matrix degradation in chondrocyte lines derived from the IFT88 mutant ORPK mouse, which assemble fewer primary cilia. In this study by Coveney et al. (2018), ORPK chondrocytes had increased generation of the ARGS and AGEG aggrecan neoepitopes relative to WT cells, but did not exhibit increased expression of aggrecan-degrading proteases or Hh target genes[193]. Instead, the rate of endocytosis of the proteases

ADAMTS-5 and MMP-13 was reduced in ORPK cells to a similar extent as treatment of WT cells with RAP, which previously inhibited protease endocytic clearance and increased matrix degradation in cartilage (Section 1.2.4). These results therefore indicated that disruption of the primary cilium upon mutation of IFT88 resulted in increased protease activity via impaired LRP-1-mediated endocytosis.

To determine the mechanism by which the primary cilium may regulate protease endocytosis, Coveney et al. (2018) first tested whether the impaired endocytosis of ORPK chondrocytes was related to increased LRP-1 receptor shedding (described in Section 1.2.4). Extracellular levels of LRP-1α were qualitatively increased in ORPK chondrocytes relative to WT chondrocytes, indicative of elevated shedding. Protein levels of the sheddase MMP-14 were also increased, although levels of the ADAM-17 sheddase were reduced.

Coveney et al. (2018) also found that the distribution of the LRP-1 receptor was altered in ORPK chondrocytes, which might have contributed to the reduced rate of endocytosis. Specifically, the transmembrane β-chain of LRP-1 in was mainly localised in the quadrant of WT cells containing the primary cilium, and even appeared as a focal area of staining at the base of the cilium in some cells. This pattern of distribution was observed less frequently in ORPK cells: in half of the ORPK cells imaged, LRP-1β was distributed evenly throughout the cell. Coveney et al. (2018) therefore hypothesised that the reduced rate of endocytosis in ORPK cells was due to loss of a periciliary, IFT88-dependent structure that facilitates efficient LRP-1 internalisation, and that this structure was the ciliary pocket.

As described in Section 1.3.1, the ciliary pocket is a pit formed around the axoneme and ciliary membrane through invagination of the plasma membrane during ciliogenesis. The ciliary pocket is similar to a structure called the flagellar pocket, which is found in protozoan parasites such as *Trypanosoma brucei* and is the sole site of endocytosis and exocytosis[194]. The ciliary pocket has also been shown to be a site of vesicular activity in mammalian cells including primary mouse

chondrocytes, in which vesicles were found along the ciliary pocket membrane by electron microscopy[195]. Furthermore, Molla-Herman et al. (2010) found that markers of clathrin-coated pits, which are formed during clathrin-mediated endocytosis, were present at the ciliary pocket in a retinal pigment epithelial cell line[137]. This group also found that these pits were enriched in the ciliary pocket membrane relative to the rest of the plasma membrane, raising the possibility that the rate of internalisation of endocytic cargo, such as the LRP-1 receptor, is enhanced at the ciliary pocket.

Whilst the ciliary pocket has not been directly examined in WT and ORPK chondrocytes, previous studies have linked disruption of IFT88 to impaired endocytosis. One example is a study by Clement et al. (2013), who investigated the role of the primary cilium in the regulation of Transforming growth factor beta (TGF-β) signalling, which has been shown to be enhanced by endocytosis of TGF-β receptors[196]. They found that the TGF-β-induced localisation of the TGF-β receptor type I to the base of the cilium in human fibroblasts was dependent on endocytosis, and, in contrast to WT mouse embryonic fibroblasts, was absent in ORPK mouse embryonic fibroblasts. The authors proposed that this was due to disrupted clathrin-mediated endocytosis at the ciliary pocket, as the periciliary concentration of the clathrin endocytic adaptor protein Clathrin assembly lymphoid myeloid leukaemia (CALM) seen in WT cells was abolished in ORPK cells.

Other properties of the primary cilium and periciliary region might also contribute to enhanced endocytosis in this region. One possibility is that the ciliary membrane itself contains endocytic microdomains. Schou et al. (2017) found that the kinesin KIF13B was recruited to the ciliary transition zone by NPHP4 in mouse fibroblasts, where it was required for formation of a microdomain containing caveolin-1 (CAV-1), which is a protein required for the other major endocytic pathway, caveolae-mediated endocytosis[197]. KIF13B has also been shown to have a role in regulating LRP-1-mediated endocytosis. Deletion of KIF13B *in vivo* reduced the uptake of

LRP-1 ligands and reduced the colocalization of LRP-1 and CAV-1-labelled caveolae observed in WT cells *in vitro*[198].

Another possibility is that the rate of LRP-1-mediated endocytosis is increased in the periciliary region through increased recycling of LRP-1 back to the periciliary membrane. This increased recycling might be related to the close proximity of the primary cilium to compartments of the endosomal system (Figure 1.7), from which internalised receptors can be returned to the plasma membrane. One such compartment is the early endosome, where endocytosed cargo is sorted and also directly returned to the cell surface via the "fast" recycling pathway[199,200]. A focal area of staining for a marker of the early endosome, Early endosomal antigen-1 (EEA1) was present

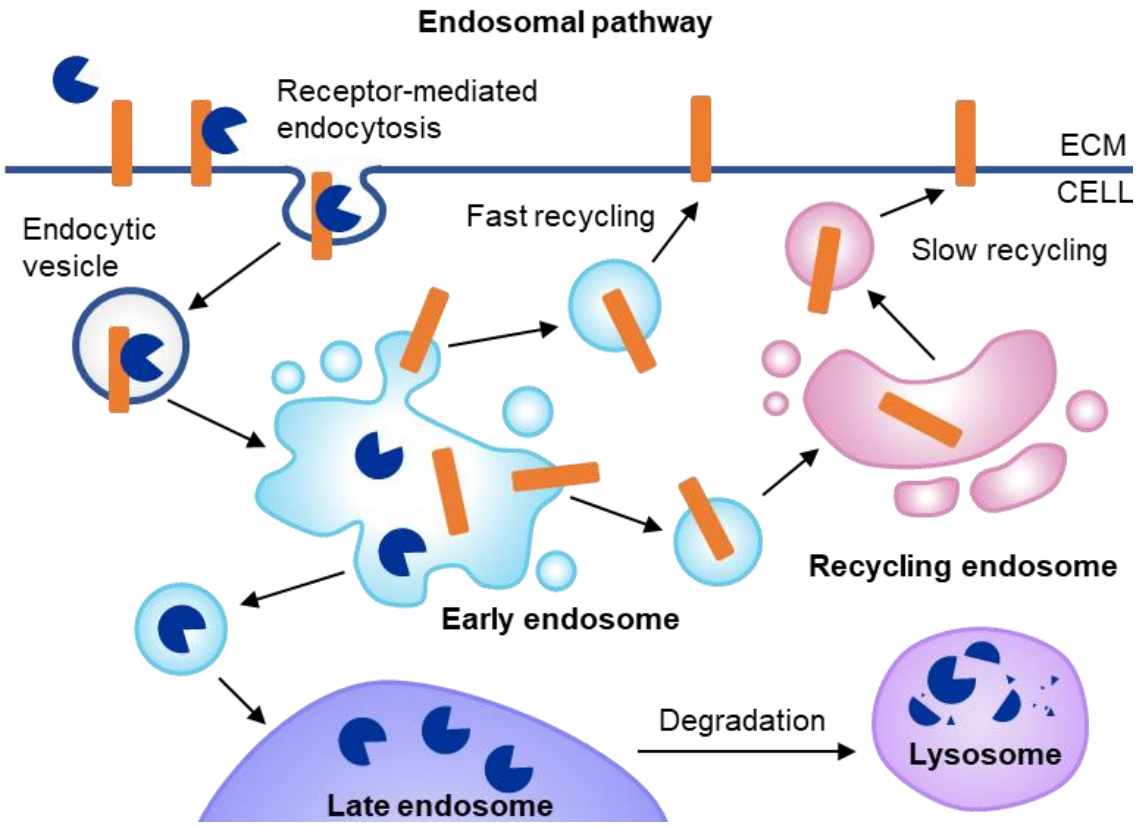

Figure 1.7 Trafficking through the endosomal pathway. Receptor-mediated endocytosis of extracellular proteins results in internalisation of these proteins in endocytic vesicles. The endocytic cargo is then sorted at the early endosome. Proteins destined for degradation are trafficked to the late endosome and then the lysosome. Other proteins are returned to the cell membrane directly from the early endosome (the "fast" recycling pathway) or via the recycling endosome (the "slow" recycling pathway). Adapted from Grant and Donaldson, 2011.

at the base of the cilium in primary mouse chondrocytes[195] and human synoviocytes[201]. Recycling endosomes, which return cargo to the plasma membrane via the "slow" recycling pathway, have also been shown to be concentrated in the pericentriolar region, and even interact with components of the appendages of the mother centriole[202]. Furthermore, Nandadasa et al. (2019), detected recycling endosomes containing a protein, ADAMTS-9, at the base of the cilium, where ADAMTS-9 was subsequently showed to be involved in the docking of ciliary vesicles during ciliogenesis[203]. The appearance of these vesicles was abolished upon knockdown of LRP-1 or LRP-2, leading the authors to propose that LRP-1 and LRP-2 are somehow involved in ADAMTS-9 recycling to the cilium.

In summary, there are a number of ways in which the primary cilium and its associated structures, such as the ciliary pocket and centrosome, could regulate the rate of endocytosis. However, the exact molecular mechanisms by which ciliary proteins could interact with the endocytic machinery and the endosomal system to modulate endocytosis, are unknown.

1.4 Thesis aims and objectives

The broad aim of my thesis was to gain further insight into how protease activity is regulated in chondrocytes. The rationale for investigating the regulation of protease activity was that cartilage matrix proteolysis is one of the main features of the development of osteoarthritis, which is one of the leading causes of global disability[1], but there are currently no disease-modifying drugs to treat osteoarthritis. Further characterisation of mechanisms that regulate protease activity could help to identify new therapeutic targets that restore physiological levels of protease activity in disease.

To address this aim, I focused on investigating how the primary cilium was involved in protease activity regulation. The Wann group has previously seen that mutation of the ciliary protein IFT88 increased protease activity and inhibited LRP-1-mediated protease clearance *in vitro*. Other studies have identified links between the periciliary region and processes that regulate the rate of endocytosis. I thus hypothesised that the primary cilium regulates the extracellular matrix-degrading activity of proteases by facilitating the formation of a periciliary area of efficient LRP-1-mediated protease endocytosis.

During my PhD project, I tried to address this hypothesis. The aims of my project were as follows:

- Aim 1 – further test whether the primary cilium is required for the regulation of protease activity. To do this, I knocked down a small panel of ciliary proteins with siRNAs and measured protease activity
- Aim 2 – test whether increases in protease activity upon knockdown of ciliary proteins were associated with disruption of endocytosis-independent mechanisms of protease activity regulation
- Aim 3 – test whether increases in protease activity upon knockdown of ciliary proteins were associated with disruption of endocytosis-dependent mechanisms of protease activity regulation

CHAPTER 2

Materials and methods

2.1 Cell culture

2.1.1 Materials

The following materials were used for cell culture experiments: Low glucose Dulbecco's Modified Eagle's Medium (Sigma-Aldrich, T3924), Trypsin-EDTA solution (Sigma-Aldrich, T3924), Recombinant Mouse IFN-gamma Protein (R&D Systems, 485-MI-100), Dulbecco's Phosphate Buffered Saline (Sigma-Aldrich, D8537), Fetal Bovine Serum (Sigma-Aldrich, F7524), L-glutamine (Sigma-Aldrich, G7513), Penicillin-Streptomycin (Sigma-Aldrich, P4333), Trypan blue solution (Sigma-Aldrich, T8154), Actinomycin D from Streptomyces sp. (Sigma-Aldrich, A9415), CT1746 (CellTech Therapeutics), Cyclopamine (Enzo Life Sciences, BML-GR334-0001), Dynasore (Sigma-Aldrich, 324410), and Dimethyl sulfoxide (DMSO) (Sigma-Aldrich, D2650).

2.1.2 Cell lines

Two cell lines were used in this thesis: a WT mouse chondrocyte cell line, and an ORPK mouse chondrocyte cell line containing a hypomorphic mutation affecting the protein IFT88[167]. Both lines were generated from chondrocytes isolated from WT or ORPK mice bred with Immortomouse mice as previously described[179]. These mice expressed mutant, interferon-γ-inducible, temperature-sensitive SV40 large T antigen (TAg), which inhibits tumour suppressor proteins such as p53 and thus promotes cell proliferation[204]. To maintain immortalisation during passage, cells were cultured in "immortalisation" media containing interferon-γ (low-glucose Dulbecco's Modified Eagle's Medium (DMEM) with 2.5 mM L-glutamine, 88 UN/ml penicillin, 88 µg/ml streptomycin, 10% volume/volume (v/v) FBS and 10 ng/ml recombinant mouse interferon-γ) at the permissible temperature for SV40 TAg expression (33 °C). Cells were grown in a humidified incubator with 5% carbon dioxide and passaged every three or four days. The passage numbers of the cultured cell lines were between 30 and 50.

The chondrocytes used to generate the cell lines used in this thesis were sternal chondrocytes isolated from 4-day-old mice by digestion with collagenase type II (2 mg/ml) for 4 hours at 37

°C[179], and were thus likely a mixture of articular and growth plate chondrocytes. Previous work by the Wann group showed that the cell lines expressed aggrecan and type II collagen at RNA level and sGAG at protein level but not type X collagen, so were likely not derived from hypertrophic chondrocytes. To obtain a phenotype closer to that of primary chondrocytes, which exhibit low levels of proliferation *in situ*, cells were moved to culture conditions that were non-permissible for immortalisation during the experimental time course. Specifically, experiments were conducted in "experimental" media that did not contain interferon-γ (low-glucose DMEM with 2.5 mM L-glutamine, 88 UN/ml penicillin, 88 µg/ml streptomycin and 10% v/v FBS), and at 37 °C.

For experiments, WT or ORPK cells grown in 75 cm^2 vented cell culture flasks were trypsinised and centrifuged at 601 x g and 20 °C for 3 minutes. The resulting cell pellet was resuspended in experimental media. To determine the number of viable cells, the Trypan Blue dye exclusion assay was used, which enables discrimination between live cells with intact cell membranes that prevent uptake of dyes such as Trypan blue, and dead cells with compromised membranes[205]. 5 µl of the cell suspension was mixed with equal volumes of Trypan Blue and loaded onto a haemocytometer. Trypan Blue-excluding cells were counted using a brightfield microscope with 10x objective to give an estimate of the number of live cells per ml of cell suspension. The cell suspension was diluted with experimental media as required to achieve a seeding density of 20,000 cells/cm^2 in plastic cell culture 12-well plates.

After cells were grown to full confluence at 37 °C for 64 hours, cells were washed in PBS then serum-free experimental media (low-glucose DMEM with 2.5 mM L-glutamine, 88 UN/ml penicillin and 88 µg/ml streptomycin), before a further 1-hour period of serum-starvation in serum-free experimental media. Most experiments were then conducted over a 24-hour time course in serum-free experimental media. Serum starvation was used to reduce non-specific signal due to bovine serum albumin (BSA) during western blotting of conditioned media

samples, but also to promote ciliation by inducing cell cycle arrest. Similarly, conducting experiments when cells were at full confluence induced cell cycle arrest due to contact inhibition. At the end of the experimental time course, conditioned media was collected, as well as lysates for RNA or protein expression analysis, as described below in Sections 2.3 and 2.4.

2.1.3 Inhibitors used in cell culture experiments

The following molecules were also used to disrupt various cellular processes in cell culture experiments (Table 2.1). All molecules were added to serum-free media at the indicated experimental concentrations at the start of the experimental time course.

Inhibitor concentration was selected based on the results of previous studies and previous work in the lab. 1 µg/ml actinomycin D was used because this concentration has been shown to inhibit the transcription of most RNA species, including mRNA, *in vitro*[206]. 10 µM CT1746 was used as an inhibitor of aggrecan degradation because this concentration has previously been shown to inhibit the activity of the major aggrecanase ADAMTS-5 (1 nM) by my co-supervisor Dr Linda Troeberg (University of East Anglia). 10 µM cyclopamine was used because Thompson et al. (2015) found that this concentration effectively inhibited expression of the Hh pathway target genes *PTCH1* and *GLI1* in isolated bovine chondrocytes[192]. 80 µM dynasore was used because this concentration almost completely inhibited ADAMTS-5 endocytosis in primary porcine chondrocytes in a previous study[117]. As a vehicle-only control, cells were treated with the same volume of DMSO as was used to dissolve each inhibitor.

Table 2.1 Pharmacological inhibitors used in cell culture experiments

Molecule	Mechanism of action	Reconstitution solvent	Concentration
Actinomycin D	Intercalates in DNA, inhibiting transcription[206]	DMSO (5 mg/ml stock)	1 µg/ml
CT1746	Inhibits matrix metallo-proteases[207]	DMSO (100 mM stock)	10 µM
Cyclopamine	Smoothened antagonist that inhibits Hh pathway signalling[208]	DMSO (4 mg/ml stock)	10 µM
Dynasore	Inhibits the GTPase dynamin required for endocytosis [117,209,210]	DMSO (16 mg/mL stock)	80 µM

2.2 siRNA-mediated gene knockdown

2.2.1 Materials

The following reagents were used for experiments in this section: 5x siRNA Buffer (Horizon Discovery, B-002000-UB-100), Lipofectamine™ RNAiMAX Transfection Reagent (Invitrogen, 13778075) and Opti-MEM Reduced serum media (Gibco, 31985062), ON-TARGETplus Non-targeting Control Pool (Dharmacon, D-001810-10-05), and ON-TARGETplus SMARTpool siRNA targeting mouse *Adamts4* (L-055337-01-0005), *Adamts5* (L-048495-01-0005), *Ap2a1* (L-043307-01-0005), *Cltc* (L-063954-00-0005), *Ift88* (L-050417-00-0005), *Kif3a* (L-042111-01-0005), *Lrp1* (L-040764-00-0005), *Nphp4* (L-055006-01-0005), and *Ttbk2* (L-047640-00-0005).

2.2.2 siRNA knockdown protocol

Knockdown of target genes was achieved using siRNAs. siRNAs are nucleic acids that are complementary to a sequence within target mRNA. siRNAs are incorporated into an endogenous complex of proteins called the RNA-induced silencing complex (RISC) that mediates degradation of the target mRNA, and thus reduces gene expression[211]. Dharmacon ON-TARGETplus SMARTpool siRNAs were used, which contain siRNAs recognising four different sequences in the targeted mRNA.

Cells were transfected with siRNAs 16 hours after seeding in cell culture plates, when confluence was at 50-60%. siRNAs were reconstituted in 5x siRNA buffer diluted in RNase-free water and used at a concentration of 10 nM. This concentration was chosen because treatment of cells with 10 nM siRNA resulted in a similar knockdown efficiency to when higher, potentially more cytotoxic concentrations of 25 and 50 nM were used (Appendix figure 7A). Lipofectamine RNAiMAX Transfection Reagent was used to introduce siRNAs into cells. For each well of cells, 4.5 µl lipofectamine was mixed with 1.5 µl siRNA and 300 µl optiMEM, then incubated at 37 °C for 5 minutes. The siRNA-containing solution was then added to the experimental media in

which cells were seeded, to give a total volume of 900 µl per well of a 12-well cell culture plate. The experimental time course was then started 48 hours after transfection.

2.3 Analysis of RNA expression

2.3.1 Materials

The sources of materials used in this section were as follows: Qiagen RNeasy Mini kit (Qiagen, 74104), RNase Inhibitor (Applied Biosystems, N8080119), Ethanol (Fischer, E/066SDP/17), High-Capacity cDNA Reverse Transcription Kit (Applied Biosystems, 4368814), TaqMan Gene Expression Assay probes (Thermo Fisher, 4331182), White PCR plate, 384 well, skirted (Grenier, 785235), AMPLIseal™ plate sealer, transparent (Grenier, 676040), and TaqMan™ Fast Universal PCR Master Mix (2X), no AmpErase™ UNG (Applied Biosystems, 4352042).

2.3.2 Isolation of RNA from chondrocyte cell lines

The Qiagen RNeasy Mini kit was used to isolate RNA from cell lysates. After collection of conditioned media, cells were placed on ice and washed with PBS. Cells were lysed with 350 µl RLT buffer and a cell scraper, homogenised with a 1 ml syringe and 21-gauge needle, and mixed with an equal volume of 70% ethanol to facilitate the binding of total RNA to a membrane within RNeasy Mini spin columns. Biological and chemical contaminants were then removed by passing 700 µl RW1 buffer and two lots of 500 µl RPE buffer through the columns by centrifugation at 11,655 x g for 30 seconds. RNA was then eluted into RNase-free water. RNA yield and purity were checked using a Nanodrop spectrophotometer, with purity assessed by comparing the ratios of absorbance at 260 nm and 280 nm (260/280), and 260 nm and 230 nm (260/230), with the expected values of 2.0 and 2.0-2.2 respectively.

2.3.3 cDNA synthesis

cDNA was synthesised using the Applied Biosystems High-Capacity cDNA Reverse Transcription Kit. RNA was diluted with RNase-free water to a concentration of 37.87 ng/µl. 13.2 µl diluted RNA (500 ng RNA) was mixed with 0.8 µl 2'-deoxynucloside 5'-triphosphates (dNTPs), 2 µl reverse transcription buffer, 2 µl random primers, 1 µl RNase inhibitor and 1 µl reverse transcriptase, giving a total reaction volume of 20 µl. Synthesis and subsequent amplification of cDNA was performed using a thermocycler at 25 °C for 10 minutes, 37 °C for 120 minutes and 85 °C for 5 minutes. cDNA samples were then transferred to ice and cDNA yield was measured using the Nanodrop spectrophotometer, with purity measured by comparison with the expected 260/280 ratio of 1.8.

2.3.4 Quantitative polymerase chain reaction

Quantitative PCR (qPCR) with TaqMan probes was used for measuring gene expression. This method involves amplifying cDNA by PCR in the presence of fluorescent dye-labelled probes that bind to a sequence within the target gene[212]. As cDNA containing this target sequence is amplified by Taq DNA polymerase, the target sequence-bound probe is cleaved by the 5'→3' exonuclease activity of the polymerase, resulting in release of the fluorescent reporter dye FAM at the 5' end of the probe from a 3' non-fluorescent quencher molecule and thus an increase in FAM fluorescence. During the exponential phase of cDNA amplification, fluorescence intensity increases proportionally with levels of cDNA containing the target sequence. Comparison of the number of amplification cycles required to reach a fixed threshold of fluorescence (known as the cycle threshold or C_T) is used to give an indication of relative target gene expression. To control for any differences in starting levels of cDNA or amplification efficiency between samples, a probe detecting a reference gene sequence that is expressed equally in all conditions was used to normalise target expression levels. The probes used in this project are listed in Table 2.2 below with *18s* used as the reference gene (supplier ID Mm02601776_g1).

Table 2.2 Table of TaqMan probes used to measure gene expression

Target gene	Protein	Species	Supplier ID
Adamts1	ADAMTS-1	Mouse	Mm01176187_m1
Adamts4	ADAMTS-4	Mouse	Mm00556068_m1
Adamts5	ADAMTS-5	Mouse	Mm00478620_m1
Ap2a1	Adaptor-related protein complex 2, alpha 1 subunit	Mouse	Mm00475919_m1
Cltc	Clathrin, heavy polypeptide	Mouse	Mm01303974_m1
Gli1	Gli1	Mouse	Mm00494654_m1
Gli2	Gli2	Mouse	Mm01293116_m1
Ift88	IFT88	Mouse	Mm00493664_m1
Kif3a	KIF3A	Mouse	Mm01288585_m1
Lrp1	LRP-1	Mouse	Mm00464608_m1
Mmp13	MMP-13	Mouse	Mm00439491_m1
Nphp4	NPHP4	Mouse	Mm00463212_m1
Ptch1	PTCH1	Mouse	Mm00436026_m1
Ttbk2	TTBK2	Mouse	Mm00453709_m1

Experiments were conducted in a 384-well PCR plate. In each well, 1 µl cDNA (1.0-1.5 µg) was mixed with 5 µl 2x TaqMan Fast Universal PCR Master Mix, 3.5 µl RNase-free water and 0.5 µl TaqMan probe. Technical triplicates were run for each sample. No-template controls, in which cDNA was replaced with RNase-free water, were used to check for non-specific probe binding. Filled plates were sealed with an AMPLIseal plate sealer and centrifuged at 179 x g for 1 minute, before loading into the Applied Biosystems Viia7 Real-Time PCR System. Comparative C_T experiments were then set up using the Quant Studio Real-Time PCR software (version 1.3), and the PCR reaction was run according to the following method: hold stage of 50 °C for 2 minutes and 95 °C for 10 minutes, then PCR stage of 95 °C for 15 seconds and 60 °C for 1 minute, repeated for 40 cycles.

C_T data was exported to Microsoft Excel and used to calculate relative gene expression levels using the delta C_T ($\Delta\Delta C_T$) method developed by Livak and Schmittgen[213]. The following calculations were then performed to:

1. Normalise target gene expression to reference gene (*18s*) expression in each sample

$$\Delta C_T = C_{T,target} - C_{T,ref}$$

2. Calculate fold change in target expression, normalised to reference gene expression, relative to mean normalised expression in control samples (non-targeting siRNA-treated cells in RNAi experiments, or WT cells for all other experiments)

$$\Delta\Delta C_T = \left(\left(C_{T,target} - C_{T,ref}\right)_{sample} - \left(MeanC_{T,target} - MeanC_{T,ref}\right)_{control}\right)$$

3. Exponentially transform logarithmic C_T data

$$Fold\ change\ in\ normalised\ target\ gene\ expression\ relative\ to\ control = 2^{-\Delta\Delta C_T}$$

Relative target gene expression data was then plotted using GraphPad Prism (version 9). As described in Livak and Schmittgen's original study, use of the $\Delta\Delta C_T$ method for quantifying gene expression was validated by calculating ΔC_T from C_T values for *18s* (reference gene) and *Ift88* (used as an example target gene) when different volumes of WT cDNA were used (Figure 2.1A). Mean ΔC_T did not change across the different cDNA dilutions tested, indicating that the amplification efficiency of both reference and target gene probes was approximately equal, which is required for the $\Delta\Delta C_T$ method to be valid[213]. *18s* was chosen as the reference gene because *18s* expression was stable across the experimental conditions used in this thesis, as indicated by the similar *18s* C_T values across conditions (Figure 2.1B, p>0.05 for all comparisons).

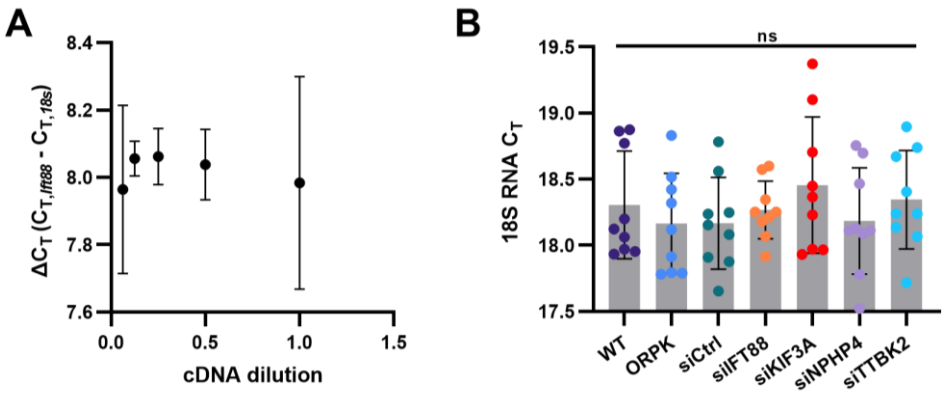

Figure 2.1 Amplification of *Ift88* and *18s* TaqMan probes was equal over a range of cDNA dilutions. ***A***) WT cells were incubated in serum-free media for 24 hours. Expression of *Ift88* was measured by qPCR, then normalised to *18s* expression. Mean ± SD, one experiment conducted in triplicate using one cell subculture (n=3). ***B***) Raw cycle threshold (C_T) values for the *18s* reference gene across the experimental conditions used in this thesis (WT, ORPK or siRNA-treated cells). Mean ± SD, three independent experiments conducted in triplicate using separate cell subcultures (n=9). ns p>0.05, one-way ANOVA with Tukey's multiple comparisons test.

2.4 Analysis of protein expression

2.4.1 Materials

The sources of materials used in this section were as follows: cOmplete™, Mini Protease Inhibitor Cocktail (Roche, 11836153001), Pierce BCA Protein Assay (Thermo Fisher, 23227), Sodium chloride (Sigma-Aldrich, 55886), Nonidet™ P40 Substitute (NP-40) (Sigma-Aldrich, 74385), Trizma® base (Sigma-Aldrich, T1503), Trichloroacetic acid (Sigma-Aldrich, T0699), Acetone >=99% (Sigma-Aldrich, 24201), 2-mercaptoethanol (MP Biomedicals, 194705), Laemmli Sample Buffer 4X (Bio-Rad, 1610747), Chameleon Duo Pre-Stained Protein Ladder (LI-COR, 928-6000), NuPAGE™ MOPS SDS Running Buffer 20X (Invitrogen, NP0001), NuPAGE™ 4-12% Bis-Tris Protein Gels, 1.5 mm, 15-well (Invitrogen, NP0336), Mini Gel Tank (Life Technologies, A25977), Immun-Blot PVDF Membrane (Bio-Rad, 1620177), PerfectBlue™ Tank Electro Blotter (VWR, PEQL52-WEB-10), Glycine (Sigma-Aldrich, G7126), Methanol (Fisher Scientific, M/4000/PC17), Revert™ 700 Total Protein Stain for Western Blot Normalization (LI-COR, 926-11011), Glacial acetic acid (VWR, 20104.298), Sodium hydroxide (Sigma-Aldrich, S8045), Trizma® hydrochloride (Sigma-Aldrich, T3252), IRDye® 680RD Goat anti-Mouse IgG Secondary Antibody (LI-COR, 925-68070), IRDye 800CW Donkey anti-Rabbit IgG Secondary Antibody (LI-COR, 926-32213), Polyclonal Swine Anti-Rabbit Immunoglobulins/HRP (Dako, P0217), Novex® Sharp Pre-stained Protein Standard (Invitrogen, LC5800), Tween 20 (Sigma-Aldrich, P1379), Clarity™ Western ECL substrate (Bio-Rad, 170-5061), NuPAGE™ 3-8% Tris-Acetate Protein Gels, 1.5 mm, 10-well (Invitrogen, EA0378), NuPAGE™ Tris-Acetate SDS Running Buffer 20X (Invitrogen, LA0041), and HiMark™ Pre-stained Protein Standard (Invitrogen, LC5699).

2.4.2 Cell lysis

To analyse the expression of intracellular or cell surface proteins, cells were lysed at the end of the experimental time course. Collection of the non-nuclear, cytoplasmic cell fraction was performed with NP-40 lysis buffer (150 mM sodium chloride, 1.0% NP-40, 50 mM Tris in

deionised water, pH 8.0) in the presence of the cOmplete Mini Protease Inhibitor Cocktail (one tablet per 10 ml) and 50 µM sodium orthovanadate to preserve phosphate groups on proteins. Cells were incubated in NP-40 buffer for 5 minutes on ice and lifted from the culture surface using a cell lifter, followed by a further 5 minutes of incubation. Cell lysates were homogenised with a 1 ml syringe and 21-gauge needle and centrifuged at 9632 x g for 10 minutes at 4 °C. The supernatant was collected and analysed with the BCA assay to measure total protein, or frozen at -20 °C.

2.4.3 Measurement of total protein concentration with the BCA assay

The total protein concentration of cell lysates was determined using the bicinchoninic acid (BCA) assay. This assay involves measuring a colour change produced by the generation of reduced copper ions by proteins and subsequent interaction with BCA[214]. 10 µl of sample was added to a 96-well cell culture plate and incubated with 200 µl BCA reagents from the Pierce BCA Protein Assay kit for 30 minutes. Serially diluted BSA in lysis buffer (concentration range 31.25-2000 µg/ml) was used as protein standards of known concentration, with lysis buffer used as a blank sample. Absorbance was measured at 562 nm using a FLUOstar Omega plate reader. Total protein concentration was calculated from a standard curve of absorbance of BSA protein standards. Lysates were then diluted as required with ultrapure water to standardise protein concentration across samples.

2.4.4 Precipitation of conditioned media

To obtain sufficient levels of extracellular proteins such as TIMP-3 and LRP-1α for detection by western blot, conditioned media samples were precipitated using trichloroacetic (TCA) acid. TCA acid was added to conditioned media at a final concentration of 5% v/v and incubated at room temperature (20 °C) for 45 minutes. Samples were centrifuged at 11,655 x g for 15 minutes at 4 °C, and the supernatant discarded. The resulting protein pellet was washed with ice-cold acetone for 10 minutes at -20 °C and spun again for 15 minutes before the acetone was removed

and pellets left for 1 hour to facilitate evaporation of any remaining acetone. Proteins were denatured as below.

2.4.5 Western blotting

Sodium dodecyl sulfate-polyacrylamide gel electrophoresis (SDS-PAGE): Denaturation of lysates or conditioned media for western blotting under reducing conditions was performed with 2.5% beta-mercaptoethanol in 4x Laemmli buffer (277.8 mM Tris-hydrochloride, 44.4% v/v glycerol, 4.4% lithium dodecyl sulfate, 0.02% bromophenol blue, pH 6.8). Samples were then boiled for 5 minutes at 100 °C and loaded onto 4-12% Bis-Tris NuPAGE gels. The Chameleon Duo Pre-stained Protein Ladder was also loaded to estimate the molecular weight of proteins in samples. Gel electrophoresis was run for 1 hour 15 minutes at 150 V in 1x MOPS buffer in a gel tank.

Transfer of proteins to membranes: Separated proteins were then transferred to a polyvinylidene fluoride (PVDF) membrane using a wet transfer system (Peqlab PerfectBlue Tank Electro Blotter) run at 100 V for 1 hour 30 minutes in 1x transfer buffer (10x transfer buffer (1.9 M glycine, 0.2 M Tris base diluted with deionised water), 20% v/v methanol in deionised water).

Total protein stain: For analysis of proteins in conditioned media, a total protein stain was used as a loading control. Directly after transfer, membranes were incubated in 5 ml LI-COR Revert total protein stain for 5 minutes. After washing in Revert wash solution (6.7% v/v glacial acetic acid, 30% methanol in deionised water), membranes were imaged using the LI-COR Odyssey CLX system, and images quantified as below. Membranes were destained using the Revert destaining solution (0.1 M sodium hydroxide, 30% methanol in deionised water) and rinsed in deionised water. Membranes were then incubated in 5% milk made up in 1x Tris-buffered saline (TBS) (10x TBS (0.1 M Tris-hydrochloride (Tris-HCl), 46 mM Tris base, 1.5 M sodium chloride) diluted with deionised water, pH 7.6) containing 0.1% Tween-20 (TBST) for 1 hour on a shaker (75 revolutions per minute (RPM)) to reduce non-specific binding of primary antibodies to the membrane. Protein remaining in gels was visualised by staining with Coomassie dye (0.5%

weight/volume (w/v) Coomassie Brilliant Blue dye (R-250), 40% v/v methanol, 10% v/v acetic acid, 50% deionised water).

Incubation of membranes with primary and secondary antibodies: Membranes were incubated overnight at 4 °C in primary antibodies diluted with 5% milk. The antibodies and dilutions used for western blotting are presented in . Membranes were then washed in TBST for 10 minutes three times, before incubation with secondary antibodies at room temperature, as described below.

Detection: Two different detection systems were used for visualisation of immunospecific bands on western blot membranes.

1) Near-infrared (NIR) fluorescence detection – Membranes were incubated with secondary antibodies conjugated to near-infrared fluorescent dyes with different emission spectra, enabling visualisation of two different proteins on the same membrane. The secondary antibodies used here were IRDye 800CW Donkey anti-Rabbit and IRDye 680RD Goat anti-Mouse antibodies, which were made up in 5% milk at a dilution of 1:5000 and incubated with membranes for 1 hour. After three washes in TBST, blots were rinsed in TBS, dried at room temperature for 40 minutes and imaged using the LI-COR Odyssey CLX imaging system. Acquisition parameters were set at 160 µm resolution, medium quality, and auto exposure for all blots.
2) Electrochemiluminescence (ECL) detection – Membranes were incubated with anti-swine secondary antibodies conjugated to horseradish peroxidase (HRP) enzyme for 2 hours, followed by three further 10-minute washes in TBST. Membranes were rinsed in TBS, incubated for 5 minutes in 1 ml Pierce ECL Plus western blotting substrate and the chemiluminescent signal produced was captured using the Syngene G:Box Chemi-XX6 system and GeneSys software (version 1.8). Blots were exposed for 10 seconds, 30 seconds, 1 minute and 2 minutes, and the resulting images were merged to produce a final image.

Table 2.3 Antibodies used for western blotting

Antibody target	Supplier	Host species	Clonality	Dilution
ADAMTS-5	Abcam (ab41037)	Rabbit	Polyclonal	1:250
ADAMTS-5 (catalytic domain)	Gendron et al., 2007[55]	Rabbit	Polyclonal	1:1000
Aggrecan neoepitope AGEG	Troeberg et al., 2008[104]	Rabbit	Monoclonal	1:5000
Beta-actin	Novus Biologicals (8H10D10)	Mouse	Monoclonal	1:5000
FLAG [clone M2]	Sigma-Aldrich (F1084)	Mouse	Polyclonal	1:500
IFT88	Proteintech (13967-1-AP)	Rabbit	Polyclonal	1:1000
KIF3A	Abcam (ab11259)	Rabbit	Polyclonal	1:1000
LRP-1α	Sigma-Aldrich (L2295)	Rabbit	Polyclonal	1:1000
LRP-1β [clone EPR3724]	Abcam (ab92544)	Rabbit	Monoclonal	1:1000
NPHP4	Proteintech (13812-1-AP)	Rabbit	Polyclonal	1:1000
TIMP-3	Sigma-Aldrich (AB6000)	Rabbit	Polyclonal	1:1000
TTBK2	Atlas (HPA018113)	Rabbit	Polyclonal	1:500
Secondary antibodies				
IRDye 800CW Donkey anti-Rabbit IgG Secondary Antibody	LI-COR (926-32213)	Donkey	Polyclonal	1:5000
IRDye 680RD Goat anti-Mouse IgG Secondary Antibody	LI-COR (926-68070)	Goat	Polyclonal	1:5000

Quantification of blots: When fluorescence detection was used, quantification was performed in Image Studio Lite (version 5.2). Regions of interest containing immunoreactive bands were first defined using the "Draw Rectangle" function. Background-corrected signal was calculated by subtracting the product of average pixel intensity of the background (defined as the 3-pixel-wide area around the region of interest) and the total number of pixels in the region of interest, from the sum of pixel intensities within the region of interest. Signal values were exported to Microsoft Excel and normalised to signal of the loading control. Data was then plotted using GraphPad Prism.

β-actin was chosen as a loading control for cell lysates based on previous work by the Wann group that showed that β-actin protein expression was more stable than β-tubulin across

experimental conditions in which the primary cilium was disrupted. Another loading control, glyceraldehyde 3-phosphate dehydrogenase (GAPDH), was not used due to previously reported links between primary cilia assembly and glycolysis[215]. The Revert total protein stain was used as a loading control for conditioned media.

For ECL western blots, Fiji (version 2.0) software was used for quantification. Lanes of the blot containing immunoreactive bands were defined using the "Rectangular Selections" tool. Profile plots of density within each lane were generated, and the peaks in density corresponding to immunoreactive bands were measured and used to indicate signal intensity. Normalisation to loading controls was performed as above.

Non-reducing conditions: These conditions were used for detection of LRP-1α, as the antibody recognising this protein works optimally under non-reducing conditions. During sample preparation, protein pellets were resuspended in sample buffer without beta-mercaptoethanol and were not boiled. Samples were loaded into 3-8% Tris-acetate gels and run in Tris-acetate buffer. All other parts of the western blot method were kept the same as reducing condition blots.

2.5 Measurement of protease activity

2.5.1 Materials

The sources of materials used in this section were as follows: Aggrecan from bovine articular cartilage (Sigma-Aldrich, A1960), Ethylenediaminetetraacetic acid (EDTA) (Sigma, Aldrich, E6758), Sodium acetate (Sigma-Aldrich, S7545), Chondroitinase ABC from Proteus vulgaris (Sigma-Aldrich, C3667-10UN, Endo-β-galactosidase from Bacteroides fragilis (Sigma-Aldrich, G6920), AGEG (gift from Professor Hideaki Nagase, University of Oxford), Recombinant Human IL-1β (PeproTech, 200-01B), Recombinant Human IL-1α (PeproTech, 200-01A), Guanidine

hydrochloride (Sigma-Aldrich, G4505), Caesium chloride (BDH, 443795Y), 1,9-Dimethylmethylene Blue dye (SERVA 20333), Sodium formate (Sigma-Aldrich, 247596), Chondroitin sulfate sodium salt from shark cartilage (Sigma-Aldrich, C4384), and biopsy punch, 6.0 mm diameter (Stiefel, 05-SF002.07/97).

2.5.2 Aggrecan overlay assay

The aggrecan overlay assay was used to measure protease activity in cell lines, as described in Ismail et al. (2015)[60]. Cells were seeded in monolayer as in Section 2.1.2. At the start of the experimental time course, 50 µg/ml purified bovine aggrecan in serum-free experimental media was added to cells. In some experiments, IL-1β or IL-1β at 10 or 50 ng/ml was added at the same time. 24 hours later, conditioned media was collected and deglycosylated to facilitate movement of the aggrecan core protein through the gel during western blotting. Specifically, 150 µl conditioned media was incubated for 16 hours overnight at 37 °C on a shaker (75 RPM) with 0.001 UN/µg chondroitin sulfate-degrading chondroitinase ABC and keratan sulfate-degrading endo-β-galactosidase in deglycosylation buffer (200 mM Tris base, 100 mM EDTA and 200 mM sodium acetate in deionised water, pH 7.5). Samples were concentrated by acetone precipitation, in which 1 ml ice-cold acetone was added and samples incubated at -20 °C for 1 hour and 30 minutes, followed by centrifugation at 11,655 x g for 30 minutes at 4 °C. The resulting protein pellet was then air dried and denatured as in Section 2.4.5. Western blot analysis of denatured samples was conducted under reducing conditions using a rabbit polyclonal antibody recognising the N-terminal AGEG neoepitope on aggrecan fragments produced by proteolytic cleavage at the aggrecan Glu^{1771}-Ala^{1772} bond[104] in the CS2 domain. This neoepitope was chosen over the ARGS neoepitope, which is indicative of cleavage that results in loss of almost the entire aggrecan molecule, and therefore may be more pathologically relevant than the CS2 domain cleavage that is indicated by AGEG generation. This was because of differences in the amino acid sequence of mouse and bovine aggrecan, which meant that

proteases secreted from mouse chondrocytes in my experimental system may not have recognised the interglobular domain cleavage site of bovine aggrecan.

2.5.3 Bovine aggrecan purification

Guanidine hydrochloride-mediated extraction of proteoglycans from bovine cartilage was used to provide aggrecan for the aggrecan overlay assay. Articular cartilage from the proximal surface of the bovine metacarpophalangeal joint of 18-24 month old animals was dissected, as described in Thompson et al. (2014)[216], and frozen at -20°C at Queen Mary, University of London. The resulting 1 cm^2 pieces of dissected cartilage were then thawed at the Kennedy Institute and mixed with 6 M guanidine hydrochloride made up in deionised water at 7.5-times the volume of cartilage, at 4 °C for 72 hours. The cOmplete, Mini protease inhibitor cocktail (1 tablet used per 10 mL extraction solution) were also added to the mixture to reduce degradation of extracted proteoglycans by serine, cysteine or metalloproteinases.

After 72 hours, larger pieces of proteoglycan-extracted dissected cartilage were removed with a metal spatula, and small debris was removed by centrifuging the extraction solution at 17,237 x g for 10 minutes at 4 °C and then collecting the supernatant. Aggrecan was then separated out from other proteoglycans by density gradient centrifugation. Caesium chloride was added to the solution to give a final density of 1.5 g/ml. Samples were then spun at 99,284 x g in an ultracentrifuge for 48 hours at 4 °C and split into six fractions. The fractions containing aggrecan were identified using the DMMB assay (see Section 2.5.5 below for protocol) and pooled. Caesium chloride was added as before to give a final density of 1.5 g/ml and spun in an ultracentrifuge using the same settings. Aggrecan-containing fractions were again pooled, dialysed three times in 2 l ultrapure water for 24 hours, freeze-dried and weighed before being used in the overlay assay. Generation of the AGEG aggrecan neoepitope was the same when cells were incubated with either aggrecan purified in the lab or commercially purified aggrecan

(Figure 2.2). AGEG signal was also the same when ECL or NIR fluorescence detection methods were used for western blotting.

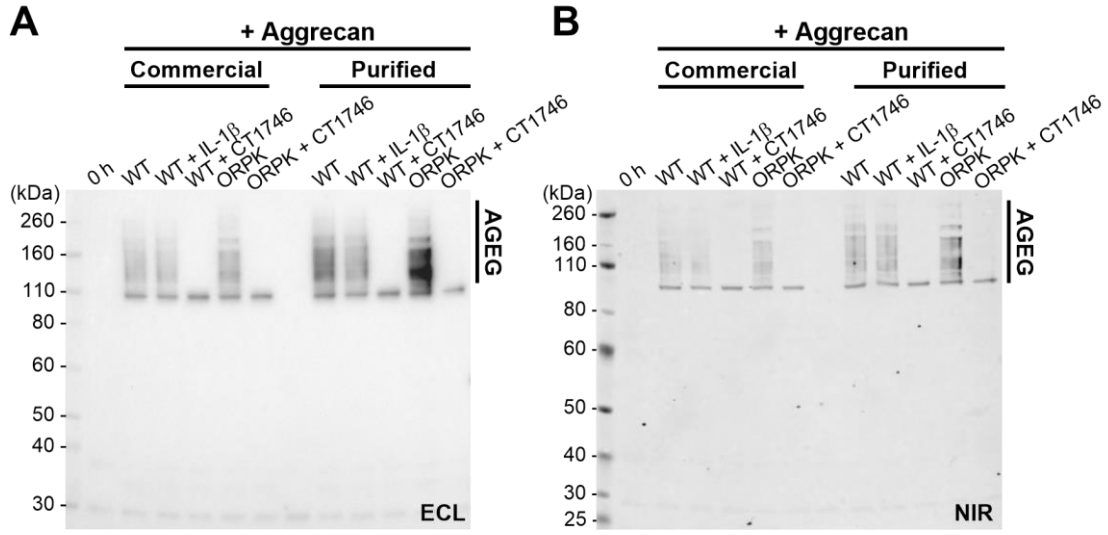

Figure 2.2 AGEG aggrecan neoepitope generation by WT and ORPK mouse chondrocyte cell lines was the same when cells were incubated with commercially sourced or lab-purified aggrecan. ***A***) WT and ORPK cells were incubated with or without 50 µg/ml aggrecan from Sigma-Aldrich (Commercial) or purified in the lab (Purified), 10 ng/ml IL-1β or the metalloprotease inhibitor CT1746, for 24 hours. AGEG neoepitope in conditioned media was detected by western blot, with ECL detection or ***B***) near-infrared fluorescence detection. Blots representative of one experiment conducted in triplicate using one cell subculture (n=3).

2.5.4 Cell-explant co-culture system

As an alternative method of measuring protease activity, porcine articular cartilage explants were used as a matrix substrate for proteases secreted from mouse chondrocyte line cells. The 1,9-dimethylmethylene blue (DMMB) colourimetric assay was used to measure release of negatively charged sulphated sGAG from the explants due to matrix degradation by mouse proteases[217].

Porcine articular cartilage explants were collected from the metacarpophalangeal joint of 3-6-month-old animals using a 6.00 mm biopsy punch under sterile conditions and freeze-thawed once. WT or ORPK cells were seeded in monolayer on Transwell® plates, as in Section 2.1.2. At the start of the experimental time course, porcine explants were placed in permeable

membrane inserts within the plate, enabling proteases secreted from mouse cells to access the porcine cartilage matrix. At each time point, conditioned media was collected and sGAG content analysed using the DMMB assay.

2.5.5 DMMB assay

DMMB dye was reconstituted in ethanol and made up to a concentration of 16 µg/ml (29 nM sodium formate in deionised water, pH 3) as described in Wann et al. (2012)[179]. 40 µl of conditioned media and 250 µl DMMB dye was added to each well of a 96-well cell culture plate. Chondroitin sulfate from shark cartilage in serum-free media (concentration range 1.125-50 µg/ml) was used as a standard, with serum-free media used as a blank sample. Absorbance at 595 nm was measured immediately after adding DMMB dye using a FLUOstar Omega plate reader. sGAG concentration was calculated from a standard curve of absorbance of chondroitin sulfate standards. sGAG release was normalised to the wet weight of explants.

2.6 Measurement of ADAMTS-5 endocytosis

2.6.1 Materials

Materials used in this section were FLAG-tagged ADAMTS-5-3 (gift from Dr Kazuhiro Yamamoto, University of Liverpool), RAP (gift from Dr Linda Troeberg, University of East Anglia), Low protein binding microcentrifuge tubes, 1.5 mL (Thermo-Fisher, 90410) and Transferrin from Human Serum, Alexa Fluor™ 647 Conjugate (Invitrogen, T23366).

2.6.2 ADAMTS-5 uptake assay

To investigate the effect of ciliary protein knockdown on ADAMTS-5 endocytosis, extracellular levels of exogenous, recombinant ADAMTS-5 with a C-terminal FLAG protein tag over a time course were analysed by western blot, as described by Yamamoto et al. (2013 and 2017)[117,193].

A FLAG-tagged ADAMTS-5 domain deletion mutant lacking the second thrombospondin domain and the spacer domain (ADAMTS-5-3)[55] was used, which retained its aggrecanolytic activity and ability to be endocytosed[117]. ADAMTS-5-3 was purified using HEK293 cells expressing a vector encoding human ADAMTS-5-3 by Dr Kazuhiro Yamamoto at the University of Liverpool. ADAMTS-5-3 protein in the conditioned media of HEK293 cells was then concentrated using an anti-FLAG-agarose column, as described in Gendron et al. (2007)[55].

Cells were seeded as in Section 2.1.2. At the start of the experimental time course, cells were incubated with serum-free experimental media containing 10 nM recombinant human ADAMTS-5-3. This concentration was chosen because it produced detectable signal in previous ADAMTS-5 endocytosis assays conducted by the Wann group. Cells were incubated with or without 500 nM human RAP, which was expressed in *Escherichia coli* and purified by Dr Linda Troeberg as described in Yamamoto et al. (2013)[117]. This RAP concentration was chosen as it effectively inhibited ADAMTS-5 endocytosis in the mouse chondrocyte cell line in the Wann group's previous study[193]. 0.2% FBS was added to the media to aid protein precipitation during sample preparation for western blotting, by seeding the protein pellet. For the 0-hour time point, media containing FLAG-tagged ADAMTS-5-3 (FLAG-ADAMTS-5) was added to cells then immediately collected in low protein binding tubes, which were used to reduce loss of signal due to FLAG-ADAMTS-5 sticking to plastic. Media was then collected at 2, 4 or 8 hours and concentrated by TCA precipitation, as described in Section 2.4.4. Samples were denatured and analysed via western blot using an anti-FLAG antibody.

2.6.3 Transferrin uptake assay

To validate the effect of endocytic protein knockdown or inhibition of receptor-mediated endocytosis, uptake of fluorescently tagged transferrin was measured. Cells were seeded on glass coverslips as in Section 2.1.2. At the start of the experimental time course, cells were incubated with 10 ng/ml Alexa-Fluor-647-conjugated transferrin in serum-free media. At 10, 30

or 90 minute time points, cells were washed with an acidic solution (0.1 M glycine and 150 mM sodium chloride in deionised water, pH 3) to remove surface-bound transferrin[218] (Figure 2.3). Cells were then fixed with 4% PFA, stained with anti-acetylated α-tubulin antibodies and imaged by epifluorescence microscopy as below in Section 2.7.2.

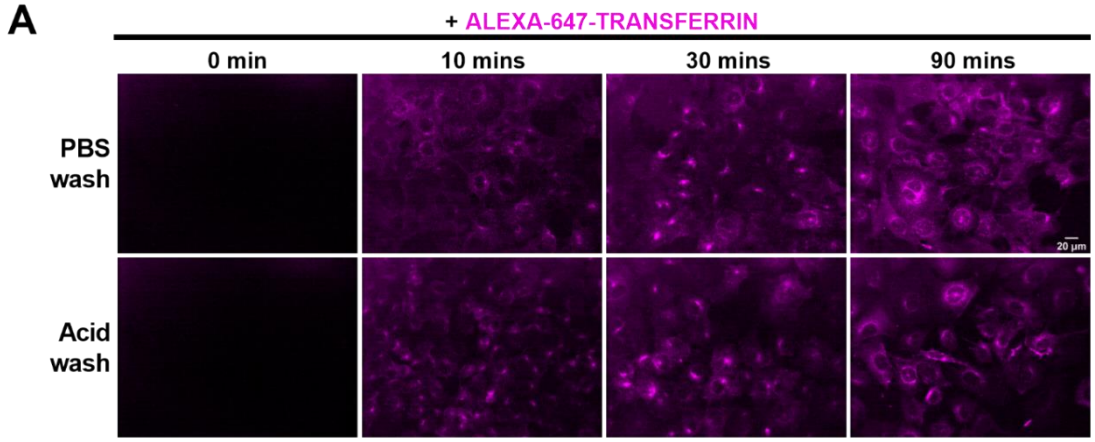

Figure 2.3 Effect of an acid wash to remove surface-bound transferrin. ***A***) WT cells were incubated with 10 ng/ml Alexa-647-conjugated transferrin in serum-free media for 0, 10, 30 or 90 minutes. Cells were washed with PBS or acid wash before fixation, then imaged by epifluorescence microscopy. Images representative of one experiment conducted in triplicate using one cell subculture (n=3). Scale bar 20 µM.

2.7 Microscopy

2.7.1 Materials

Materials used in this section included Glass coverslips, 13 mm, 1.5 thickness (VWR, 631-0150), Paraformaldehyde (PFA) (Sigma-Aldrich, P6148), Triton™ X-100 (Sigma-Aldrich, T8787), Phosphate buffered saline (PBS), low phosphate, 10X (VWR, 437117K), Goat serum (Sigma-Aldrich, G9023), Bovine Serum Albumin (Sigma-Aldrich, A9418), 4',6-Diamidino-2-Phenylindole, Dihydrochloride (DAPI) (Invitrogen, D1306), ProLong™ Gold Antifade Mountant (Invitrogen, P36930), F(ab')2-Goat Anti-Mouse IgG (H+L) Cross-Adsorbed Secondary Antibody, Alexa Fluor™

488 (Invitrogen, A11017), Alexa Fluor™ 555 Goat Anti-Rabbit (H+L) Secondary Antibody (Invitrogen, A21428), Rabbit IgG, polyclonal Isotype Control (Abcam, ab37415), Sucrose (S8501, Sigma-Aldrich), Magnesium chloride (Sigma-Aldrich, 1374248), Piperazine-N,N'-bis(2-ethanesulfonic acid) (PIPES) (P1851, Sigma-Aldrich) and Ethylene glycol-bis(β-aminoethyl ether)-N,N,N',N'-tetraacetic acid (EGTA) (324626, Sigma-Aldrich).

2.7.2 Immunofluorescence staining

Cells were seeded on 13 mm glass coverslips in a 24-well cell culture plate at a density of 20,000 cells/cm^2. At the end of the experimental time course, cells were washed in PBS and fixed with 4% paraformaldehyde (PFA) (4% PFA w/v in 1x PBS, pH 8.9) for 7 minutes at 37 °C, before two further washes in PBS. Cells were permeabilised with 0.5% Triton X-100 in PBS for 5 minutes on a shaker (75 RPM) at room temperature, followed by blocking with 5% goat serum in 0.1% BSA/PBS for 45 minutes to reduce non-specific antibody binding. Cells were then incubated with primary antibody in 0.1% BSA/PBS overnight at 4 °C.

After primary antibody incubation, cells were washed in 0.1% BSA/PBS three times for 5 minutes and incubated with Alexa Fluor anti-mouse and/or anti-rabbit secondary antibodies in PBS (Table 2.4). Cells were washed again in 0.1% BSA/PBS and nuclei were stained with 1 µg/ml 4',6-diamino-2-phenylindole (DAPI) in PBS. Coverslips were rinsed in PBS and mounted on glass slides with ProLong Gold antifade mountant.

To check for non-specific staining introduced by secondary antibodies, cells were incubated without primary antibodies ("no primary antibody" control) in 0.1% BSA/PBS overnight then incubated with secondary antibodies as above. To control for non-specific staining introduced by primary antibodies, cells were incubated with IgG (isotype control; 1:1000 dilution) in 0.1% BSA/PBS overnight, then incubated with secondary antibodies.

Table 2.4 Antibodies used for immunofluorescence

Antibody target	Supplier	Host species	Clonality	Dilution
Acetylated α-tubulin	Sigma-Aldrich (T7451)	Mouse	Monoclonal	1:2000
ARL13b	Proteintech (1771-1-AP)	Rabbit	Polyclonal	1:1000
EEA1	Abcam (ab2900)	Rabbit	Polyclonal	1:1000
Secondary antibodies				
Goat anti-Rabbit IgG (H+L) Cross-Adsorbed Secondary Antibody, Alexa Fluor 555	Invitrogen (A-21428)	Goat	Polyclonal	1:500
F(ab')2-Goat anti-Mouse IgG (H+L) Cross-Adsorbed Secondary Antibody, Alexa Fluor 488	Invitrogen (A-11017)	Goat	Polyclonal	1:500

2.7.3 EEA1 staining

For staining of the early endosome marker EEA1, before fixation, cells were washed with 250 µL of the "cytoskeletal buffer" developed by Hua and Ferland[219] (300 mM sucrose, 3 mM magnesium chloride, 10 mM PIPES, 50 µM Triton X-100, 50 µM EGTA in deionsed water, pH 6.9) then fixed in 4% PFA made up in cytoskeletal buffer. Cells were then permeabilised and incubated with primary and secondary antibodies as above.

2.7.4 Ciliation measurement with epifluorescence microscopy

To measure levels of ciliation across different experimental groups, cells were stained with antibodies recognising the primary cilia-localised proteins acetylated α-tubulin and ARL13B (Table 2.4). Blinding to experimental groups during ciliation measurement was carried out by another researcher through labelling of slides with random numbers; labels were then removed once ciliation measurements were collected. A Zeiss Axio Scope A1 microscope with a 100x oil-immersion objective was used to count the number of DAPI-stained nuclei and primary cilia present in 25 fields of view per coverslip. Acetylated α-tubulin staining was primarily used to

count cilia, with ARL13B staining used to confirm the identity of cilia. The following equation was used to calculate the percentage of ciliated cells in each field of view:

$$Ciliation\ (\%) = \frac{Number\ of\ cilia}{Number\ of\ cells} \times 100$$

Ciliation data was then plotted using GraphPad Prism.

2.7.5 Confocal microscopy

The Olympus FLUOVIEW 1200 confocal microscope with a 60x oil-immersion objective was used for confocal microscopy. A zoom factor of 1.4x and image size of 1600x1600 pixels was used, giving a pixel size of 0.188 µm in the XY plane. Optical sections were taken every 0.400 µm in the Z plane, with pixel size of 0.814 µm. Images were then exported into Fiji, which was used to create maximum intensity projections of z-stacks.

For measurement of primary cilia length, images of cells stained with anti-acetylated α-tubulin or anti-ARL13B antibodies were collected from 5 fields of view per coverslip. Maximum intensity projections were created as above in Fiji. Cilia lengths were measured using the segmented line tool, exported into GraphPad Prism and plotted in scatter graphs.

2.8 Statistical tests

Cell culture experiments were performed in three replicate wells of a cell culture plate per experimental condition. Most experiments were conducted at least three separate times using three different subcultures of the same chondrocyte line, to give n=9.

The Shapiro-Wilk normality test plus visual inspection of Q-Q plots were used in all datasets to determine which descriptive statistics and statistical tests should be used. In addition to each individual replicate, the mean value of normally distributed data was presented graphically, with

error bars representing the standard deviation (SD). For non-normally distributed data, the median value and error bars representing the interquartile range (IQR) were presented.

In experiments where more than two experimental conditions were compared to controls, a one-way Analysis of variance (ANOVA) test with Tukey's multiple comparisons test, or Kruskal-Wallis test with Dunn's multiple comparisons test in the case of non-parametric data, were used to test for statistically significant differences. When these tests were used, multiplicity-adjusted p values were presented. When only one experimental condition was compared to control cells, two-tailed Student's t-test or the Mann-Whitney test for non-parametric data were used.

The extracellular half-life of FLAG-tagged ADAMTS-5 was calculated by fitting data from the ADAMTS-5 endocytosis assay to a one-phase exponential decay curve.

Statistical significance was set at a p value of 0.05.

CHAPTER 3

Identification of TTBK2 as a regulator of ADAMTS-5-mediated aggrecan degradation

3.1 Introduction

As discussed in Section 1.3, a number of studies have demonstrated associations between the primary cilium and the regulation of the extracellular matrix. For example, disruption of proteins involved in cilia assembly and function, such as IFT80, have been shown to affect the expression of cartilage matrix components in the growth plate during post-natal cartilage development[174]. These changes in matrix synthesis are thought to be due to disruption of signalling pathways regulated by the primary cilium, such as the Hh pathway[152], which in turn leads to altered chondrocyte differentiation.

In addition to matrix anabolism, the primary cilium has been indirectly linked to cartilage matrix catabolism through its regulation of the Hh pathway, as genetic activation of Hh signalling increased cartilage matrix degradation and expression of matrix-degrading proteases such as ADAMTS-5 in adult mice[75]. Direct disruption of ciliary proteins, such as constitutive mutation of members of the BBSome complex, also resulted in changes consistent with matrix degradation *in vivo*, including reduced articular cartilage thickness and reduced proteoglycan staining[188]. However, it is not known whether these changes are due to altered matrix anabolism during development or increased matrix catabolism in adulthood.

To gain further insight into the mechanism by which the primary cilium might regulate cartilage catabolism, the Wann group previously conducted a study to measure matrix proteolysis upon mutation of the ciliary protein IFT88, which I worked on during an undergraduate research project. In this study, a chondrocyte cell line derived from ORPK mice expressing a hypomorphic mutant form of IFT88 exhibited increased proteolysis of one of the major components of the cartilage matrix, aggrecan[193]. These ORPK cells also had impaired uptake of the aggrecan-degrading proteases ADAMTS-5 and MMP-13 by LRP-1-mediated endocytosis, which was previously shown by Yamamoto et al. (2013) to regulate protease activity in primary human chondrocytes[117]. Yamamoto and colleagues also found that LRP-1-mediated endocytosis of

proteases was reduced in osteoarthritic cartilage[120]; therefore, drugs targeting proteins that regulate LRP-1-mediated uptake could enhanced protease endocytosis and reduce cartilage loss in osteoarthritis.

Based on the Wann group's previous work, I hypothesised that the primary cilium is required for efficient endocytosis of proteases and thus regulates protease extracellular activity, as discussed in Section 1.3.3. Whilst there are a number of potential mechanisms by which the primary cilium regulates endocytosis, the exact molecular mechanism is unknown. Also, apart from IFT88 in the Wann group's previous study, no other ciliary proteins have been directly shown to regulate protease activity.

3.1.1 Aims and objectives

In this chapter, I aimed to determine whether the primary cilium is required for the regulation of aggrecan-degrading protease activity. I hypothesised that the primary cilium regulates protease activity by increasing the rate of LRP-1-mediated endocytosis of proteases, through contributing to the formation of a periciliary region of enhanced endocytosis.

To address this aim, my first objective was to validate a method for measuring protease activity in a mouse chondrocyte cell line when different ciliary proteins were depleted. The method I used was the aggrecan overlay assay, which has been used to measure the aggrecan-degrading activity of human chondrocytes[60], but has not been fully validated in the mouse chondrocyte cell line used here. The assay involved co-culturing cells with purified bovine aggrecan and subsequently detecting the neoepitopes on protease-generated aggrecan fragments via western blot (Figure 3.1). The neoepitope detected in this thesis was AGEG, which is present at the N-terminus of bovine aggrecan fragments generated from cleavage at the $Glu^{1771\sim1772}Ala$ bond within the second chondroitin sulfate-rich region[53].

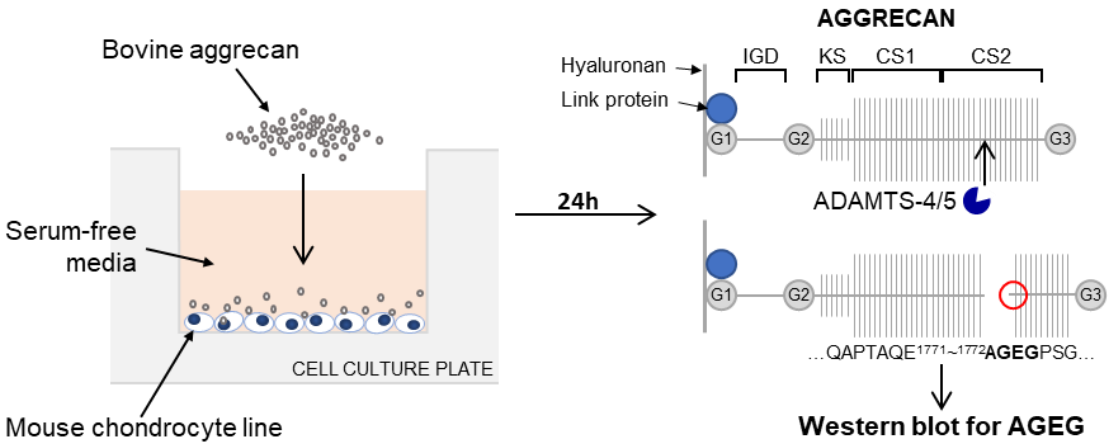

Figure 3.1 Aggrecan overlay assay and AGEG neoepitope detection. To measure protease activity in a mouse chondrocyte cell line, cells were grown in monolayer then incubated with purified bovine aggrecan in serum-free media for 24 hours. To measure aggrecan degradation by proteases secreted from the cells, levels of the aggrecan neoepitope AGEG in conditioned media were determined by western blot. The AGEG neoepitope is generated by cleavage in the second chondroitin sulfate-rich region (CS2) of aggrecan by proteases such as ADAMTS-4 and ADAMTS-5.

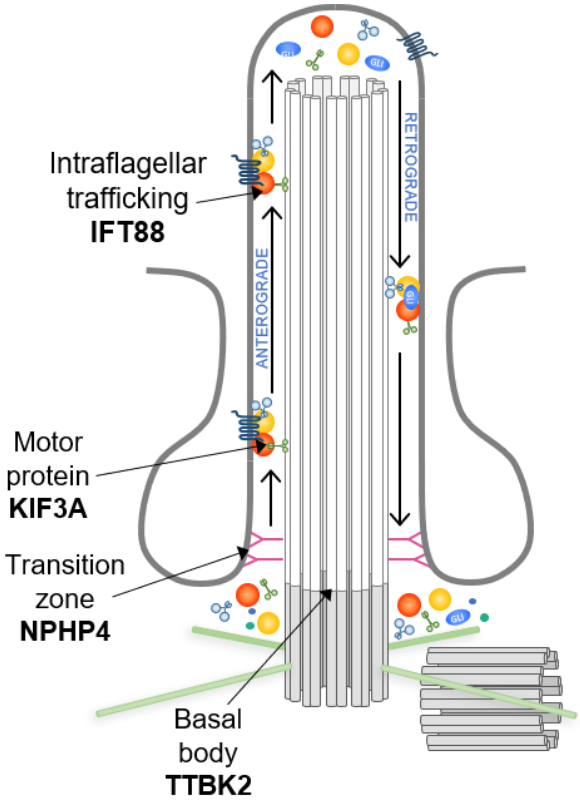

Figure 3.2 Function and localisation of candidate regulators of protease activity. IFT88 is part of a protein complex, which, together with the motor protein KIF3A, traffics cargo from the cell body into the cilium (anterograde intraflagellar transport (IFT)). NPHP4 is involved in maintenance of the transition zone and is also involved in caveolae-dependent endocytosis at the ciliary membrane. The kinase TTBK2 regulates maturation of the centriole into the basal body, which then forms the axoneme.

The second objective of this chapter was to use the aggrecan overlay assay to measure aggrecanolytic protease activity when ciliary proteins were knocked down with siRNAs. To determine which cilia protein-regulated processes are involved in the regulation of protease activity, four proteins with different roles in cilia formation and function were depleted. These proteins were:

- IFT88 itself, to enable disruption of anterograde IFT-regulated processes (Figure 3.2)
- the motor protein KIF3A, which is also involved in anterograde IFT and, like IFT88, is frequently targeted to model cilia disruption[152,220,221]
- the transition zone protein NPHP4, which is one of the only ciliary proteins directly shown to have a role in endocytosis[197]
- TTBK2, a centriolar kinase involved in the earliest stages of ciliogenesis[140].

3.2 Results

3.2.1 Validation of the aggrecan overlay assay and subsequent AGEG neoepitope detection as an indicator of protease activity

To test whether the AGEG aggrecan neoepitope could be detected by western blot, live cartilage explants from three different porcine metacarpophalangeal joints were incubated over a 72-hour time course with or without 10 ng/ml IL-1β, a proinflammatory cytokine which induces proteolytic cartilage matrix degradation[51,60]. Immunoreactive bands at approximately the molecular weight reported for AGEG-containing fragments (120-130 kDa[53,60]) were observed after 24 hours. Signal intensity increased over time, and upon IL-1β treatment relative to untreated explants at 24 and 48 hours (Figure 3.3A). Similar bands were also detected when purified bovine aggrecan was incubated either with 1 nM FLAG-tagged recombinant human ADAMTS-5-3 over a 24-hour time course (Figure 3.3B). AGEG signal increased over time, and

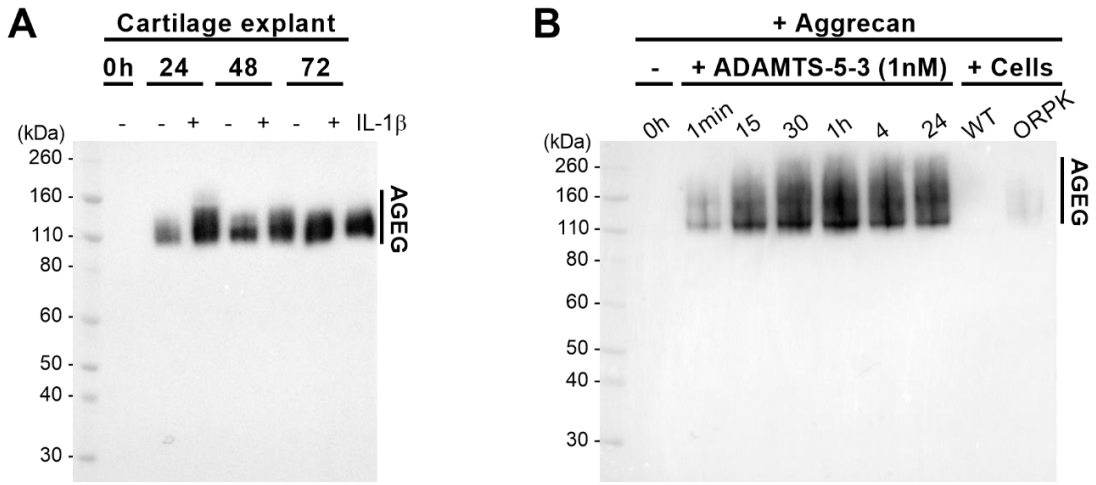

Figure 3.3 The AGEG neoepitope was generated upon degradation of purified aggrecan and aggrecan within the cartilage matrix. ***A***) Live porcine cartilage explants were incubated with or without 10 ng/ml IL-1β for 24, 48 or 72 hours. AGEG neoepitope in conditioned media was detected by western blot, with ECL detection. Blot representative of one experiment conducted using explants from three separate porcine metacarpophalangeal joints (n=3). ***B***) 1 nM FLAG-tagged human ADAMTS-5-3 was incubated with 100 µg/ml purified bovine aggrecan over a time course, or WT and ORPK cells were incubated with 50 µg/ml aggrecan for 24 hours. AGEG neoepitope was detected in conditioned media by western blot (ECL). Blot representative of one experiment conducted in triplicate (n=3).

was elevated in conditioned media from ORPK cells relative to that of WT cells, which is consistent with previous studies[193]. In summary, the AGEG neoepitope could be consistently detected upon cleavage of ECM-associated aggrecan by porcine chondrocytes, and cleavage of purified aggrecan by recombinant ADAMTS-5 or mouse chondrocyte cell lines.

To gain further confidence that AGEG neoepitope generation by the chondrocyte cell lines was indicative of protease activity, WT cells were treated with different forms and concentrations of interleukin-1 (IL-1), which has been shown to induce proteolytic aggrecan degradation in chondrocytes[60]. AGEG generation by WT cells was not affected by treatment with IL-1β at 10 ng/ml (Figure 3.4A, quantified in B; p>0.9999) or 50 ng/ml (Figure 3.4C, quantified in D; p=0.9910). WT cells were also treated with 50 ng/ml IL-1α, which has a greater affinity for the IL-1 receptor than IL-1β[222], and thus was hypothesised to potentially have a greater effect on

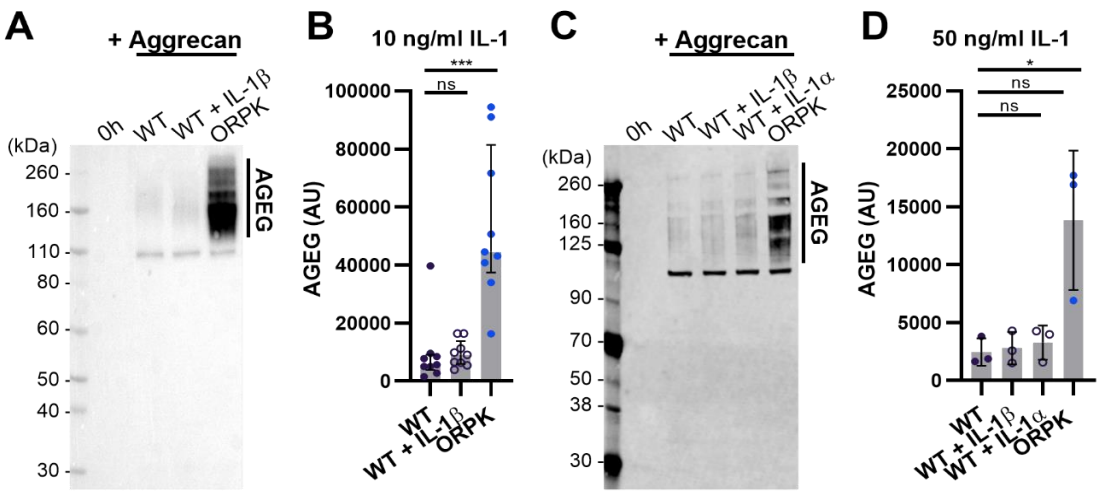

Figure 3.4 AGEG aggrecan neoepitope generation by WT and ORPK mouse chondrocyte cell lines was not responsive to interleukin-1. ***A***) WT and ORPK cells were incubated with 50 µg/ml aggrecan with or without 10 ng/ml IL-1β for 24 hours. AGEG neoepitope in conditioned media was detected by western blot, with ECL detection. Blot representative of three independent experiments conducted in triplicate using separate cell subcultures (n=9). ***B***) Quantification of AGEG levels in *A*). Median ± interquartile range (IQR). *** p<0.001, ns p>0.05, Kruskal-Wallis test with Dunn's multiple comparisons test. ***C***) WT and ORPK cells were incubated with 50 µg/ml aggrecan with or without 50 ng/ml IL-1β or IL-1α for 24 hours. AGEG neoepitope was detected by western blot, with near-infrared fluorescence (NIR) detection. Blot representative of three independent experiments conducted in triplicate using one cell subculture (n=3). ***D***) Quantification of AGEG in *C*). Mean ± SD. * p<0.05, ns p>0.05, one-way ANOVA with Tukey's multiple comparisons test.

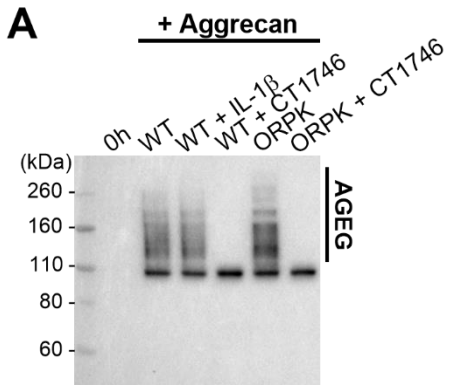

Figure 3.5 AGEG generation in WT and ORPK chondrocyte cell lines was mediated by metalloproteases. ***A***) WT and ORPK cells were incubated with 50 µg/ml aggrecan with or without the metalloprotease inhibitor CT1746 (10 µM), for 24 hours. AGEG in conditioned media was detected by western blot (ECL detection). Blot representative of one experiment conducted in triplicate using one cell subculture (n=3).

protease activity. However, IL-1α also had no effect on AGEG generation (Figure 3.4C, quantified in D; p=0.9884). As an alternative way of validating that AGEG generation in the aggrecan overlay assay was indicative of protease activity, WT and ORPK cells were treated with CT1746, which is a broad-spectrum inhibitor of matrix-degrading metalloproteinases, including aggrecanases[223]. AGEG signal between 120 and 250 kDa was abolished in WT and ORPK cells treated with 10 nM CT1746 (Figure 3.5). A band of around 100 kDa was unaffected by CT1746 treatment or the cell type used, indicating that this was non-specific signal. In summary, these results showed that generation of the AGEG neoepitope was indicative of aggrecan cleavage by metalloproteases.

To determine which proteases were responsible for aggrecan cleavage, AGEG generation was measured after the two main aggrecanolytic proteases, ADAMTS-4 and ADAMTS-5[61], were depleted from WT cells using siRNAs. Mean expression of *Adamts4* RNA was reduced by 50% in cells treated with siRNA targeting the *Adamts4* gene (siADAMTS4 cells) relative to cells treated with a non-targeting siRNA (siCtrl cells), as measured by qPCR (Figure 3.6A). Mean expression of *Adamts5* RNA was reduced by over 60% in siADAMTS5 cells relative to siCtrl cells (Figure 3.6B).

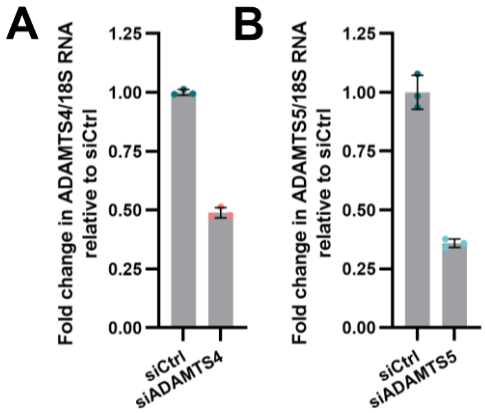

Figure 3.6 siRNA knockdown of *Adamts4* and *Adamts5* in WT cells. ***A***) RNA was isolated from siRNA-treated cells incubated with 50 µg/ml aggrecan for 24 hours. Expression of *Adamts4* or ***B***) *Adamts5* was measured by qPCR, normalised to *18s* expression and presented as a fold change relative to siCtrl. Mean ± SD, one experiment in triplicate using one cell subculture (n=3).

AGEG generation by these cells was subsequently measured by western blotting, and aggrecan incubated with FLAG-tagged ADAMTS-5-3 (FLAG-ADAMTS-5) was used as a positive control for AGEG signal. NIR fluorescence detection was used in these blots, which enabled use of the Revert total protein stain as a loading control, and also produced very similar signal to ECL detection in AGEG western blots with serially diluted conditioned media samples (Appendix figure 1, p. 219).

Knockdown of *Adamts4* had no effect on AGEG signal relative to siCtrl cells qualitatively (Figure 3.8A) or upon quantification and normalisation to total protein (Figure 3.8B, p>0.9999). In contrast, AGEG signal with or without normalisation to total protein was reduced upon knockdown of *Adamts5* relative to siCtrl cells (p=0.0333). AGEG generation by siADAMTS5 cells was similar to that of siCtrl cells treated with CT1746. These results indicate that ADAMTS-5 is responsible for the majority of aggrecan proteolysis in these cells.

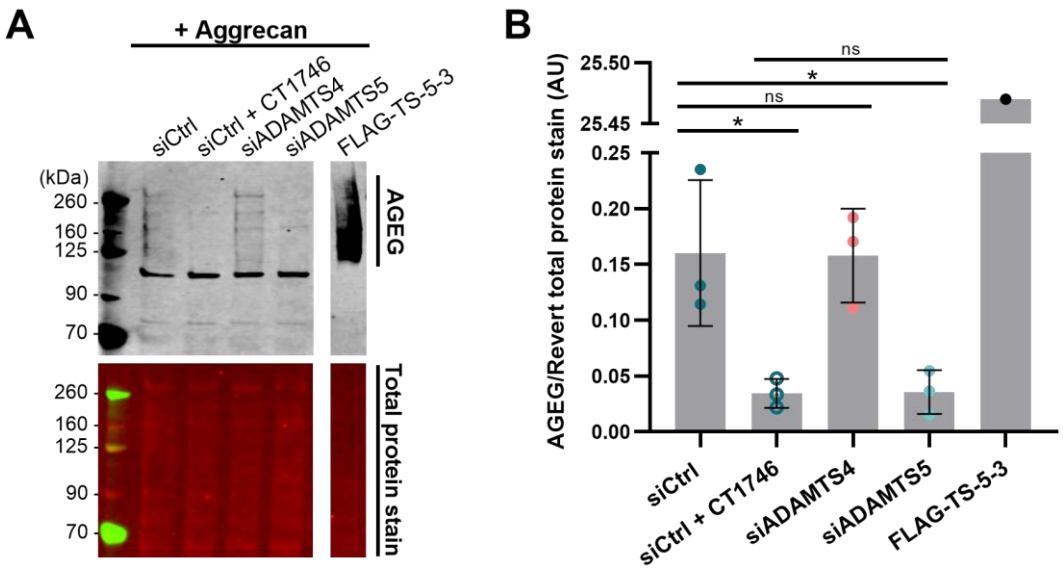

Figure 3.7 AGEG generation in the WT cell line was mediated by ADAMTS-5. ***A***) siCtrl, siADAMTS4 and siADAMTS5 cells were incubated with 50 µg/ml aggrecan with or without 10 µM CT1746 for 24 hours. AGEG neoepitope in conditioned media was detected by western blot, with near-infrared fluorescence detection (800 nm channel). Revert total protein stain was imaged in the 700 nm channel. Blot representative of one experiment conducted in triplicate using one cell subculture (n=3). ***B***) Quantification of AGEG levels in *A*), normalised to Revert total protein stain. Mean ± SD. * p<0.05, ns p>0.05, one-way ANOVA with Tukey's multiple comparisons test.

Alternative methods of measuring protease activity were also tested. To measure the ability of the WT and ORPK chondrocyte cell lines to degrade aggrecan within a cartilage matrix, cells were co-cultured with freeze-thawed porcine cartilage explants, and sGAG release into the media was then analysed using the DMMB assay (Appendix figure 2A, p.220). Some sGAG was released from explants alone, particularly at 8 and 48 hours (Appendix figure 2B). sGAG release in the co-culture system was thus corrected for release from explants alone at the same time point. Whilst GAG release was increased in the ORPK cell-explant co-culture relative to the WT cell-explant co-culture at 16 and 48 hours (Appendix figure 2C), sGAG release was the same in both conditions at 16 hours and even reduced in the ORPK cell-explant co-culture relative to that of WT at 8 hours. No statistically significant differences between WT and ORPK conditions were observed at any time point, and measurements of sGAG release between samples were highly variable; therefore, the assay was not used further.

Detection of chondroitinase-resistant remnants of GAG chains attached to full-length and degraded aggrecan was also tested as a method of measuring general aggrecanolytic protease activity. These GAG stubs were detected using the 2-B-6 antibody[55,224] (Appendix figure 3C, p.221) after purified aggrecan was incubated with FLAG-ADAMTS-5-3 or WT and ORPK cells. Multiple bands at approximately the expected molecular weights of 2-B-6-positive aggrecan fragments[55] were detected in aggrecan samples incubated with FLAG-ADAMTS-5-3. Signal intensity of these 2-B-6 bands and AGEG bands on the same blot increased with chondroitinase concentration (Appendix figure 3A). 2-B-6 signal was also increased in conditioned media from ORPK cells incubated with aggrecan relative to conditioned media from WT cells (Appendix figure 3B). However, due to weak signal and thus low sensitivity, the 2-B-6 antibody was not used in the rest of this thesis. Instead, use of AGEG neoepitope detection as an indicator of protease activity was continued for all further experiments.

3.2.2 Validation of ciliary gene knockdown in a mouse chondrocyte cell line

The aggrecan overlay assay and AGEG neoepitope detection were then used to measure aggrecan proteolysis upon knockdown of four proteins with different ciliary roles. siRNA pools targeting *Ift88*, *Kif3a*, *Nphp4* or *Ttbk2*, or a non-targeting control siRNA pool, were transfected into cells 16 hours after seeding on cell culture plates. At this time point, few cells had exited the cell cycle and started to form a primary cilium (Figure 3.9). Transfection of cells before cilia assembly had occurred enabled the siRNAs targeting ciliary genes to have an effect on this process before aggrecan was added 48 hours later. Therefore, by the end of the overlay assay 72 hours after cells were transfected, cilia had assembled in siCtrl cells, and fewer cilia had assembled in cells in which ciliary genes had been knocked down, such as in siTTBK2 cells.

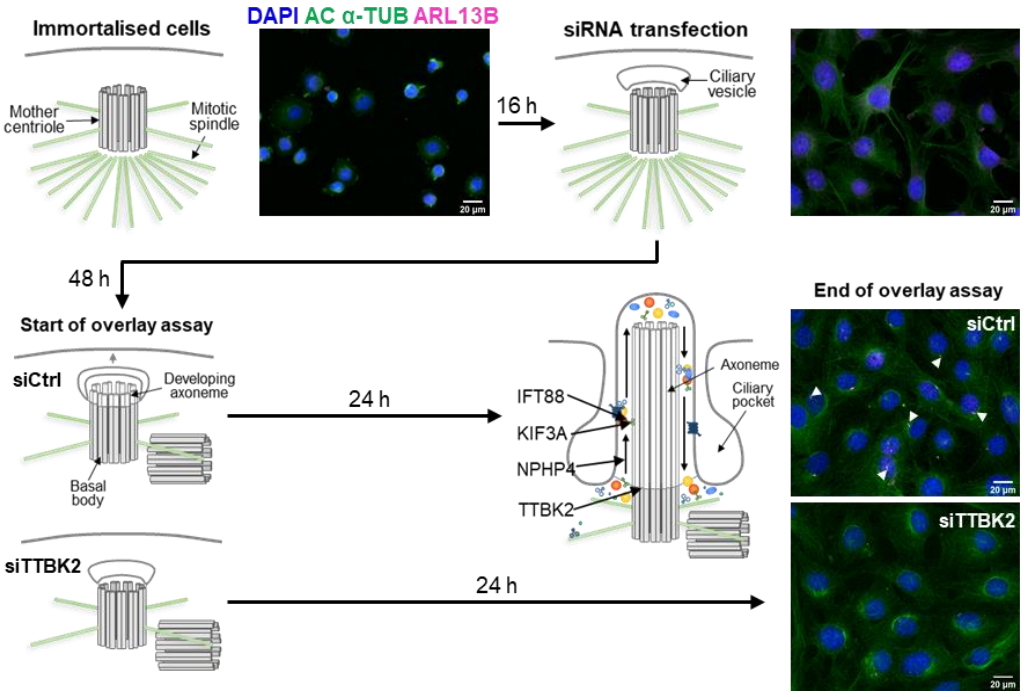

Figure 3.9 Assembly of primary cilia during the experimental time course. WT cells were seeded in an immortalised state, in which cells were still dividing and thus could not assemble a primary cilium, as shown in images of cells stained for the cilia markers acetylated α-tubulin and ARL13B. Cells were transfected with non-targeting siRNA or siRNAs targeting four different ciliary proteins 16 hours after seeding, at which point cells were 50-60% confluent and still had not assembled any primary cilia. 48 hours later at the start of the experimental time course, cells had reached 100% confluence and had exited the cell cycle, enabling cilia assembly to proceed. At the end of the time course, siCtrl cells exhibited staining for primary cilia (white arrowheads), whereas in cells treated with siRNAs targeting ciliary genes such as *TTBK2* before cilia assembly had started, fewer cilia were visible.

At the end of the aggrecan overlay assay, cell lysates or RNA were collected and analysed by western blot or qPCR respectively to validate ciliary gene knockdown. Expression of *Ift88*, *Kif3a*, *Nphp4* and *Ttbk2* RNA was reduced by 50-70% in each knockdown condition relative to siCtrl cells (Figure 3.10A). In western blots, a band corresponding to the molecular weight of IFT88 (93 kDa) was present in WT and siCtrl cell lysates probed with an anti-IFT88 antibody, and

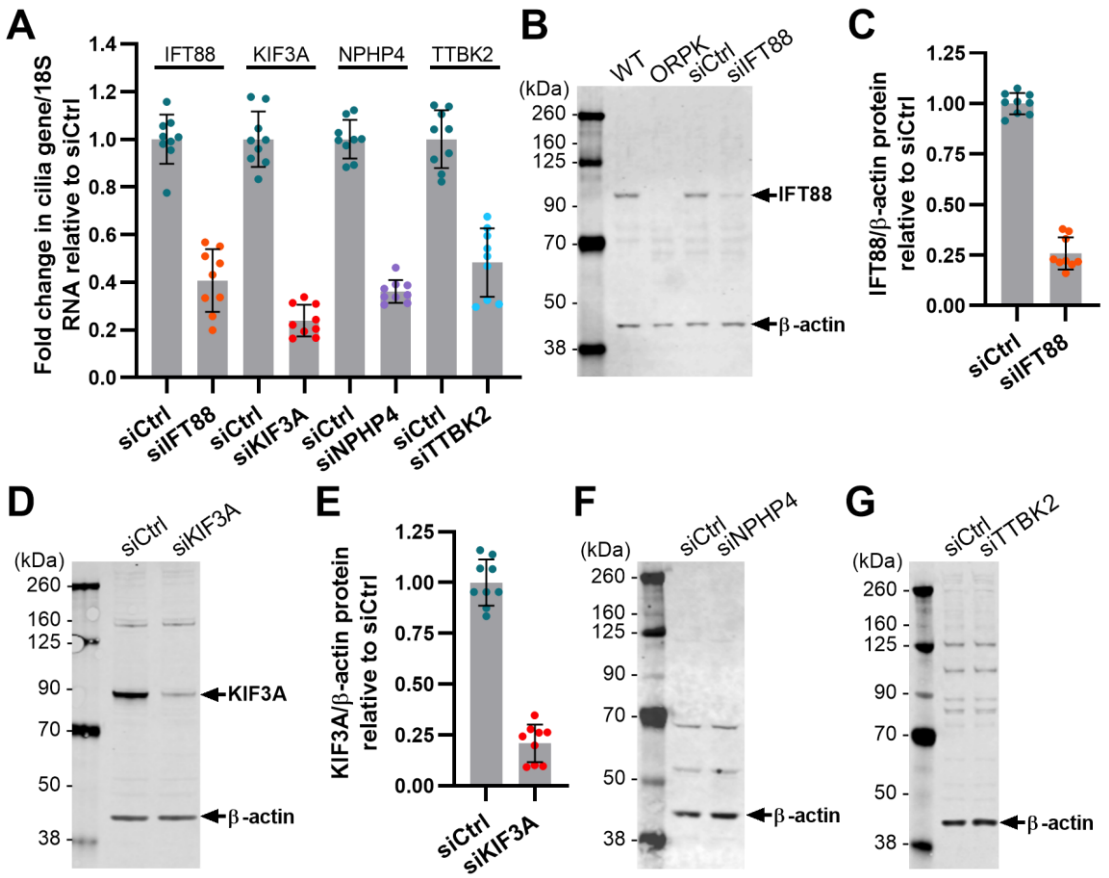

Figure 3.10 siRNA-mediated knockdown of ciliary proteins in a WT chondrocyte cell line. ***A***) RNA was isolated from siRNA-treated cells after incubation with 50 µg/ml aggrecan for 24 hours. Expression of IFT88, KIF3A, NPHP4 or TTBK2 RNA was measured by qPCR, then normalised to *18s* expression and presented as a fold change relative to siCtrl. Mean ± SD, three independent experiments conducted in triplicate using separate cell subcultures (n=9). ***B***) Cell lysates were collected at the end of the aggrecan overlay assay. IFT88 was detected in WT, ORPK, siCtrl and siIFT88 cell lysates by western blot, with β-actin loading control. ***C***) Fold change in IFT88 levels in *B*), normalised to β-actin, relative to siCtrl. Mean ± SD. ***D***) Western blot analysis of KIF3A in siCtrl and siKIF3A cells, with β-actin loading control. ***E***) Fold change in KIF3A levels in *D*), normalised to β-actin, relative to siCtrl. Mean ± SD, n=9. ***F***) Western blot analysis of NPHP4 in siCtrl and siNPHP4 cells, and ***G***) TTBK2 in siCtrl and siTTBK2 cells, with β-actin loading control. All blots are representative of three independent experiments conducted in triplicate using separate cell subcultures (n=9).

disappeared partially in siIFT88 lysates and completely in ORPK lysates (Figure 3.10B), indicating that this band was full-length IFT88. Quantification of IFT88 protein signal showed that knockdown efficiency was around 75% (Figure 3.10C). In validating *Kif3a* knockdown at protein level, a band at the expected molecular weight for KIF3A (80 kDa) was present at qualitatively reduced levels in siKIF3A cells relative to siCtrl. Quantification of these bands showed that knockdown efficiency of KIF3A was around 80% (Figure 3.10D and E).

However, western blots performed with serially diluted siCtrl lysates showed that whilst the IFT88 signal increased linearly with mass of protein present, the β-actin signal plateaued at higher protein amounts (Appendix figure 4, p.222). Therefore, calculation of knockdown efficiency after normalisation to β-actin could have resulted in incorrect estimation of efficiency, due to the saturation of β-actin signal at higher concentrations of total protein. Western blot analysis of NPHP4 and TTBK2 protein expression in siNPHP4 and siTTBK2 cells did not show any siRNA-sensitive bands of the expected molecular weights of 157 and 137 kDa respectively (Figure 3.10 F and G); therefore, the knockdown efficiency of *Nphp4* and *Ttbk2* at protein level could not be determined.

The effect of ciliary gene knockdown on ciliation was also assessed. Fluorescence microscopy was used to visualise two markers of the cilium: acetylated α-tubulin, which is enriched in the ciliary axoneme[225], and ARL13B, which is a GTPase present in the ciliary membrane[226] (Figure 3.11). Cells were first stained without primary antibodies targeting these markers or with an isotype control to check for non-specific staining (Appendix figure 5, p.223). No staining was observed when no primary antibodies were used. Some staining was observed in the IgG isotype-treated cells, but this staining was diffuse and unlike the focal staining that was observed in untreated siCtrl cells and identified as primary cilia.

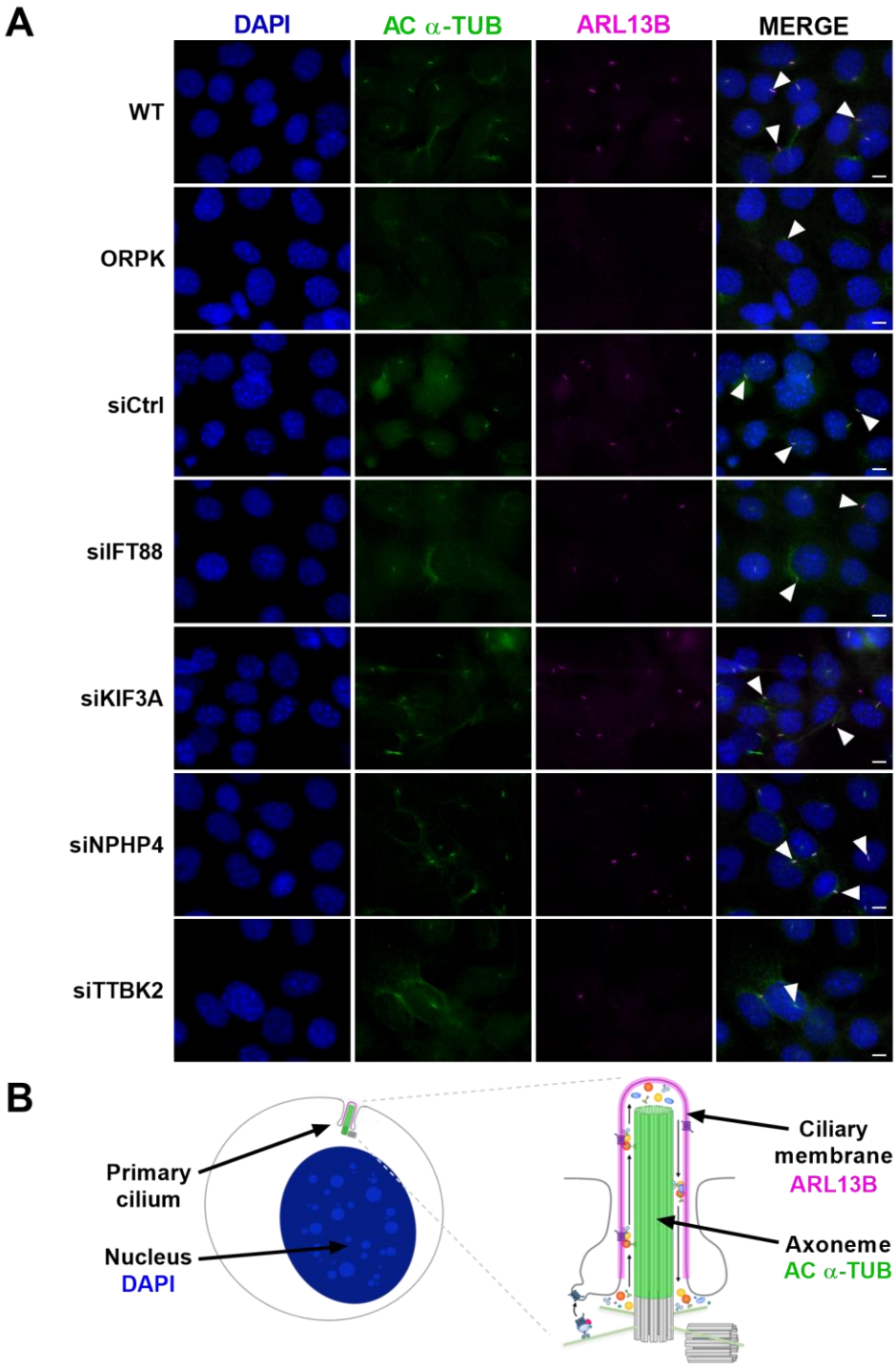

Figure 3.11 Effect of ciliary gene knockdown on ciliation. ***A***) WT, ORPK or siRNA-treated cells were incubated in serum-free media for 24 hours. Cells were fixed and stained with antibodies targeting acetylated α-tubulin (green) and ARL13b (magenta), and counterstained with DAPI (blue) to visualise cell nuclei. Cells were imaged using a Zeiss Axioscope epifluorescence microscope across 25 fields of view per coverslip. Scale bar 10 µm. White arrowheads indicate cilia. Images representative of triplicate coverslips across three independent experiments using separate cell subcultures (n=9). ***B***) Schematic of primary cilia in these cells. ARL13B is a marker of the ciliary membrane, and acetylated α-tubulin indicates the presence of the ciliary axoneme.

Ciliation in ORPK cells was reduced relative to WT cells, with only 7% of cells assembling a primary cilium (Figure 3.12A, p<0.0001). The percentage of ciliated cells was also statistically significantly reduced to around 25% in siIFT88, siKIF3A and siTTBK2 cells and 32% in siNPHP4 cells, relative to siCtrl cells in which half of the cells assembled a cilium (p<0.0001 for all comparisons). Cell number, as indicated by the presence of DAPI-stained nuclei, was statistically significantly increased upon knockdown of all four ciliary genes, with the largest increase observed in siKIF3A cells (Figure 3.12B, p<0.001 for siNPHP4 versus siCtrl, p>0.0001 for all other comparisons).

Cilia length was also measured in confocal microscopy images of stained cells, although length was unchanged across all conditions when either acetylated α-tubulin or ARL13B staining was used to measure length, including in siTTBK2 cells relative to siCtrl cells (Appendix figure 6, p.224, p>0.9999 for both acetylated α-tubulin and ARL13B-stained-cilia).

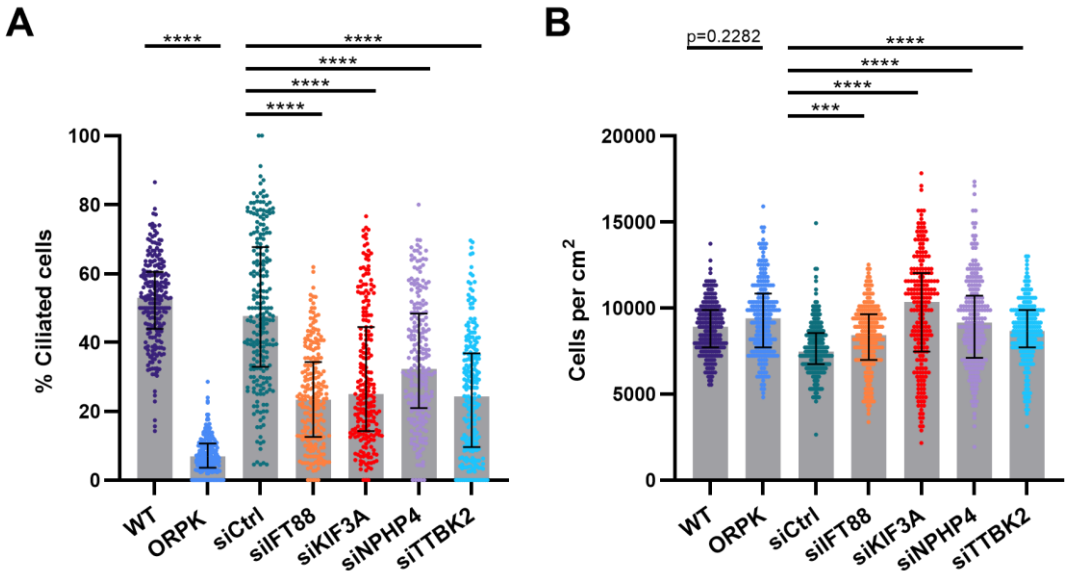

Figure 3.12 Knockdown of ciliary genes reduces ciliation. ***A***) WT, ORPK or siRNA-treated cells were incubated in serum-free media for 24 hours and stained for the cilia markers acetylated α-tubulin and ARL13B. DAPI-stained cells and acetylated α-tubulin- and ARL13B-stained cilia were counted in 25 fields of view of one coverslip. Cilia number was divided by cell number to calculate the percentage of ciliated cells for each field of view. ***B***) Cell number counted across 25 fields of view was used to calculate the number of cells present per cm^2. Median ± IQR. *** p<0.001, **** p<0.0001, p values >0.05 shown on graph, Kruskal-Wallis test with Dunn's multiple comparisons test. Three independent experiments were conducted in triplicate using separate cell subcultures (n=9).

3.2.3 Knockdown of *Ttbk2* increased AGEG neoepitope generation in the aggrecan overlay assay

The effect of knocking down IFT88, KIF3A, *Nphp4* or *Ttbk2* on aggrecanolytic protease activity was then studied using the aggrecan overlay assay and subsequent AGEG neoepitope detection. As seen previously by Coveney et al. (2013)[193], ORPK cells exhibited a statistically significant increase in AGEG generation relative to WT cells (Figure 3.13, p=0.0004), although AGEG signal was highly variable between samples. Knockdown of either IFT88, KIF3A or *Nphp4* had no effect on AGEG generation relative to siCtrl cells (p>0.9999).

Knockdown of *Ttbk2* had the larger effect on AGEG generation than knockdown of the other ciliary genes, with a 3-fold increase in median AGEG generation relative to siCtrl observed. However, this increase in AGEG generation in siTTBK2 cells was not statistically significant (p>0.9999). Also, as observed across conditions, AGEG levels were variable between samples of

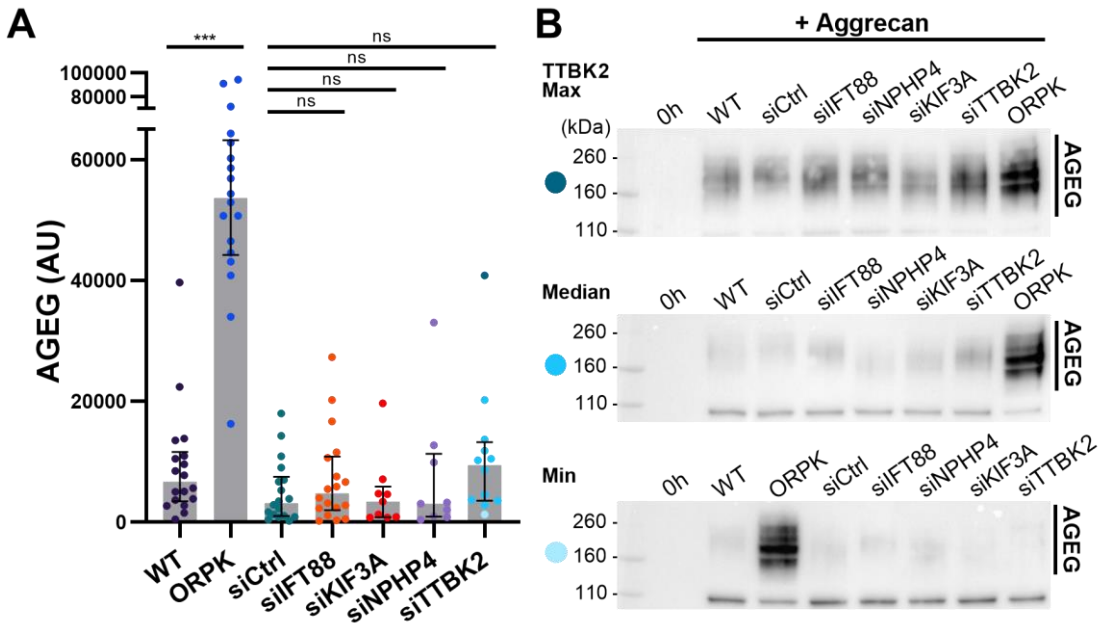

Figure 3.13 Knockdown of *Ttbk2* resulted in increased AGEG generation in a WT chondrocyte cell line. ***A***) WT, ORPK or siRNA-treated cells were incubated with 50 µg/ml aggrecan for 24 hours. AGEG neoepitope in conditioned media was detected by western blot with ECL detection, then quantified. Median ± IQR, at least three independent experiments conducted in triplicate using separate cell subcultures (minimum n=9). *** p<0.001, ns p>0.9999, Kruskal-Wallis test with Dunn's multiple comparisons test. ***B***) Blots representative of maximum (top), median (middle) and minimum (bottom) AGEG signal in siTTBK2 samples across experiments (n=9).

conditioned media from siTTBK2 cells. In some western blots, AGEG generation was greatly increased in siTTBK2 cells relative to siCtrl (Figure 3.13B, top panel), whereas in others AGEG levels were the same as or lower than levels in siCtrl (Figure 3.13B, middle and bottom panels).

As knockdown of *Ttbk2* was the only ciliary gene knockdown condition to have any qualitative effect on AGEG generation despite the high variation in AGEG signal, TTBK2 was further investigated as a candidate ciliary protein that could regulate aggrecan proteolysis. To check when the maximum aggrecanolytic activity of siTTBK2 cells occurred, the aggrecan overlay assay was conducted over a 72-hour time course. Western blotting with NIR fluorescence detection was used in this experiment, as this detection method was associated with lower AGEG signal variation than ECL detection (Appendix figure 1C, p.219) and enabled use of the Revert total protein stain as a loading control. Only one replicate of each sample was analysed, but AGEG generation was qualitatively increased in siCtrl conditioned media over time (Figure 3.14A). The large increase in AGEG generation by siCtrl cells at 72 hours was not quantified as this increase was possibly due to impaired general cell function after 72 hours in serum-free media, although

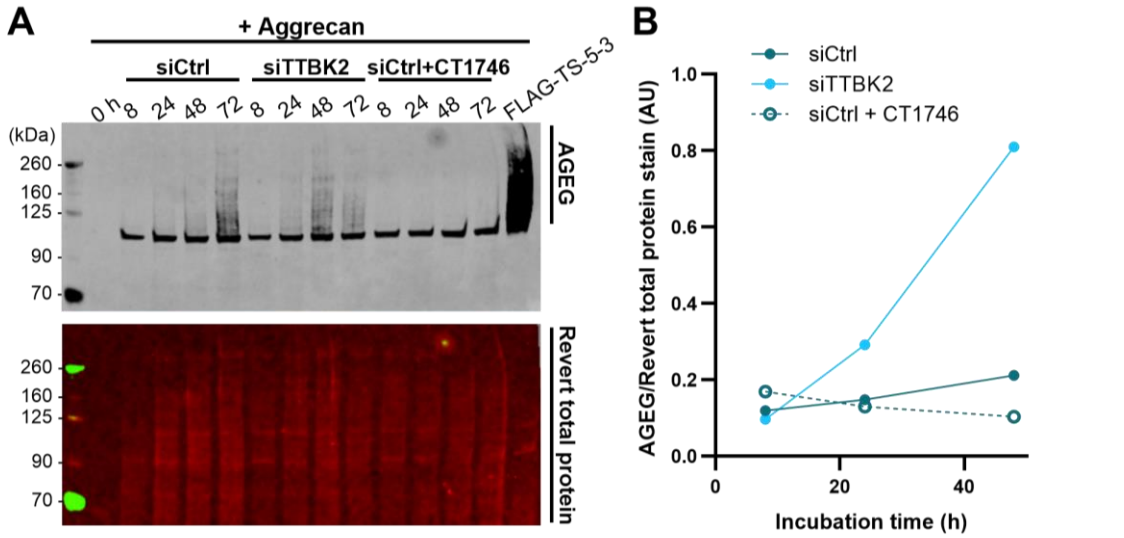

Figure 3.14 AGEG generation increased over time upon TTBK2 knockdown. ***A***) siCtrl and siTTBK2 cells were incubated with 50 µg/ml aggrecan with or without 10 nM CT1746, for 8, 24, 48 or 72 hours. AGEG neoepitope in conditioned media was detected by western blot with near-infrared fluorescence detection (800 nm channel). Revert total protein stain was imaged in the 700 nm channel. Experiment conducted once using one cell subculture (n=1). ***B***) Quantification of AGEG levels in *A*), normalised to Revert total protein stain.

this would need to be confirmed by measuring cell viability. No signal was seen in media of siCtrl cells treated with the metalloproteinase inhibitor CT1746 at any time point (Figure 3.14A). Quantification of this blot showed that there was a 2-fold increase in AGEG generation in siTTBK2 cells relative to siCtrl cells at 24 hours, similar to the increase seen in Figure 3.13, and a larger, 4-fold increase was observed at 48 hours (Figure 3.14B). Ideally, I would have repeated the experiment at 48 hours, but did not have sufficient time.

To determine whether increasing *Ttbk2* knockdown efficiency would further increase AGEG generation, AGEG levels were measured when cells were treated with increasing concentrations of *Ttbk2*-targeting siRNA (Appendix figure 7, p.225). Whilst the use of 25 and 50 nM siRNA resulted in 5 to 10% lower *Ttbk2* expression than the 10 nM siRNA used in all previous experiments, increasing siRNA concentration had no effect on AGEG generation. At all three siRNA concentrations, AGEG generation was qualitatively higher in siTTBK2 cells relative to siCtrl cells, but could not be quantified due to the high levels of non-specific signal present in blots from this experiment.

To confirm that AGEG generation in siTTBK2 cells was due to the action of ADAMTS-5, which was shown to be the main aggrecanolytic protease in this cell line in Figure 3.8, AGEG generation was measured when cells were treated with siRNAs targeting both *Ttbk2* and *Adamts5*. siCtrl, siTTBK2 and siADAMTS5 cells were treated with an additional 10 nM non-targeting siRNA, thus ensuring that the total concentration of siRNA present in all conditions was 20 nM.

Knockdown of *Adamts5* alone or in combination with *Ttbk2* resulted in a 70 to 80% reduction in *Adamts5* RNA expression relative to siCtrl cells (Figure 3.15A). Similarly, *Ttbk2* expression was reduced by over 60% relative to siCtrl cells upon knockdown of *Ttbk2* alone or in combination with *Adamts5* (Figure 3.15B). Knockdown of *Adamts5* alone had no effect on *Ttbk2* expression ($p=0.1836$), whereas knockdown of *Ttbk2* resulted in a statistically significant 1.7-fold increase in *Adamts5* expression ($p=0.0002$). The contribution of this increase in *Adamts5* expression to

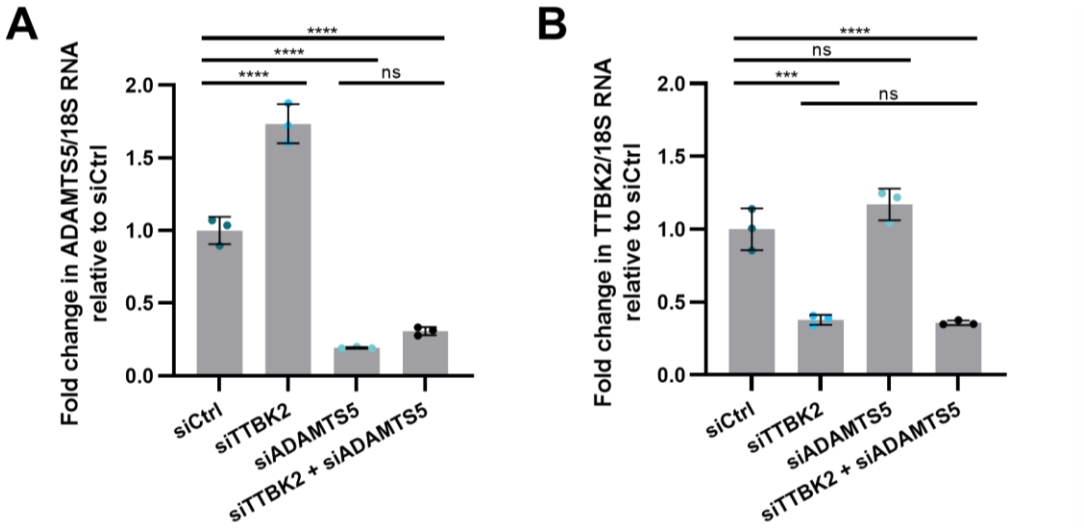

Figure 3.15 Combined knockdown of *Adamts5* and *Ttbk2*. *A*) RNA was isolated from siRNA-treated cells after incubation with 50 µg/ml aggrecan for 24 hours. Expression of *Adamts5* or ***B***) *Ttbk2* RNA was measured by qPCR, then normalised to *18s* expression and presented as a fold change relative to siCtrl. Mean ± SD, one experiment conducted in triplicate using one cell subculture (n=3). *** p<0.001, **** p<0.0001, ns p>0.05, one-way ANOVA with Tukey's multiple comparisons test.

overall aggrecan proteolysis in siTTBK2 cells was investigated further in experiments presented in Section 4.2.1.

The effect of single or combined knockdown of *Ttbk2* and *Adamts5* on AGEG generation was then analysed by western blot. *Ttbk2* knockdown alone resulted in a statistically significant, 6-fold increase in AGEG levels normalised to total protein, relative to siCtrl cells (Figure 3.16, p=0.0019). In contrast, almost no AGEG signal was detectable when *Ttbk2* was knocked down in combination with *Adamts5*, which was a statistically significant reduction in AGEG generation relative to knockdown of *Ttbk2* alone (p=0.0006). These results indicate that the increased aggrecan-degrading protease activity upon *Ttbk2* knockdown was mainly mediated by ADAMTS-5.

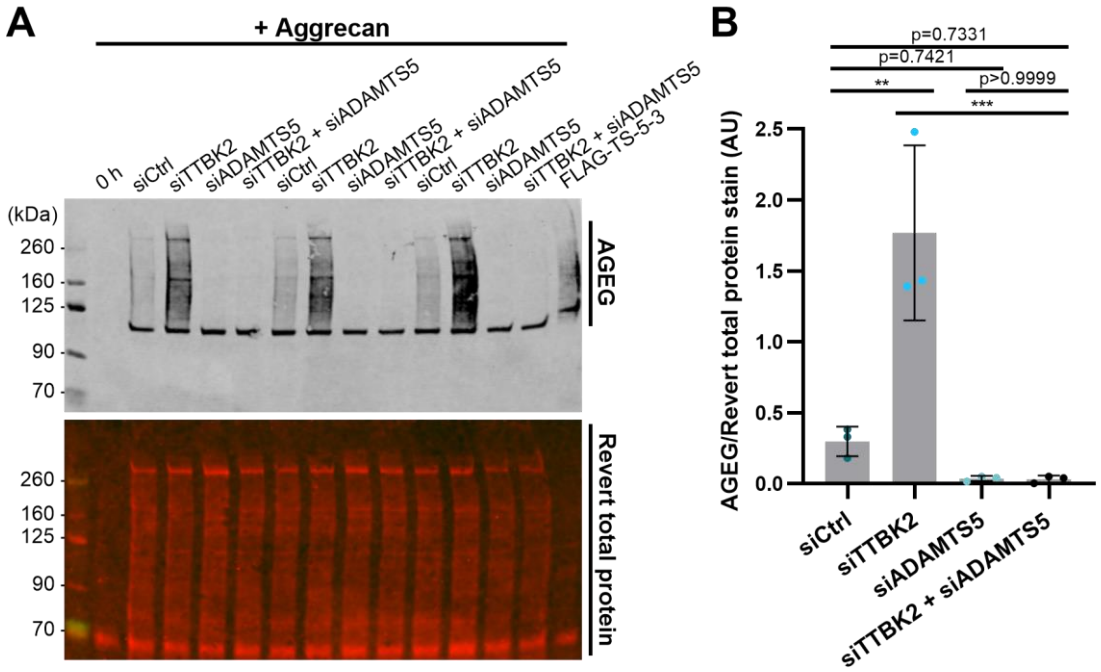

Figure 3.16 Increased AGEG generation upon *Ttbk2* knockdown was abolished with combined knockdown of *Adamts5*. *A*) siRNA-treated cells were incubated with 50 µg/ml aggrecan for 24 hours. AGEG neoepitope in conditioned media was detected by western blot with near-infrared fluorescence detection (800 nm channel). Revert total protein stain was imaged in the 700 nm channel. Blot representative of one experiment conducted in triplicate using one cell subculture (n=3). ***B***) Quantification of AGEG levels in *A*), normalised to Revert total protein stain. Mean ± SD, n=3. ** $p<0.01$, *** $p<0.001$, ns $p>0.05$, one-way ANOVA with Tukey's multiple comparisons test.

3.3 Discussion

3.3.1 Summary

In this chapter, I aimed to determine whether the primary cilium is involved in the regulation of aggrecan proteolysis, by measuring protease activity when genes encoding proteins with different roles in cilia assembly and function were knocked down with siRNAs in a mouse chondrocyte cell line. I found that generation of the AGEG aggrecan neoepitope by these cells was indicative of ADAMTS-5-dependent aggrecan degradation, as AGEG generation was inhibited by a broad-spectrum metalloprotease inhibitor or knockdown of *Adamts5*, which encodes the major aggrecanolytic protease in mice. I then found that knockdown of IFT88, KIF3A or *Nphp4* had no effect on AGEG generation despite reducing ciliation, indicating that the presence of the primary cilium may not be required for the regulation of protease activity. However, knockdown of *Ttbk2* resulted in increased ADAMTS-5-mediaed AGEG production, and therefore the centriolar kinase TTBK2 might be a novel regulator of ADAMTS-5 activity.

3.3.2 AGEG generation by a mouse chondrocyte cell line was indicative of protease activity

Conditioned media from live porcine cartilage explants was used as a positive control for western blot analysis of the AGEG aggrecan neoepitope. Given that proteoglycans such as aggrecan constitute around 10% of cartilage[227], each explant contained around 800 µg aggrecan, thus providing plenty of substrate for aggrecan-degrading proteases secreted by porcine chondrocytes. AGEG signal in explant conditioned media increased over time and upon treatment with the cytokine IL-1β, which has been shown to induce generation of the aggrecan interglobular domain neoepitope ARGS in porcine articular cartilage explants[228] and AGEG and ARGS generation in human cartilage explants and human chondrocytes in monolayer[60]. AGEG generation also increased over time when purified bovine aggrecan was incubated with 1 nM recombinant human ADAMTS-5. This is consistent with previous studies using recombinant

ADAMTS-5[54], including the form of ADAMTS-5 used in this thesis (ADAMTS-5-3) that lacks the spacer and second thrombospondin domains and has been shown to degrade bovine aggrecan by western blot analysis using antibodies against ARGS and other neoepitopes[55]. Similar AGEG signal was detected in conditioned media when WT and ORPK cells were incubated with 25 µg aggrecan, and the elevated AGEG generation observed in ORPK cells was consistent with the group's previous studies[193]. In summary, the AGEG signal observed in three different experimental systems in this chapter (porcine cartilage explants, purified ADAMTS-5 and cells of a mouse chondrocyte cell line) was consistent with the results of previous studies of aggrecanolytic protease activity.

In contrast to porcine explants, cells of the WT mouse chondrocyte cell line did not exhibit increased AGEG generation in response to IL-1. This result was unexpected based on previous work showing that IL-1 induces aggrecan proteolysis in chondrocytes, including the Wann group's previous study, in which 50 ng/ml IL-1β was shown to increase AGEG and ARGS generation in the WT chondrocyte cell line[193]. However, in other experiments, I observed the expected effect of interventions previously shown to modulate aggrecan proteolysis. For example, AGEG generation in WT and ORPK cells was inhibited by the broad-spectrum metalloprotease inhibitor CT1746. This compound was first identified as an inhibitor of gelatinases in a mouse model of lung cancer[229], and has also been shown to inhibit collagen breakdown in mouse bone explant cultures[207] and aggrecan degradation *in vitro*[223].

Furthermore, siRNA-mediated knockdown of *Adamts5*, but not *Adamts4*, reduced AGEG generation. These results confirm that ADAMTS-5 is the primary aggrecan-degrading protease in this chondrocyte cell line, which is consistent with previous studies in mouse chondrocytes. For example, using a surgical model of osteoarthritis, Glasson et al. (2004) showed that histological cartilage degradation in mice upon deletion of the ADAMTS-4 catalytic domain was similar to WT mice, as was IL-1-induced proteoglycan loss and NITEGE neoepitope generation in

mouse cartilage explants[56]. In contrast, ADAMTS-5 catalytic domain deletion resulted in protection against aggrecan degradation in the same model of osteoarthritis, and exhibited less proteoglycan release and a large reduction in NITEGE staining in articular cartilage relative to control mice[57]. ADAMTS-5 has also been shown to have increased intrinsic catalytic activity relative to ADAMTS-4[230]. In summary, the inhibition of AGEG generation by CT1746 and *Adamts5* knockdown in my experiments validated the aggrecan overlay assay and subsequent AGEG detection as a method for measuring aggrecanolytic protease activity.

3.3.3 Changes in protease activity did not correlate with changes in ciliation

After validation, the aggrecan overlay assay and AGEG neoepitope detection were used to measure proteolytic aggrecan degradation when different ciliary genes were depleted, and thus test whether the primary cilium is required for regulation of protease activity. Before this, the effect of siRNA-mediated ciliary gene knockdown on ciliation was characterised by staining of acetylated α-tubulin and ARL13B, which are markers of the two main structures of the cilium, the ciliary axoneme and membrane respectively. IFT88 knockdown resulted in around a 50% reduction in ciliation relative to siCtrl cells, which was expected given the essential role of IFT88 in cilia assembly[144] and observations of reduced ciliation upon IFT88 knockdown in other chondrocytic mouse cell lines[145]. Similar reductions in cilia assembly were observed upon knockdown of *Ttbk2*, which is required for initiation of ciliogenesis through removing the protein CP110 from the distal centriole[139,140], and knockdown of KIF3A, which has been shown to reduce cilia assembly in cartilage *in vivo*[175]. The effect of *Nphp4* knockdown on ciliation was smaller, which is consistent with the reported function of NPHP4 at the transition zone rather than in cilia assembly[151]. Cilia length was also investigated, given that changes in length have been associated with altered cilia function; for example, Thompson et al. (2016) found that lithium chloride treatment of bovine articular chondrocytes increased cilia length but also inhibited Ihh-induced Hh signalling[231]. However, cilia length was unaffected by knockdown of these ciliary genes.

Despite the reduction in ciliation observed, siRNA-mediated knockdown of IFT88, KIF3A or *Nphp4* had no effect on AGEG generation, with only *Ttbk2* knockdown resulting in increased AGEG signal. No previous studies have looked directly at whether NPHP4 regulates protease activity or has a role in cartilage homeostasis, but mutation of IFT88 in ORPK cells has previously been shown to increase AGEG production. It was therefore surprising that that protease activity was not affected by knockdown of IFT88 or KIF3A, which are both involved in anterograde IFT during ciliogenesis. This lack of correlation between ciliation and AGEG generation across the different experimental conditions implied that simply the presence of the main structures of the primary cilium (i.e. the axoneme and ciliary membrane) was not required for regulation of protease activity. Supporting this hypothesis, Kaushik et al. (2009) found that ciliation was unaffected in adult mouse cartilage upon mutation of BBSome complex proteins, which were required for cilia assembly and regulation of ciliary membrane composition *in vitro*[148]*,* but cartilage thickness and proteoglycan content were reduced[188].

Therefore, the elevated AGEG generation in ORPK cells could instead be a consequence of the non-ciliary defects that have been observed in ORPK mice. For example, ORPK mice exhibited increased rates of cell proliferation in pancreatic and renal tissues[232–234], although ORPK cell number was not statistically significantly increased relative to WT cells in my experiments. In chondrocytes, the ORPK mutation has also been shown to affect the actin and tubulin cytoskeleton throughout the cell[176,235], which in turn could affect various cellular processes. The potential existence of multiple defects in ORPK cells meant that the exact cause of increased protease activity in these cells would be difficult to identify; therefore, the mechanism of elevated aggrecan proteolysis in ORPK cells was not investigated further in this thesis.

Another possible explanation for the lack of effect of IFT88 and KIF3A knockdown on protease activity is that proteins were only partially depleted, with around 20% of control levels of IFT88 protein remaining in siIFT88 cells. Furthermore, the estimated knockdown efficiency at protein

level could have been incorrect due to the non-linearity of β-actin signal that was used as a loading control. This explanation is unlikely as TTBK2 knockdown resulted in increased AGEG generation and was the least efficient at RNA level, but the use of null cells or improving siRNA knockdown efficiency would provide further certainty that IFT88, KIF3A and NPHP4 do not have a role in regulating protease activity.

3.3.4 TTBK2 is a regulator of aggrecanolytic ADAMTS-5 activity

Whilst the primary cilium itself was not required for the regulation of protease activity in the mouse chondrocyte cell line, I found evidence that the centriolar kinase TTBK2 is involved in regulating aggrecan proteolysis. Knockdown of *Ttbk2* increased AGEG generation by three-fold in initial experiments, and then six-fold in later experiments, in which AGEG signal was normalised to total protein to control for differences in loading, and a less variable western blot detection method was used. This increase in AGEG generation was abolished upon combined knockdown of *Adamts5* and *Ttbk2*, and was therefore mediated by ADAMTS-5.

TTBK2 has not been linked to cartilage degradation in any previous studies. The function of TTBK2 has mainly been investigated in tissues of the central nervous system, as mutations in the *TTBK2* gene cause the neurodegenerative disorder spinocerebellar ataxia 11 (SCA11)[236], and in ciliogenesis. Identification of a TTBK2 mutant mouse with defects in Hh pathway-regulated embryonic patterning by Goetz et al. (2012) led to the discovery of the role of TTBK2 in the initiation of cilia assembly[140]. They found that TTBK2 phosphorylated the centriolar protein CP110, resulting in removal of this protein from the distal centriole and permitting elongation of the axoneme. TTBK2 has subsequently been found to phosphorylate various other proteins involved in ciliogenesis[237]. As knockdown of two other proteins that are essential for cilia assembly, IFT88 and KIF3A, did not affect AGEG generation, it is unlikely that the increased ADAMTS-5 activity observed upon *Ttbk2* knockdown is related to impaired axoneme formation, as discussed above. Knockdown of *Ttbk2* could have resulted in changes to the ultrastructure of

cilia, centrosomes and the surrounding cellular region that in turn disrupted protease activity regulation by an unknown mechanism, but such changes were not detectable by the epifluorescence microscopy used in this thesis.

Studies of the non-ciliary functions of TTBK2 also do not provide much insight into how knockdown of *Ttbk2* could increase ADAMTS-5 activity. Watanabe et al. (2015) found that TTBK2 is involved in the regulation of microtubule dynamics, and therefore could regulate many different cellular processes, including proliferation[238]. However, cell number did not correlate with AGEG generation upon ciliary gene knockdown, and thus the increased AGEG generation upon *Ttbk2* knockdown is unlikely to be simply due to an increase in the total number of ADAMTS-5-secreting cells. Watanabe et al. (2015) also showed that TTBK2 interacted with components of the endocytic machinery such as subunits of the clathrin adaptor protein 2 (AP-2) complex in rat brain lysates. Furthermore, TTBK2 has been indirectly linked to endocytosis in other studies; for example, Nieding et al. (2016) found that TTBK2 modulates the activity of the glutamate receptor kainate through regulating its plasma membrane abundance, possibly via endocytosis and subsequent RAB5-dependent transport of kainate to the early endosome[239]. Considering these previous results, together with the Wann group's previous findings that mutation of IFT88 in ORPK cells resulted in impaired LRP-1-mediated endocytosis of proteases, I hypothesised that knockdown of *Ttbk2* increased ADAMTS-5 activity by disrupting endocytic uptake of ADAMTS-5. However, the exact mechanism by which TTBK2 regulates endocytosis and could thus be involved in extracellular protease clearance, is unknown.

To directly determine the cause of elevated AGEG generation upon *Ttbk2* knockdown, I investigated whether various mechanisms of protease activity regulation were disrupted by *Ttbk2* knockdown, including endocytosis, and the results of these experiments are presented in the following chapters.

3.3.5 Strengths and limitations

Detection of the AGEG neoepitope in conditioned media by western blot was shown in this chapter to be a valid indicator of aggrecanolytic protease activity. One advantage of using the AGEG neoepitope is that signal is relatively stable over time, unlike signal of neoepitopes such as KEEE and GLGS, which can disappear at later time points due to further degradation of aggrecan fragments containing these neoepitopes[54]. However, cleavage in the second chondroitin sulfate-rich region of aggrecan to produce the AGEG neoepitope is potentially less important to aggrecan function than cleavage in the interglobular domain, which results in loss of the majority of the aggrecan core protein and is indicated by neoepitopes such as ARGS. Detection of ARGS was assumed to be impossible in this experimental system due to differences in the interglobular domain amino acid sequences of mouse and bovine aggrecan. Specifically, mouse proteases secreted by the chondrocyte cell lines used here cleave a site in the mouse interglobular domain to produce the ALGS neoepitope, and therefore may not recognise the ARGS sequence found in bovine aggrecan as a cleavage site.

The major limitation of using AGEG detection by western blot to detect proteolytic aggrecan degradation was the high level of variation in AGEG signal across samples. This variability was likely introduced at a number of points during the experiment, such as loss of protein during the precipitation steps required for AGEG neoepitope detection, impaired protein separation by SDS-PAGE due to improper sample deglycosylation, and the absence of a loading control. Normalisation of the AGEG signal to the Revert total protein stain thus helped to reduce variation between samples, as did the use of near-infrared fluorescence detection, which was associated with less variation between blots than ECL detection and was possibly due to greater control over western blot exposure time. However, AGEG signal was still non-linear with NIR detection, resulting in potential overestimation of larger changes in AGEG and limited detection of small changes in AGEG. Therefore, measurement of protease activity using an additional assay

would help to provide more certainty that the differences in ADAMTS-5 activity observed in this chapter are real.

Two alternative approaches for measuring aggrecanolytic protease activity in the mouse chondrocyte cell line were tested. Measurement of sGAG release with the DMMB assay was used as an indicator of degradation of aggrecan in porcine cartilage explants by proteases secreted by cells of WT and ORPK chondrocyte cell lines. However, the limited sensitivity of the assay and passive sGAG release from explants led to even higher levels of variation and a reduced ability to detect differences in protease activity compared to western blotting. Whilst a statistically significant, 6-fold increase in AGEG generation was observed in ORPK cells relative to WT cells by western blot, sGAG release by ORPK cells corrected for passive explant release was not statistically significantly different to that of WT cells.

Detection of chondroitinase-resistant chondroitin sulfate stubs using the 2B6 antibody was also tested as an indicator of general aggrecanolytic activity, although it was not used further due to the limited sensitivity of the assay. Other approaches that have been used for measuring protease activity include enzyme-linked immunosorbent assays (ELISAs)[60,240,241]. These are more quantitative than western blotting but are based on detection of the ARGS neoepitope, which is not possible in the experimental system in this chapter as discussed above. Another possible approach, which is not based on detection of neoepitopes, is the use of peptide probes that fluoresce upon cleavage by selected proteases. For example, MMP-selective probes have been used to detect protease activity *in vitro* and *in vivo* in mouse models of rheumatoid arthritis[242] and osteoarthritis[243], with probe activation correlating with histological cartilage damage during disease progression in both models.

3.3.6 Conclusions

In this chapter, I have shown that the aggrecan overlay assay and subsequent neoepitope detection is a valid method for measuring aggrecanolytic protease activity in a mouse

chondrocyte cell line. This meant that detection of the AGEG neoepitope in this assay could then be used to identify ciliary proteins that regulate protease activity. Knockdown of IFT88, KIF3A or *Nphp4* with siRNAs had no effect on protease activity despite resulting in reduced cilia assembly, thus providing evidence that the cilium itself is not involved in the regulation of proteases. In contrast, knockdown of *Ttbk2* resulted in elevated AGEG generation, which was further increased when variation in the assay was reduced through the use of a loading control. This increase in AGEG generation was abolished upon combined knockdown of ADAMTS-5. Therefore, TTBK2 was identified as a novel regulator of ADAMTS-5 activity.

As few proteins have been shown to be directly involved in the regulation of protease activity, the study of how TTBK2 regulates ADAMTS-5 activity could provide further insight into the molecular mechanisms by which protease activity is regulated in cartilage. Confirmation of this result in an experimental system that better preserves the physiological chondrocyte phenotype and use of an alternative protease activity assay would help to determine the physiological relevance and reproducibility of this result.

In the following chapters, I investigated whether processes known to regulate ADAMTS-5 activity were disturbed upon *Ttbk2* knockdown and contributed to the elevated protease activity observed in this chapter.

CHAPTER 4

Investigation of endocytosis-independent mechanisms of ADAMTS-5 activity regulation upon *Ttbk2* knockdown

4.1 Introduction

In the previous chapter, I found that knockdown of *Ttbk2* in a mouse chondrocyte cell line increased aggrecan degradation by ADAMTS-5. I hypothesised that TTBK2 regulates ADAMTS-5 activity through regulation of LRP-1-mediated endocytosis of proteases, as the Wann group has previously observed that this process is impaired upon mutation of another ciliary protein, IFT88, in ORPK cells[193], and TTBK2 has been shown to interact with components of the endocytic machinery[238].

However, there is evidence that disruption of TTBK2 affects cellular processes that in turn have been linked to endocytosis-independent mechanisms of protease activity regulation. For example, TTBK2 mutant mice had embryonic defects characteristic of altered Hh pathway signalling, such as loss of ventral neural cell types[140], and modulation of Hh signalling has been shown to affect proteolytic cartilage degradation *in vivo*, as discussed in Section 1.3.3. Specifically, Lin et al. (2009) found that genetic activation of the Hh pathway increased proteoglycan loss, aggrecan and collagen neoepitope generation, and *Adamts5* expression in adult mice[75]. Furthermore, the elevated *ADAMTS5* expression in human osteoarthritic cartilage explants stimulated with recombinant Ihh was reduced upon knockdown of the transcription factor RUNX2, indicating that the Hh pathway could regulate protease activity through upregulation of protease expression at RNA level.

As discussed in Section 1.2, post-transcriptional mechanisms may also make an important contribution to the regulation of protease activity, as some studies have reported that changes in protease RNA levels do not always correlate with activity. For example, Ismail et al. (2015) found that aggrecan neoepitope generation by primary human chondrocytes in response to IL-1 was mediated by ADAMTS-5, but *ADAMTS5* expression was unchanged relative to non-IL-1-treated cells[60]. ADAMTS-5 activity is post-transcriptionally regulated directly by the endogenous protease inhibitor TIMP-3, which has been shown to inhibit aggrecan neoepitope generation by

recombinant ADAMTS-5 and ADAMTS-4 *in vitro*[98] and in IL-1-stimulated porcine cartilage explants[99]. Deletion of TIMP-3 in mice also increased cartilage matrix degradation and generation of aggrecan and collagen neoepitopes[100], illustrating the importance of TIMP-3 in cartilage matrix homeostasis *in vivo*. Disruption of TIMP-3 may also occur during the development of osteoarthritis, as Morris et al. (2010) found that protein levels of TIMP-3 were reduced in more damaged regions of human osteoarthritic cartilage relative to regions of lower grade damage[103]. ADAMTS-5 activity is also regulated through post-transcriptional activation of the inactive ADAMTS-5 zymogen through cleavage of the C-terminal prodomain. The proprotein convertase responsible for ADAMTS-5 activation has not been definitively identified, and candidates include furin[96] and PACE4[95].

In summary, ADAMTS-5 activity can be regulated at a number of different levels, not just via endocytosis.

4.1.1 Aims and objectives

In this chapter, I aimed to determine whether knockdown of *Ttbk2* increased ADAMTS-5-mediated aggrecan proteolysis through disruption of endocytosis-independent mechanisms that regulate ADAMTS-5 activity.

My first objective in addressing this aim was to investigate the expression of *Adamts5* at RNA level upon *Ttbk2* knockdown in a mouse chondrocyte cell line, and then test whether any changes in *Adamts5* transcription contributed to increased aggrecan proteolysis. The second objective was to test the effect of activation of the Hh signalling pathway in the mouse chondrocyte cell line on AGEG neoepitope generation, and to determine whether the Hh pathway was activated upon *Ttbk2* knockdown. The third objective was to assess the effect of *Ttbk2* knockdown on levels of the endogenous protease inhibitor TIMP-3. The final objective was to investigate activation of ADAMTS-5 upon *Ttbk2* knockdown.

4.2 Results

4.2.1 Increased *Adamts5* RNA expression upon *Ttbk2* knockdown did not contribute to increased AGEG generation

To determine whether the increased aggrecan proteolysis in *Ttbk2* knockdown cells observed in Chapter 3 was due to changes in transcriptional regulation of ADAMTS-5 activity, I measured the expression of *Adamts5* at RNA level using qPCR. *Adamts5* RNA levels upon ciliary gene knockdown were compared to test whether there was a correlation between transcriptional changes and AGEG generation in my experimental system. siTTBK2 cells exhibited around a 20% increase in *Adamts5* RNA expression relative to siCtrl cells, although this increase was not statistically significant (Figure 4.1, p=0.0738). A similar increase in *Adamts5* expression was observed upon KIF3A knockdown (Figure 4.1, p=0.3058), which had no effect on AGEG production (Figure 3.13, p.97). In contrast, median *Adamts5* expression in ORPK cells, which generated high levels of AGEG, was not statistically significantly different to WT cells, although expression was variable across samples (Figure 4.1, p>0.9999). Therefore, whilst knockdown of *Ttbk2* resulted in a small increase in *Adamts5* expression, there was no correlation between AGEG generation and *Adamts5* expression across cells in which ciliary genes were disrupted.

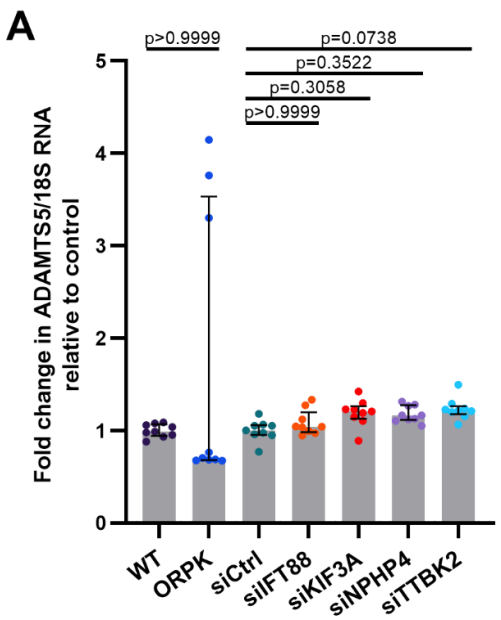

Figure 4.1 Knockdown of *Ttbk2* increased *Adamts5* RNA expression by 20%. RNA was isolated from siRNA-treated cells incubated with 50 µg/ml aggrecan for 24 hours. Expression of *Adamts5* RNA was measured by qPCR, then normalised to *18s* expression and presented as a fold change relative to control (WT for ORPK; siCtrl for all other conditions). Median ± IQR, three independent experiments conducted in triplicate using separate cell subcultures (n=9). p values shown on graph, Kruskal-Wallis test with Dunn's multiple comparisons test.

To directly test whether increased *Adamts5* expression contributed to elevated ADAMTS-5 activity upon *Ttbk2* knockdown, AGEG generation was measured when siCtrl and siTTBK2 cells were treated with the transcriptional inhibitor actinomycin D or the vehicle control DMSO during the aggrecan overlay assay. Cells treated with 1 or 5 µg/ml actinomycin D exhibited a large, statistically significant reduction in expression of the reference gene *18s* relative to vehicle-treated cells, thus validating actinomycin D as a transcriptional inhibitor in this experimental system (Figure 4.2A, p>0.0001). In this experiment, *Ttbk2* knockdown in vehicle-treated cells did not affect *Adamts5* expression relative to vehicle-treated siCtrl cells (Figure 4.2B).

A two-fold increase in AGEG generation was observed upon *Ttbk2* knockdown, although as seen in Chapter 3, this was again not statistically significant (Figure 4.3, p=0.9076). Treatment with 1 or 5 µg/ml actinomycin D resulted in a large reduction in *Adamts5* transcription in both siCtrl

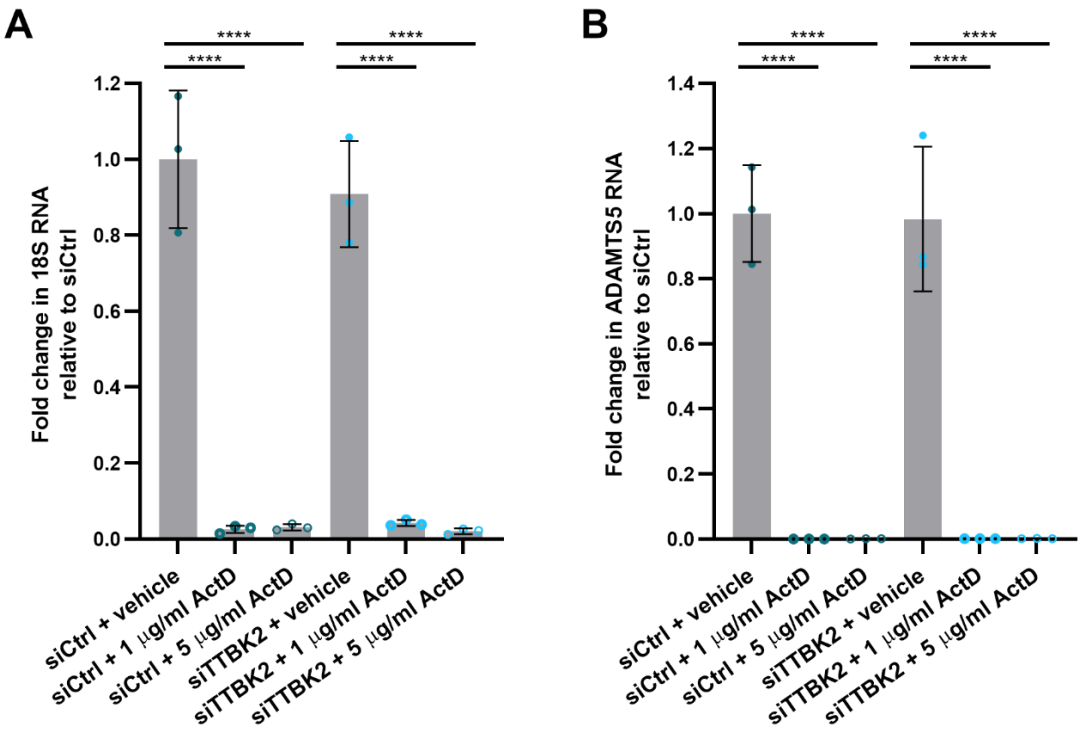

Figure 4.2 Actinomycin D inhibited transcription of *Adamts5*. *A*) RNA was isolated from siCtrl and siTTBK2 cells after incubation with 50 µg/ml aggrecan with or without DMSO, 1 µg/ml actinomycin D or 5 µg/ml actinomycin D, for 24 hours. Expression of *18s* or ***B*)** *Adamts5* RNA was measured by qPCR, and presented as a fold change relative to control. Mean ± SD, one experiment conducted in triplicate using one cell subculture (n=3). **** p<0.0001, ns p>0.9999, one-way ANOVA with Tukey's multiple comparisons test.

and siTTBK2 cells (Figure 4.2B, p<0.0001 for all comparisons). This actinomycin D-induced reduction in *Adamts5* expression in siCtrl and siTTBK2 cells did not result in any statistically significant reductions in AGEG generation relative to vehicle-treated cells, as would be expected if ADAMTS-5 activity was transcriptionally regulated over the 24-hour time course of the aggrecan overlay assay (Figure 4.3). Unlike 1 µg/ml actinomycin D, treatment of siTTBK2 cells with 5 µg/ml actinomycin D resulted in a small, 30% reduction in mean AGEG production relative to vehicle-treated siTTBK2 cells (Figure 4.3B), although this was also not statistically significant (p=0.9568) and *Adamts5* expression was the same in siTTBK2 cells treated with 1 or 5 µg/ml actinomycin D (Figure 4.2B). In summary, these results indicate that the increase in *Adamts5* RNA levels observed in siTTBK2 cells did not significantly affect ADAMTS-5 activity during the aggrecan overlay assay, although AGEG levels in this experiment were very variable.

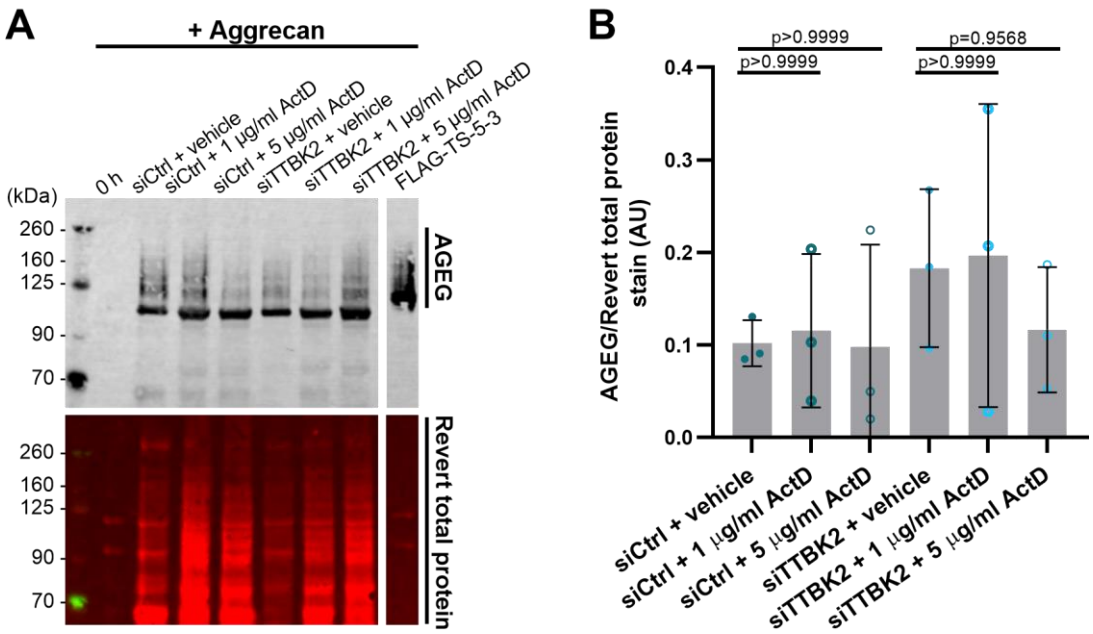

Figure 4.3 Actinomycin D-induced inhibition of *Adamts5* transcription had no effect on AGEG generation upon *Ttbk2* knockdown. *A*) siCtrl and siTTBK2 cells were incubated with 50 µg/ml aggrecan with or without DMSO, 1µg/ml actinomycin D or 5 µg/ml actinomycin, for 24 hours. AGEG neoepitope in conditioned media was detected by western blot with near-infrared fluorescence detection (800 nm channel). Revert total protein stain was imaged in the 700 nm channel. Blot representative of one experiment conducted in triplicate using one cell subculture (n=3). ***B*)** Quantification of AGEG levels in *A*), normalised to Revert total protein stain. Mean ± SD. p values shown on graph, one-way ANOVA with Tukey's multiple comparisons test.

The expression of other proteases capable of generating the AGEG neoepitope was also investigated. Levels of *Adamts4* and *Mmp13* RNA were unaffected in siTTBK2 cells relative to siCtrl cells (Figure 4.4A and C, p>0.9999 and p=0.7901 respectively). *Adamts1* expression was statistically significantly increased only in siTTBK2 cells (Figure 4.4, p=0.0045), with no changes observed in other conditions. However, as indicated by the reduction in *18s* expression upon actinomycin D treatment, the expression of most genes, including *Adamts1*, was possibly inhibited during the assay in Figure 4.3. As actinomycin D treatment did not significantly affect AGEG generation in siTTBK2 cells during this assay, *Adamts1* expression was unlikely to contribute to the increased AGEG generation detected in siTTBK2 cells over 24 hours.

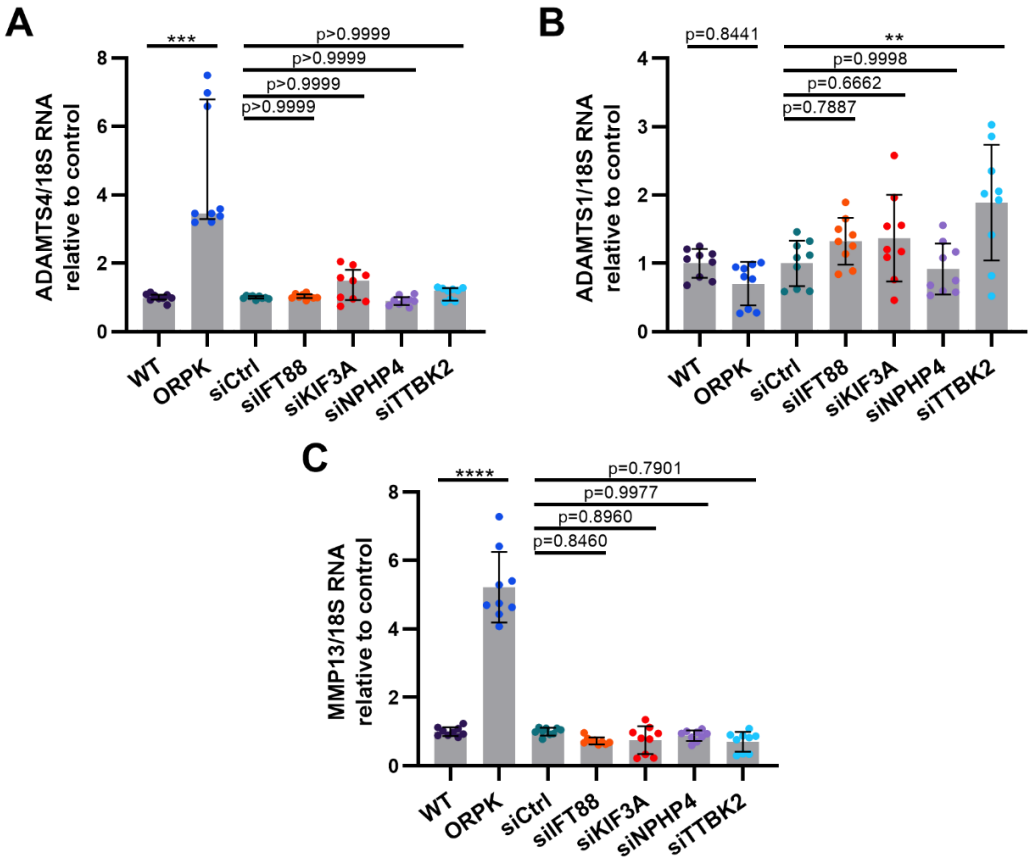

Figure 4.4 Expression of other proteases upon *Ttbk2* knockdown. *A*) RNA was isolated from cells after incubation with 50 µg/ml aggrecan for 24 hours. Expression of *Adamts4*, ***B*)** *Adamts1* or ***C*)** *Mmp13* RNA was measured by qPCR, then normalised to *18s* expression and presented as a fold change relative to control (WT for ORPK; siCtrl for all other conditions). In *A*), median ± IQR. p values shown on graph, Kruskal-Wallis test with Dunn's multiple comparisons test. In *B*) and *C*), mean ± SD. p values shown on graph, one-way ANOVA with Tukey's multiple comparisons test. Three independent experiments were conducted in triplicate using separate cell subcultures (n=9).

4.2.2 Activation of the hedgehog signalling pathway in the mouse chondrocyte cell line did not affect AGEG generation

To determine whether constitutive activation of the Hh pathway contributed to increased ADAMTS-5 activity upon *Ttbk2* knockdown, the expression of the Hh pathway target genes *Ptch1* and *Gli1* was measured by qPCR when ciliary genes were knocked down. To validate that any increased *Ptch1* and *Gli1* expression was indicative of Hh pathway activation, siCtrl cells were incubated with recombinant Ihh (r-Ihh) to directly stimulate the pathway. siCtrl cells exhibited a dose-dependent increase in *Ptch1* and *Gli1* expression upon r-Ihh treatment. Treatment with 1 µg/ml r-Ihh resulted in a statistically significant 30% increase in *Ptch1* expression relative to untreated cells (Figure 4.6A, p=0.0219). The r-Ihh-induced increases in *Gli1* expression were greater than the increases in *Ptch1* expression: treatment with 0.5 or 1 µg/ml r-Ihh statistically significantly increased *Gli1* expression by three- or four-fold respectively (Figure 4.6C, p=0.0049 and p=0.0003).

When ciliary genes were knocked down, no statistically significant differences in baseline *Ptch1* expression were observed, including in siTTBK2 cells (Figure 4.6B, p>0.9999). *Gli1* expression was statistically significantly increased by 60% in siTTBK2 cells relative to siCtrl cells (Figure 4.6D, p=0.0100), indicating that *Ttbk2* knockdown resulted in constitutive Hh pathway activation. However, changes in *Gli1* expression did not correlate with changes in AGEG production, as a similar 60% increase was observed in siKIF3A cells relative to controls cells (p=0.0047).

To directly determine whether constitutive Hh pathway activation upon *Ttbk2* knockdown contributed to increased ADAMTS-5 activity, measurement of AGEG generation was attempted in siTTBK2 cells treated with the Hh pathway inhibitor cyclopamine[208,244]. Whilst treatment of r-Ihh-treated siCtrl cells with 10 µM cyclopamine restored *Ptch1* and *Gli1* expression to the levels observed in vehicle-treated cells (Appendix figure 8, p.226), cyclopamine had no effect on *Ptch1* or *Gli1* expression in siTTBK2 cells (p=0.2694 and p=0.9998 respectively).

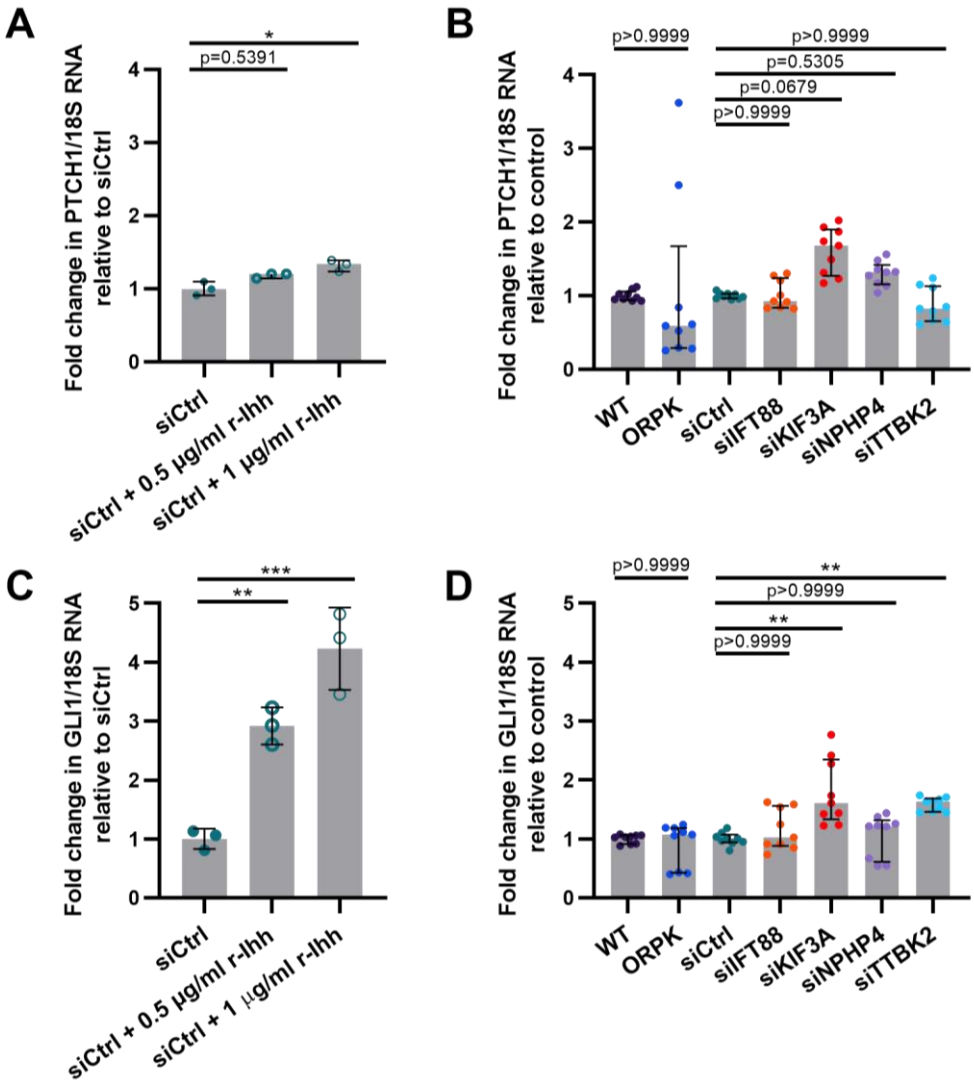

Figure 4.6 Knockdown of *Ttbk2* increased the expression of the hedgehog pathway target gene *Gli1*. *A*) and *B*) RNA was isolated from siRNA-treated cells incubated with or without 0.5 or 1 µg/ml recombinant Indian hedgehog (r-Ihh), after incubation with 50 µg/ml aggrecan for 24 hours. Expression of *Ptch1* or ***C*)** and ***D*)** *Gli1* RNA was measured by qPCR, then normalised to 18S expression and presented as a fold change relative to siCtrl. In *A*), *B*) and *C*), median ± IQR. * p<0.05, ** p<0.01, *** p<0.001, p values >0.05 shown on graph, Kruskal-Wallis test with Dunn's multiple comparisons test. In *D*), mean ± SD. ** p<0.01, p values >0.05 shown on graph, one-way ANOVA with Tukey's multiple comparisons test. Three independent experiments were conducted in triplicate using separate cell subcultures (n=9).

In light of the failure of cyclopamine to inhibit Hh signalling in siTTBK2 cells, the role of Hh pathway activation in increasing ADAMTS-5 activity upon *Ttbk2* knockdown was instead investigated indirectly by measuring AGEG generation when the pathway was activated in siCtrl

cells by r-Ihh. However, treatment of siCtrl cells with 0.5 or 1 µg/ml r-Ihh had no effect on AGEG generation (Figure 4.7, p=0.9886 and p=0.2818 respectively). These results indicated that constitutive activation of the Hh pathway upon *Ttbk2* knockdown did not affect AGEG production in my experimental system.

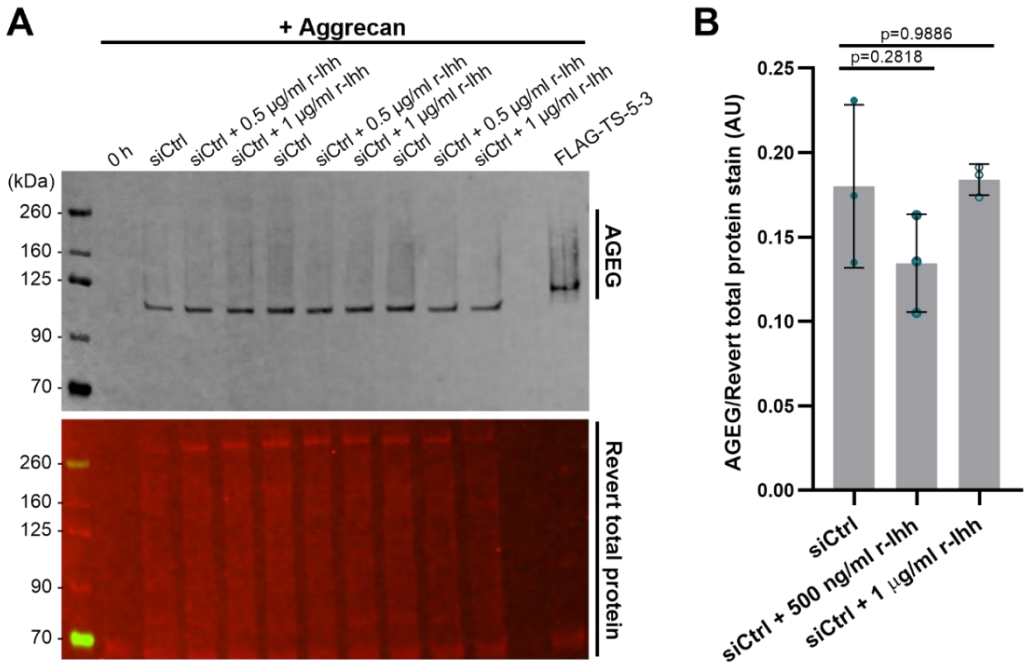

Figure 4.7 Activation of the hedgehog pathway with recombinant Indian hedgehog did not affect AGEG generation in the mouse chondrocyte cell line. ***A***) siCtrl cells treated with or without 0.5 or 1 µg/ml recombinant Indian hedgehog (r-Ihh), were incubated with 50 µg/ml aggrecan for 24 hours. AGEG neoepitope in conditioned media was detected by western blot with near-infrared fluorescence detection (800 nm channel). Revert total protein stain was imaged in the 700 nm channel. Blot representative of one experiment conducted in triplicate using one cell subculture (n=3). ***B***) Quantification of AGEG levels in *A*), normalised to Revert total protein stain. Mean ± SD. p values shown on graph, one-way ANOVA with Tukey's multiple comparisons test.

4.2.3 Knockdown of *Ttbk2* did not affect levels of the endogenous protease inhibitor TIMP-3

Having concluded that the increased ADAMTS-5-mediated aggrecan proteolysis upon *Ttbk2* knockdown was not associated with increased *Adamts5* gene transcription (Figure 4.3), I studied post-transcriptional mechanisms of ADAMTS-5 activity regulation in siTTBK2 cells.

I first tested whether *Ttbk2* knockdown increased *Adamts5* activity through loss of the main endogenous inhibitor of ADAMTS-5, TIMP-3. Extracellular levels of TIMP-3 in conditioned media were measured by western blot using an antibody against TIMP-3. siCtrl cells were treated with the sGAG heparin as a positive control for extracellular TIMP-3 signal, as heparin has been shown to inhibit LRP-1-mediated endocytosis of extracellular TIMP-3[110]. The signal intensity of two bands at the expected molecular weight for the glycosylated and non-glycosylated forms of TIMP-3 (around 24 and 30 kDa respectively) increased upon heparin treatment, thus validating these bands as extracellular TIMP-3 (Figure 4.8A). Quantification of these bands showed that heparin treatment resulted in a 70-fold increase in the median levels of extracellular, non-glycosylated TIMP-3 and a four-fold increase in glycosylated TIMP-3, relative to untreated siCtrl cells (Figure 4.8B and C, p=0.0021 and p=0.0043 respectively). Non-glycosylated and glycosylated TIMP-3 were unaffected by *Ttbk2* knockdown, with only a small increase in both forms of TIMP-3 observed in siTTBK2 cells (p>0.9999 for both comparisons), indicating that the increased ADAMTS-5 activity upon *Ttbk2* knockdown was not due to reduced extracellular TIMP-3 levels.

Western blot analysis of intracellular TIMP-3 in cell lysates was also attempted (Appendix figure 9, p.227). Three bands were detected, and signal intensity of the band at the expected molecular weight of the TIMP-3 dimer (50 kDa) did not change across any of the conditions tested, including siCtrl and siTTBK2 cells (Appendix figure 9B, p=0.9183). However, as TIMP-3-mediated inhibition of ADAMTS-5 occurs in the extracellular matrix, extracellular TIMP-3 is the most

functionally relevant form and thus western blot analysis of intracellular TIMP-3 was not optimised further.

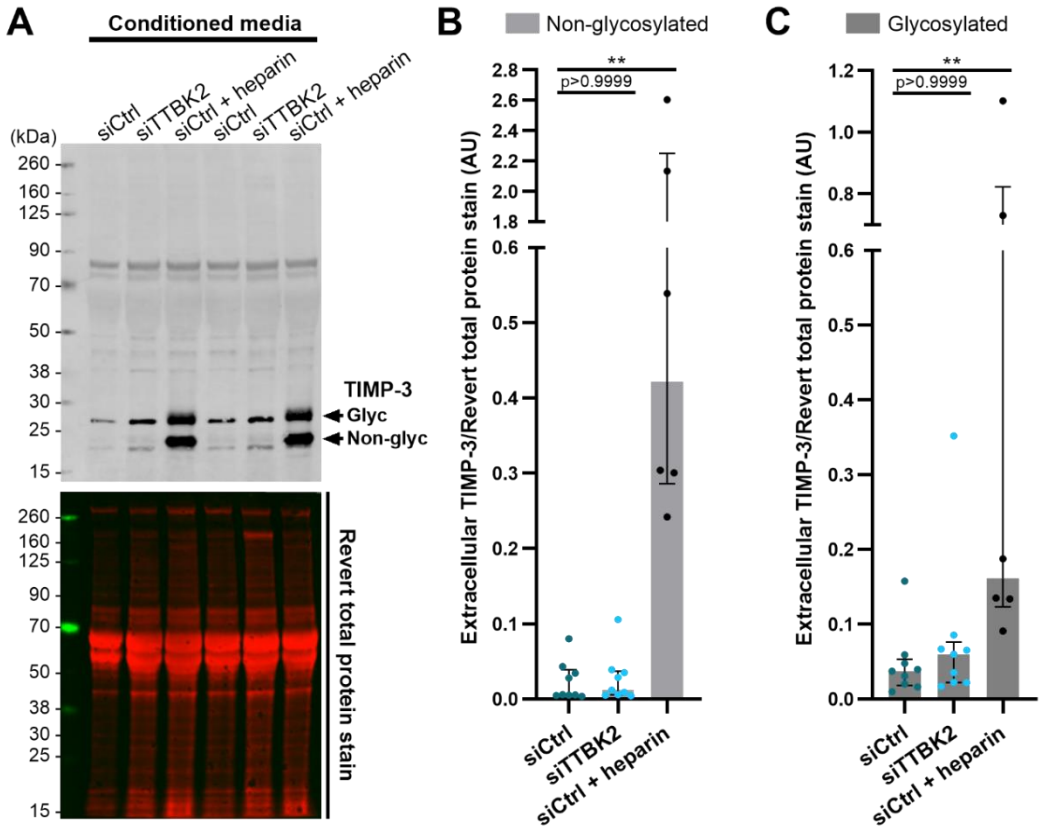

Figure 4.8 Knockdown of *Ttbk2* did not affect extracellular levels of TIMP-3. *A*) siCtrl and siTTBK2 cells were incubated with or without 200 mg/ml heparin in serum-free media for 24 hours. Extracellular TIMP-3 in conditioned media was detected by western blot with near-infrared fluorescence detection (800 nm channel). Revert total protein stain was imaged in the 700 nm channel. Blot shows two sets of replicates representative of three independent experiments conducted in triplicate using separate cell subcultures (n=9). ***B*)** Quantification of non-glycosylated TIMP-3 or ***C*)** glycosylated TIMP-3 in *A*), normalised to Revert total protein stain. Median ± IQR. ** p<0.01, p values >0.05 shown on graph, Kruskal-Wallis test with Dunn's multiple comparisons test.

4.2.4 Measurement of ADAMTS-5 activation

I also tested whether *Ttbk2* knockdown increased ADAMTS-5 activity by increasing the activation of inactive ADAMTS-5 zymogens. As ADAMTS-5 activation has been proposed to occur both in the cytoplasm and extracellularly, detection of pro- and active forms of ADAMTS-5 protein was attempted in cell lysates and conditioned media. During western blot analysis of intracellular ADAMTS-5 in cell lysates, no specific bands sensitive to knockdown of *Adamts5* were observed (Appendix figure 10, p.227), and therefore the effect of *Ttbk2* knockdown on intracellular ADAMTS-5 activation could not be determined.

I then tried to detect extracellular ADAMTS-5 in conditioned media by western blot. Treatment of cells with heparin was used as a positive control for extracellular ADAMTS-5 signal because heparin has been shown to inhibit the endocytosis of extracellular ADAMTS-5 in porcine chondrocytes[117]. The signal intensity of two bands at the expected molecular weight for active ADAMTS-5 (80 kDa) and pro-ADAMTS-5 (100 kDa) increased upon heparin treatment of siCtrl and siTTBK2 cells, but not siADAMTS5 cells (Figure 4.9A), indicating that these bands were pro- and active ADAMTS-5. Bands of a similar size were detected in cells that were not treated with heparin, but signal was very low. Subsequent quantification of these bands and normalisation to total protein showed that there was no difference in pro- and active ADAMTS-5 signal between conditioned media from siCtrl and siADAMTS5 cells (Figure 4.9B, $p>0.9999$). Therefore, levels of ADAMTS-5 protein were too low in cells that were not treated with heparin to be detected above background, and these blots could not be used to make conclusions about activation of ADAMTS-5 upon *Ttbk2* knockdown.

There were other bands of molecular weights below 80 kDa that appear to have increased signal intensity in conditioned media from siCtrl cells. For example, a band of around 65 kDa was present in two of the three siCtrl conditioned media samples analysed but not in siTTBK2 or siADAMTS5 conditioned media (Figure 4.9A, indicated by a single asterisk). Similarly, signal

intensity of a 52 kDa band was increased in some siCtrl conditioned media samples relative to siTTBK2 and siADAMTS5 conditioned media, and in heparin-treated siCtrl cells (Figure 4.9A, double asterisk). These differences in signal intensity of the 65 and 52 kDa bands indicated that there could be more proteolytic processing of active ADAMTS-5 to even smaller forms of the protease, which have been shown to be less active[55], in siCtrl cells relative to siTTBK2 cells.

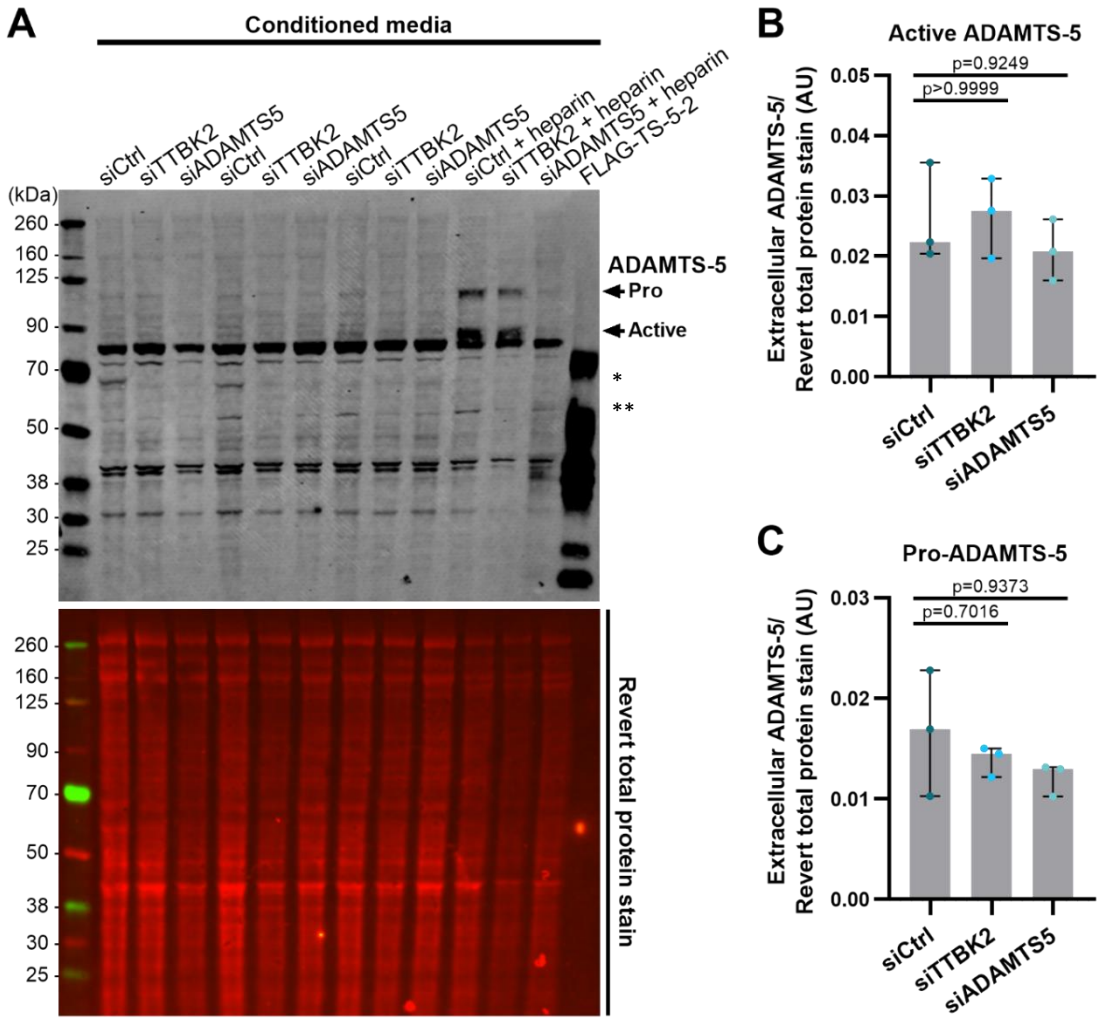

Figure 4.9 Knockdown of *Ttbk2* did not appear to affect extracellular levels of ADAMTS-5. *A*) siCtrl, siTTBK2 and siADAMTS5 were incubated with or without 200 mg/ml heparin in serum-free media for 24 hours. Extracellular ADAMTS-5 in conditioned media was detected by western blot with near-infrared fluorescence detection (800 nm channel). Revert total protein stain was imaged in the 700 nm channel. FLAG-tagged ADAMTS-5-2 was used as a positive control for ADAMTS-5 signal. One experiment conducted in triplicate using one cell subculture (n=3). ***B*)** Quantification of active ADAMTS-5 or ***C*)** pro-ADAMTS-5 in *A*), normalised to Revert total protein stain. Mean ± SD. p values >0.05 shown on graph, one-way ANOVA with Tukey's multiple comparisons test.

However, without more quantitative analysis of the forms of ADAMTS-5 present, especially the highly active full-length form, the relevance of such differences in processing to overall ADAMTS-5 activity could not be determined.

4.3 Discussion

4.3.1 Summary

In this chapter, I aimed to determine whether the endocytosis-independent mechanisms known to regulate ADAMTS-5 activity were disturbed upon *Ttbk2* knockdown in a mouse chondrocyte cell line. I found that inhibition of *Adamts5* transcription with actinomycin D had no effect on the increased AGEG generation observed upon *Ttbk2* knockdown, indicating that increased *Adamts5* expression during the aggrecan overlay assay does not contribute to increased ADAMTS-5 activity. I also showed that, whilst there was evidence of constitutive Hh pathway activation when *Ttbk2* was knocked down, direct activation of Hh signalling with r-Ihh had no effect on AGEG generation in my experimental system. Furthermore, knockdown of *Ttbk2* had no effect on extracellular levels of the physiological ADAMTS-5 inhibitor TIMP-3. Finally, I investigated whether ADAMTS-5 activation was altered by *Ttbk2* knockdown, but extracellular active and pro-ADAMTS-5 could only be detected in positive control samples.

4.3.2 Knockdown of *Ttbk2* increased ADAMTS-5 activity during the aggrecan overlay assay via disruption of post-transcriptional mechanisms

Knockdown of *Ttbk2* increased the expression of *Adamts5* by 20%, which was not statistically significant. Increased *Adamts4* expression was also observed upon *Ttbk2* knockdown, as well as a statistically significant, two-fold increase in *Adamts1* expression. However, as shown in Section 3.2.1, AGEG generation upon *Ttbk2* knockdown was primarily mediated by ADAMTS-5. Previous studies have also shown that the aggrecan-degrading activities of ADAMTS-4 and ADAMTS-1 are much lower than that of ADAMTS-5; for example, in contrast to ADAMTS-5 deletion, ADAMTS-4 or ADAMTS-1 deletion in mouse models of osteoarthritis did not reduce cartilage loss or aggrecan neoepitope generation relative to WT mice[58,69]. I also showed that ADAMTS-4 did not contribute to AGEG generation in my experiments. Therefore, it is likely that increased

expression of *Adamts1* and *Adamts4* did not cause increased AGEG generation upon *Ttbk2* knockdown.

Knockdown of KIF3A increased *Adamts5* expression to a similar extent as *Ttbk2* knockdown, but, as shown in Chapter 3, KIF3A depletion had no effect on AGEG generation. This result implied that increases in *Adamts5* expression during the aggrecan overlay assay did not increase ADAMTS-5 aggrecanolytic activity. Supporting this, AGEG generation upon *Ttbk2* knockdown was not significantly reduced when *Adamts5* expression was inhibited with actinomycin D over the 24-hour time course of the assay. Therefore, the increased aggrecan proteolysis observed upon *Ttbk2* knockdown was due to disruption of post-transcriptional regulation of ADAMTS-5 activity.

These results are consistent with other studies that have shown that ADAMTS-5 activity in cartilage is primarily regulated post-transcriptionally rather than transcriptionally, although few have tested this directly. For example, Naito et al. (2007) found that *ADAMTS5* expression was the same in osteoarthritic and non-osteoarthritic human cartilage[62], and thus did not correlate with the increased ADAMTS-5 activity observed in osteoarthritis, which is demonstrated by the increased generation of aggrecan neoepitopes[245]. Furthermore, Kevorkian et al. (2004) found that expression of both *ADAMTS5* and *ADAMTS4* was statistically significantly downregulated in osteoarthritis[42].

Other studies have observed a lack of correlation between *ADAMTS5* expression and ADAMTS-5 activity *in vitro*. Flannery et al. (1999) showed that treatment of primary human chondrocytes with the pro-catabolic cytokine IL-1 had no effect on *ADAMTS1*, *ADAMTS4* or *ADAMTS5* expression, despite increasing ARGS neoepitope generation[246]. In bovine articular cartilage explants, Tortorella et al. (2001) found that IL-1-induced sGAG release and production of aggrecan neoepitopes were not associated with increased *ADAMTS5* expression[247]. IL-1 treatment did increase *ADAMTS4* expression in this study, but ADAMTS-4 is a less active

aggrecanase than ADAMTS-5[55], and subsequent work by Pratta et al. (2003) showed that IL-1 may regulate ADAMTS-5 activity at post-transcriptional levels by increasing ADAMTS-4 activation[248]. Ismail et al. (2015) also showed that IL-1 regulated ADAMTS-5 activity through post-transcriptional mechanisms. They found that IL-1-induced increases in AGEG and ARGS neoepitope production in primary human chondrocytes were mediated by ADAMTS-5, but occurred independently of changes in *ADAMTS5* expression[60]. Instead, IL-1 stimulation resulted in activation of JNK2 signalling, which in turn impaired LRP-1-mediated endocytosis of extracellular ADAMTS-5 protein by increasing shedding of the LRP-1 receptor.

Proteins that are directly involved in *ADAMTS5* transcription may also affect post-transcriptional regulation of ADAMTS-5 activity. For example, Kobayashi et al. (2013) identified the NFκB family member RelA as the transcription factor that most strongly induces *ADAMTS5* promoter activity[89]. Inhibition of IL-1-induced proteoglycan release upon deletion of RelA in primary mouse chondrocytes was associated with reduced *Adamts5* expression, but, as the authors mentioned, could also have been due to reduced activation of pro-ADAMTS-5 by the RelA-induced protease, MMP-3[249].

In contrast to the studies discussed above, other groups have shown that *ADAMTS5* and *ADAMTS4* expression was upregulated in osteoarthritic cartilage relative to non-osteoarthritic cartilage[61], and correlated with severity of cartilage degeneration in disease[63]. IL-1 has also been shown to increase *ADAMTS4* and *ADAMTS5* expression in isolated human chondrocytes[250]. These differences in results could have occurred due to the high levels of variation associated with human samples, differences in techniques used to measure expression, and differences in the number of samples analysed. But, as illustrated by the work of Ismail et al. (2015) and other groups, the existence of multiple post-transcriptional mechanisms of ADAMTS-5 activity regulation means that protease activity cannot always be inferred from protease expression alone. Measurement of ADAMTS-5-mediated AGEG generation upon direct inhibition of

transcription in the experiments presented in this chapter provides further evidence that transcriptional changes do not always affect aggrecan-degrading protease activity.

4.3.3 Knockdown of *Ttbk2* increased ADAMTS-5 activity via a Hh-independent mechanism

Expression of the Hh pathway target gene *Gli1* was statistically significantly increased upon *Ttbk2* knockdown, indicative of constitutive activation of the pathway. However, as with *Adamts5* expression, Hh pathway target gene expression upon knockdown of other ciliary genes did not correlate with AGEG generation; for example, *Ptch1* and *Gli1* expression were increased when KIF3A was knocked down. Furthermore, direct activation of the Hh pathway in the mouse chondrocyte cell line with r-Ihh had no effect on AGEG generation. Taken together, these results indicate that the increased ADAMTS-5 activity upon *Ttbk2* knockdown was not due to constitutive Hh pathway activation.

My findings are consistent with the results of Thompson et al. (2015), who showed that sGAG release from bovine or human articular cartilage explants was unaffected by activation of the Hh pathway with r-Ihh or inhibition of any constitutive Hh signalling with cyclopamine[192]. Members of the Wann group have also recently shown that increased Hh pathway signalling caused by post-natal, cartilage-specific deletion of IFT88 in mice, was not associated with increased aggrecanase-generated NVTEGE neoepitope staining in articular cartilage[178].

However, other studies have provided direct evidence that modulation of the Hh pathway alters protease activity. For example, Lin et al. (2009) found that genetic activation of the Hh pathway *in vivo* reduced proteoglycan content in articular cartilage, and also increased the generation of the aggrecan neoepitope NVTEGE and the collagen neoepitope C1,2C by immunohistochemistry[75]. Zhou et al. (2014) also showed that inhibition of Hh signalling via cartilage-specific deletion of Ihh in a surgical mouse model of osteoarthritis reduced MMP activity, which was detected using fluorescent activity-based probes[185]. More indirect,

correlative evidence came from work with human cartilage samples. Expression of *PTCH1* and *GLI1* was increased in the most severely histologically damaged areas of osteoarthritic human cartilage relative to the least affected areas[75], and immunohistochemical staining of cartilage showed that Ihh levels increased with severity of osteoarthritis[184]. Weber et al. (2020) also found that the Hh agonist Smoothened agonist (SAG) increased generation of the C1,2C type II collagen neoepitope and the NITEGE aggrecan neoepitope in porcine cartilage explants by western blot[251]. However, the lack of molecular weight markers and absence of positive or negative controls for protease activity make it difficult to confirm the identity of the immunoreactive bands presented in this study.

The difference between my results showing that Hh pathway activation does not increase aggrecan proteolysis, and the results of studies such as that of Lin et al. (2009), could be due to the presence of additional factors *in vivo* that link Hh pathway activation to protease activity regulation. One such factor could be mechanical loading, which was absent in the unloaded cells of my experimental system, given that mechanical strain has been shown to activate the Hh pathway in isolated chondrocytes[216]. Replication of my experiments in mechanically loaded cells could help to further understand these differences. Also, as proposed by Thompson et al. (2015), another factor missing from *in vitro* experimental systems is the long-term effects on chondrocyte differentiation caused by modulation of Hh signalling[192]. To determine whether increased Hh signalling induced by loss of cilia is responsible for cartilage matrix degradation *in vivo*, future studies should directly measure protease activity upon disruption of ciliary proteins with and without pharmacological Hh inhibition. To directly measure protease activity, neoepitope antibody staining or protease-activated fluorescent peptide probes that have been used for *in vivo* imaging of MMP activity[243], could be used.

Another explanation is that the main mechanisms by which Hh signalling regulates protease activity are transcriptional, whereas ADAMTS-5 activity was not transcriptionally regulated

during the time course of my experiments. These mechanisms include activation of the transcription factor RUNX2, which regulated *ADAMTS5* promoter activity[73] and interacted directly with GLI2 *in vitro*[252]. Other mechanisms proposed control of protease transcription through regulation of the Wnt pathway[187] and the cholesterol biosynthesis pathway[186].

In summary, activation of the Hh pathway upon *Ttbk2* knockdown in my experiments did not contribute to increased ADAMTS-5 activity.

4.3.4 Knockdown of *Ttbk2* increased ADAMTS-5 activity via a TIMP-3-independent mechanism

After finding that *Ttbk2* knockdown increased ADAMTS-5 activity via a post-transcriptional mechanism, I investigated whether this increased ADAMTS-5 activity was due to loss of the main endogenous ADAMTS-5 inhibitor, TIMP-3[98].

Heparin treatment of the mouse chondrocyte cell line increased extracellular levels of TIMP-3, as expected based on previous observations that GAGs such as heparin inhibit LRP-1-mediated endocytosis of TIMP-3[104,105]. *Ttbk2* knockdown had no effect on extracellular levels of either glycosylated or non-glycosylated TIMP-3, which have been shown to have the same capacity for inhibiting ADAMTS-4 and ADAMTS-5 activity[253]. This was not surprising as TTBK2 has not been directly linked to TIMP-3 in any previous studies. The *Timp3* gene is upregulated by Hh pathway signalling[254], which was constitutively active upon *Ttbk2* knockdown. However, I did not observe significant increases in TIMP-3 when *Ttbk2* was knocked down, and such an increase would not explain the increase in ADAMTS-5 activity in these cells. Therefore, the increased AGEG generation when *Ttbk2* was knocked down in my experiments was not due to impaired inhibition of ADAMTS-5 via reduced levels of extracellular TIMP-3.

4.3.5 Knockdown of *Ttbk2* did not appear to affect extracellular activation of ADAMTS-5

I also tested whether *Ttbk2* knockdown resulted in upregulation of another post-transcriptional mechanism: activation of inactive pro-ADAMTS-5 by proprotein convertases such as PACE4[95], furin and PC7[96], which have not previously been linked to TTBK2 or other ciliary proteins. These candidate proprotein convertases can act intracellularly, at the cell surface, or in the extracellular environment[255], so I tried to measure pro- and active-ADAMTS-5 levels in cell lysates and conditioned media.

As expected based on previous work showing that heparin inhibited ADAMTS-5 uptake in porcine chondrocytes[117], treatment of cells with heparin in my experiments increased levels of pro- and active ADAMTS-5 in conditioned media, but not upon *Adamts5* knockdown. However, no striking changes in extracellular levels of pro- or active ADAMTS5 were detected in heparin-treated cells upon *Ttbk2* knockdown, and almost no specific signal was detected in conditioned media from non-heparin-treated cells. No specific bands were detected in cell lysates, as signal was unaffected by *Adamts5* knockdown. Therefore, to determine whether increased ADAMTS-5 activation contributed to increased ADAMTS-5 activity upon *Ttbk2* knockdown, more sensitive methods of measuring pro- and active ADAMTS-5 levels would be required.

Bands at lower molecular weights than active ADAMTS-5 were detected in conditioned media from control cells. The signal intensity of these bands was reduced upon knockdown of *Ttbk2* but also *Adamts5*. Therefore, these bands could represent further-processed forms of active ADAMTS-5, although the use of other controls such as a secondary antibody-only blot or pre-incubation of membranes with a blocking peptide, would give more confidence that these bands are specific. These smaller forms of ADAMTS-5 may have reduced activity, as Gendron et al. (2007) found that sequential deletion of the ADAMTS-5 C-terminal ancillary domains resulted in progressively lower aggrecan proteolysis *in vitro*[55]. Domain deletion ADAMTS-4 mutant

proteases also have variable aggrecanolytic activity[256], and small forms of ADAMTS-4 have been detected in human articular cartilage[91] and in porcine chondrocyte cultures[257]. These observations therefore raise the possibility that the increased ADAMTS-5 activity upon *Ttbk2* knockdown could be due to reduced C-terminal processing of ADAMTS-5 relative to control cells. However, development of a more sensitive, quantitative method of detecting forms of ADAMTS-5 is required to test this.

4.3.6 Strengths and limitations

I decided to directly test whether the 20% increase in *Adamts5* expression contributed to increased AGEG generation upon *Ttbk2* knockdown because upregulation of *Adamts5* expression does not always correlate with increased expression, as discussed above (Section 4.3.2). To do this, I measured AGEG generation when cells were treated with 1 or 5 μg/ml actinomycin D, as 1 μg/ml actinomycin D has been shown to inhibit the transcription of most RNA species, including mRNA, using radiolabelling assays[206]. Whilst actinomycin D treatment had no effect on mean AGEG generation during the aggrecan overlay assay in control cells or upon *Ttbk2* knockdown, AGEG levels were more variable in treated cells compared to untreated cells. This could have been due to inhibited transcription of other genes encoding proteins involved in protease activity regulation, as actinomycin D is a non-selective inhibitor. This lack of selectivity was demonstrated by inhibition of not only *Adamts5* expression, but also expression of the *18*s reference gene in treated cells. Also, actinomycin D could have also disrupted transcriptional processes essential for cell survival, as 24-hour treatment of primary human chondrocytes with 0.2 μg/ml actinomycin D was previously shown to increase cell death[258]. These potential off-target effects and cytotoxicity of actinomycin D make it difficult to determine whether my results were indicative of inhibition of *Adamts5* transcription alone. To address this, inducible *Adamts5* knockdown could be used to more selectively inhibit *Adamts5* transcription during the aggrecan overlay assay.

Another approach to assess the functional consequences of increased *Adamts5* expression upon *Ttbk2* knockdown without the use of pharmacological agents, would be to measure levels of ADAMTS-5 protein during the 24-hour time course of the aggrecan overlay assay. This approach would help to determine whether the increased ADAMTS-5 activity upon *Ttbk2* knockdown was caused by increased ADAMTS-5 protein synthesis due to increased *Adamts5* transcription, or by post-transcriptional dysregulation of existing ADAMTS-5 synthesised before the start of the assay. As ADAMTS-5 could not be detected at protein level, an inhibitor of protein translation, such as cycloheximide, could be used during the aggrecan overlay assay as an alternative way to test whether new ADAMTS-5 synthesis contributed to increased ADAMTS-5 activity upon *Ttbk2* knockdown.

To assess Hh signalling upon *Ttbk2* knockdown, I measured expression of the genes *Gli1* and *Ptch1*, which are both well-characterised targets of the Hh pathway[259]. Only *Gli1* expression was increased upon *Ttbk2* knockdown, so to be more certain that the Hh signalling was constitutively activated, another indicator of pathway activation could have been analysed. An example of this is analysis of levels of full-length and repressor forms of GLI3 by western blot, as Hh pathway activation reduced production of the smaller, repressor form of GLI3 *in vitro* and *in vivo,* which in turn resulted in de-repression of *Gli1* transcription[260].

To directly assess the contribution of constitutive Hh pathway activation to elevated aggrecan proteolysis upon *Ttbk2* knockdown, I tried to measure AGEG production upon inhibition of Hh signalling with cyclopamine. This small molecule has been shown to bind and antagonise the positive effector of the Hh pathway, Smo[244], which results in inhibition of Hh pathway signalling; for example, cyclopamine treatment of fibroblasts *in vitro* resulted in reduced *Gli*- and *Ptch1*-luciferase reporter activity in response to Shh[208]. However, the increased *Gli1* expression observed when *Ttbk2* was knocked down was unaffected by cyclopamine treatment. As cyclopamine reduced *Ptch1* and *Gli1* expression in r-Ihh-treated siCtrl cells, this lack of effect

was not due to the use of an insufficient concentration of cyclopamine (10 μM), which was chosen based on the effective dose previously reported for primary bovine articular chondrocytes[192].

Another possibility is that increased GLI-mediated transcription of Hh targets upon *Ttbk2* knockdown occurred in a Smo-independent manner via non-canonical pathways, which has been observed in the context of cancer. For example, Thayer et al. (2003) showed that cyclopamine treatment of certain pancreatic cancer cell lines did not affect *Gli1* transcription[261]. Also, in normal human fibroblast cell lines, *Gli1* expression could be induced by recombinant TGF-β, which was not affected by cyclopamine[262]. Therefore, inhibition of GLI-mediated transcription with molecules such as GANT61, which is a GLI antagonist that acts downstream of Smo by preventing GLI1 binding to DNA[263], could be required to more definitively determine the contribution of canonical or non-canonical activation of the Hh pathway to increased ADAMTS-5 activity upon *Ttbk2* knockdown.

Another limitation of the experiments in this chapter was the limited sensitivity of detection of ADAMTS-5 protein by western blot. Issues with detection of endogenous ADAMTS-5 have previously been reported; for example, Gendron et al. (2007) could not successfully detect ADAMTS-5 in IL-1α-treated porcine cartilage explants and estimated that large amounts of cartilage would be required for ADAMTS-5 to be present in detectable levels[55]. Some groups have been able to detect endogenous ADAMTS proteases: Kashiwagi et al. (2004) observed bands at the expected molecular weight of ADAMTS-4 in IL-1α-treated pig articular cartilage[256]. Malfait et al. (2002) detected endogenous ADAMTS-5 in the extracellular matrix extracted from normal and osteoarthritic human cartilage, with ADAMTS-4 also observed in osteoarthritic samples only[50]. In conditioned media from primary mouse chondrocytes, Luo et al. (2020) saw bands at the expected molecular weight for ADAMTS-5[264]. However, the identities of the bands in these studies were not validated, such as through knockdown of ADAMTS-5.

Nevertheless, the methods of sample preparation in these studies in which ADAMTS-5 was successfully detected, such as recombinant TIMP-3-mediated affinity purification of ADAMTS-5 in conditioned media described by Kashiwagi et al. (2004), could be useful for measuring ADAMTS-5 protein levels upon *Ttbk2* knockdown in future experiments. Such methods could also enable the use of another indicator of activation, the SISR neoepitope, which is generated at the N-terminus of ADAMTS-5 when the pro-domain is cleaved by proprotein convertases such as PACE4 *in vitro* and *in situ* in bovine cartilage explants[95]. The expression and activity of ADAMTS-5-activating proprotein convertases could also be investigated upon *Ttbk2* knockdown, but evidence of altered activation would first be required to determine the relevance of any changes in furin, PACE4 or other convertases to the increased ADAMTS-5 activity.

4.3.7 Conclusions

In this chapter, I have shown that knockdown of *Ttbk2* increased ADAMTS-5 activity during the aggrecan overlay assay independently of increased *Adamts5* expression. This result further highlights that expression of *Adamts5* at RNA level needs to be measured alongside, rather than instead of, indicators of proteolytic activity. I also showed that the increased ADAMTS-5 activity observed upon *Ttbk2* knockdown was not due to constitutive Hh pathway activation, as r-Ihh-activated Hh signalling did not affect AGEG generation in my experimental system. Identification of an inhibitor of Hh target gene expression when *Ttbk2* is knocked down, and subsequent measurement of aggrecan proteolysis, would be required to more directly address the role of Hh signalling in regulating protease activity in these cells.

Through investigating post-transcriptional mechanisms, I showed that knockdown of *Ttbk2* did not affect extracellular levels of TIMP-3, and therefore the increased ADAMTS-5 activity was not due to loss of TIMP-3-mediated inhibition of the protease. Due to the low sensitivity of ADAMTS-5 protein detection by western blot, I could not make any conclusions about ADAMTS-5 activation upon *Ttbk2* knockdown, and therefore further optimisation of this assay is required.

As most endocytosis-independent mechanisms were ruled out as the process by which knockdown of *Ttbk2* increased ADAMTS-5 activity in this chapter, I next investigated whether *Ttbk2* knockdown impaired endocytosis-dependent regulation of ADAMTS-5 activity.

CHAPTER 5

Investigation of endocytosis-dependent mechanisms of ADAMTS-5 activity regulation upon *Ttbk2* knockdown

5.1 Introduction

In the previous chapter, I found that the increased ADAMTS-5 activity upon knockdown of *Ttbk2* was not associated with changes in protease transcription, Hh signalling or the endogenous protease inhibitor TIMP-3. In this chapter, I tried to determine whether the mechanism by which knockdown of *Ttbk2* increased ADAMTS-5 activity was through impaired endocytosis of ADAMTS-5.

As discussed in Sections 1.2.3 and 1.2.4, studies have shown that the activities of various MMPs and TIMP-3 are regulated by endocytosis mediated by the cell surface receptor LRP-1. Considering these studies and previous observations that ADAMTS-5 activity did not correlate with *Adamts5* expression in cartilage[62], Yamamoto et al. (2013) proposed that ADAMTS-5 activity was regulated post-transcriptionally via regulation of extracellular ADAMTS-5 levels by endocytosis[117]. They observed that dead porcine cartilage explants had increased ADAMTS-5 activity relative to live cartilage, and that this was associated with a reduced ability to clear extracellular, exogenous ADAMTS-5. To determine whether the clearance of ADAMTS-5 in live cartilage was due to endocytosis, they investigated the effect of dynasore. This is an inhibitor of the protein dynamin, which is involved in endocytic vesicle formation in the two main endocytic pathways, clathrin- and caveolae-dependent endocytosis[210]. Dynasore reduced ADAMTS-5 clearance in live cartilage to the level observed in dead cartilage, whereas an inhibitor of caveolae-dependent endocytosis, β-cyclodextrin, had no effect, leading the authors to conclude that ADAMTS-5 clearance was due to clathrin-dependent endocytosis.

Yamamoto et al. (2013) also found that ADAMTS-5 clearance in live porcine cartilage was reduced by the protein RAP. RAP is a physiological competitive antagonist of LDL receptors that is found in the endoplasmic reticulum and acts as a molecular chaperone for LRP-1, inhibiting its ligand-binding ability during trafficking through the secretory pathway before LRP-1 reaches the cell surface[109]. siRNA-mediated knockdown of LRP-1 also reduced ADAMTS-5 endocytosis in

human chondrocytes, albeit to a lesser extent than RAP. However, neither RAP nor LRP-1 knockdown completely inhibited ADAMTS-5 clearance, raising the possibility that LRP-1-independent endocytic pathways might contribute to ADAMTS-5 endocytosis. The existence of such pathways was proposed by Scilabra et al. (2013) in the context of TIMP-3 endocytosis, as they found that, similarly to ADAMTS-5, TIMP-3 endocytosis was not completely inhibited by RAP or in LRP-1-deficient cells[105].

Nevertheless, Yamamoto et al. (2013) concluded that LRP-1-mediated endocytosis had a role in the regulation of the extracellular activity of ADAMTS-5, and subsequently demonstrated the clinical significance of this mechanism of ADAMTS-5 regulation in osteoarthritis. They found that ADAMTS-5 clearance was impaired in osteoarthritic human cartilage relative to healthy cartilage[120]. Shedding of the extracellular, ligand-binding α-chain of the LRP-1 receptor was also increased in osteoarthritic cartilage and, as discussed in Section 1.2.4, LRP-1 receptor shedding has been shown to inhibit the endocytic uptake of MMPs. Antibodies inhibiting the enzymes (known as "sheddases") responsible for LRP-1 cleavage, ADAM-17 and MMP-14, increased the endocytic capacity of osteoarthritic cartilage, demonstrating the translational potential of modulating LRP-1-mediated endocytosis.

Yamamoto et al. (2013) also found that internalised FLAG-tagged ADAMTS-5 in porcine and human chondrocytes colocalised with EEA-1, which is a marker of the sorting site of endocytic cargo, the early endosome[117]. Both FLAG-tagged ADAMTS-5 and EEA1 were mainly, but not exclusively, localised to one region of the cell. The Wann group hypothesised that this region contained the primary cilium because endocytic activity has been detected at the cilium and its surrounding area (the "periciliary" region). For example, Molla-Herman et al. (2010) found that the membrane of the ciliary pocket was enriched with clathrin-coated pits relative to the rest of the plasma membrane[137]. In the WT mouse chondrocyte cell line used in this thesis, the Wann group subsequently found that internalised FLAG-tagged ADAMTS-5 and the transmembrane β-

chain of LRP-1 itself also localised to the cellular region that contained the primary cilium, although EEA1 was evenly distributed throughout the cytoplasm[193]. Impaired cilia assembly in IFT88 mutant ORPK cells was also associated with loss of this concentrated LRP-1 distribution and reduced uptake of FLAG-tagged ADAMTS-5, as well as increased generation of aggrecan neoepitopes.

Following these results, I hypothesised that the periciliary region is a region of highly efficient endocytosis, where the rate of protease endocytosis is increased. There are a number of possible mechanisms by which endocytosis could be more efficient in the periciliary region (Figure 5.1):

1) The enrichment of clathrin-coated pits in the ciliary pocket membrane relative to the rest of the cell, as observed by Molla-Herman et al. (2010)[137], could increase the rate of internalisation of endocytic cargo, such as LRP-1, at the ciliary pocket.
2) The rate of recycling of internalised LRP-1 back to the periciliary membrane could be increased relative to the rest of the plasma membrane, due to the close proximity between the primary cilium and components of the endosomal pathway. These components could include the early endosome, as EEA1 was concentrated at the base of the cilium in primary mouse chondrocytes[195]. The early endosome is where endocytic cargo is sorted and also rapidly recycled directly to the plasma membrane[199]. Recycling endosomes, where internalised membrane proteins are targeted back to the cell surface, have also been shown to interact with the appendages of the mother centriole at the base of the cilium, and disruption of centriolar proteins altered the recycling rate of the transferrin receptor[202]. As discussed in Section 3.3.3, I showed that disruption of the main components of the primary cilium (the axoneme and the ciliary membrane) upon knockdown of ciliary genes was not always associated with increased ADAMTS-5 activity. However, whether there was a correlation between changes in the organisation

of the ciliary pocket and periciliary endosomal compartments potentially caused by knockdown of ciliary genes such as *Ttbk2*, and ADAMTS-5 activity, remained unexplored.

3) Ciliary proteins directly interact with the endocytic machinery. Such proteins could include TTBK2, which has been shown to directly interact with the endocytic machinery, such as clathrin adaptor proteins of the AP-2 complex[238].

I therefore hypothesised that TTBK2 is required for efficient LRP-1-mediated clearance of extracellular proteases, by contributing to the establishment of an area of enhanced endocytosis in the periciliary region.

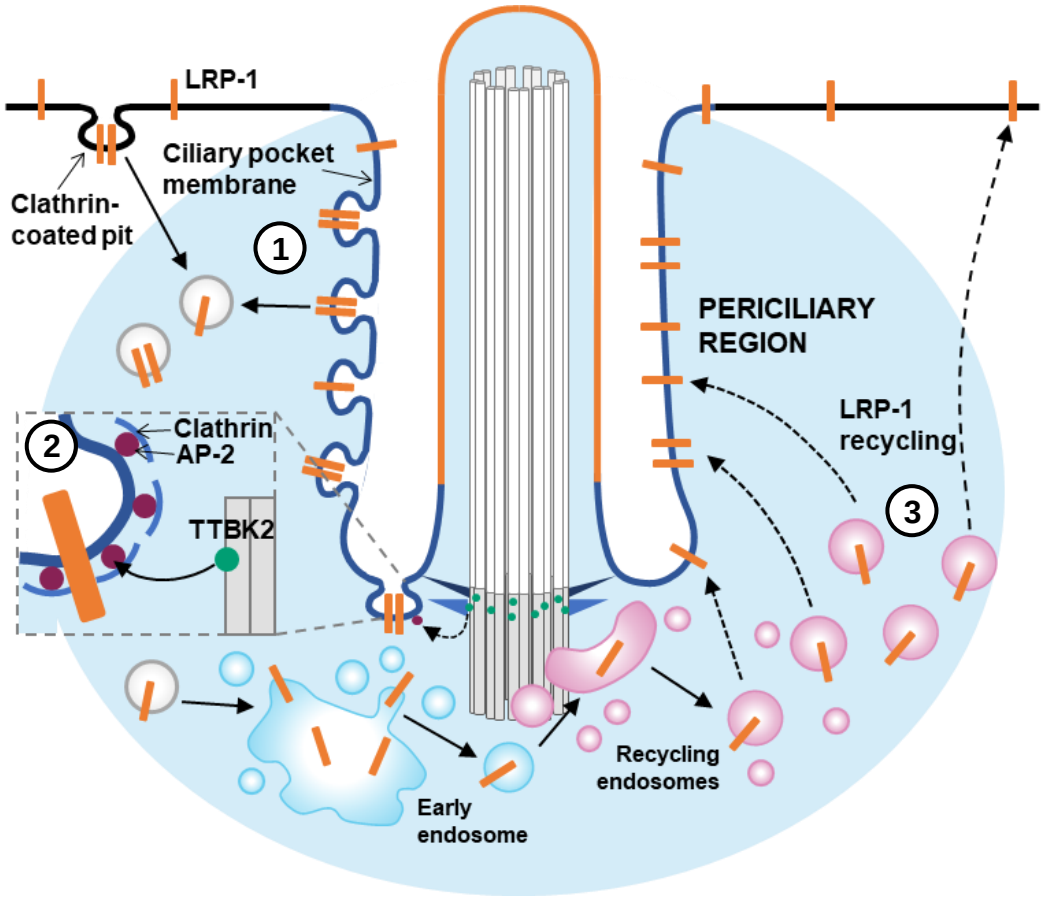

Figure 5.1 Potential mechanisms of enhanced endocytosis in the periciliary region. 1) Internalisation of endocytic cargo could be increased in the periciliary region due to enrichment of clathrin-coated pits in the ciliary pocket membrane, or **2**) via cilia-associated proteins such as TTBK2 interacting directly with the endocytic machinery to stimulate endocytosis in this region. **3**) Recycling of internalised proteins may also be increased at the periciliary membrane due to the close proximity to components of the endosomal pathway, such as the recycling endosome and potentially the early endosome.

5.1.1 Aims and objectives

In this chapter, I tested the hypothesis that knockdown of *Ttbk2* increased ADAMTS-5 activity by impairing LRP-1-mediated endocytosis of ADAMTS-5.

The primary objective of this chapter was to directly measure ADAMTS-5 endocytosis upon *Ttbk2* knockdown in a mouse chondrocyte cell line using the functional assay previously used by Yamamoto et al. (2013) in human and porcine cartilage and chondrocytes[117], and by the Wann group in the same cell line[193]. The assay involved incubating cells with recombinant FLAG-tagged ADAMTS-5 over a time course. Specifically, I used the domain-deletion mutant of ADAMTS-5, ADAMTS-5-3, that was missing the spacer and second thrombospondin domains, but contained the first thrombospondin domain required for endocytosis[117]. To validate the assay, cells were incubated with heparin (Figure 5.2), which almost completely inhibited TIMP-3 clearance in the HTB94 chondrosarcoma cell line[105], and fully inhibited internalisation of FLAG-tagged ADAMTS-5, as assessed by microscopy, in porcine chondrocytes[117]. The endocytosis inhibitor dynasore was also used to validate that clearance of extracellular ADAMTS-5 was the result of endocytosis. siRNA-mediated knockdown of the genes encoding clathrin heavy chain (*Cltc*) or the α1 subunit of the clathrin adaptor protein complex AP-2 (*Ap2α1*), was used to test whether ADAMTS-5 is endocytosed via clathrin-dependent pathways, as seen in previous studies[117]. RAP and knockdown of LRP-1 were used to confirm that LRP-1 was the receptor that predominantly mediated ADAMTS-5 clearance in my experimental system.

Alongside assessing endocytic function, I addressed a secondary objective, which was to examine the expression and localisation of LRP-1 upon *Ttbk2* knockdown. I also measured extracellular levels of LRP-1α to determine the effect of *Ttbk2* knockdown on LRP-1 shedding. To determine whether knockdown of *Ttbk2* affected organisation of endosomal compartments, I attempted to optimise immunofluorescence staining for the early endosome marker EEA1 in the mouse chondrocyte cell line, to clarify the discrepancies in EEA1 distribution between the

Wann group's previous work, and studies in primary porcine chondrocytes[117] and mouse chondrocytes[195].

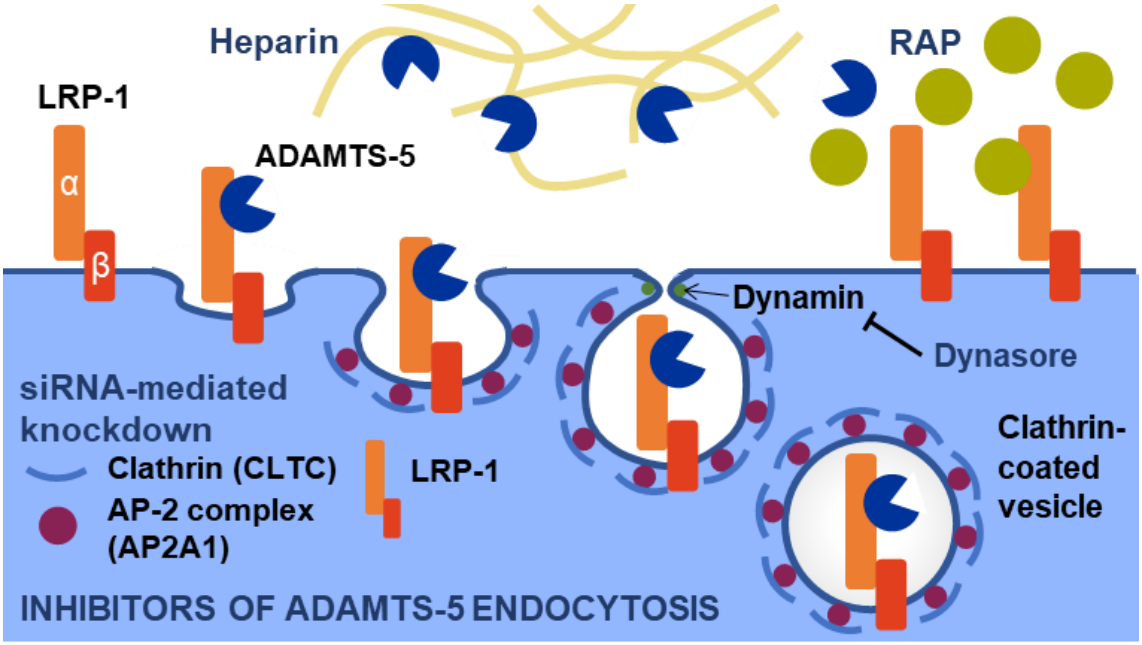

Figure 5.2 Inhibitors of ADAMTS-5 endocytosis. The inhibitors used were heparin, which sequesters ADAMTS-5 extracellularly and reduces binding to LRP-1; dynasore, which inhibits the dynamin protein required for endocytic vesicle formation during clathrin- and caveolae-dependent endocytosis; RAP, which competes with ADAMTS-5 for binding to LRP-1; and siRNA-mediated knockdown of LRP-1 itself, and two proteins crucial for clathrin-dependent endocytosis, clathrin heavy chain (CLTC) and the α1 subunit of the AP-2 complex (AP2A1).

5.2 Results

5.2.1 Validation of an ADAMTS-5 endocytosis assay

To measure endocytosis of ADAMTS-5 in the mouse chondrocyte cell line, cells were incubated with FLAG-ADAMTS-5 over a time course. Levels of extracellular FLAG-ADAMTS-5 in conditioned media were then measured by western blot using an anti-FLAG antibody.

In initial experiments, WT cells were incubated with 10 nM FLAG-tagged ADAMTS-5-3 over the 120-minute time course used in the Wann group's previous experiments with this cell line[193]. A band at the expected molecular weight for FLAG-tagged ADAMTS-5-3 (52 kDa[55]) was observed in conditioned media at the 0-hour time point (Figure 5.3A). Unlike in previous experiments, the levels of extracellular FLAG-ADAMTS-5 in WT conditioned media did not decrease by much across the 120-minute time course, thus limiting the ability to detect differences in endocytic rate between experimental conditions. The time course was therefore extended to 8 hours, and qualitatively larger differences in extracellular FLAG-ADAMTS-5 levels were observed between time points (Figure 5.3B). A similar reduction in extracellular FLAG-ADAMTS-5 over time was observed when an antibody recognising the catalytic domain of ADAMTS-5 was used for western blot analysis of conditioned media (Appendix figure 11, p.228).

Quantification of anti-FLAG blots showed that extracellular FLAG-ADAMTS-5 was rapidly cleared from the media during the first 2 hours of the assay (Figure 5.3C). After this, the rate of clearance began to plateau between 2 and 4 hours, and to a greater extent between 4 and 8 hours. At 8 hours, around 80% of the FLAG-ADAMTS-5 added at the start of the assay had been cleared from the media. However, the non-linearity of FLAG-ADAMTS-5 signal at lower amounts of protein (Appendix figure 12, p.229) could mean that extracellular FLAG-ADAMTS-5 levels were even lower at this time point. The half-life of extracellular FLAG-ADAMTS-5 in WT cells was around 75 minutes.

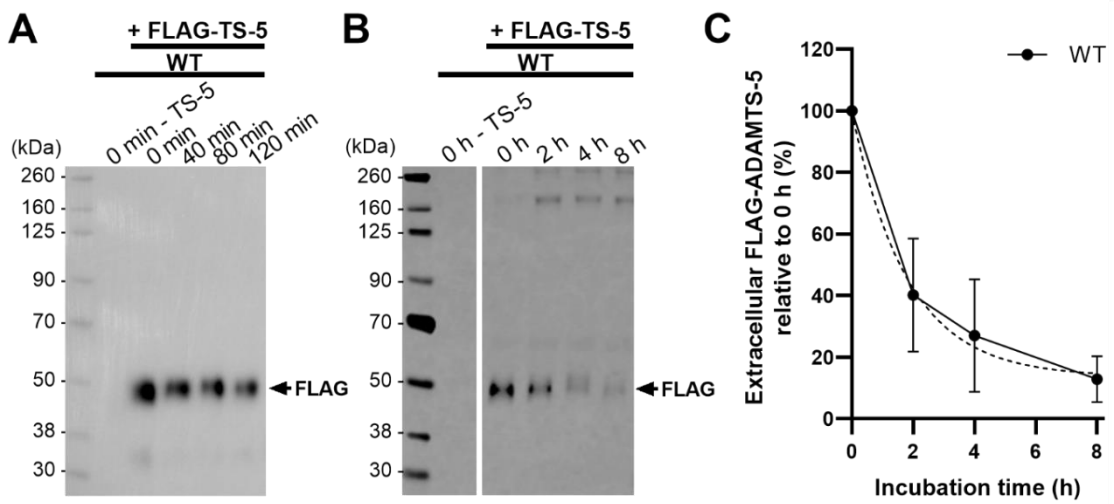

Figure 5.3 Extracellular FLAG-tagged ADAMTS-5 was cleared from the culture medium by WT cells. ***A***) WT cells were incubated with or without 10 nM FLAG-tagged ADAMTS-5-3 in serum-free media for 0, 40, 80 and 120 minutes, or ***B***) 0, 2, 4 and 8 hours. Extracellular levels of FLAG-ADAMTS-5 in conditioned media were detect by western blot using an anti-FLAG antibody. Blots representative of two independent experiments conducted in triplicate using separate cell subcultures (n=6). ***C***) Quantification of extracellular FLAG-ADAMTS-5-3 levels in *B*), calculated as a percentage relative to levels at 0 hours. Mean ± SD, n=6. Dashed line is one-phase exponential decay curve fitted to data, as determined by non-linear regression analysis.

To confirm that the ADAMTS-5 clearance I observed was the result of endocytosis, cells were treated with 200 µg/ml heparin during the assay. Only two time points (2 hours and 8 hours) were analysed due to the limited supply of FLAG-ADAMTS-5. Extracellular levels of FLAG-ADAMTS-5 were qualitatively increased at 2 hours, and to a greater extent at 8 hours, in siCtrl cells treated with heparin relative to untreated cells (Figure 5.4A). Quantification of blots and normalisation to total protein also showed that heparin treatment increased the mean levels of extracellular FLAG-ADAMTS-5, particularly at 8 hours when FLAG-ADAMTS-5 levels in heparin-treated siCtrl cells were double the levels observed in untreated cells (Figure 5.4B). These differences were not statistically significant (p=0.9266 and 0.4333 at 2 and 8 hours respectively), which was possibly due to the high levels of variation in FLAG-ADAMTS-5 signal between the three replicate samples analysed in each condition.

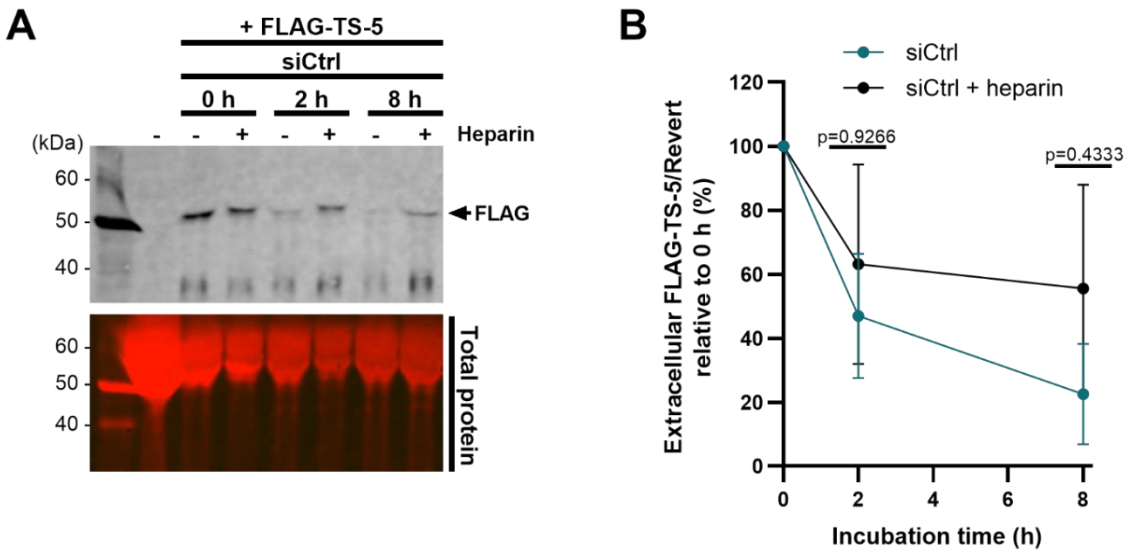

Figure 5.4 Clearance of extracellular FLAG-ADAMTS-5 was inhibited by heparin. ***A***) siCtrl cells were incubated with or without 10 nM FLAG-tagged ADAMTS-5-3 and 200 µg/ml heparin in serum-free media for 0, 2 and 8 hours. Extracellular levels of FLAG-ADAMTS-5 in conditioned media were detected by western blot using an anti-FLAG antibody with near-infrared fluorescence detection (800 nm channel). Revert total protein stain was imaged in the 700 nm channel. Blot representative of one experiment conducted in triplicate using one cell subculture (n=3). ***B***) Quantification of extracellular FLAG-ADAMTS-5-3 levels in *A*), normalised to Revert total protein stain, relative to levels at 0 hours in each condition. Mean ± SD. p values >0.05 shown on graph, one-way ANOVA with Tukey's multiple comparisons test.

To gain further confidence that ADAMTS-5 clearance in these cells was due to endocytosis, dynasore was used to more selectively inhibit endocytic uptake. The ability of dynasore to inhibit endocytosis was first assessed by measuring internalisation of fluorescently labelled transferrin, which has been used as an indicator of endocytic capacity[210]. In untreated WT cells, punctate, peri-nuclear transferrin signal was observed, which increased in intensity over the 90-minute time course, as assessed by epifluorescence microscopy (Appendix figure 13, p.230). However, similar intracellular punctate signal was observed in WT cells treated with dynasore via confocal microscopy, together with large areas of intense signal that were not present in untreated cells. Therefore, in the absence of clear inhibition of transferrin endocytosis, dynasore was not used in the ADAMTS-5 endocytosis assay to conserve FLAG-ADAMTS-5.

5.2.2 ADAMTS-5 clearance was not affected by disruption of clathrin-dependent endocytosis

To determine whether ADAMTS-5 endocytosis occurred via the clathrin-dependent pathway in my experimental system, the clathrin-related endocytic proteins clathrin heavy chain and the α1 subunit of the AP-2 complex were depleted with siRNAs. Expression of *Cltc* and *Ap2a1* RNA was reduced by over 90% relative to siCtrl cells in siCLTC and siAP2A1 cells respectively (Figure 5.5).

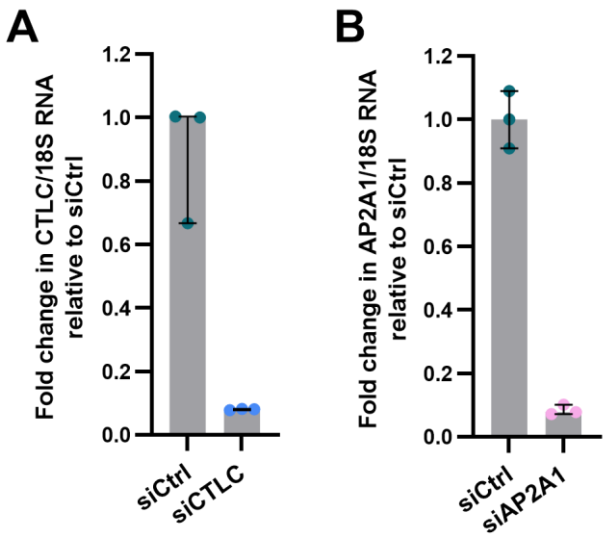

Figure 5.5 siRNA knockdown of clathrin-related endocytic proteins CLTC and AP2A1. ***A***) RNA was isolated from siRNA-treated cells incubated in serum-free media for 24 hours. Expression of *Cltc* or ***B***) *Ap2a1* was measured by qPCR, then normalised to *18s* expression and presented as a fold change relative to siCtrl. Median ± IQR, one experiment conducted in triplicate using one cell subculture (n=3).

Knockdown of *Cltc*, and to a lesser extent *Ap2a1*, also resulted in a reduction in transferrin endocytosis, as less internalised transferrin was observed after 30 and 90 minutes relative to siCtrl cells (Figure 5.6A). There was some intracellular, punctate transferrin signal in siCLTC and siAP2A1 cells, as assessed by confocal microscopy (Figure 5.6B), indicating that transferrin endocytosis was not completely inhibited.

In contrast to the effects on transferrin uptake observed by microscopy, knockdown of *Cltc* and *Ap2a1* had very little effect on FLAG-ADAMTS-5 endocytosis (Figure 5.7A). Quantification and normalisation of FLAG-ADAMTS-5 signal showed that mean levels of extracellular FLAG-ADAMTS-5 were not statistically significantly different upon *Cltc* or *Ap2a1* knockdown relative to siCtrl cells at all time points (Figure 5.7B; p=0.8037, 0.8193 and >0.9999 for siCLTC cells

relative to siCtrl at 2, 4 and 8 hours respectively; p=0.7661, >0.9999 and 0.9904 for siAP2A1 cells).

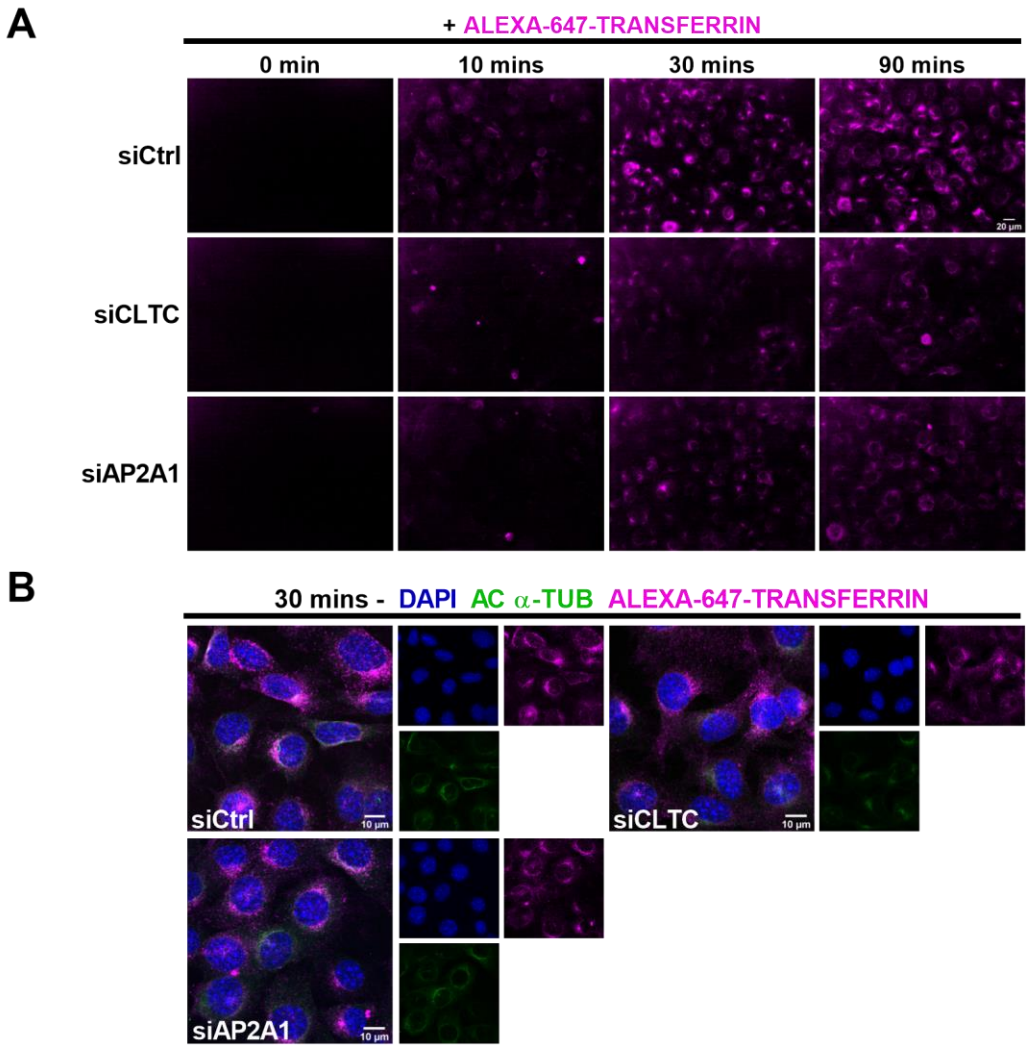

Figure 5.6 Knockdown of *Cltc* or *Ap2a1* partially reduced fluorescently labelled transferrin internalisation. ***A***) siRNA-treated cells were incubated with 10 ng/ml Alexa-647-conjugated transferrrin in serum-free media for 0, 10, 30 or 90 minutes. Cells fixed and imaged by epifluorescence microscopy. Scale bar 20 µm. ***B***) After fixation, cells were stained with antibodies targeting acetylated α-tubulin (green), and counterstained with DAPI (blue) to visualise cell nuclei. Cells were imaged using an Olympus FV1200 confocal microscope across three fields of view. Maximum projection images were created in ImageJ. Images representative of one experiment conducted in triplicate using one cell subculture (n=3). Scale bar 10 µm.

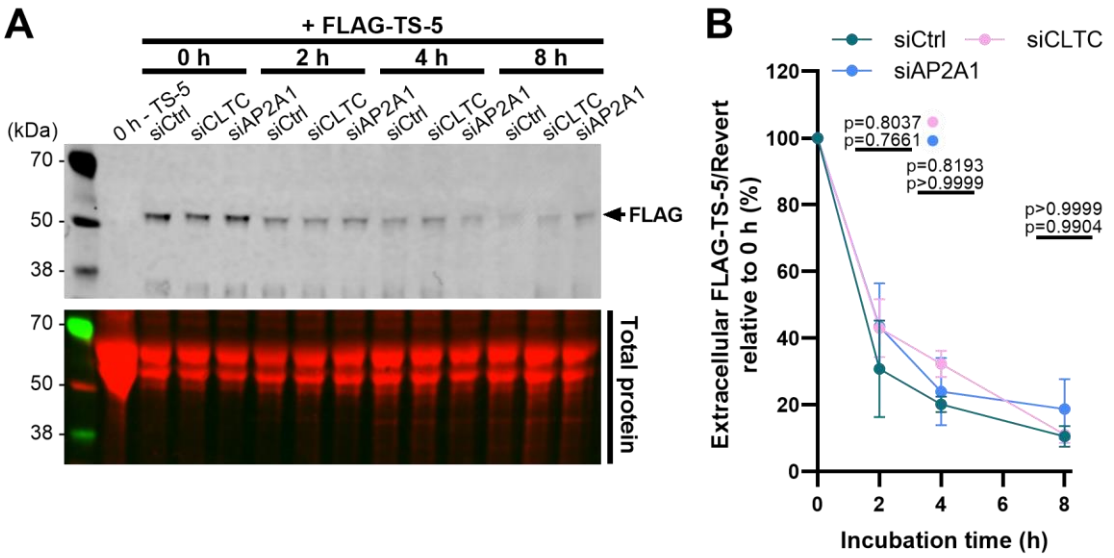

Figure 5.7 Knockdown of *Cltc* or *Ap2a1* did not affect ADAMTS-5 endocytosis. ***A***) siCtrl, siCLTC or siAP2A1 cells were incubated with or without 10 nM FLAG-tagged ADAMTS-5-3 in serum-free media for 0, 2, 4 and 8 hours. Extracellular levels of FLAG-ADAMTS-5 in conditioned media were detected by western blot using an anti-FLAG antibody with near-infrared fluorescence detection (800 nm channel). Revert total protein stain was imaged in the 700 nm channel. Blot representative of one experiment conducted in triplicate using one cell subculture (n=3). ***B***) Quantification of extracellular FLAG-ADAMTS-5-3 levels in *A*), normalised to Revert total protein stain, relative to levels at 0 hours in each condition. Mean ± SD. p values >0.05 shown on graph, one-way ANOVA with Tukey's multiple comparisons test.

5.2.3 ADAMTS-5 clearance was not affected by disruption of LRP-1-dependent endocytosis

To determine the LRP-1-dependence of ADAMTS-5 endocytosis, LRP-1 was knocked down with siRNAs. Expression of *Lrp1* RNA was reduced by 80% in siLRP1 cells relative to siCtrl cells (Figure 5.14), and LRP-1β protein was reduced by 90% (Figure 5.12C).

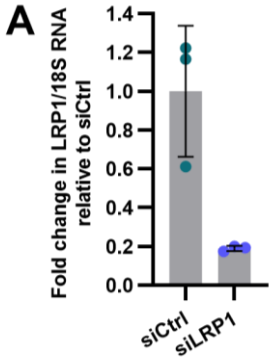

Figure 5.8 siRNA knockdown of *Lrp1*. *A*) RNA was isolated from siRNA-treated cells incubated in serum-free media for 24 hours. Expression of *Lrp1* RNA was measured by qPCR, then normalised to *18s* expression and presented as a fold change relative to siCtrl. Mean ± SD, one experiment conducted in triplicate using one cell subculture (n=3).

However, no large differences in extracellular FLAG-ADAMTS-5 levels were observed between siLRP1 and siCtrl cells (Figure 5.9). The mean levels of extracellular FLAG-ADAMTS-5 in siLRP1 cells were only around 5% higher than siCtrl cells at each time point, which was not a statistically

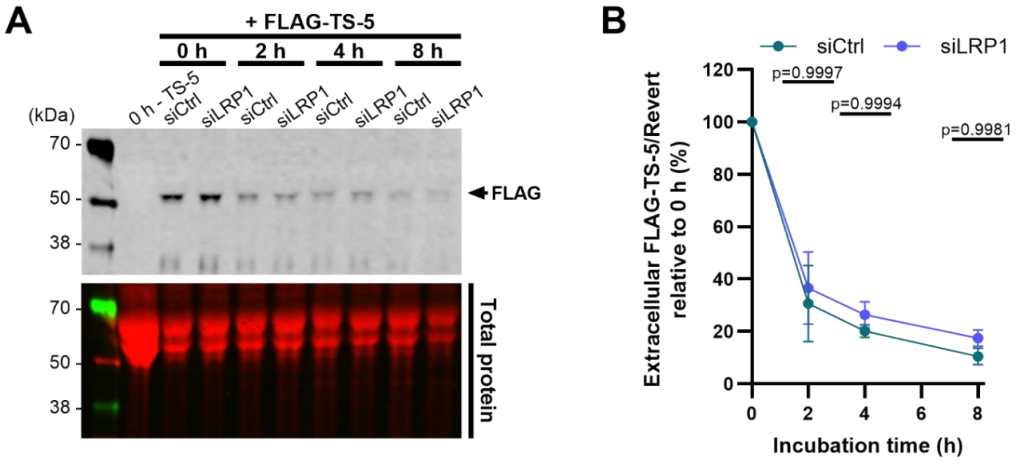

Figure 5.9 Knockdown of LRP-1 did not affect ADAMTS-5 endocytosis. *A*) siCtrl and siLRP1 cells were incubated with or without 10 nM FLAG-ADAMTS-5-3 in serum-free media for 0, 2, 4 and 8 hours. Extracellular levels of FLAG-ADAMTS-5 in conditioned media were detected by western blot using an anti-FLAG antibody with near-infrared fluorescence detection (800 nm channel). Revert total protein stain was imaged in the 700 nm channel. Blot representative of one experiment conducted in triplicate using one cell subculture (n=3). ***B***) Quantification of extracellular FLAG-ADAMTS-5-3 levels in *A*), normalised to Revert total protein stain, relative to levels at 0 hours in each condition. Mean ± SD. p values >0.05 shown on graph, one-way ANOVA with Tukey's multiple comparisons test.

significant difference (Figure 5.9 B; p=0.9997, 0.9994 and 0.9981 at 2, 4 and 8 hours respectively).

To test whether this lack of ADAMTS-5 endocytosis inhibition was due to incomplete LRP-1 knockdown, endocytosis was measured when cells were treated with the LRP-1 competitive antagonist RAP. Extracellular FLAG-ADAMTS-5 levels were not qualitatively affected by treatment with 0.5 µM RAP relative to non-treated siCtrl cells (Figure 5.10A). No statistically significant, quantitative differences were observed between RAP-treated and untreated cells at any time point (Figure 5.10B; p>0.9999 at 2, 4 and 8 hours), although normalisation to total protein was not possible because the experiment was conducted before the Revert total protein stain was acquired.

In a separate experiment, levels of extracellular FLAG-ADAMTS-5 were qualitatively increased in some samples when 0.5 µM RAP was used or when 1 µM RAP was pre-incubated with cells for

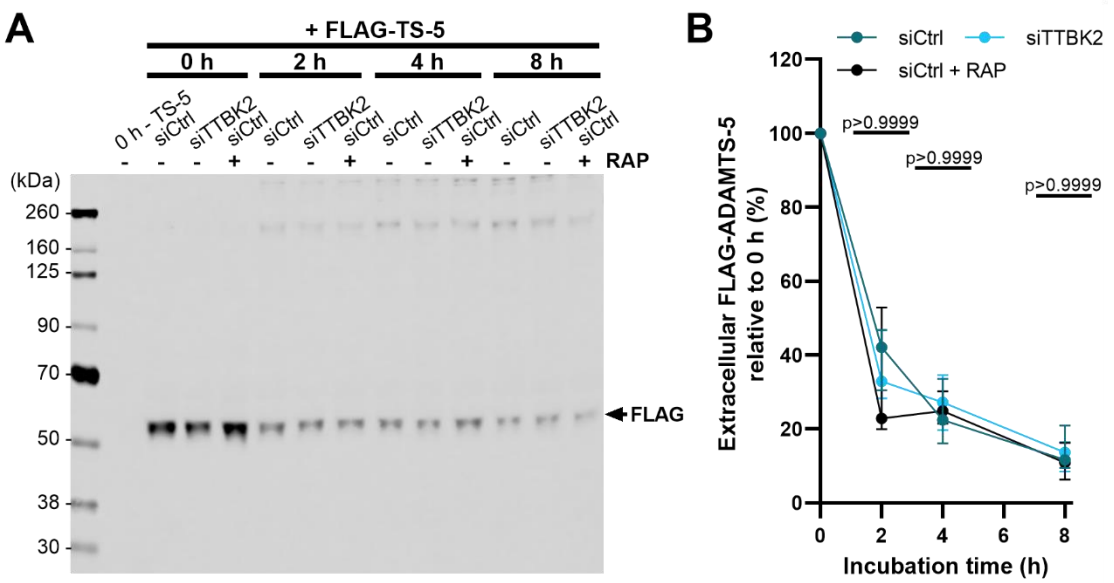

Figure 5.10 The LRP-1 competitive antagonist RAP did not affect ADAMTS-5 endocytosis. ***A***) siCtrl and siTTBK2 were incubated with or without 10 nM FLAG-tagged ADAMTS-5-3 and 0.5 µM RAP in serum-free media for 0, 2, 4 or 8 hours. Extracellular levels of FLAG-ADAMTS-5 in conditioned media were detected by western blot using an anti-FLAG antibody. Blot representative of two independent experiments conducted in triplicate using one cell subculture (n=6). ***B***) Quantification of extracellular FLAG-ADAMTS-5-3 levels in *A*), calculated as a percentage relative to levels at 0 hours. Median ± IQR. p values >0.05 shown on graph, Kruskal-Wallis test with Dunn's multiple comparisons test.

2 hours before FLAG-ADAMTS-5 was added (Appendix figure 14, p.231). However, this was not consistently observed across samples and the total number of samples analysed was small (n=2).

In summary, disruption of clathrin-mediated endocytosis through knockdown of *Cltc* or *Ap2a1*, or disruption of LRP-1-mediated endocytosis through LRP-1 knockdown or RAP treatment, had no effect on ADAMTS-5 endocytosis in my experimental system. As heparin and RAP had a much greater effect on ADAMTS-5 endocytosis in previous studies, these results could be because I used the wrong time course: the largest differences in the rate of endocytosis between conditions could have occurred before the earliest time point or after the latest time point in my experiments, and therefore were not detected. Alternatively, these results could be due to ADAMTS-5 being cleared by other endocytic pathways in my experimental system, which were potentially disrupted upon *Ttbk2* knockdown.

5.2.4 Knockdown of *Ttbk2* had no effect on ADAMTS-5 endocytosis

To determine whether ADAMTS-5 endocytosis was impaired upon *Ttbk2* knockdown, siCtrl and siTTBK2 cells were incubated with FLAG-ADAMTS-5. Expression of *Ttbk2* RNA was reduced by around 70% in siTTBK2 cells relative to siCtrl cells at both 0 and 8 hours (Appendix figure 15, p.231). However, knockdown of *Ttbk2* had no qualitative effect on ADAMTS-5 endocytosis (Figure 5.10A), and no statistically significant differences in quantified extracellular FLAG-ADAMTS-5 were observed between siTTBK2 and siCtrl cells at any time point (Figure 5.10B; p>0.9999 at 2, 4 and 8 hours).

Similar results were obtained in a better-controlled, repeat experiment, in which total protein was used as a loading control. Knockdown of *Ttbk2* had no effect on extracellular FLAG-ADAMTS-5 levels normalised to total protein at any time point relative to siCtrl cells (Figure 5.11B; p>0.9999), whereas heparin increased extracellular levels of ADAMTS-5 at 4 and 8 hours, albeit

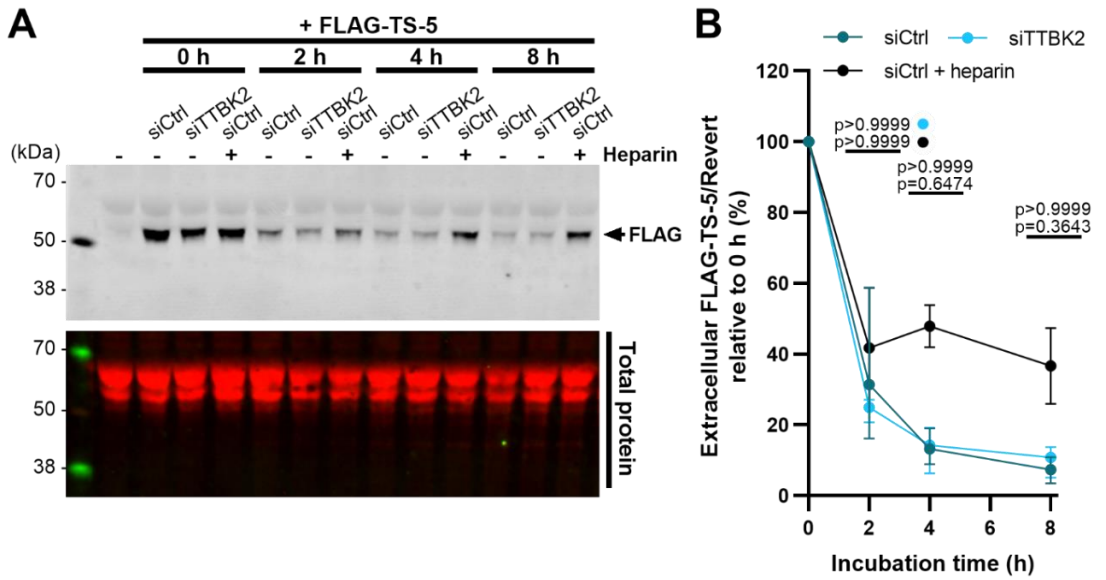

Figure 5.11 Knockdown of *Ttbk2* did not affect ADAMTS-5 endocytosis. *A*) siCtrl and siTTBK2 cells were incubated with or without 10 nM FLAG-tagged ADAMTS-5-3 and 200 µg/ml heparin in serum-free media for 0, 2, 4 and 8 hours. Extracellular levels of FLAG-ADAMTS-5 in conditioned media were detected by western blot using an anti-FLAG antibody with near-infrared fluorescence detection (800 nm channel). Revert total protein stain was imaged in the 700 nm channel. Blot representative of one experiment conducted in triplicate using one cell subculture (n=3). ***B*)** Quantification of extracellular FLAG-ADAMTS-5-3 levels in *A*), normalised to Revert total protein stain, relative to levels at 0 hours in each condition. Mean ± SD.

not statistically significantly ($p>0.9999$, $p=0.6474$ and $p=0.3643$ at 2, 4 and 8 hours). Therefore, knockdown of *Ttbk2* did not affect ADAMTS-5 endocytosis in my experimental system.

5.2.5 Knockdown of *Ttbk2* did not affect LRP-1 expression, localisation or shedding

Alongside the functional endocytosis assay, the effect of *Ttbk2* knockdown on LRP-1 itself was examined, given that LRP-1-mediated endocytosis has been shown in previous studies to be the predominant mechanism of ADAMTS-5 endocytic clearance. Knockdown of *Ttbk2* or other ciliary genes had no effect on the expression of *Lrp1* at RNA level relative to siCtrl cells (Figure 5.12A; p>0.9999 for all comparisons). Levels of LRP-1β (65 kDa) in cell lysates were also unaffected by knockdown of *Ttbk2* (Figure 5.12B and C; p>0.9999).

To determine the effect of *Ttbk2* knockdown on LRP-1 shedding, LRP-1α levels in conditioned media were measured by western blot. A band at the expected molecular weight of LRP-1α (515

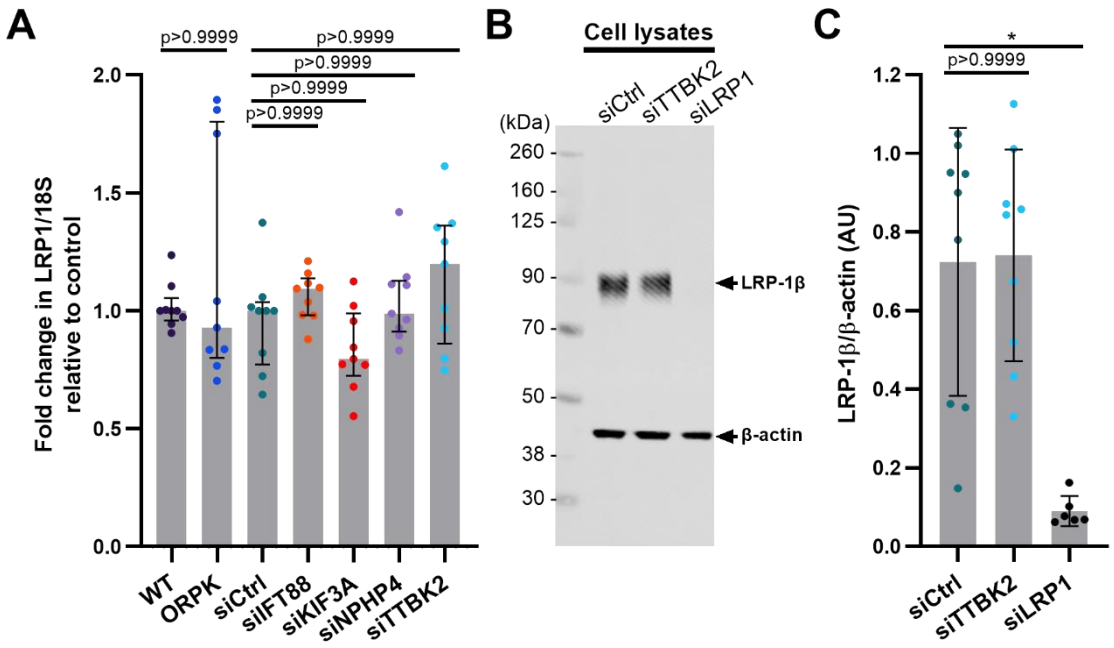

Figure 5.12 Knockdown of *Ttbk2* did not affect expression of *Lrp1* RNA or LRP-1β protein. *A*) RNA was isolated from siRNA-treated cells after incubation in serum-free media for 24 hours. Expression of *Lrp1* RNA was measured by qPCR, then normalised to *18s* expression and presented as a fold change relative to control (WT for ORPK; siCtrl for all other conditions). Median ± IQR, three independent experiments conducted in triplicate using separate cell subcultures (n=9). p values shown on graph, Kruskal-Wallis test with Dunn's multiple comparisons test. ***B***) LRP-1β in siRNA-treated cell lysates was detected by western blot, with β-actin used as a loading control. Blot representative of three independent experiments conducted in triplicate using separate cell subcultures (n=9). ***C***) Quantification of LRP-1β levels in *A*), normalised to β-actin. Mean ± SD. * p<0.05, p values >0.05 shown on graph, one-way ANOVA with Tukey's multiple comparisons test.

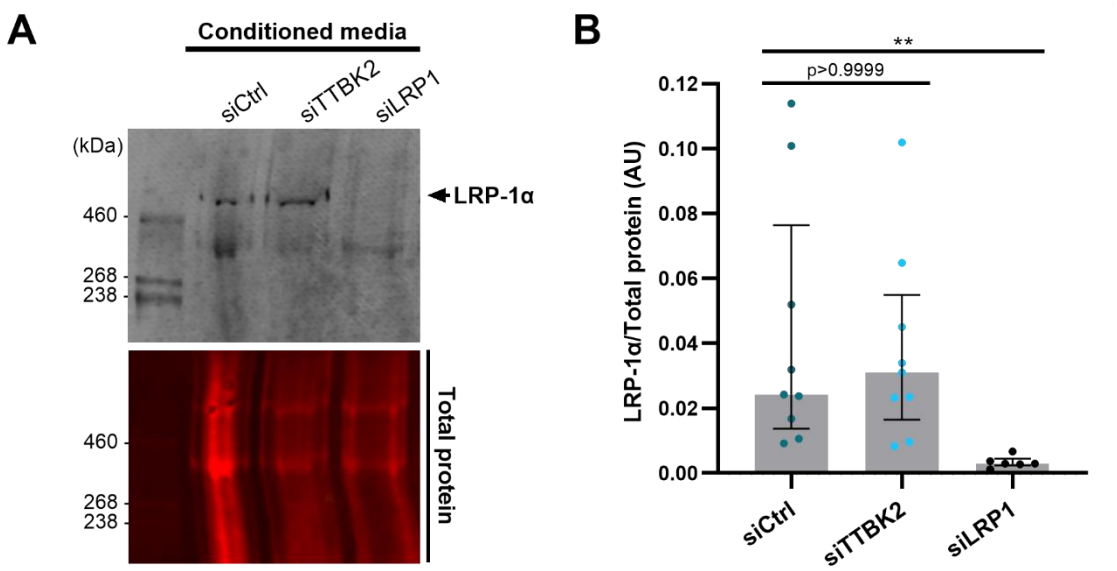

Figure 5.13 Knockdown of *Ttbk2* did not affect extracellular levels of the LRP-1α protein. ***A***) siCtrl, siTTBK2 and siLRP1 cells were incubated in serum-free media for 24 hours. Extracellular LRP-1α in conditioned media was detected by western blot with near-infrared fluorescence detection (800 nm channel). Revert total protein stain was imaged in the 700 nm channel. Blot representative of three independent experiments conducted in triplicate using separate cell subcultures (n=9). ***B***) Quantification of LRP-1α in *A*), normalised to Revert total protein stain. Median ± IQR. ** p<0.01, p values >0.05 shown on graph, Kruskal-Wallis test with Dunn's multiple comparisons test.

kDa) was detected in conditioned media from siCtrl cells but not siLRP1 cells, thus validating this band as LRP-1α (Figure 5.13A). Quantification of this band and normalisation to total protein showed that extracellular LRP-1α levels, and thus LRP-1 shedding, were not affected by *Ttbk2* knockdown (Figure 5.13B; p>0.9999).

The cellular distribution of LRP-1β was assessed by confocal microscopy to determine whether knockdown of *Ttbk2* affected the periciliary localisation of LRP-1β previously observed by the Wann group in this cell line. Punctate, perinuclear LRP-1β staining was observed in both siCtrl and siTTBK2 cells (Figure 5.15). In some siCtrl cells, LRP-1β staining was concentrated on the side of the cell where the acetylated α-tubulin-stained primary cilium was present. LRP-1β staining frequently co-localised with non-cilia-associated acetylated α-tubulin staining in siCtrl and siTTBK2 cells. Overall, LRP-1β localisation was not strikingly different upon *Ttbk2* knockdown.

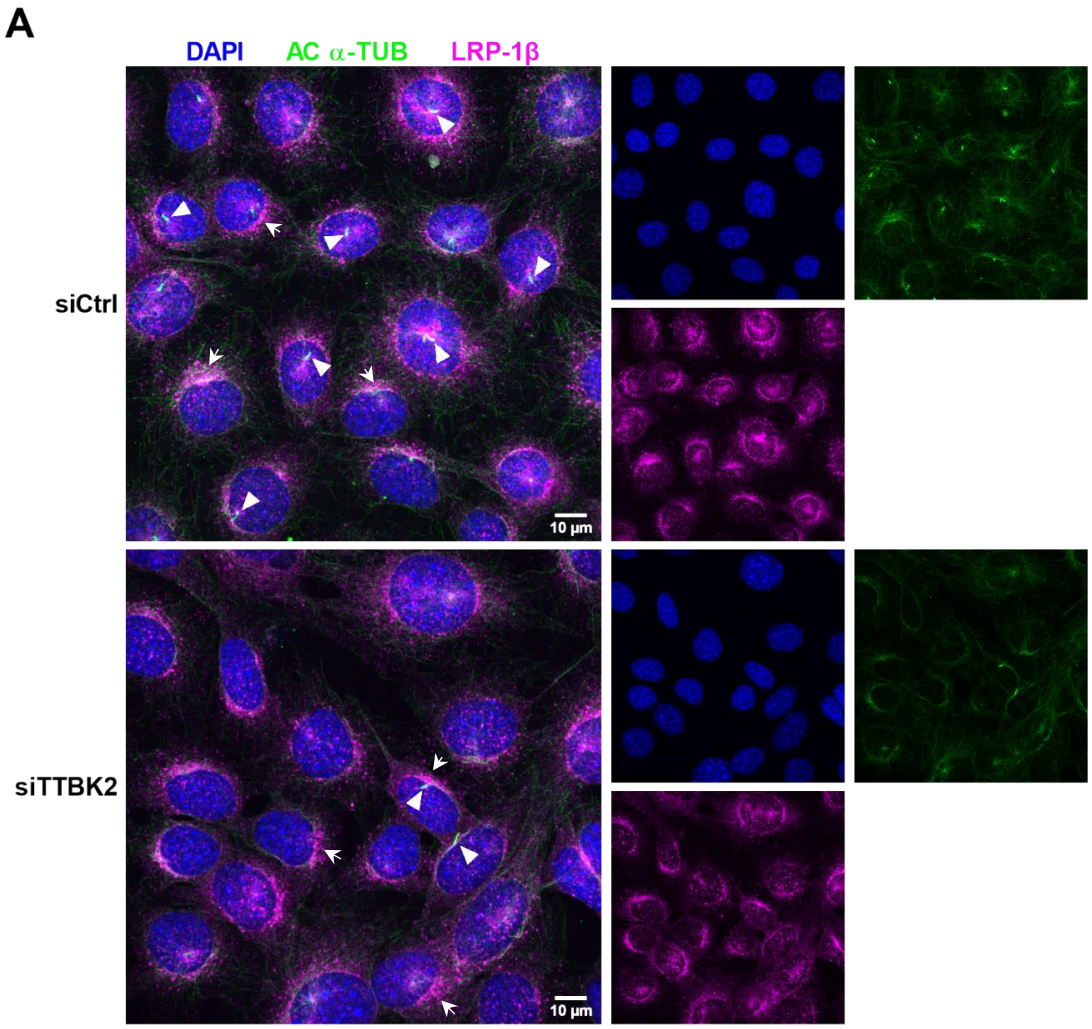

Figure 5.15 Knockdown of *Ttbk2* did not affect LRP-1β localisation. ***A***) siCtrl and siTTBK2 cells were incubated in serum-free media for 24 hours. Cells were fixed and stained with antibodies targeting acetylated α-tubulin (green) and LRP-1β (magenta), and counterstained with DAPI (blue) to visualise cell nuclei. Cells were imaged using an Olympus FV1200 confocal microscope across three fields of view per coverslip. Maximum projection images were created in ImageJ. Images shown are representative of one experiment conducted in triplicate using one cell subculture (n=3). Scale bar 10 µm. White arrowheads indicate cilia; white arrows indicate areas of concentrated LRP-1β staining.

I also attempted to investigate the localisation of different endosomal compartments upon *Ttbk2* knockdown, and first tried to determine whether the early endosome marker EEA1 was localised to periciliary region, as previously reported in primary mouse chondrocytes[195] but not observed in the Wann group's previous work[193].

To do this, cells were stained with two different antibodies targeting EEA1, after fixation under conditions shown by Hua and Ferland to better preserve cilia- and microtubule-associated structures than PFA fixation[219]. Specifically, cells were washed with a "cytoskeletal buffer" that was used by Hua and Ferland to aid tubulin polymerisation and stabilise microtubules, before fixation. Use of the cytoskeletal buffer revealed focal areas of EEA1 staining by a rabbit antibody at the base of the cilium (Appendix figure 16A, p.232). This staining was even more concentrated at the base of the cilium when PFA was made up in cytoskeletal buffer (Figure 5.16). However, no such concentrated EEA1 distribution was observed with or without cytoskeletal buffer when

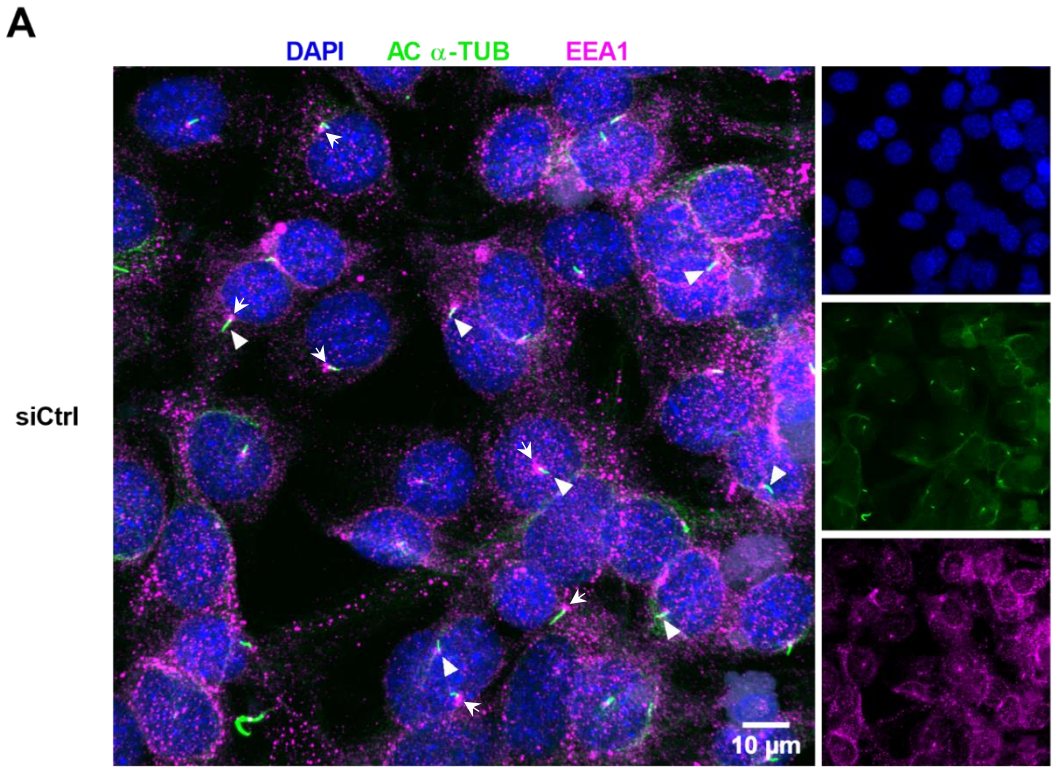

Figure 5.16 A marker of the early endosome, Early endosomal antigen 1, was concentrated at the base of the primary cilium. ***A***) siCtrl cells were incubated in serum-free media for 24 hours. Cells were washed with cytoskeletal buffer and fixed in PFA made up in cytoskeletal buffer. Cells were then stained with antibodies targeting acetylated α-tubulin (green) and Early endosomal antigen 1 (EEA1) (magenta, rabbit antibody), then counterstained with DAPI (blue). Cells were imaged using an Olympus FV1200 confocal microscope across three fields of view per coverslip. Maximum projection images were created in ImageJ. Images shown are representative of one experiment conducted in triplicate using one cell subculture (n=3). Scale bar 10 µm. White arrowheads indicate cilia; white arrows indicate areas of EEA1 concentration at the base of the primary cilium.

a mouse EEA1 antibody was used (Appendix figure 16B), casting doubt on whether the focal areas of EEA1 staining seen in Figure 5.16 were real. In light of this uncertainty, EEA1 localisation upon *Ttbk2* knockdown was not tested.

5.3 Discussion

5.3.1 Summary

In this chapter, I aimed to determine whether disruption of ADAMTS-5 endocytosis was the cause of the increased ADAMTS-5 activity observed upon *Ttbk2* knockdown in Chapter 2. I found that treatment of siCtrl cells with heparin, which has been shown to almost completely inhibit ADAMTS-5[117] and TIMP-3[105] endocytosis, resulted in a relatively small, non-statistically significant inhibition of ADAMTS-5 endocytic clearance in my experiments. However, in contrast to previous studies, neither disruption of genes encoding proteins involved in clathrin-mediated endocytosis, nor disruption of LRP-1 inhibited ADAMTS-5 clearance. I also found that knockdown of *Ttbk2* did not affect LRP-1 expression, shedding or localisation. Whilst EEA1 staining with one antibody appeared to be concentrated at the base of the cilium after optimisation of fixation conditions, which was consistent with previous reports in chondrocytes, this result could not be replicated with another antibody and therefore the focal EEA1 staining observed may be non-specific.

5.3.2 Evaluation of the ADAMTS-5 endocytosis assay

To measure ADAMTS-5 endocytosis upon *Ttbk2* knockdown in the WT mouse chondrocyte cell line, I used the assay previously used by the Wann group. In the group's previous study, almost all of the FLAG-ADAMTS-5 added at the start of the assay had been cleared by 80 minutes in WT cells[193]. However, in my experiments, FLAG-ADAMTS-5 was detected in conditioned media even after 120 minutes. This apparent difference in the rate of endocytosis between my results and the group's previous results is likely because of differences in sample preparation for western blotting. Specifically, to conserve the limited stock of FLAG-ADAMTS-5, I used 10 nM FLAG-ADAMTS-5 rather than the 20 nM used previously, but I also concentrated the conditioned media by TCA precipitation. The addition of this precipitation step meant that I analysed around 12-times more FLAG-ADAMTS-5 protein per time point by western blotting than in the Wann

group's previous experiments. To obtain larger differences in levels of FLAG-ADAMTS-5 between time points and thus improve the range of the assay, I extended the time course to 8 hours, by which point almost all of the FLAG-ADAMTS-5 added at the start of the assay had been cleared. Also, the reduction in extracellular FLAG-ADAMTS-5 levels over time was unlikely to be simply due to cleavage of the FLAG protein tag, as similar signal was observed when an anti-FLAG antibody or an anti-ADAMTS-5 catalytic domain antibody were used for western blotting. Conducting the assay in the presence of protease inhibitors could help to further rule out protease degradation.

Treatment of cells with heparin was used to validate that the clearance of extracellular ADAMTS-5 I observed was due to endocytic uptake. Heparin is thought to inhibit endocytosis of LRP-1 ligands such as TIMP-3 by sequestering these ligands in the extracellular environment[104]. Previous studies have shown that heparin more effectively inhibited endocytosis of ADAMTS-5 in porcine chondrocytes[117] and radiolabelled TIMP-3 in HTB94 cells[105], than RAP. Consistent with these previous studies, I found that heparin treatment increased extracellular levels of FLAG-ADAMTS-5 at 4 and 8 hours. However, extracellular levels of FLAG-ADAMTS-5 at 2 hours were similar in cells treated with or without heparin.

In light of heparin only partially inhibiting ADAMTS-5 clearance, I tested alternative approaches for inhibiting endocytosis, to gain further confidence that the results of this assay were a valid indication of the endocytic capacity of cells in my experimental system. I considered using dynasore, which selectively inhibits the endocytic machinery directly, unlike heparin which inhibits endocytosis through binding the endocytic cargo. Dynasore has been shown to block the endocytosis of a variety of ligands, including transferrin and low-density lipoprotein in cell lines[210], and ADAMTS-5 uptake in porcine cartilage explants[117]. However, I found that dynasore did not completely inhibit transferrin endocytosis in the WT mouse chondrocyte cell line, as punctate, cell-associated transferrin signal was observed in both vehicle- and dynasore-treated

cells. Furthermore, large areas of dense transferrin signal were seen only in dynasore-treated cells. These areas may represent surface-bound transferrin that was not internalised, although cells were washed with an acid wash before fixation to remove surface-bound ligand. This transferrin signal is not typically observed upon treatment of cells with dynasore[210]; thus, the exact cause of this signal is unclear, and dynasore was not used further.

The other approach I tested to further validate the ADAMTS-5 endocytosis assay, and also to identify the endocytic pathways used to clear extracellular ADAMTS-5 in my experimental system, was knockdown of endocytic proteins using siRNAs. I depleted clathrin heavy chain, which is required for one of the two major endocytic pathways, clathrin-dependent endocytosis, and the α1 subunit of the AP-2 complex, which is also required for clathrin-dependent endocytosis and has also been shown to interact with TTBK2 in rat brain lysates[238]. Knockdown of the genes encoding these proteins was around 90% efficient at RNA level and resulted in a reduction in transferrin uptake. These results were consistent with previous studies such as Hinrichsen et al. (2003), who found that siRNA-mediated knockdown of clathrin heavy-chain or the α subunit of AP-2 in HeLa cells inhibited the endocytosis of fluorescently labelled transferrin[265].

However, knockdown of *Cltc* or *Ap2a1* did not strikingly inhibit ADAMTS-5 endocytosis, and resulted in only a small, statistically insignificant increase in extracellular FLAG-ADAMTS-5 levels at each time point relative to siCtrl cells. This result was unexpected on the basis of the work of Yamamoto et al. (2013). They found that inhibition of the other major endocytic pathway, caveolae-mediated endocytosis, through the use of cholesterol-depleting compound β-cyclodextrin, had no effect on ADAMTS-5 endocytosis in porcine cartilage explants[117]. Endocytosis of other ADAMTSs and matrix-associated molecules has also been shown to be clathrin-dependent. For example, siRNA-mediated knockdown of LRP-1 or inhibition of clathrin-mediated endocytosis with the drug chlorpromazine, reduced the internalisation of connective

tissue growth factor (CTGF) in a human chondrocytic cell line, and β-cyclodextrin treatment had no effect on CTGF endocytosis[266]. Nandadasa et al. (2019) also found that the presence of endocytic vesicles containing ADAMTS-9 was reduced upon siRNA knockdown of clathrin heavy chain, LRP-1 or LRP-2, or pharmacological inhibition of clathrin-mediated endocytosis with the small molecule Pitstop 2 *in vitro*[203].

One explanation for the lack of inhibition of ADAMTS-5 clearance upon *Cltc* or *Ap2a1* knockdown is that ADAMTS-5 endocytosis occurs via caveolae-dependent endocytosis in my experimental system. A few studies have identified associations between LRP-1 and caveolae-mediated endocytosis. For example, using cell fractionation, Boucher et al. (2002) found that LRP-1 was present in higher levels in caveolae-containing cell membrane fractions relative to the non-caveolae membrane in human fibroblasts[267]. Also, knockout of the kinesin KIF13B, which colocalised with LRP-1 and the core caveolae protein caveolin-1 but not clathrin, reduced endocytosis of the LRP-1 ligand LDL in mouse embryonic fibroblasts[198]. However, a functional link between LRP-1, ADAMTS-5 and caveolae has not been identified.

Given that other groups have directly demonstrated the importance of clathrin in ADAMTS endocytosis, it is more likely that the lack of inhibition of ADAMTS-5 endocytosis upon *Cltc* and *Ap2a1* knockdown was due to issues with the set-up of the ADAMTS-5 endocytosis assay. For example, the difference in the rate of endocytosis between siCLTC or siAP2A1 cells and siCtrl cells might have been greater before the first time point analysed (2 hours) or after the final time point (8 hours). Also, the high variation associated with western blot analysis of FLAG-ADAMTS-5 made it more difficult to determine with any certainty that small differences in the rates of endocytosis were real. The ineffective inhibition of endocytosis by heparin provided further support to this idea that the assay was not able to detect the largest differences in the rate of endocytosis, as heparin has previously been shown to almost completely inhibit ADAMTS-5 internalisation[117].

Consistent with this technical explanation for why targeting the clathrin-dependent endocytic pathway had no effect on ADAMTS-5 clearance in my experiments, knockdown of the receptor shown to mediate the majority of ADAMTS-5 endocytosis, LRP-1, did not affect extracellular FLAG-ADAMTS-5 levels. This lack of inhibition of endocytosis was observed despite an 80% reduction in *Lrp1* RNA expression and a 90% reduction in LRP-1β protein levels. Levels of extracellular FLAG-ADAMTS-5 were also unaffected by 500 nM RAP, which was unexpected based on the results of previous studies. For example, treatment of isolated human chondrocytes or live porcine cartilage explants with 500 nM RAP increased extracellular levels of FLAG-ADAMTS-5, as assessed via western blot, and reduced intracellular levels of FLAG-ADAMTS-5, as assessed via microscopy[117]. The Wann group has also seen that RAP increased extracellular levels of FLAG-ADAMTS-5 in the WT mouse chondrocyte cell line used in this thesis, although ADAMTS-5 uptake was not completely inhibited by RAP[193].

It is also possible that the absence of inhibition of ADAMTS-5 endocytosis upon LRP-1 knockdown or RAP treatment was because ADAMTS-5 endocytosis in my experimental system was not predominantly mediated by LRP-1. Supporting the existence of an LRP-1-independent endocytic pathway, both Scilabra et al. (2013) and Yamamoto et al. (2013) observed incomplete RAP-mediated inhibition of TIMP-3 and ADAMTS-5 uptake respectively[105,117]. Furthermore, TIMP-3 endocytosis was observed in LRP-1 deficient mouse embryonic fibroblasts, at approximately half the rate of WT cells[105]. Scilabra et al. proposed that urokinase plasminogen activator receptor-associated protein (uPARAP)/Endo180 potentially mediated TIMP-3 endocytosis via an LRP-1-independent pathway, as it has been shown to bind to the pro-enzyme form of the LRP-1 ligand urokinase plasminogen activator[268]. However, deletion of uPARAP/Endo180 had no effect on MMP-13 endocytosis in mouse dermal fibroblasts *in vitro*[268], and no other non-LRP-1 receptors have been experimentally shown to mediate protease uptake.

In summary, the results in this chapter imply that my experiments were not correctly set up to detect the largest differences in the rate of ADAMTS-5 endocytosis between conditions. Multiple studies, including previous work by the Wann group in the same cell line that was used in this thesis, have provided evidence that ADAMTS-5 endocytosis in chondrocytes occurs via LRP-1-mediated, clathrin-dependent endocytosis. However, I found that disruption of LRP-1 or clathrin-mediated endocytosis via multiple approaches had no effect on ADAMTS-5 clearance in my experimental system. There are biological explanations for this lack of inhibition, such as most ADAMTS-5 endocytosis being mediated by another receptor or via caveolae-mediated endocytosis. However, the evidence for the existence of such pathways in the context of protease endocytosis is weak, and the incomplete inhibition of ADAMTS-5 endocytosis by heparin indicated that the differences between my results and the results of previous studies are most likely due to technical issues.

Knockdown of *Ttbk2* had no effect on extracellular levels of FLAG-ADAMTS-5 at any time point in my experiments. However, considering the limitations of the assay discussed above, it is possible that any inhibition of ADAMTS-5 endocytosis caused by *Ttbk2* knockdown was not detectable. Therefore, further optimisation of the ADAMTS-5 uptake assay or use of an alternative endocytosis assay is required before disruption of endocytosis can be definitively ruled out as the mechanism by which *Ttbk2* knockdown increased ADAMTS-5 activity.

5.3.3 LRP-1 expression, localisation or shedding was unaffected by knockdown of *Ttbk2*

My original hypothesis for how knockdown of *Ttbk2* increased ADAMTS-5 activity was that endocytosis mediated by LRP-1 was impaired, as previous studies had shown that this receptor was important for the regulation of extracellular ADAMTS-5 clearance and, in turn, its aggrecan-degrading activity in cartilage[117]. Therefore, alongside conducting the functional endocytosis assay, which ultimately could not be used to definitively demonstrate a role for LRP-1 in

ADAMTS-5 endocytosis in my experimental system, I tested whether *Ttbk2* knockdown affected the LRP-1 receptor itself.

I found that expression of *Lrp1* RNA or LRP-1β protein was not affected by *Ttbk2* knockdown. Previous studies have reported that regulation of LRP-1-mediated endocytosis mainly occurs through LRP-1 shedding (as discussed in Section 1.2.4). During this process, the LRP-1 receptor is proteolytically cleaved, resulting in the release of the entire ligand-binding α-chain and part of the β-chain into the extracellular environment[121]. LRP-1 shedding has been shown to increase protease activity in chondrocytes through reducing the endocytic capacity of cells, but also the activity of ADAMTS-5 bound to soluble, shed LRP-1 was around 3-fold greater than that of free ADAMTS-5[120]. However, in my experiments, extracellular LRP-1α levels and thus LRP-1 shedding was unaffected by *Ttbk2* knockdown. There are also no links in the literature between TTBK2 and LRP-1 expression or shedding.

LRP-1β localisation was also examined to investigate whether *Ttbk2* knockdown disrupted the periciliary distribution of LRP-1β previously seen by the Wann group, which possibly represented an area of enhanced endocytosis. Consistent with the group's previous study, I saw that LRP-1β staining in siCtrl cells was frequently concentrated on, but not exclusively localised to, the side of the cell where the primary cilium was assembled. Similar LRP-1β staining was observed upon TTBK2 knockdown, which resulted in reduced assembly of the main ciliary structures (the axoneme and ciliary membrane, as shown in Chapter 3). This result indicated that the ciliary axoneme might not be required for establishing the hypothesised periciliary region of increased LRP-1 endocytosis and recycling.

Instead, in control cells and upon *Ttbk2* knockdown, there was more colocalisation of LRP-1β with non-ciliary acetylated α-tubulin staining than with the ciliary axoneme itself, which frequently occupied only a small area of the cell near the regions of intense LRP-1β staining. This colocalisation raises the possibility that the periciliary distribution of LRP-1β might be related to

microtubule-mediated vesicular trafficking at the centrosome, which has previously been shown to be the site of the recycling endosome[269]. Ciliary proteins might still have a role in organising LRP-1 localisation, as the subdistal appendages acquired by the mother centriole during ciliogenesis have been shown to anchor recycling endosomes and regulate the recycling rate of transferrin[202]. Also, as the LRP-1β staining in my experiments represented both intracellular and surface-bound LRP-1β, part of the concentrated LRP-1β staining observed could be due to increased levels of LRP-1β on the cell surface in this region. This in turn could be due to concentration of LRP-1 in clathrin-coated pits, which have been shown to be enriched at the ciliary pocket membrane[137]. Further work is required to investigate where exactly LRP-1 is present in the cell, such as through imaging the recycling endosome via Rab11 staining and labelling surface versus intracellular LRP-1 via surface biotinylation.

I began to investigate the organisation of endosomal compartments by trying to visualise the early endosome. I found that after fixing cells with PFA, the early endosome marker EEA1 was distributed evenly through the cell, as the Wann group had seen previously. The use of a buffer designed by Hua and Ferland to stabilise microtubules, referred to as cytoskeletal buffer[219], resulted in the appearance of focal EEA1 staining at the base of the cilium, similar to previous studies in primary mouse chondrocytes[195]. However, this focal EEA1 staining could not be replicated with an alternative anti-EEA1 antibody and I did not include any negative controls for antibody specificity, such as staining cells upon siRNA-mediated knockdown of EEA1 or without primary antibodies. Therefore, I cannot be certain that the focal, ciliary-localised EEA1 staining observed was specific. Other approaches, such as the expression of EEA1 tagged with a fluorescent protein, would be required to determine which pattern of EEA1 staining observed in these experiments was real.

5.3.4 Strengths and limitations

As discussed in Section 5.2.1, the ADAMTS-5 endocytosis assay I used in this chapter potentially had a few major limitations. The main possible limitation was that the largest differences in endocytic rate between conditions might have occurred outside the 8-hour time course, thus explaining the ineffectiveness of RAP and other endocytosis-targeting molecules in my experiments. Possible solutions to address this would be to measure extracellular FLAG-ADAMTS-5 levels at later time points, or during the first 2 hours of the assay, when around 60% of the exogenous ADAMTS-5 added at the start of the time course was taken up by WT cells. Conducting the assay on ice could help to slow down the initial rapid phase of ADAMTS-5 uptake, and thus help to determine whether the greatest differences in uptake between conditions occurred immediately after FLAG-ADAMTS-5 was added to cells.

Another fundamental limitation of the assay, which would still be present even if the time course was optimised, was the high variation in FLAG-ADAMTS-5 signal between samples. Signal variation was particularly high at the 0-hour time point, when ADAMTS-5 levels were expected to be the same across all conditions and, importantly, to which signal at all other time points was normalised. One possible explanation for this variation was that FLAG-ADAMTS-5 stuck to plastic surfaces during cell culture and western blot preparation, leading to loss of protein from samples. Evidence of this was observed by other members of the Wann group and in other studies; for example, Yamamoto et al. (2013) showed that there was a small reduction in extracellular FLAG-ADAMTS-5 signal over time even when the uptake assay was conducted without cells[117]. I used low protein-binding tubes to try to minimise this issue, but variation between samples was still high. Repeating the experiment further could have also helped to increase certainty that the small differences observed between conditions were real, but most experiments were limited to only three replicates due to the low supply of FLAG-tagged ADAMTS-5.

Considering these limitations of the ADAMTS-5 endocytosis assay, an alternative endocytosis assay should be set up to study the endocytic capacity of cells upon *Ttbk2* knockdown, alongside further optimisation of the current assay. One alternative approach would be to measure intracellular levels of FLAG-tagged ADAMTS-5 in cell lysates over time by western blotting, although this would not overcome the issues with signal variation discussed above. Levels of internalised FLAG-ADAMTS-5 could instead be visualised via microscopy, which was used in this cell line in the Wann group's previous work but would be no more quantitative then western blotting.

Another approach would be to label endogenous ADAMTS-5, such as through expression of a fluorescently tagged protease, and then study the endocytic process with live-cell microscopy. This would eliminate one of the issues of studying endocytosis through incubating cells with a tagged, exogenous protease: FLAG-tagged ADAMTS-5 was rapidly taken up by cells, whereas detectable increases in endogenous ADAMTS-5 activity occur over a longer time period. For example, as seen in Chapter 3, AGEG generation was undetectable after incubation of cells with aggrecan for 8 hours, which is when the majority of FLAG-ADAMTS-5 had been endocytosed during the ADAMTS-5 endocytosis assay. Visualisation of endogenous ADAMTS-5 internalisation could therefore enable endocytosis and AGEG generation to be measured along the same time course. This could give a better indication of whether differences in the rate of ADAMTS-5 endocytosis are functionally relevant to ADAMTS-5 activity.

In summary, development of a protease endocytosis assay that can accurately detect changes in the rate of endocytosis over a greater range than the current assay, should be prioritised in future studies of the mechanism of TTBK2-mediated ADAMTS-5 regulation. The ability to detect small differences in endocytic rate is particularly important in the context of ADAMTS-5, which has extremely potent aggrecan-degrading activity: as seen in Section 3.2.1, incubation of 1 nM recombinant ADAMTS-5 with aggrecan for only one minute resulted in AGEG-positive aggrecan

fragment production. The potency of proteases means that only a small change in the processes regulating ADAMTS-5 activity, such as a small reduction in the rate of endocytosis, could have a very large, cumulative effect on matrix degradation over time. Therefore, it may be very difficult to detect the exact cause of increased protease activity *in vitro*, such as upon *Ttbk2* knockdown, and also in people with osteoarthritis, which is a disease that develops over many years. Approaches for measuring protease activity during the progression of osteoarthritis, such as quantitative *in vivo* imaging of protease activity using the fluorescent probes mentioned in Section 3.3.5, could reveal the dynamics of protease activity dysregulation in disease and thus give further insight into the potential mechanisms of osteoarthritis pathogenesis.

5.3.5 Conclusions

In this chapter, I proposed that the assay used to test whether ADAMTS-5 endocytosis was impaired upon *Ttbk2* knockdown in my experimental system, had multiple limitations that prevented the detection of differences in the rate of endocytosis between conditions. Supporting this proposal, I found that ADAMTS-5 endocytosis was only partially inhibited by heparin in my experiments, in contrast to previous studies. Furthermore, ADAMTS-5 endocytosis was unaffected by siRNA-mediated disruption of proteins required for clathrin-dependent endocytosis, which is the pathway previously shown to be used for the majority of ADAMTS-5 uptake. Despite evidence from previous studies showing that LRP-1 predominantly mediates ADAMTS-5 endocytosis, inhibition of LRP-1-dependent endocytosis through RAP treatment or LRP-1 knockdown had no effect on ADAMTS-5 endocytosis in my experiments.

Therefore, even though knockdown of *Ttbk2* was shown to have no effect on ADAMTS-5 using this assay, disruption of endocytosis cannot yet be ruled out as the cause of increased ADAMTS-5 activity upon *Ttbk2* knockdown. In this chapter, I have also shown that knockdown of *Ttbk2* did not affect RNA or protein levels of LRP-1. LRP-1 shedding or LRP-1β localisation were also

unaffected by *Ttbk2* knockdown. Therefore, any defects in endocytosis upon *Ttbk2* knockdown were unlikely to be due to altered expression, distribution or shedding of LRP-1.

In conclusion, further investigation of endocytosis upon *Ttbk2* knockdown is required, such as through optimisation of the current assay and development of new approaches to directly measure endocytosis.

CHAPTER 6

Discussion

6.1 Summary

In this thesis, I aimed to gain further insight into the mechanisms regulating cartilage extracellular matrix proteolysis, by investigating whether the primary cilium was involved in the regulation of matrix-degrading proteases. I hypothesised that ciliary proteins regulate the extracellular activity of these proteases, by facilitating the formation of a periciliary area of efficient LRP-1-mediated protease endocytosis. Consistent with the first part of this hypothesis, I found that siRNA-mediated knockdown of *Ttbk2*, which encodes a centriolar kinase required for cilia assembly, increased ADAMTS-5-mediated aggrecan proteolysis in a mouse chondrocyte line.

I have also obtained some insight into the molecular mechanism by which TTBK2 regulates the activity of ADAMTS-5. In Chapter 3, I found that siRNA-mediated knockdown of three ciliary proteins, including IFT88, reduced assembly of the main structures of the cilium (the axoneme and ciliary membrane) but did not affect aggrecan proteolysis *in vitro*. I hypothesised that the ciliary axoneme was not required for the regulation of protease activity, and therefore TTBK2 may regulate ADAMTS-5 activity independently of its role in facilitating cilia axoneme assembly.

In Chapter 4, I concluded that small changes in ADAMTS-5 RNA levels upon *Ttbk2* knockdown did not contribute to increased ADAMTS-5 activity in my experimental system, as inhibition of transcription with actinomycin D did not affect AGEG neoepitope generation over 24 hours. Therefore, TTBK2 likely regulates ADAMTS-5 activity mainly at post-transcriptional levels. I also found that activation of Hh signalling with recombinant Ihh did not affect ADAMTS-5 activity. This result implied that Hh pathway activation upon *Ttbk2* knockdown did not contribute to increased ADAMTS-5 activity. Levels of the physiological protease inhibitor TIMP-3 were also unaffected by *Ttbk2* knockdown; therefore, the increased ADAMTS-5 activity observed upon *Ttbk2* knockdown was not due to loss of TIMP-3-mediated inhibition of ADAMTS-5.

In Chapter 5, I prioritised directly assessing whether *Ttbk2* knockdown had a functional effect on the rate of endocytosis of extracellular ADAMTS-5. However, the potential limitations of the ADAMTS-5 endocytosis assay meant that, even though *Ttbk2* knockdown during the assay had no effect on ADAMTS-5 clearance, impaired endocytosis cannot yet be definitively ruled out as the cause of increased ADAMTS-5 activity upon *Ttbk2* knockdown.

6.2 Potential mechanisms of protease activity regulation by TTBK2

6.2.1 LRP-1-mediated endocytosis of ADAMTS-5

Whilst I did not identify exactly how TTBK2 regulated ADAMTS-5 activity, there are a number of potential mechanisms of ADAMTS-5 activity regulation that could have been disturbed upon *Ttbk2* knockdown and thus could be investigated in future studies. One cilia-related possibility is that *Ttbk2* knockdown disrupts the formation of non-axonemal ciliary structures such as the ciliary pocket (Figure 6.1A). The ciliary pocket was enriched with clathrin-coated pits relative to the plasma membrane in an epithelial cell line[137]. This may facilitate an increase in the rate of LRP-1 internalisation in this region and could partly explain the concentrated LRP-1β distribution observed in Chapter 5. The role of TTBK2 in ciliary pocket formation is unknown, although Absalon et al. (2008) showed that siRNA-mediated knockdown of other proteins involved in ciliogenesis, such as IFT88, in the protozoan parasites trypanosomes resulted in altered formation of the flagellar pocket[270]. This is a structure analogous to the ciliary pocket and the exclusive site of endocytosis and exocytosis. Consistent with this, the authors also showed that IFT88 knockdown disturbed endocytosis of a fluorescently labelled dye.

To study the structure of the ciliary pocket upon *Ttbk2* knockdown, electron microscopy could be used, although a few ciliary pocket markers have been identified that could be visualised by fluorescence microscopy. These include the serine-threonine kinase Akt, which was detected at the base of the ciliary pocket by immunofluorescence and electron microscopy in RPE1 cells[271].

Lu et al. (2015) also showed that the protein EHD1, was concentrated at the ciliary pocket membrane by immunofluorescence staining with super-resolution structured illumination (SIM) microscopy, and immunogold labelling combined with electron microscopy[136].

The exact mechanism by which the ciliary pocket is enriched with clathrin-coated pits is also unknown, but could be related to membrane phosphoinositide composition. The exact lipid

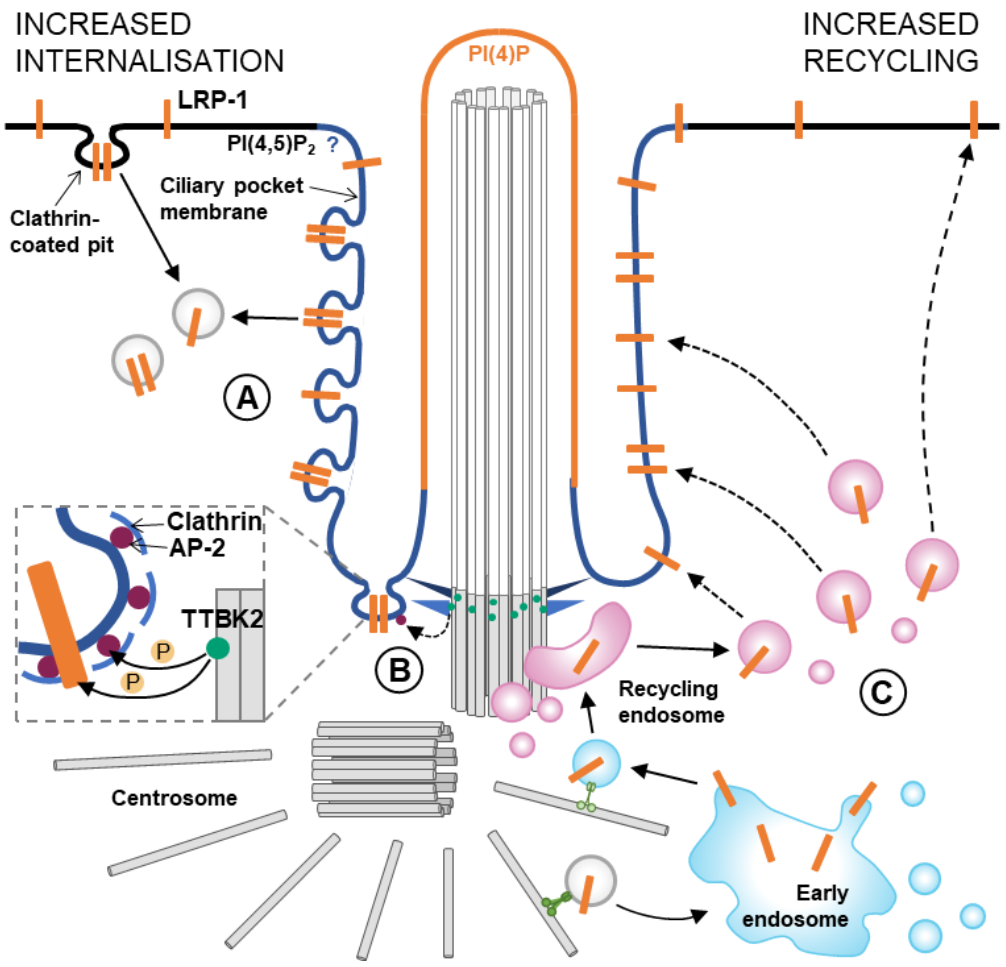

Figure 6.1 Potential direct and indirect mechanisms of regulation of LRP-1-mediated endocytosis by TTBK2. ***A***) Through its role in regulating ciliogenesis, TTBK2 might be required for the formation of the ciliary pocket. This may be a site of increased internalisation of endocytic cargo such as LRP-1 due to the increased presence of clathrin-coated pits, which in turn could be related to the unique phosphoinositide composition of the ciliary membrane. ***B***) TTBK2 could interact with and phosphorylate endocytic adaptor proteins, such as the AP-2 complex, or LRP-1 itself to increase the rate of endocytosis in the pericentriolar region. ***C***) TTBK2 could contribute to increased recycling of LRP-1 back to the plasma membrane in the vicinity of the centrioles, by maintaining the pericentriolar localisation of the recycling endosome through an unknown mechanism.

composition of the ciliary pocket membrane has not been defined. However, the ciliary membrane has been shown to have low levels of phosphatidylinositol 4,5-bisphosphate ($PI(4,5)P_2$) and high levels of phosphatidylinositol 4-phosphate (PI(4)P) in neuronal stem cells using anti-phosphatidylinositol phosphate (PIP) antibodies[272] and in IMCD3 cell lines using fluorescently labelled PIP sensors[273], due to the action of the phosphatase INPP5E. Maintenance of this PIP composition has important consequences for ciliary function in regulating Hh signalling events, through controlling ciliary entry of the Hh negative regulator G protein-coupled receptor 161 (GPR161)[272,273]. The flagellar pocket of trypanosomes has also been shown to be enriched with $PI(4,5)P_2$ and disruption of this enrichment through siRNA-mediated knockdown of a trypanosome PIP kinase reduced transferrin endocytosis[274]. Investigation of the ciliary pocket structure and membrane composition could provide further insight into how *Ttbk2* knockdown could affect protease endocytosis.

Another possibility is that TTBK2 increases LRP-1 internalisation through interactions with endocytic adaptor proteins, which could thus be disturbed upon *Ttbk2* knockdown. Watanabe et al. (2015) found that the α1, α2 and β subunits of the clathrin adaptor protein complex AP-2 interact with the catalytic domain of TTBK2 in rat brain lysates[238]. Previous studies have also showed that phosphorylation of AP-2 complex subunits regulates clathrin-mediated endocytosis. Fessart et al. (2007) showed that phosphorylation of AP-2 complex β subunit controls the initial rate of endocytosis of angiotensin II type 1 receptor *in vitro*, by regulating binding of the β-subunit to another endocytic adaptor protein β-arrestin, which links clathrin-coated pits and GPCRs[275].

Knockdown of TTBK2 could also affect the rate of protease endocytosis by disrupting recycling of the internalised LRP-1 receptor back to the plasma membrane. One possible mechanism is that *Ttbk2* knockdown alters LRP-1 phosphorylation, which has been shown to regulate the binding of Sorting nexin 17 (SNX17)[276]. SNX17 has been shown to co-localise with LRP-1 in early

endosomes[277], where it is involved in re-routing endocytic cargo away from the lysosomal degradation pathways, and into the recycling pathways[278]. Supporting this potential role of SNX17 in LRP-1 recycling, Van Kerkhof et al. (2005) found that mutation of SNX17 interaction sites in the LRP-1β cytoplasmic domain *in vitro* resulted in reduced cell surface levels of LRP-1, increased LRP-1 degradation, and reduced endocytosis of the LRP-1 ligand α2-macroglobulin[277]. Testing whether TTBK2 and LRP-1 interact by co-immunoprecipitation, plus measurement of LRP-1 phosphorylation alongside protease endocytosis, could help to determine whether any reduced ADAMTS-5 clearance upon *Ttbk2* knockdown is related to altered LRP-1 phosphorylation. To do this, detection of TTBK2 at protein level would need to be optimised, as I could not detect specific signal in cell lysates during western blot analysis of TTBK2.

As discussed in Section 5.3.3, TTBK2 could also be involved in LRP-1 recycling through maintaining the pericentriolar localisation of recycling endosomes, which have been shown to be regulated by subdistal appendage proteins associated with the mother centriole[202]. The close proximity of the recycling endosome to the centrioles could enhance the rate of LRP-1 recycling back to the membrane in this region, relative to the plasma membrane further away from the recycling endosome. This enhanced rate of LRP-1 recycling could then increase the efficiency of LRP-1-mediated endocytosis in the pericentriolar region, by increasing the number of LRP-1 receptors on the cell surface available for binding extracellular proteases. Whether this pericentriolar region of efficient endocytosis exists and how TTBK2 is involved in its establishment, are both unknown. Speculatively, TTBK2 might be linked to recycling endosomes through its role in promoting microtubule polymerisation by phosphorylating and thus antagonising the microtubule depolymerase KIF2A[238]. Treatment of human cell lines with the microtubule-depolymerising drug nocodazole resulted in loss of pericentrosomal recycling endosomes, which were instead peripherally distributed in cells[279]. Further investigation of recycling endosome localisation through staining for the recycling endosome marker Rab11, measurement of LRP-1 surface levels, and visualisation of the cytoskeleton, would be required

to determine whether this possible mechanism for increasing the rate of endocytosis in the pericentriolar region is disturbed upon *Ttbk2* knockdown.

6.2.2 Cilia-independent mechanisms of ADAMTS-5 activity regulation by TTBK2

Cilia-independent functions of TTBK2 may also be required for the regulation of ADAMTS-5 activity by various mechanisms, and could be investigated in future studies. TTBK2 could indirectly regulate multiple cellular processes that affect ADAMTS-5 activity through its role in regulating microtubule dynamics[238]. Such cellular processes may include the protease endocytosis and LRP-1 receptor recycling discussed in Section 6.2.1, as the microtubule cytoskeleton is essential for vesicular trafficking. Previous studies have also demonstrated links between other cytoskeletal components, and both transcriptional and post-transcriptional processes regulating protease activity. For example, disruption of the actin cytoskeleton with cytochalasin D resulted in increased expression of various MMPs and increased activation of MMP-2 in human dermal fibroblasts[280], whereas acrylamide-mediated disruption of vimentin intermediate filaments in primary bovine chondrocytes reduced MMP-2 activation and collagen degradation[281]. Altered organisation of actin[282] and vimentin intermediate filaments[283] has been observed in osteoarthritic chondrocytes.

As ADAMTS-5 activity in my experimental system was not regulated at RNA level, as shown in Chapter 4, any protease activity-altering cytoskeletal changes downstream of *Ttbk2* knockdown would likely affect post-transcriptional processes such as ADAMTS-5 activation. The technical limitations of my experiments meant that I could not rule out whether conversion of pro-ADAMTS-5 to active ADAMTS-5 was elevated upon *Ttbk2* knockdown. Therefore, activation of pro-ADAMTS-5 should be further investigated in future studies as a potential mechanism by which TTBK2 regulates ADAMTS-5 activity, such as by determining whether the expression of molecules involved in this process are altered upon *Ttbk2* knockdown. These molecules include proprotein convertases such as PACE4[95] and furin[96], but also proteins that have been indirectly

linked to protease activation such as syndecan-4. Echtermeyer et al. (2009) found that deletion of syndecan-4 in mice reduced histological cartilage damage upon induction of osteoarthritis via DMM, which they proposed was due to reduced activation of ADAMTS-5 by MMP-3, although there is no direct experimental evidence for MMP-3-mediated conversion of pro- to active ADAMTS-5[249]. Genome-wide transcriptomic or proteomic analysis could also help to identify other cellular pathways that are disturbed upon *Ttbk2* knockdown and could be linked to dysregulation of ADAMTS-5 activity.

6.3 Identification of TTBK2 as a novel regulator of ADAMTS-5 activity

6.3.1 Implications for osteoarthritis

Osteoarthritis is one of the leading causes of disability globally[1], but currently the only recommended treatments are joint replacement surgery in severe disease and symptomatic relief[32]. There are currently no disease-modifying osteoarthritis drugs (DMOADs) available to slow the progression of the disease. Many of the proposed DMOADs targeting the proteases responsible for cartilage loss, such as protease inhibitors[126] and IL-1 antagonists[127], have failed to alter structural changes or pain in people with osteoarthritis in clinical trials, and have multiple side effects. The discovery of molecules involved in protease activity regulation is therefore important clinically, as it could lead to the identification of more selective therapeutic targets.

The finding that *Ttbk2* knockdown resulted in increased ADAMTS-5-mediated aggrecan degradation *in vitro* means that TTBK2 could be a potential therapeutic target in osteoarthritis. However, TTBK2 is expressed throughout the body and is essential for cell function, as illustrated by the human disease spinocerebellar ataxia 11 (SCA11), which results in the death of various neuronal cell types due to a truncating mutation of TTBK2[236]. Also, expression of a SCA11 TTBK2 mutation in mice resulted in embryonic lethality[284] and a TTBK2-null mutation resulted in severe embryonic defects *in vivo*[140]. Therefore, modulation of TTBK2 expression or function to in turn

modulate ADAMTS-5 activity could result in multiple adverse effects in chondrocytes, in which the cilium is thought to have an important role in mechanotransduction[178], and in other cell types, meaning that TTBK2 alone is likely to be a poor therapeutic target.

To reduce disruption of other cellular processes, another approach for a TTBK2-targeting osteoarthritis drug would be to disrupt the interaction between TTBK2 and the currently unknown proteins involved in the mechanism of TTBK2-mediated regulation of ADAMTS-5, particularly if these proteins have few or even no other functions in the cell. Therapeutically targeting protein-protein interactions has been investigated in the context of other diseases. For example, Vu et al. (2013) developed a small molecule that inhibited the interaction between a negative regulator of the tumour suppressor p53, Mouse double minute 2 homolog (MDM2) and p53, by mimicking the MDM2-interacting sites of p53[285]. This molecule reduced the growth of human osteosarcoma-derived tumours in mice. Identification of TTBK2 interactors could help with design of a similar drug that results in reduction of ADAMTS-5 activity.

Another important factor that should be considered in designing a potential TTBK2-related osteoarthritis drug is that ADAMTS-5 has an important role in maintaining normal matrix turnover and thus matrix homeostasis, as illustrated by the conditions associated with ADAMTS-5 deficiency discussed below in Section 6.3.2. Therefore, the use of a drug that results in complete inhibition of matrix-degrading ADAMTS-5 activity may cause fibrosis-related side effects similar to those seen in clinical trials of MMP inhibitors[126]. One possible solution to this is that, if TTBK2 regulates ADAMTS-5 via endocytosis, as discussed in Section 6.2.1, physiological levels of extracellular ADAMTS-5 could be preserved by pharmacologically modulating the rate of endocytosis with a drug targeting the TTBK2-ADAMTS-5 regulatory mechanism.

Other considerations when designing a potential TTBK2-related osteoarthritis drug include that the drug should also target sources of ADAMTS-5 within the joint other than chondrocytes, which have been the main focus of the experiments in this thesis. Weng et al. (2016) detected

ADAMTS-5 in synovial membrane tissue and synovial fluid from non-osteoarthritic human knee joints by western blot and ELISA respectively, and found that ADAMTS-5 levels were increased in osteoarthritic samples[286]. Rogers-DeCotes et al. (2021) also saw ADAMTS-5 expression in trabecular bone of the mouse temporomandibular joint via immunohistochemical staining[287]. The contribution of ADAMTS-5 secreted by either chondrocytes, bone cells or synovial cells to overall cartilage matrix degradation in osteoarthritis is unknown. Therefore, to ensure complete inhibition of pathological ADAMTS-5 activity in the joint, a drug targeting TTBK2-regulated cartilage matrix proteolysis should modulate ADAMTS-5 activity to similar extents in each cell type of the joint. To start to address this, my experiments in this thesis and any further mechanism-focused experiments should be repeated in bone and synovial cells alongside chondrocytes in future studies of the role of TTBK2 in ADAMTS-5 activity regulation. For example, as primary cilia are assembled by synoviocytes[201] and bone cells such as osteoblasts[288], measurement of aggrecan proteolysis upon ciliary protein disruption in these cells would help to determine the involvement of the primary cilium in the regulation of protease activity in other joint tissues outside cartilage.

6.3.2 Implications in diseases beyond osteoarthritis

Dysregulation of ADAMTS-5 activity is part of the pathogenesis of diseases other than osteoarthritis. Due to its role in cleaving the central nervous system-specific proteoglycan brevican that is present in the brain ECM, ADAMTS-5 has been associated with regulation of cancer cell invasion in glioblastoma, which is a common malignant brain tumour with a very low survival rate[289]. For example, Nakada et al. (2005) found that ADAMTS-5 protein levels were increased in glioblastoma brain samples relative to healthy controls, and that overexpression of ADAMTS-5 *in vitro* resulted in increased invasion through a brevican-containing matrix[290]. Viapiano et al. (2008) also found that injection of glioblastoma cell lines expressing uncleavable brevican due to a mutation in the ADAMTS-5 cleavage site into mouse brains, resulted in smaller tumour formation and increased survival relative to injection of WT cells[291].

ADAMTS-5-mediated cleavage of the proteoglycan versican has also been linked to the development of brain vascular lesions called cerebral cavernous malformations (CCM). In a mouse model of CCM, conditional knockdown of ADAMTS-5 in endothelial cells reduced CCM lesion volume, whereas induction of ADAMTS-5 expression increased angiogenesis-promoting versican fragment production and resulted in even more severe lesion formation[292]. Impaired ADAMTS-5-mediated versican and aggrecan degradation has also been linked to thoracic aortic aneurysm and dissection[293], and defects affecting the aorta were observed upon deletion of ADAMTS-5 *in vivo*[294,295]. Further study of the mechanism by which *Ttbk2* knockdown increased ADAMTS-5 activity could therefore help in the development of new therapies to restore normal ADAMTS-5 activity in these diseases.

LRP-1 also has a role in the pathogenesis of other diseases. For example, Kanekiyo et al. (2011) found that siRNA-mediated knockdown of LRP-1 in mouse neuronal cell lines or treatment of primary mouse neurons with anti-LRP-1 antibodies reduced the endocytosis of amyloid beta peptides, the aggregation of which causes neurodegenerative conditions such as Alzheimer's disease[296]. Rauch et al. (2020) also saw that endocytosis of another protein with a crucial role in neurodegeneration, tau, was impaired when LRP-1 was depleted via CRISPR/Cas9 technology in a human neuroglioma cell line or upon treatment of cells with RAP[297]. These studies highlight how further investigation of the effect of TTBK2 knockdown on LRP-1-mediated endocytosis could have wider relevance outside osteoarthritis.

6.4 Strengths and limitations

I chose a mouse chondrocyte cell line to investigate the contribution of ciliary proteins to the regulation of protease activity due to the tractable nature of this system. These cells could be easily genetically modified to deplete a range of proteins of interest, which would have likely been more difficult and time consuming in other experimental systems, such as primary cells or

generation of knockout mice. However, one of the main disadvantages of using a cell line, and specifically a chondrocyte cell line in monolayer culture, is the potential loss of the cellular phenotype observed *in vivo*. Numerous studies have shown that serial culture of primary chondrocytes results in a change in morphology from the rounded appearance seen *in vivo* to a more fibroblastic, flattened shape, as well as a reduction in expression of cartilage matrix molecules such as type II collagen[298–300]. This dedifferentiation of chondrocytes has even been shown to affect primary cilia. Serial passaging of primary bovine articular chondrocytes resulted in progressive loss of cilia and altered Hh signalling[301]. The effects of dedifferentiation on the phenotype of chondrocytes can be alleviated by culturing cells in 3D. For example, expression of the type II collagen gene was increased in a mouse chondrocyte cell line cultured in alginate beads relative to monolayer cultures[302]. Culture of human articular chondrocytes in alginate beads or cell pellets also increased sGAG generation and expression of chondrogenic markers relative to chondrocytes in monolayer, although type II collagen expression at protein level was increased across all three conditions[303].

Given the importance of 3D culture for maintaining chondrocyte phenotype *in vitro*, cartilage explants could provide a more physiological experimental system that is also rich in cartilage matrix substrate. However, use of bovine or porcine tissue explants is hampered by the lack of reagents for genetic modification in these species. Also, whilst an siRNA-based approach has been used to investigate the molecular basis of protease activity regulation in human cartilage explants[61], the availability of human samples, and particularly non-osteoarthritic control samples, is limited. In summary, repeating the experiments presented in this chapter in systems that better preserve the chondrocyte phenotype, such as 3D culture of primary chondrocytes, would help to determine whether the results in this thesis are also valid in more biologically and physiologically relevant systems.

Another limitation of my experimental system was the limited knockdown efficiency achieved with siRNAs. This, combined with the limited sensitivity and range of assays such as western blot analysis of ADAMTS-5 protein and potentially the ADAMTS-5 endocytosis assay, meant that the cellular changes that resulted in increased ADAMTS-5 activity upon *Ttbk2* knockdown were potentially undetectable. Use of higher concentrations of siRNA increased *Ttbk2* knockdown efficiency by only 10% and had no effect on AGEG generation. Therefore, to avoid any cytotoxic effects of using even higher doses of siRNA to achieve more efficient knockdown, future experiments could use an alternative technique for depleting ciliary proteins. For example, the CRISPR/Cas9 system has been used in various cell lines to deplete ciliary proteins such as IFT88, albeit with different levels of efficacy[304,305]. Other options include the use of small molecule inhibitors, such as a recently described inhibitor of both TTBK2 and the central nervous system-specific TTBK1[306], to investigate the role of TTBK2-mediated phosphorylation in the regulation of ADAMTS-5 activity, or the use of chondrocytes isolated from TTBK2-null mice.

Other limitations include the use of only one reference gene for qPCR. As shown in Chapter 2, expression of the reference gene used in this thesis (*18s*) was stable across experimental conditions. However, to improve the reliability of my gene expression data, I could have evaluated the stability of a panel of reference genes in my experiments and used at least two of the most stable reference genes in every qPCR experiment, as recommended in the Minimum Information for Publication of Quantitative Real-Time PCR Experiments (MIQE) guidelines[307]. Another limitation was the incomplete validation of β-actin as a loading control during western blotting of cell lysates. As discussed in Section 2.4.5, previous work by the Wann group and previous studies on the role of primary cilia in metabolism suggested that the loading controls β-tubulin and GAPDH would not be stably expressed when ciliary proteins were disrupted. However, primary cilia have also been linked to the actin cytoskeleton[137]. Also, I did not directly check whether levels of β-actin were stable across experimental conditions, such as by

comparing β-actin signal to Revert total protein signal when ciliary genes were targeted with siRNAs.

6.5 Future work

In future studies, the generation and study of the musculoskeletal phenotype of TTBK2-null mice would help to address the two major limitations of my work in a chondrocyte cell line discussed above. As constitutive, whole-body knockdown of TTBK2 resulted in severe embryonic defects in mice[140], cartilage-specific deletion of TTBK2 would need to be used *in vivo* to reduce potential disruption of non-cartilaginous tissues. Also, as the primary cilium has an important role in cartilage development via Hh signalling[170], deletion of TTBK2 would need to be induced in adult mice to ensure that any cartilage matrix changes observed are not a result of altered cartilage development. To achieve cartilage-specific, inducible deletion of TTBK2, mice expressing tamoxifen-inducible Cre-recombinase in aggrecan-expressing cells could be used. Injection of tamoxifen has been shown to result in successful disruption of reporter gene expression in articular chondrocytes of these mice after skeletal maturity[308]. Histological analysis of proteoglycan content and immunohistochemical detection of aggrecan neoepitopes could then be used to investigate cartilage matrix catabolism upon TTBK2 knockdown *in vivo*.

Another direction for future work would be to investigate whether TTBK2 is involved in the pathogenesis of osteoarthritis. A potential starting point in addressing this question would be to determine whether *TTBK2* expression is reduced in osteoarthritic cartilage relative to non-osteoarthritic cartilage. *TTBK2* expression could be measured in the lab via qPCR in human cartilage samples, or bioinformatics tools such as SkeletalVis could be used to explore existing RNA-seq and microarray datasets looking at gene expression changes in osteoarthritis. SkeletalVis is an online repository of transcriptomics data from over 300 studies relevant to skeletal biology and disease, including osteoarthritis[309]. A preliminary search of the SkeletalVis database showed that, in the study that analysed the highest number of osteoarthritic and non-

osteoarthritic human articular cartilage samples, *TTBK2* expression was statistically significantly downregulated in osteoarthritis[310].

However, one issue with analysis of gene expression to address whether TTBK2 is involved in osteoarthritis, is that any post-transcriptional dysregulation of TTBK2 function in disease would be missed. Measurement of TTBK2 protein expression would partially solve this problem. Although, based on my failure to identify TTBK2 by western blot in mouse chondrocyte cell line lysates containing high amounts of cellular, non-matrix-associated proteins, obtaining enough healthy and osteoarthritic cartilage to detect TTBK2 at protein level could be very difficult. Another problem is that TTBK2 expression and function may not be affected in osteoarthritis, and instead, the molecules downstream of TTBK2 that facilitate its regulation of ADAMTS-5 activity are disturbed. However, in the absence of a clear understanding of how knockdown of TTBK2 increases ADAMTS-5 activity, the identity of these molecules is unknown.

Further investigation into the molecular and cellular mechanism by which *Ttbk2* knockdown increases ADAMTS-5 activity therefore forms the other major direction of future work. As discussed in Section 4.3.6, there are many possible experiments to strengthen the evidence that *Ttbk2* knockdown does not affect transcriptional, Hh-dependent and TIMP-3-dependent mechanisms of ADAMTS-5 activity regulation. To investigate protease activation, the development of more sensitive methods to detect ADAMTS-5 protein is required in future experiments. As discussed in Section 5.3.4, developing alternative ADAMTS-5 endocytosis assays will also form a crucial part of any future studies addressing this mechanistic question. Also, as discussed above in Section 0, there are a number of hypotheses for how knockdown of TTBK2 could disrupt LRP-1-mediated endocytosis, which should be tested alongside measurement of endocytic rate with functional assays.

6.6 Conclusions

In this thesis, I have identified a novel regulator of cartilage extracellular matrix degradation, which is the centriolar kinase TTBK2. I have shown that *Ttbk2* knockdown increased ADAMTS-5-mediated aggrecan proteolysis in a mouse chondrocyte cell line. This result could be important in the context of a disease characterised by increased protease activity, osteoarthritis, for which there are currently no drugs to stop its progression.

Determining the molecular mechanism of action of TTBK2 will provide further insight into the potential of molecules involved in TTBK2-ADAMTS-5 regulatory axis as therapeutic targets, and the work I have conducted has helped to rule out some important protease-regulating processes. I have found evidence that *Ttbk2* knockdown increased ADAMTS-5 activity via a non-transcriptional, Hh-independent and TIMP-3 independent mechanism. However, further work is required to understand the role of TTBK2 in another major mechanism regulating proteolytic matrix catabolism, protease endocytosis. Further investigation into the mechanism of action of TTBK2 could therefore help in the development of new strategies to modulate protease activity and ultimately restore normal levels of protease activity in osteoarthritis.

REFERENCES

1. Cross, M. *et al.* The global burden of hip and knee osteoarthritis: Estimates from the Global Burden of Disease 2010 study. *Ann. Rheum. Dis.* **73**, 1323–1330 (2014).

2. Kluzek, S. *et al.* Painful knee but not hand osteoarthritis is an independent predictor of mortality over 23 years follow-up of a population-based cohort of middle-aged women. *Ann. Rheum. Dis.* **75**, 1749–1756 (2016).

3. Safiri, S. *et al.* Global, regional and national burden of osteoarthritis 1990-2017: A systematic analysis of the Global Burden of Disease Study 2017. *Ann. Rheum. Dis.* **79**, 819–828 (2020).

4. Hunziker, E. B., Quinn, T. M. & Häuselmann, H. J. Quantitative structural organization of normal adult human articular cartilage. *Osteoarthr. Cartil.* **10**, 564–572 (2002).

5. Buckwalter, J. A., Mow, V. C. & Ratcliffe, A. Restoration of injured or degenerated articular cartilage. *J. Am. Acad. Orthop. Surg.* **2**, 192–201 (1994).

6. Karim, A., Amin, A. K. & Hall, A. C. The clustering and morphology of chondrocytes in normal and mildly degenerate human femoral head cartilage studied by confocal laser scanning microscopy. *J. Anat.* **232**, 686–698 (2018).

7. Clarke, I. C. Articular cartilage: a review and scanning electron microscope study. 1. The interterritorial fibrillar architecture. *J. Bone Joint Surg. Br.* **53**, 732–750 (1971).

8. Muir, H., Bullough, P. & Maroudas, A. The distribution of collagen in human articular cartilage with some of its physiological implications. *J. Bone Joint Surg. Br.* **52**, 554–563 (1970).

9. Bank, R. A., Soudry, M., Maroudas, A., Mizrahi, J. & Tekoppele, J. M. The increased swelling and instantaneous deformation of osteoarthritic cartilage is highly correlated with collagen degradation. *Arthritis Rheum.* **43**, 2202–2210 (2000).

10. Venn, M. & Maroudas, A. Chemical composition and swelling of normal and osteoarthrotic femoral head cartilage. I. Chemical composition. *Ann. Rheum. Dis.* **36**, 121–129 (1977).

11. Schmidt, M. B., Mow, V. C., Chun, L. E. & Eyre, D. R. Effects of proteoglycan extraction on the tensile behavior of articular cartilage. *J. Orthop. Res.* **8**, 353–363 (1990).

12. Armstrong, C. G. & Mow, V. C. Variations in the intrinsic mechanical properties of human articular cartilage with age, degeneration, and water content. *J. Bone Joint Surg. Am.* **64**,

88–94 (1982).

13. Pritzker, K. P. H. *et al.* Osteoarthritis cartilage histopathology: Grading and staging. *Osteoarthr. Cartil.* **14**, 13–29 (2006).

14. Lane, N. E. *et al.* OARSI-FDA initiative: Defining the disease state of osteoarthritis. *Osteoarthr. Cartil.* **19**, 478–482 (2011).

15. Hollander, A. P. *et al.* Increased damage to type II collagen in osteoarthritic articular cartilage detected by a new immunoassay. *J. Clin. Invest.* **93**, 1722–1732 (1994).

16. Mankin, H. J., Dorfman, H., Lippiello, L. & Zarins, A. Biochemical and metabolic abnormalities in articular cartilage from osteo-arthritic human hips. II: Correlation of morphology with biochemical and metabolic data. *J. Bone Joint Surg Am.* **53**, 523–37 (1971).

17. Glyn-Jones, S. *et al.* Osteoarthritis. *The Lancet* **386**, 376–387 (2015).

18. Li, B. & Aspden, R. M. Mechanical and material properties of the subchondral bone plate from the femoral head of patients with osteoarthritis or osteoporosis. *Ann. Rheum. Dis.* **56**, 247–254 (1997).

19. Felson, D. T. *et al.* Defining radiographic osteoarthritis for the whole knee. *Osteoarthr. Cartil.* **5**, 241–250 (1997).

20. Oehler, S., Neureiter, D., Meyer-Scholten, C. & Aigner, T. Subtyping of osteoarthritic synoviopathy. *Clin. Exp. Rheumatol.* **20**, 633–640 (2002).

21. Ludwig, T. E., McAllister, J. R., Lun, V., Wiley, J. P. & Schmidt, T. A. Diminished cartilage-lubricating ability of human osteoarthritic synovial fluid deficient in proteoglycan 4: Restoration through proteoglycan 4 supplementation. *Arthritis Rheum.* **64**, 3963–3971 (2012).

22. Oliveria, S. A., Felson, D. T., Reed, J. I., Cirillo, P. A. & Walker, A. M. Incidence of symptomatic hand, hip, and knee osteoarthritis among patients in a health maintenance organization. *Arthritis Rheum.* **38**, 1134–1141 (1995).

23. Rasheed, Z., Akhtar, N. & Haqqi, T. M. Advanced glycation end products induce the expression of interleukin-6 and interleukin-8 by receptor for advanced glycation end product-mediated activation of mitogen-activated protein kinases and nuclear factor-κB in human osteoarthritis chondrocytes. *Rheumatology* **50**, 838–851 (2011).

24. Bank, R. A., Bayliss, M. T., Lafeber, F. P. J. G., Maroudas, A. & Tekoppele, J. M. Ageing and zonal variation in post-translational modification of collagen in normal human articular cartilage: The age-related increase in Non-Enzymatic Glycation affects biomechanical properties of cartilage. *Biochem. J.* **330**, 345–351 (1998).

25. Martin, J. A., Ellerbroek, S. M. & Buckwalter, J. A. Age-related decline in chondrocyte response to insulin-like growth factor-I: The role of growth factor binding proteins. *J. Orthop. Res.* **15**, 491–498 (1997).

26. Tachmazidou, I. *et al.* Identification of new therapeutic targets for osteoarthritis through genome-wide analyses of UK Biobank data. *Nat. Gen.* **51**, 230–236 (2019).

27. Blagojevic, M., Jinks, C., Jeffery, A. & Jordan, K. P. Risk factors for onset of osteoarthritis of the knee in older adults: a systematic review and meta-analysis. *Osteoarthr. Cartil.* **18**, 24–33 (2010).

28. Altman, R. *et al.* Development of criteria for the classification and reporting of osteoarthritis: Classification of osteoarthritis of the knee. *Arthritis Rheum.* **29**, 1039–1049 (1986).

29. Lohmander, L. S., Östenberg, A., Englund, M. & Roos, H. High prevalence of knee osteoarthritis, pain, and functional limitations in female soccer players twelve years after anterior cruciate ligament injury. *Arthritis Rheum.* **50**, 3145–3152 (2004).

30. Räsänen, P. *et al.* Effectiveness of hip or knee replacement surgery in terms of quality-adjusted life years and costs. *Acta Orthop.* **78**, 108–115 (2007).

31. Bayliss, L. E. *et al.* The effect of patient age at intervention on risk of implant revision after total replacement of the hip or knee: a population-based cohort study. *Lancet* **389**, 1424–1430 (2017).

32. Bannuru, R. R. *et al.* OARSI guidelines for the non-surgical management of knee, hip, and polyarticular osteoarthritis. *Osteoarthr. Cartil.* **27**, 1578–1589 (2019).

33. Moore, E. E. *et al.* Fibroblast growth factor-18 stimulates chondrogenesis and cartilage repair in a rat model of injury-induced osteoarthritis. *Osteoarthr. Cartil.* **13**, 623–631 (2005).

34. Sennett, M. L. *et al.* Sprifermin treatment enhances cartilage integration in an in vitro repair model. *J. Orthop. Res.* **36**, 2648–2656 (2018).

35. Hochberg, M. C. *et al.* Effect of intra-articular sprifermin vs placebo on femorotibial joint cartilage thickness in patients with osteoarthritis: The FORWARD randomized clinical trial. *JAMA* **322**, 1360–1370 (2019).

36. Mohan, G. *et al.* Pre-emptive, early, and delayed alendronate treatment in a rat model of knee osteoarthritis: Effect on subchondral trabecular bone microarchitecture and cartilage degradation of the tibia, bone/cartilage turnover, and joint discomfort. *Osteoarthr. Cartil.* **21**, 1595–1604 (2013).

37. Vaysbrot, E. E., Osani, M. C., Musetti, M. C., McAlindon, T. E. & Bannuru, R. R. Are bisphosphonates efficacious in knee osteoarthritis? A meta-analysis of randomized controlled trials. *Osteoarthr. Cartil.* **26**, 154–164 (2018).

38. Knäuper, V., López-Otin, C., Smith, B., Knight, G. & Murphy, G. Biochemical characterization of human collagenase-3. *J. Biol. Chem.* **271**, 1544–1550 (1996).

39. Billinghurst, R. C. *et al.* Enhanced cleavage of type II collagen by collagenases in osteoarthritic articular cartilage. *J. Clin. Invest.* **99**, 1534–1545 (1997).

40. Dahlberg, L. *et al.* Selective enhancement of collagenase-mediated cleavage of resident type II collagen in cultured osteoarthritic cartilage and arrest with a synthetic inhibitor that spares collagenase 1 (Matrix metalloproteinase 1). *Arthritis Rheum.* **43**, 673–682 (2000).

41. Tetlow, L. C., Adlam, D. J. & Woolley, D. E. Matrix metalloproteinase and proinflammatory cytokine production by chondrocytes of human osteoarthritic cartilage; Associations with degenerative changes. *Arthritis Rheum.* **44**, 585–594 (2001).

42. Kevorkian, L. *et al.* Expression Profiling of Metalloproteinases and Their Inhibitors in Cartilage. *Arthritis Rheum.* **50**, 131–141 (2004).

43. Neuhold, L. A. *et al.* Postnatal expression in hyaline cartilage of constitutively active human collagenase-3 (MMP-13) induces osteoarthritis in mice. *J. Clin. Invest.* **107**, 35–44 (2001).

44. Little, C. B. *et al.* Matrix metalloproteinase 13-deficient mice are resistant to osteoarthritic cartilage erosion but not chondrocyte hypertrophy or osteophyte development. *Arthritis Rheum.* **60**, 3723–3733 (2009).

45. Kafienah, W., Brömme, D., Buttle, D. J., Croucher, L. J. & Hollander, A. P. Human cathepsin K cleaves native type I and II collagens at the N-terminal end of the triple helix. *Biochem.*

J. **331**, 727–732 (1998).

46. Dejica, V. M. *et al.* Cleavage of type II collagen by cathepsin K in human osteoarthritic cartilage. *Am. J. Pathol.* **173**, 161–169 (2008).

47. Hayami, T., Zhuo, Y., Wesolowski, G. A., Pickarski, M. & Duong, L. T. Inhibition of cathepsin K reduces cartilage degeneration in the anterior cruciate ligament transection rabbit and murine models of osteoarthritis. *Bone* **50**, 1250–1259 (2012).

48. Sandy, J. D., Neame, P. J., Boynton, R. E. & Flannery, C. R. Catabolism of aggrecan in cartilage explants: Identification of a major cleavage site within the interglobular domain. *J. Biol. Chem.* **266**, 8683–8685 (1991).

49. Sandy, J. D. & Verscharen, C. Analysis of aggrecan in human knee cartilage and synovial fluid indicates that aggrecanase (ADAMTS) activity is responsible for the catabolic turnover and loss of whole aggrecan whereas other protease activity is required for C-terminal processing in vivo. *Biochem. J.* **358**, 615–626 (2001).

50. Malfait, A. M., Liu, R. Q., Ijiri, K., Komiya, S. & Tortorella, M. D. Inhibition of ADAM-TS4 and ADAM-TS5 prevents aggrecan degradation in osteoarthritic cartilage. *J. Biol. Chem.* **277**, 22201–22208 (2002).

51. Dingle, J. T., Page Thomas, D. P., King, B. & Bard, D. R. In vivo studies of articular tissue damage mediated by catabolin/interleukin 1. *Ann. Rheum. Dis.* **46**, 527–533 (1987).

52. Tortorella, M. D. *et al.* Purification and cloning of aggrecanase-1: A member of the ADAMTS family of proteins. *Science* **284**, 1664–1666 (1999).

53. Tortorella, M. D. *et al.* Sites of aggrecan cleavage by recombinant human aggrecanase-1 (ADAMTS-4). *J. Biol. Chem.* **275**, 18566–18573 (2000).

54. Tortorella, M. D., Liu, R. Q., Burn, T., Newton, R. C. & Arner, E. Characterization of human aggrecanase 2 (ADAM-TS5): Substrate specificity studies and comparison with aggrecanase 1 (ADAM-TS4). *Matrix Biol.* **21**, 499–511 (2002).

55. Gendron, C. *et al.* Proteolytic activities of human ADAMTS-5: Comparative studies with ADAMTS-4. *J. Biol. Chem.* **282**, 18294–18306 (2007).

56. Glasson, S. S. *et al.* Characterization of and osteoarthritis susceptibility in ADAMTS-4-knockout mice. *Arthritis Rheum.* **50**, 2547–2558 (2004).

57. Glasson, S. S. *et al.* Deletion of active ADAMTS5 prevents cartilage degradation in a

murine model of osteoarthritis. *Nature* **434**, 644–648 (2005).

58. Stanton, H. *et al.* ADAMTS5 is the major aggrecanase in mouse cartilage in vivo and in vitro. *Nature* **434**, 648–652 (2005).

59. Larkin, J. *et al.* Translational development of an ADAMTS-5 antibody for osteoarthritis disease modification. *Osteoarthr. Cartil.* **23**, 1254–1266 (2015).

60. Ismail, H. M. *et al.* Interleukin-1 acts via the JNK-2 signaling pathway to induce aggrecan degradation by human chondrocytes. *Arthritis Rheum.* **67**, 1826–1836 (2015).

61. Song, R. H. *et al.* Aggrecan degradation in human articular cartilage explants is mediated by both ADAMTS-4 and ADAMTS-5. *Arthritis Rheum.* **56**, 575–585 (2007).

62. Naito, S. *et al.* Expression of ADAMTS4 (aggrecanase-1) in human osteoarthritic cartilage. *Pathol. Int.* **57**, 703–711 (2007).

63. Bau, B. *et al.* Relative messenger RNA expression profiling of collagenases and aggrecanases in human articular chondrocytes in vivo and in vitro. *Arthritis Rheum.* **46**, 2648–2657 (2002).

64. Fan, Z., Bau, B., Yang, H., Soeder, S. & Aigner, T. Freshly isolated osteoarthritic chondrocytes are catabolically more active than normal chondrocytes, but less responsive to catabolic stimulation with interleukin-1β. *Arthritis Rheum.* **52**, 136–143 (2005).

65. Plaas, A. *et al.* Aggrecanolysis in human osteoarthritis: confocal localization and biochemical characterization of ADAMTS5-hyaluronan complexes in articular cartilages. *Osteoarthr. Cartil.* **15**, 719–734 (2007).

66. Fosang, A. J., Last, K., Knäuper, V., Murphy, G. & Neame, P. J. Degradation of cartilage aggrecan by collagenase-3 (MMP-13). *FEBS Lett.* **380**, 17–20 (1996).

67. Carlos Rodríguez-Manzaneque, J. *et al.* ADAMTS1 cleaves aggrecan at multiple sites and is differentially inhibited by metalloproteinase inhibitors. *Biochem. Biophys. Res. Commun.* **293**, 501–508 (2002).

68. Tortorella, M. & Malfait, A. Will the real aggrecanase(s) step up: Evaluating the criteria that define aggrecanase activity in osteoarthritis. *Curr. Pharm. Biotechnol.* **9**, 16–23 (2008).

69. Little, C. B. *et al.* ADAMTS-1-knockout mice do not exhibit abnormalities in aggrecan

turnover in vitro or in vivo. *Arthritis Rheum.* **52**, 1461–1472 (2005).

70. Hou, W. S., Li, Z., Büttner, F. H., Bartnik, E. & Brömme, D. Cleavage site specificity of cathepsin K toward cartilage proteoglycans and protease complex formation. *Biol. Chem.* **384**, 891–897 (2003).

71. Pratta, M. A. *et al.* Aggrecan protects cartilage collagen from proteolytic cleavage. *J. Biol. Chem.* **278**, 45539–45545 (2003).

72. Jiménez, M. J. G. *et al.* Collagenase 3 is a target of Cbfa1, a transcription factor of the runt gene family involved in bone formation. *Mol. Cell. Biol.* **19**, 4431–4442 (1999).

73. Thirunavukkarasu, K., Pei, Y. & Wei, T. Characterization of the human ADAMTS-5 (aggrecanase-2) gene promoter. *Mol. Biol. Rep.* **34**, 225–231 (2007).

74. Kamekura, S. *et al.* Contribution of Runt-related transcription factor 2 to the pathogenesis of osteoarthritis in mice after induction of knee joint instability. *Arthritis Rheum.* **54**, 2462–2470 (2006).

75. Lin, A. C. *et al.* Modulating hedgehog signaling can attenuate the severity of osteoarthritis. *Nat. Med.* **15**, 1421–1425 (2009).

76. Yan, D., Chen, D. & Im, H. J. Fibroblast growth factor-2 promotes catabolism via FGFR1-Ras-Raf-MEK1/2- ERK1/2 axis that coordinates with the PKCδ pathway in human articular chondrocytes. *J. Cell. Biochem.* **113**, 2856–2865 (2012).

77. Tetsunaga, T. *et al.* Regulation of mechanical stress-induced MMP-13 and ADAMTS-5 expression by RUNX-2 transcriptional factor in SW1353 chondrocyte-like cells. *Osteoarthr. Cartil.* **19**, 222–232 (2011).

78. Burleigh, A. *et al.* Joint immobilization prevents murine osteoarthritis and reveals the highly mechanosensitive nature of protease expression in vivo. *Arthritis Rheum.* **64**, 2278–2288 (2012).

79. Vincent, T. L. Mechanoflammation in osteoarthritis pathogenesis. *Semin. Arthritis Rheum.* **49**, S36–S38 (2019).

80. Kapoor, M., Martel-Pelletier, J., Lajeunesse, D., Pelletier, J. P. & Fahmi, H. Role of proinflammatory cytokines in the pathophysiology of osteoarthritis. *Nat. Rev. Rheumatol.* **7**, 33–42 (2011).

81. Kobayashi, M. *et al.* Role of interleukin-1 and tumor necrosis factor α in matrix

degradation of human osteoarthritic cartilage. *Arthritis Rheum.* **52**, 128–135 (2005).

82. Clements, K. M. *et al.* Gene deletion of either interleukin-1β, interleukin-1β -converting enzyme, inducible nitric oxide synthase, or stromelysin 1 accelerates the development of knee osteoarthritis in mice after surgical transection of the medial collateral ligament and partial medial meniscectomy. *Arthritis Rheum.* **48**, 3452–3463 (2003).

83. Ryu, J. H. *et al.* Interleukin-6 plays an essential role in hypoxia-inducible factor 2α-induced experimental osteoarthritic cartilage destruction in mice. *Arthritis Rheum.* **63**, 2732–2743 (2011).

84. Beekhuizen, M. *et al.* An explorative study comparing levels of soluble mediators in control and osteoarthritic synovial fluid. *Osteoarthr. Cartil.* **21**, 918–922 (2013).

85. Dai, S. M., Shan, Z. Z., Nishioka, K. & Yudoh, K. Implication of interleukin 18 in production of matrix metalloproteinases in articular chondrocytes in arthritis: Direct effect on chondrocytes may not be pivotal. *Ann. Rheum. Dis.* **64**, 735–742 (2005).

86. Inoue, H. *et al.* High levels of serum IL-18 promote cartilage loss through suppression of aggrecan synthesis. *Bone* **42**, 1102–1110 (2008).

87. Plater-Zyberk, C. *et al.* Therapeutic effect of neutralizing endogenous IL-18 activity in the collagen-induced model of arthritis. *J. Clin. Invest.* **108**, 1825–1832 (2001).

88. Liacini, A., Sylvester, J., Li, W. Q. & Zafarullah, M. Inhibition of interleukin-1-stimulated MAP kinases, activating protein-1 (AP-1) and nuclear factor kappa B (NF-κB) transcription factors down-regulates matrix metalloproteinase gene expression in articular chondrocytes. *Matrix Biol.* **21**, 251–262 (2002).

89. Kobayashi, H. *et al.* Transcriptional induction of ADAMTS5 protein by nuclear factor-κB (NF-κB) family member RelA/p65 in chondrocytes during osteoarthritis development. *J. Biol. Chem.* **288**, 28620–28629 (2013).

90. Knäuper, V. *et al.* Cellular mechanisms for human procollagenase-3 (MMP-13) activation. Evidence that MT1-MMP (MMP-14) and gelatinase A (MMP-2) are able to generate active enzyme. *J. Biol. Chem.* **271**, 17124–17131 (1996).

91. Gao, G. *et al.* Activation of the proteolytic activity of ADAMTS4 (aggrecanase-1) by C-terminal truncation. *J. Biol. Chem.* **277**, 11034–11041 (2002).

92. Moldovan, F. *et al.* Modulation of collagenase 3 in human osteoarthritic cartilage by

activation of extracellular transforming growth factor β: Role of furin convertase. *Arthritis Rheum.* **43**, 2100–2109 (2000).

93. Wang, P. *et al.* Proprotein convertase furin interacts with and cleaves pro-ADAMTS4 (Aggrecanase-1) in the trans-golgi network. *J. Biol. Chem.* **279**, 15434–15440 (2004).

94. Tortorella, M. D. *et al.* ADAMTS-4 (aggrecanase-1): N-Terminal activation mechanisms. *Arch. Biochem. Biophys.* **444**, 34–44 (2005).

95. Malfait, A. M. *et al.* Proprotein convertase activation of aggrecanases in cartilage in situ. *Arch. Biochem. Biophys.* **478**, 43–51 (2008).

96. Longpré, J. M. *et al.* Characterization of proADAMTS5 processing by proprotein convertases. *Int. J. Biochem. Cell Biol.* **41**, 1116–1126 (2009).

97. Murphy, G. & Willenbrock, F. Tissue inhibitors of matrix metalloendopeptidases. *Methods Enzymol.* **248**, 496–510 (1995).

98. Kashiwagi, M., Tortorella, M., Nagase, H. & Brew, K. TIMP-3 Is a potent inhibitor of aggrecanase 1 (ADAM-TS4) and aggrecanase 2 (ADAM-TS5). *J. Biol. Chem.* **276**, 12501–12504 (2001).

99. Gendron, C., Kashiwagi, M., Hughes, C., Caterson, B. & Nagase, H. TIMP-3 inhibits aggrecanase-mediated glycosaminoglycan release from cartilage explants stimulated by catabolic factors. *FEBS Lett.* **555**, 431–436 (2003).

100. Sahebjam, S., Khokha, R. & Mort, J. S. Increased collagen and aggrecan degradation with age in the joints of *Timp3*$^{-/-}$ mice. *Arthritis Rheum.* **56**, 905–909 (2007).

101. Kanakis, I. *et al.* Targeted inhibition of aggrecanases prevents articular cartilage degradation and augments bone mass in the STR/ort mouse model of spontaneous osteoarthritis. *Arthritis Rheum.* **71**, 571–582 (2019).

102. Nakamura, H., Vo, P., Kanakis, I., Liu, K. & Bou-Gharios, G. Aggrecanase-selective tissue inhibitor of metalloproteinase-3 (TIMP3) protects articular cartilage in a surgical mouse model of osteoarthritis. *Sci. Rep.* **10**, (2020).

103. Morris, K. J., Cs-Szabo, G. & Cole, A. A. Characterization of TIMP-3 in human articular talar cartilage. *Connect. Tissue Res.* **51**, 478–490 (2010).

104. Troeberg, L. *et al.* Calcium pentosan polysulfate is a multifaceted exosite inhibitor of aggrecanases. *FASEB J.* **22**, 3515–3524 (2008).

105. Scilabra, S. D. *et al.* Differential regulation of extracellular tissue inhibitor of metalloproteinases-3 levels by cell membrane-bound and shed low density lipoprotein receptor-related protein 1. *J. Biol. Chem.* **288**, 332–342 (2013).

106. Herz, J., Clouthier, D. E. & Hammer, R. E. LDL receptor-related protein internalizes and degrades uPA-PAI-1 complexes and is essential for embryo implantation. *Cell* **71**, 411–421 (1992).

107. Lillis, A. P., Van Duyn, L. B., Murphy-Ullrich, J. E. & Strickland, D. K. LDL receptor-related protein 1: unique tissue-specific functions revealed by selective gene knockout studies. *Physiol. Rev.* **88**, 887–918 (2008).

108. Herz, J., Goldstein, J. L., Strickland, D. K., Ho, Y. K. & Brown, M. S. 39-kDa protein modulates binding of ligands to low density lipoprotein receptor-related protein/α2-macroglobulin receptor. *J. Biol. Chem.* **266**, 21232–21238 (1991).

109. Bu, G., Geuze, H. J., Strous, G. J. & Schwartz, A. L. 39 kDa receptor-associated protein is an ER resident protein and molecular chaperone far LDL receptor-related protein. *EMBO J.* **14**, 2269–2280 (1995).

110. Troeberg, L. *et al.* Sulfated glycosaminoglycans control the extracellular trafficking and the activity of the metalloprotease inhibitor TIMP-3. *Chem. Biol.* **21**, 1300–1309 (2014).

111. Chanalaris, A. *et al.* Suramin inhibits osteoarthritic cartilage degradation by increasing extracellular levels of chondroprotective tissue inhibitor of metalloproteinases 3. *Mol. Pharmacol.* **92**, 459–468 (2017).

112. Guns, L.-A. *et al.* Suramin increases cartilage proteoglycan accumulation in vitro and protects against joint damage triggered by papain injection in mouse knees in vivo. *RMD Open* **3**, e000604 (2017).

113. Scilabra, S. D. *et al.* Increased TIMP-3 expression alters the cellular secretome through dual inhibition of the metalloprotease ADAM10 and ligand-binding of the LRP-1 receptor. *Sci. Rep.* **8**, 14687 (2018).

114. Carreca, A. P. *et al.* Quantitative proteomics reveals changes induced by TIMP-3 on cell membrane composition and novel metalloprotease substrates. *Int. J. Mol. Sci.* **22**, 1–20 (2021).

115. Emonard, H. *et al.* Low density lipoprotein receptor-related protein mediates endocytic clearance of pro-MMP-2-TIMP-2 complex through a thrombospondin-independent

mechanism. *J. Biol. Chem.* **279**, 54944–54951 (2004).

116. Barmina, O. Y. *et al.* Collagenase-3 binds to a specific receptor and requires the low density lipoprotein receptor-related protein for internalization. *J. Biol. Chem.* **274**, 30087–30093 (1999).

117. Yamamoto, K. *et al.* LRP-1-mediated endocytosis regulates extracellular activity of ADAMTS-5 in articular cartilage. *FASEB J.* **27**, 511–521 (2013).

118. Yamamoto, K. *et al.* Low density lipoprotein receptor-related protein 1 (LRP1)-mediated endocytic clearance of a disintegrin and metalloproteinase with thrombospondin motifs-4 (ADAMTS-4): Functional differences of non-catalytic domains of ADAMTS-4 and ADAMTS-5 in LRP1 binding. *J. Biol. Chem.* **289**, 6462–6474 (2014).

119. Yamamoto, K. *et al.* MMP-13 is constitutively produced in human chondrocytes and co-endocytosed with ADAMTS-5 and TIMP-3 by the endocytic receptor LRP1. *Matrix Biol.* **56**, 57–73 (2016).

120. Yamamoto, K. *et al.* Inhibition of shedding of Low-density lipoprotein receptor–related protein 1 reverses cartilage matrix degradation in osteoarthritis. *Arthritis Rheum.* **69**, 1246–1256 (2017).

121. Quinn, K. A., Pye, V. J., Dai, Y. P., Chesterman, C. N. & Owensby, D. A. Characterization of the soluble form of the low density lipoprotein receptor-related protein (LRP). *Exp. Cell Res.* **251**, 433–441 (1999).

122. Selvais, C. *et al.* Metalloproteinase-dependent shedding of low-density lipoprotein receptor-related protein-1 ectodomain decreases endocytic clearance of endometrial matrix metalloproteinase-2 and -9 at menstruation. *Endocrinology* **150**, 3792–3799 (2009).

123. Wygrecka, M. *et al.* Shedding of low-density lipoprotein receptor-related protein-1 in acute respiratory distress syndrome. *Am. J. Respir. Crit. Care Med.* **184**, 438–448 (2011).

124. Brebion, F. *et al.* Discovery of GLPG1972/S201086, a potent, selective, and orally bioavailable ADAMTS-5 inhibitor for the treatment of osteoarthritis. *J. Med. Chem.* **64**, 2937-2952 (2021).

125. Janusz, M. J. *et al.* Induction of osteoarthritis in the rat by surgical tear of the meniscus: Inhibition of joint damage by a matrix metalloproteinase inhibitor. *Osteoarthr. Cartil.* **10**, 785–791 (2002).

126. Krzeski, P. *et al.* Development of musculoskeletal toxicity without clear benefit after administration of PG-116800, a matrix metalloproteinase inhibitor, to patients with knee osteoarthritis: A randomized, 12-month, double-blind, placebo-controlled study. *Arthritis Res. Ther.* **9**, R109 (2007).

127. Fleischmann, R. M. *et al.* A phase II trial of Lutikizumab, an anti–interleukin-1α/β dual variable domain immunoglobulin, in knee osteoarthritis patients with synovitis. *Arthritis Rheum.* **71**, 1056–1069 (2019).

128. Van Den Bosch, M. H. *et al.* Induction of canonical Wnt signaling by synovial overexpression of selected Wnts leads to protease activity and early osteoarthritis-like cartilage damage. *Am. J. Pathol.* **185**, 1970–1980 (2015).

129. Yazici, Y. *et al.* Lorecivivint, a novel intraarticular CDC-like kinase 2 and dual-specificity tyrosine phosphorylation-regulated kinase 1A inhibitor and Wnt pathway modulator for the treatment of knee osteoarthritis: A Phase II randomized trial. *Arthritis Rheum.* **72**, 1694–1706 (2020).

130. Collins, I. & Wann, A. K. T. Regulation of the extracellular matrix by ciliary machinery. *Cells* **9**, 278 (2020).

131. Wheatley, D. N. Primary cilia in normal and pathological tissues. *Pathobiology* **63**, 222–238 (1995).

132. Poole, C. A., Flint, M. H. & Beaumont, B. W. Analysis of the morphology and function of primary cilia in connective tissues: A cellular cybernetic probe? *Cell Motil.* **5**, 175–193 (1985).

133. Tucker, R. W., Pardee, A. B. & Fujiwara, K. Centriole ciliation is related to quiescence and DNA synthesis in 3T3 cells. *Cell* **17**, 527–535 (1979).

134. Tanos, B. E. *et al.* Centriole distal appendages promote membrane docking, leading to cilia initiation. *Genes Dev.* **27**, 163–168 (2013).

135. Sorokin, S. P. Reconstructions of centriole formation and ciliogenesis in mammalian lungs. *J. Cell Sci.* **3**, 207–230 (1968).

136. Lu, Q. *et al.* Early steps in primary cilium assembly require EHD1/EHD3-dependent ciliary vesicle formation. *Nat. Cell Biol.* **17**, 228–240 (2015).

137. Molla-Herman, A. *et al.* The ciliary pocket: an endocytic membrane domain at the base

of primary and motile cilia. *J. Cell Sci.* **123**, 1785–1795 (2010).

138. Benmerah, A. The ciliary pocket. *Curr. Opin. Cell Biol.* **25**, 1–7 (2013).

139. Spektor, A., Tsang, W. Y., Khoo, D. & Dynlacht, B. D. Cep97 and CP110 suppress a cilia assembly program. *Cell* **130**, 678–690 (2007).

140. Goetz, S. C., Liem, K. F. & Anderson, K. V. The spinocerebellar ataxia-associated gene tau tubulin kinase 2 controls the initiation of ciliogenesis. *Cell* **151**, 847–858 (2012).

141. Cajanek, L. & Nigg, E. A. Cep164 triggers ciliogenesis by recruiting Tau tubulin kinase 2 to the mother centriole. *Proc. Natl. Acad. Sci.* **111**, E2841–E2850 (2014).

142. Rosenbaum, J. L. & Witman, G. B. Intraflagellar transport. *Nat. Rev. Mol. Cell Biol.* **3**, 813–825 (2002).

143. Bhogaraju, S. *et al.* Molecular basis of tubulin transport within the cilium by IFT74 and IFT81. *Science* **341**, 1009–1012 (2013).

144. Pazour, G. J. *et al.* Chlamydomonas IFT88 and its mouse homologue, polycystic kidney disease gene tg737, are required for assembly of cilia and flagella. *J. Cell Biol.* **151**, 709–718 (2000).

145. Deren, M. E., Yang, X., Guan, Y. & Chen, Q. Biological and chemical removal of primary cilia affects mechanical activation of chondrogenesis markers in chondroprogenitors and hypertrophic chondrocytes. *Int. J. Mol. Sci.* **17**, 188 (2016).

146. Nonaka, S. *et al.* Randomization of left-right asymmetry due to loss of nodal cilia generating leftward flow of extraembryonic fluid in mice lacking KIF3B motor protein. *Cell* **95**, 829–837 (1998).

147. Cole, D. G. *et al.* Chlamydomonas kinesin-II-dependent intraflagellar transport (IFT): IFT particles contain proteins required for ciliary assembly in *Caenorhabditis elegans* sensory neurons. *J. Cell Biol.* **141**, 993–1008 (1998).

148. Nachury, M. V. *et al.* A core complex of BBS proteins cooperates with the GTPase Rab8 to promote ciliary membrane biogenesis. *Cell* **129**, 1201–1213 (2007).

149. Westlake, C. J. *et al.* Primary cilia membrane assembly is initiated by Rab11 and transport protein particle II (TRAPPII) complex-dependent trafficking of Rabin8 to the centrosome. *Proc. Natl. Acad. Sci. U. S. A.* **108**, 2759–2764 (2011).

150. Reiter, J. F., Blacque, O. E. & Leroux, M. R. The base of the cilium: roles for transition fibres and the transition zone in ciliary formation, maintenance and compartmentalization. *EMBO Rep.* **13**, 608–618 (2012).

151. Awata, J. *et al.* NPHP4 controls ciliary trafficking of membrane proteins and large soluble proteins at the transition zone. *J. Cell Sci.* **127**, 4714–4727 (2014).

152. Huangfu, D. *et al.* Hedgehog signalling in the mouse requires intraflagellar transport proteins. *Nature* **426**, 83–87 (2003).

153. Chiang, C. *et al.* Cyclopia and defective axial patterning in mice lacking Sonic hedgehog gene function. *Nature* **383**, 407–413 (1996).

154. Bangs, F. & Anderson, K. V. Primary cilia and mammalian hedgehog signaling. *Cold Spring Harb. Perspect. Biol.* **9**, a028175 (2017).

155. Rohatgi, R., Milenkovic, L. & Scott, M. P. Patched1 regulates hedgehog signaling at the primary cilium. *Science* **317**, 372–376 (2007).

156. Corbit, K. C. *et al.* Vertebrate Smoothened functions at the primary cilium. *Nature* **437**, 1018–1021 (2005).

157. Tuson, M., He, M. & Anderson, K. V. Protein kinase A acts at the basal body of the primary cilium to prevent Gli2 activation and ventralization of the mouse neural tube. *Development* **138**, 4921–4930 (2011).

158. Haycraft, C. J. *et al.* Gli2 and Gli3 localize to cilia and require the intraflagellar transport protein Polaris for processing and function. *PLoS Genet.* **1**, e53 (2005).

159. Keady, B. T. *et al.* IFT25 links the signal-dependent movement of hedgehog components to intraflagellar transport. *Dev. Cell* **22**, 940–951 (2012).

160. Reiter, J. F. & Leroux, M. R. Genes and molecular pathways underpinning ciliopathies. *Nat. Rev. Mol. Cell Biol.* **18**, 533–547 (2017).

161. Beales, P. L. *et al.* IFT80, which encodes a conserved intraflagellar transport protein, is mutated in Jeune asphyxiating thoracic dystrophy. *Nat. Genet.* **39**, 727–729 (2007).

162. Praetorius, H. A. & Spring, K. R. Bending the MDCK cell primary cilium increases intracellular calcium. *J. Membr. Biol.* **184**, 71–79 (2001).

163. Nauli, S. M. *et al.* Polycystins 1 and 2 mediate mechanosensation in the primary cilium of

kidney cells. *Nat. Genet.* **33**, 129–137 (2003).

164. Yoder, B. K., Hou, X. & Guay-Woodford, L. M. The polycystic kidney disease proteins, polycystin-1, polycystin-2, polaris, and cystin, are co-localized in renal cilia. *J. Am. Soc. Nephrol.* **13**, 2508–2516 (2002).

165. Mochizuki, T. *et al.* PKD2, a gene for polycystic kidney disease that encodes an integral membrane protein. *Science* **272**, 1339–1342 (1996).

166. Delling, M. *et al.* Primary cilia are not calcium-responsive mechanosensors. *Nature* **531**, 656–660 (2016).

167. Moyer, J. *et al.* Candidate gene associated with a mutation causing recessive polycystic kidney disease in mice. *Science* **264**, 1329–1333 (1994).

168. Walker, R. V. *et al.* Ciliary exclusion of Polycystin-2 promotes kidney cystogenesis in an autosomal dominant polycystic kidney disease model. *Nat. Commun.* **10**, (2019).

169. Riddle, R. D., Johnson, R. L., Laufer, E. & Tabin, C. Sonic hedgehog mediates the polarizing activity of the ZPA. *Cell* **75**, 1401–1416 (1993).

170. Vortkamp, A. *et al.* Regulation of rate of cartilage differentiation by Indian Hedgehog and PTH-related protein. *Science* **273**, 613–622 (1996).

171. Ortega, N., Behonick, D. J. & Werb, Z. Matrix remodeling during endochondral ossification. *Trends Cell Biol.* **14**, 86–93 (2004).

172. St-Jacques, B., Hammerschmidt, M. & McMahon, A. P. Indian hedgehog signaling regulates proliferation and differentiation of chondrocytes and is essential for bone formation. *Genes Dev.* **13**, 2072–2086 (1999).

173. Maeda, Y. *et al.* Indian Hedgehog produced by postnatal chondrocytes is essential for maintaining a growth plate and trabecular bone. *Proc. Natl. Acad. Sci. U. S. A.* **104**, 6382–6387 (2007).

174. Yuan, X. & Yang, S. Deletion of IFT80 impairs epiphyseal and articular cartilage formation due to disruption of chondrocyte differentiation. *PLoS One* **10**, e0130618 (2015).

175. Song, B., Haycraft, C. J., Seo, H. seon, Yoder, B. K. & Serra, R. Development of the post-natal growth plate requires intraflagellar transport proteins. *Dev. Biol.* **305**, 202–216 (2007).

176. McGlashan, S. R., Haycraft, C. J., Jensen, C. G., Yoder, B. K. & Poole, C. A. Articular cartilage and growth plate defects are associated with chondrocyte cytoskeletal abnormalities in Tg737^{orpk} mice lacking the primary cilia protein polaris. *Matrix Biol.* **26**, 234–246 (2007).

177. Li, Y. & Dudley, A. T. Noncanonical frizzled signaling regulates cell polarity of growth plate chondrocytes. *Development* **136**, 1083–1092 (2009).

178. Coveney, C. *et al.* The ciliary protein IFT88 controls post-natal cartilage thickness and influences development of osteoarthritis. *Arthritis Rheum.* doi:10.1002/art.41894 (2021).

179. Wann, A. K. T. *et al.* Primary cilia mediate mechanotransduction through control of ATP-induced Ca^{2+} signaling in compressed chondrocytes. *FASEB J.* **26**, 1663–1671 (2012).

180. Thompson, C. L., McFie, M., Paul Chapple, J., Beales, P. & Knight, M. M. Polycystin-2 is required for chondrocyte mechanotransduction and traffics to the primary cilium in response to mechanical stimulation. *Int. J. Mol. Sci.* **22**, 4313 (2021).

181. Rais, Y. *et al.* The growth plate's response to load is partially mediated by mechano-sensing via the chondrocytic primary cilium. *Cell. Mol. Life Sci.* **72**, 597–615 (2015).

182. Kitami, M. *et al.* IFT20 is required for the maintenance of cartilaginous matrix in condylar cartilage. *Biochem. Biophys. Res. Commun.* **509**, 222–226 (2019).

183. Noda, K., Kitami, M., Kitami, K., Kaku, M. & Komatsu, Y. Canonical and noncanonical intraflagellar transport regulates craniofacial skeletal development. *Proc. Natl. Acad. Sci. U. S. A.* **113**, E2589–E2597 (2016).

184. Wei, F. *et al.* Activation of Indian hedgehog promotes chondrocyte hypertrophy and upregulation of MMP-13 in human osteoarthritic cartilage. *Osteoarthr. Cartil.* **20**, 755–763 (2012).

185. Zhou, J. *et al.* Disrupting the Indian hedgehog signaling pathway in vivo attenuates surgically induced osteoarthritis progression in *Col2a1-CreER^{T2}*; Ihh$^{fl/fl}$ mice. *Arthritis Res. Ther.* **16**, R11 (2014).

186. Ali, S. A. *et al.* Regulation of cholesterol homeostasis by hedgehog signaling in osteoarthritic cartilage. *Arthritis Rheum.* **68**, 127–137 (2016).

187. Rockel, J. S. *et al.* Hedgehog inhibits β-catenin activity in synovial joint development and osteoarthritis. *J. Clin. Invest.* **126**, 1649–1663 (2016).

188. Kaushik, A. P., Martin, J. A., Zhang, Q., Sheffield, V. C. & Morcuende, J. A. Cartilage abnormalities associated with defects of chondrocytic primary cilia in Bardet-Biedl syndrome mutant mice. *J. Orthop. Res.* **27**, 1093–1099 (2009).

189. Sheffield, I. D. *et al.* Osteoarthritis-like changes in Bardet-Biedl syndrome mutant ciliopathy mice (*Bbs1*$^{M390R/M390R}$): Evidence for a role of primary cilia in cartilage homeostasis and regulation of inflammation. *Front. Physiol.* **9**, 708 (2018).

190. Chang, C. F., Ramaswamy, G. & Serra, R. Depletion of primary cilia in articular chondrocytes results in reduced Gli3 repressor to activator ratio, increased Hedgehog signaling, and symptoms of early osteoarthritis. *Osteoarthr. Cartil.* **20**, 152–161 (2012).

191. Chang, C. F. & Serra, R. Ift88 regulates Hedgehog signaling, *Sfrp5* expression, and β-catenin activity in post-natal growth plate. *J. Orthop. Res.* **31**, 350–356 (2013).

192. Thompson, C. L. *et al.* Hedgehog signalling does not stimulate cartilage catabolism and is inhibited by Interleukin-1β. *Arthritis Res. Ther.* **17**, 373 (2015).

193. Coveney, C. R. *et al.* Cilia protein IFT88 regulates extracellular protease activity by optimizing LRP-1–mediated endocytosis. *FASEB J.* **32**, 6771-6782 (2018).

194. Morgan, G. W., Allen, C. L., Jeffries, T. R., Hollinshead, M. & Field, M. C. Developmental and morphological regulation of clathrin-mediated endocytosis in *Trypanosoma brucei*. *J. Cell Sci.* **114**, 2605–2615 (2001).

195. Rich, D. R. & Clark, A. L. Chondrocyte primary cilia shorten in response to osmotic challenge and are sites for endocytosis. *Osteoarthr. Cartil.* **20**, 923–930 (2012).

196. Clement, C. A. *et al.* TGF-β signaling is associated with endocytosis at the pocket region of the primary cilium. *Cell Rep.* **3**, 1806–1814 (2013).

197. Schou, K. B. *et al.* KIF13B establishes a CAV1-enriched microdomain at the ciliary transition zone to promote Sonic hedgehog signalling. *Nat. Commun.* **8**, 14177 (2017).

198. Kanai, Y., Wang, D. & Hirokawa, N. KIF13B enhances the endocytosis of LRP1 by recruiting LRP1 to caveolae. *J. Cell Biol.* **204**, 395–408 (2014).

199. van der Sluijs, P. *et al.* The small GTP-binding protein rab4 controls an early sorting event on the endocytic pathway. *Cell* **70**, 729–740 (1992).

200. Grant, B. D. & Donaldson, J. G. Pathways and mechanisms of endocytic recycling. *Nat. Rev. Mol. Cell Biol.* **10**, 597–608 (2009).

201. Rattner, J. B., Sciore, P., Ou, Y., Van Der Hoorn, F. A. & Lo, I. K. Y. Primary cilia in fibroblast-like type B synoviocytes lie within a cilium pit: A site of endocytosis. *Histol. Histopathol.* **25**, 865–875 (2010).

202. Hehnly, H., Chen, C. T., Powers, C. M., Liu, H. L. & Doxsey, S. The centrosome regulates the Rab11-dependent recycling endosome pathway at appendages of the mother centriole. *Curr. Biol.* **22**, 1944–1950 (2012).

203. Nandadasa, S. *et al.* Secreted metalloproteases ADAMTS9 and ADAMTS20 have a non-canonical role in ciliary vesicle growth during ciliogenesis. *Nat. Commun.* **10**, 953 (2019).

204. Jat, P. S. *et al.* Direct derivation of conditionally immortal cell lines from an H-2Kb-tsA58 transgenic mouse. *Proc. Natl. Acad. Sci. U. S. A.* **88**, 5096–5100 (1991).

205. Strober, W. Trypan blue exclusion test of cell viability. *Curr. Protoc. Immunol.* **111**, A3.B.1-A3.B.3 (2015).

206. Perry, R. P. & Kelley, D. E. Inhibition of RNA synthesis by actinomycin D: Characteristic dose-response of different RNA species. *J. Cell. Physiol.* **76**, 127–139 (1970).

207. Kerkvliet, E. H. M., Docherty, A. J. P., Beertsen, W. & Everts, V. Collagen breakdown in soft connective tissue explants is associated with the level of active gelatinase A (MMP-2) but not with collagenase. *Matrix Biol.* **18**, 373–380 (1999).

208. Taipale, J. *et al.* Effects of oncogenic mutations in Smoothened and Patched can be reversed by cyclopamine. *Nature* **406**, 1005–1009 (2000).

209. Damke, H., Baba, T., Warnock, D. E. & Schmid, S. L. Induction of mutant dynamin specifically blocks endocytic coated vesicle formation. *J. Cell Biol.* **127**, 915–934 (1994).

210. Macia, E. *et al.* Dynasore, a cell-permeable inhibitor of Dynamin. *Dev. Cell* **10**, 839–850 (2006).

211. Agrawal, N. *et al.* RNA interference: Biology, mechanism, and applications. *Microbiol. Mol. Biol. Rev.* **67**, 657–685 (2003).

212. Heid, C. A., Stevens, J., Livak, K. J. & Williams, P. M. Real time quantitative PCR. *Genome Res.* **6**, 986–994 (1996).

213. Livak, K. J. & Schmittgen, T. D. Analysis of relative gene expression data using real-time quantitative PCR and the $2^{-\Delta\Delta CT}$ method. *Methods* **25**, 402–408 (2001).

214. Smith, P. K. *et al.* Measurement of protein using bicinchoninic acid. *Anal. Biochem.* **150**, 76–85 (1985).

215. Jeong, A. L. *et al.* Oncoprotein CIP 2A promotes the disassembly of primary cilia and inhibits glycolytic metabolism. *EMBO Rep.* **19**, e45 (2018).

216. Thompson, C. L., Chapple, J. P. & Knight, M. M. Primary cilia disassembly down-regulates mechanosensitive hedgehog signalling: A feedback mechanism controlling ADAMTS-5 expression in chondrocytes. *Osteoarthr. Cartil.* **22**, 490–498 (2014).

217. Farndale, R. W., Sayers, C. A. & Barrett, A. J. A direct spectrophotometric microassay for sulfated glycosaminoglycans in cartilage cultures. *Connect. Tissue Res.* **9**, 247–248 (1982).

218. Fielding, A. B., Willox, A. K., Okeke, E. & Royle, S. J. Clathrin-mediated endocytosis is inhibited during mitosis. *Proc. Natl. Acad. Sci. U. S. A.* **109**, 6572–6577 (2012).

219. Hua, K. & Ferland, R. J. Fixation methods can differentially affect ciliary protein immunolabeling. *Cilia* **6**, 5 (2017).

220. Haycraft, C. J. *et al.* Intraflagellar transport is essential for endochondral bone formation. *Development* **134**, 307–316 (2007).

221. Ezratty, E. J. *et al.* A role for the primary cilium in notch signaling and epidermal differentiation during skin development. *Cell* **145**, 1129–1141 (2011).

222. Smith, R. J. *et al.* Recombinant human interleukin-1α and recombinant human interleukin-1β stimulate cartilage matrix degradation and inhibit glycosaminoglycan synthesis. *Inflammation* **13**, 367–382 (1989).

223. Sugimoto, K., Takahashi, M., Yamamoto, Y., Shimada, K. & Tanzawa, K. Identification of aggrecanase activity in medium of cartilage culture. *J. Biochem.* **126**, 449–455 (1999).

224. Hughes, C. E., Caterson, B., Fosang, A. J., Roughley, P. J. & Mort, J. S. Monoclonal antibodies that specifically recognize neoepitope sequences generated by 'aggrecanase' and matrix metalloproteinase cleavage of aggrecan: Application to catabolism in situ and in vitro. *Biochem. J.* **305**, 799–804 (1995).

225. Piperno, G. & Fuller, M. T. Monoclonal antibodies specific for an acetylated form of α-tubulin recognize the antigen in cilia and flagella from a variety of organisms. *J. Cell Biol.* **101**, 2085–2094 (1985).

226. Cevik, S. *et al.* Joubert syndrome Arl13b functions at ciliary membranes and stabilizes

protein transport in Caenorhabditis elegans. *J. Cell Biol.* **188**, 953–969 (2010).

227. Kiani, C., Chen, L., Wu, Y. J., Yee, A. J. & Yang, B. B. Structure and function of aggrecan. *Cell Res.* **12**, 19–32 (2002).

228. Little, C. B. *et al.* Aggrecanase versus matrix metalloproteinases in the catabolism of the interglobular domain of aggrecan in vitro. *Biochem. J.* **344**, 61–68 (1999).

229. Anderson, I. C., Shipp, M. A., Docherty, A. J. & Teicher, B. A. Combination therapy including a gelatinase inhibitor and cytotoxic agent reduces local invasion and metastasis of murine Lewis lung carcinoma. *Cancer Res.* **56**, 715–718 (1996).

230. Fushimi, K., Troeberg, L., Nakamura, H., Ngee, H. L. & Nagase, H. Functional differences of the catalytic and non-catalytic domains in human ADAMTS-4 and ADAMTS-5 in aggrecanolytic activity. *J. Biol. Chem.* **283**, 6706–6716 (2008).

231. Thompson, C. L., Wiles, A., Poole, C. A. & Knight, M. M. Lithium chloride modulates chondrocyte primary cilia and inhibits Hedgehog signaling. *FASEB J.* **30**, 716–726 (2016).

232. Cano, D. A., Murcia, N. S., Pazour, G. J. & Hebrok, M. *Orpk* mouse model of polycystic kidney disease reveals essential role of primary cilia in pancreatic tissue organization. *Development* **131**, 3457–3467 (2004).

233. Zhang, Q., Davenport, J. R., Croyle, M. J., Haycraft, C. J. & Yoder, B. K. Disruption of IFT results in both exocrine and endocrine abnormalities in the pancreas of *Tg737*^{orpk} mutant mice. *Lab. Investig.* **85**, 45–64 (2005).

234. Chang, M. Y. *et al.* Haploinsufficiency of *Pkd2* is associated with increased tubular cell proliferation and interstitial fibrosis in two murine *Pkd2* models. *Nephrol. Dial. Transplant.* **21**, 2078–2084 (2006).

235. Wang, Z. *et al.* IFT88 influences chondrocyte actin organization and biomechanics. *Osteoarthr. Cartil.* **24**, 544–554 (2016).

236. Houlden, H. *et al.* Mutations in TTBK2, encoding a kinase implicated in tau phosphorylation, segregate with spinocerebellar ataxia type 11. *Nat. Genet.* **39**, 1434–1436 (2007).

237. Bernatik, O. *et al.* Phosphorylation of multiple proteins involved in ciliogenesis by Tau Tubulin kinase 2. *Mol. Biol. Cell* **31**, 1032–1046 (2020).

238. Watanabe, T. *et al.* TTBK2 with EB1/3 regulates microtubule dynamics in migrating cells

through KIF2A phosphorylation. *J. Cell Biol.* **210**, 737–751 (2015).

239. Nieding, K. *et al.* Tau tubulin kinase TTBK2 sensitivity of glutamate receptor GluK2. *Cell. Physiol. Biochem.* **39**, 1444–1452 (2016).

240. Will, H., Dettloff, M., Bendzkô, P. & Sveshnikov, P. A quantitative assay for aggrecanase activity. *J. Biomol. Tech.* **16**, 459–472 (2005).

241. Struglics, A., Hansson, M. & Lohmander, L. S. Human aggrecanase generated synovial fluid fragment levels are elevated directly after knee injuries due to proteolysis both in the inter globular and chondroitin sulfate domains. *Osteoarthr. Cartil.* **19**, 1047–1057 (2011).

242. Lim, N. H. *et al.* In vivo imaging of matrix metalloproteinase 12 and matrix metalloproteinase 13 activities in the mouse model of collagen-induced arthritis. *Arthritis Rheum.* **66**, 589–598 (2014).

243. Lim, N. H., Meinjohanns, E., Meldal, M., Bou-Gharios, G. & Nagase, H. In vivo imaging of MMP-13 activity in the murine destabilised medial meniscus surgical model of osteoarthritis. *Osteoarthr. Cartil.* **22**, 862–868 (2014).

244. Chen, J. K., Taipale, J., Cooper, M. K. & Beachy, P. A. Inhibition of Hedgehog signaling by direct binding of cyclopamine to Smoothened. *Genes Dev.* **16**, 2743–2748 (2002).

245. Lark, M. W. *et al.* Aggrecan degradation in human cartilage: Evidence for both matrix metalloproteinase and aggrecanase activity in normal, osteoarthritic, and rheumatoid joints. *J. Clin. Invest.* **100**, 93–106 (1997).

246. Flannery, C. R., Little, C. B., Hughes, C. E. & Caterson, B. Expression of ADAMTS homologues in articular cartilage. *Biochem. Biophys. Res. Commun.* **260**, 318–322 (1999).

247. Tortorella, M. D., Malfait, A. M., Deccico, C. & Arner, E. The role of ADAM-TS4 (aggrecanase-1) and ADAM-TS5 (aggrecanase-2) in a model of cartilage degradation. *Osteoarthr. Cartil.* **9**, 539–552 (2001).

248. Pratta, M. A., Scherle, P. A., Yang, G., Liu, R. Q. & Newton, R. C. Induction of aggrecanase 1 (ADAM-TS4) by interleukin-1 occurs through activation of constitutively produced protein. *Arthritis Rheum.* **48**, 119–133 (2003).

249. Echtermeyer, F. *et al.* Syndecan-4 regulates ADAMTS-5 activation and cartilage breakdown in osteoarthritis. *Nat. Med.* **15**, 1072–1076 (2009).

250. Miyaki, S. *et al.* MicroRNA-140 is expressed in differentiated human articular chondrocytes and modulates interleukin-1 responses. *Arthritis Rheum.* **60**, 2723–2730 (2009).

251. Weber, A. E. *et al.* Modulation of hedgehog signaling by kappa opioids to attenuate osteoarthritis. *Arthritis Rheum.* **72**, 1278–1288 (2020).

252. Shimoyama, A. *et al.* Ihh/Gli2 signaling promotes osteoblast differentiation by regulating Runx2 expression and function. *Mol. Biol. Cell* **18**, 2411–2418 (2007).

253. Troeberg, L. *et al.* The C-terminal domains of ADAMTS-4 and ADAMTS-5 promote association with N-TIMP-3. *Matrix Biol.* **28**, 463–469 (2009).

254. Kopinke, D., Roberson, E. C. & Reiter, J. F. Ciliary hedgehog signaling restricts injury-induced adipogenesis. *Cell* **170**, P340-P351 (2017).

255. Seidah, N. G. *et al.* The activation and physiological functions of the proprotein convertases. *Int. J. Biochem. Cell Biol.* **40**, 1111–1125 (2008).

256. Kashiwagi, M. *et al.* Altered proteolytic activities of ADAMTS-4 expressed by C-terminal processing. *J. Biol. Chem.* **279**, 10109–10119 (2004).

257. Powell, A. J., Little, C. B. & Hughes, C. E. Low molecular weight isoforms of the aggrecanases are responsible for the cytokine-induced proteolysis of aggrecan in a porcine chondrocyte culture system. *Arthritis Rheum.* **56**, 3010–3019 (2007).

258. Kim, H. A., Kim, Y. H. & Song, Y. W. Facilitation of Fas mediated apoptosis of human chondrocytes by the proteasome inhibitor and actinomycin D. *J. Rheumatol.* **30**, 550–558 (2003).

259. Goodrich, L. V., Milenković, L., Higgins, K. M. & Scott, M. P. Altered neural cell fates and medulloblastoma in mouse patched mutants. *Science* **277**, 1109–1113 (1997).

260. Wang, B., Fallon, J. F. & Beachy, P. A. Hedgehog-regulated processing of Gli3 produces an anterior/posterior repressor gradient in the developing vertebrate limb. *Cell* **100**, 423–434 (2000).

261. Thayer, S. P. *et al.* Hedgehog is an early and late mediator of pancreatic cancer tumorigenesis. *Nature* **425**, 851–856 (2003).

262. Dennler, S. *et al.* Induction of sonic hedgehog mediators by transforming growth factor-β: Smad3-dependent activation of *Gli2* and *Gli1* expression in vitro and in vivo. *Cancer*

Res. **67**, 6981–6986 (2007).

263. Lauth, M., Bergström, Å., Shimokawa, T. & Toftgård, R. Inhibition of GLI-mediated transcription and tumor cell growth by small-molecule antagonists. *Proc. Natl. Acad. Sci. U. S. A.* **104**, 8455–8460 (2007).

264. Luo, Z. *et al.* Scutellarin attenuates the IL-1β-induced inflammation in mouse chondrocytes and prevents osteoarthritic progression. *Front. Pharmacol.* **11**, 107 (2020).

265. Hinrichsen, L., Harborth, J., Andrees, L., Weber, K. & Ungewickell, E. J. Effect of Clathrin heavy chain- and α-Adaptin-specific small inhibitory RNAs on endocytic accessory proteins and receptor trafficking in HeLa cells. *J. Biol. Chem.* **278**, 45160–45170 (2003).

266. Kawata, K. *et al.* Role of LRP1 in transport of CCN2 protein in chondrocytes. *J. Cell Sci.* **125**, 2965–2972 (2012).

267. Boucher, P. *et al.* Platelet-derived growth factor mediates tyrosine phosphorylation of the cytoplasmic domain of the low density lipoprotein receptor-related protein in caveolae. *J. Biol. Chem.* **277**, 15507–15513 (2002).

268. Engelholm, L. H. *et al.* uPARAP/Endo180 is essential for cellular uptake of collagen and promotes fibroblast collagen adhesion. *J. Cell Biol.* **160**, 1009–1015 (2003).

269. McGraw, T. E., Dunn, K. W. & Maxfield, F. R. Isolation of a temperature-sensitive variant Chinese hamster ovary cell line with a morphologically altered endocytic recycling compartment. *J. Cell. Physiol.* **155**, 579–594 (1993).

270. Absalon, S. *et al.* Intraflagellar transport and functional analysis of genes required for flagellum formation in trypanosomes. *Mol. Biol. Cell* **19**, 929–944 (2008).

271. Suizu, F. *et al.* Phosphorylation-dependent Akt–Inversin interaction at the basal body of primary cilia. *EMBO J.* **35**, 1346–1363 (2016).

272. Chavez, M. *et al.* Modulation of ciliary phosphoinositide content regulates trafficking and Sonic hedgehog signaling output. *Dev. Cell* **34**, 338–350 (2015).

273. Garcia-Gonzalo, F. R. *et al.* Phosphoinositides regulate ciliary protein trafficking to modulate hedgehog signaling. *Dev. Cell* **34**, 400–409 (2015).

274. Demmel, L. *et al.* The endocytic activity of the flagellar pocket in *Trypanosoma brucei* is regulated by an adjacent phosphatidylinositol phosphate kinase. *J. Cell Sci.* **127**, 2351–2364 (2014).

275. Fessart, D. *et al.* Src-dependent phosphorylation of β2-adaptin dissoaciates the β-arrestin-AP-2 complex. *J. Cell Sci.* **120**, 1723–1732 (2007).

276. Betts, G. N., Van Der Geer, P. & Komives, E. A. Structural and functional consequences of tyrosine phosphorylation in the LRP1 cytoplasmic domain. *J. Biol. Chem.* **283**, 15656–15664 (2008).

277. Van Kerkhof, P. *et al.* Sorting nexin 17 facilitates LRP recycling in the early endosome. *EMBO J.* **24**, 2851–2861 (2005).

278. Böttcher, R. T. *et al.* Sorting nexin 17 prevents lysosomal degradation of β1 integrins by binding to the β 1-integrin tail. *Nat. Cell Biol.* **14**, 584–592 (2012).

279. Horgan, C. P., Walsh, M., Zurawski, T. H. & McCaffrey, M. W. Rab11-FIP3 localises to a Rab11-positive pericentrosomal compartment during interphase and to the cleavage furrow during cytokinesis. *Biochem. Biophys. Res. Commun.* **319**, 83–94 (2004).

280. Lambert, C. A., Colige, A. C., Munaut, C., Lapière, C. M. & Nusgens, B. V. Distinct pathways in the over-expression of matrix metalloproteinases in human fibroblasts by relaxation of mechanical tension. *Matrix Biol.* **20**, 397–408 (2001).

281. Blain, E. J., Gilbert, S. J., Hayes, A. J. & Duance, V. C. Disassembly of the vimentin cytoskeleton disrupts articular cartilage chondrocyte homeostasis. *Matrix Biol.* **25**, 398–408 (2006).

282. Pascarelli, N. A., Collodel, G., Moretti, E., Cheleschi, S. & Fioravanti, A. Changes in ultrastructure and cytoskeletal aspects of human normal and osteoarthritic chondrocytes exposed to interleukin-1β and cyclical hydrostatic pressure. *Int. J. Mol. Sci.* **16**, 26019–26034 (2015).

283. Holloway, I. *et al.* Increased presence of cells with multiple elongated processes in osteoarthritic femoral head cartilage. *Osteoarthr. Cartil.* **12**, 17–24 (2004).

284. Bouskila, M. *et al.* TTBK2 kinase substrate specificity and the impact of spinocerebellar-ataxia-causing mutations on expression, activity, localization and development. *Biochem. J.* **437**, 157–167 (2011).

285. Vu, B. *et al.* Discovery of RG7112: A small-molecule MDM2 inhibitor in clinical development. *ACS Med. Chem. Lett.* **4**, 466–469 (2013).

286. Weng, L. H., Ko, J. Y., Wang, C. J., Sun, Y. C. & Wang, F. S. Dkk-1 promotes angiogenic

responses and cartilage matrix proteinase secretion in synovial fibroblasts from osteoarthritic joints. *Arthritis Rheum.* **64**, 3267–3277 (2012).

287. Rogers-DeCotes, A. W., Porto, S. C., Dupuis, L. E. & Kern, C. B. ADAMTS5 is required for normal trabeculated bone development in the mandibular condyle. *Osteoarthr. Cartil.* **29**, 547–557 (2021).

288. Pacheco, M. *et al.* Evc works in chondrocytes and osteoblasts to regulate multiple aspects of growth plate development in the appendicular skeleton and cranial base. *Bone* **50**, 28–41 (2012).

289. Ostrom, Q. T. *et al.* CBTRUS statistical report: Primary brain and other central nervous system tumors diagnosed in the United States in 2011-2015. *Neuro. Oncol.* **20**, iv1–iv86 (2018).

290. Nakada, M. *et al.* Human glioblastomas overexpress ADAMTS-5 that degrades brevican. *Acta Neuropathol.* **110**, 239–246 (2005).

291. Viapiano, M. S., Hockfield, S. & Matthews, R. T. BEHAB/brevican requires ADAMTS-mediated proteolytic cleavage to promote glioma invasion. *J. Neurooncol.* **88**, 261–272 (2008).

292. Hong, C. C. *et al.* Cerebral cavernous malformations are driven by ADAMTS5 proteolysis of versican. *J. Exp. Med.* **217**, (2020).

293. Cikach, F. S. *et al.* Massive aggrecan and versican accumulation in thoracic aortic aneurysm and dissection. *JCI insight* **3**, e97167 (2018).

294. Dupuis, L. E. *et al. Adamts5*$^{-/-}$ mice exhibit altered aggrecan proteolytic profiles that correlate with ascending aortic anomalies. *Arterioscler. Thromb. Vasc. Biol.* **39**, 2067–2081 (2019).

295. Fava, M. *et al.* Role of ADAMTS-5 in aortic dilatation and extracellular matrix remodeling. *Arterioscler. Thromb. Vasc. Biol.* **38**, 1537–1548 (2018).

296. Kanekiyo, T. *et al.* Heparan sulphate proteoglycan and the low-density lipoprotein receptor-related protein 1 constitute major pathways for neuronal amyloid-β uptake. *J. Neurosci.* **31**, 1644–1651 (2011).

297. Rauch, J. N. *et al.* LRP1 is a master regulator of tau uptake and spread. *Nature* **580**, 381–385 (2020).

298. Holtzer, H., Abbott, J., Lash, J. & Holtzer, S. The loss of phenotypic traits by differentiated cells *in vitro*, I. Dedifferentiation of cartilage cells. *Proc. Natl. Acad. Sci.* **46**, 1533–1542 (1960).

299. Von Der Mark, K., Gauss, V., Von Der Mark, H. & Müller, P. Relationship between cell shape and type of collagen synthesised as chondrocytes lose their cartilage phenotype in culture. *Nature* **267**, 531–532 (1977).

300. Benya, P. D., Padilla, S. R. & Nimni, M. E. Independent regulation of collagen types by chondrocytes during the loss of differentiated function in culture. *Cell* **15**, 1313–1321 (1978).

301. Thompson, C. L. *et al.* Chondrocyte expansion is associated with loss of primary cilia and disrupted hedgehog signalling. *Eur. Cells Mater.* **34**, 128–141 (2017).

302. van Beuningen, H. M. *et al.* Phenotypic differences in murine chondrocyte cell lines derived from mature articular cartilage. *Osteoarthr. Cartil.* **10**, 977–986 (2002).

303. Caron, M. M. J. *et al.* Redifferentiation of dedifferentiated human articular chondrocytes: Comparison of 2D and 3D cultures. *Osteoarthr. Cartil.* **20**, 1170–1178 (2012).

304. Katoh, Y. *et al.* Practical method for targeted disruption of ciliarelated genes by using CRISPR/Cas9-mediated, homology-independent knock-in system. *Mol. Biol. Cell* **28**, 898–906 (2017).

305. Lee, J. *et al.* Loss-of-function of IFT88 determines metabolic phenotypes in thyroid cancer. *Oncogene* **23**, 1 (2018).

306. Marcotte, D. J. *et al.* The crystal structure of the catalytic domain of tau tubulin kinase 2 in complex with a small-molecule inhibitor. *Acta Crystallogr. Sect. F Struct. Biol. Commun.* **76**, 103–108 (2020).

307. Bustin, S. A. *et al.* The MIQE guidelines: Minimum information for publication of quantitative real-time PCR experiments. *Clin. Chem.* **55**, 611–622 (2009).

308. Henry, S. P. *et al.* Generation of aggrecan-CreERT2 knockin mice for inducible Cre activity in adult cartilage. *Genesis* **47**, 805–814 (2009).

309. Soul, J., Hardingham, T. E., Boot-Handford, R. P. & Schwartz, J. M. SkeletalVis: An exploration and meta-analysis data portal of cross-species skeletal transcriptomics data. *Bioinformatics* **35**, 2283–2290 (2019).

310. Fisch, K. M. *et al.* Identification of transcription factors responsible for dysregulated networks in human osteoarthritis cartilage by global gene expression analysis. *Osteoarthr. Cartil.* **26**, 1531–1538 (2018).

APPENDIX

APPENDIX FIGURES 1 – Identification of TTBK2 as a regulator of ADAMTS-5-mediated aggrecan degradation

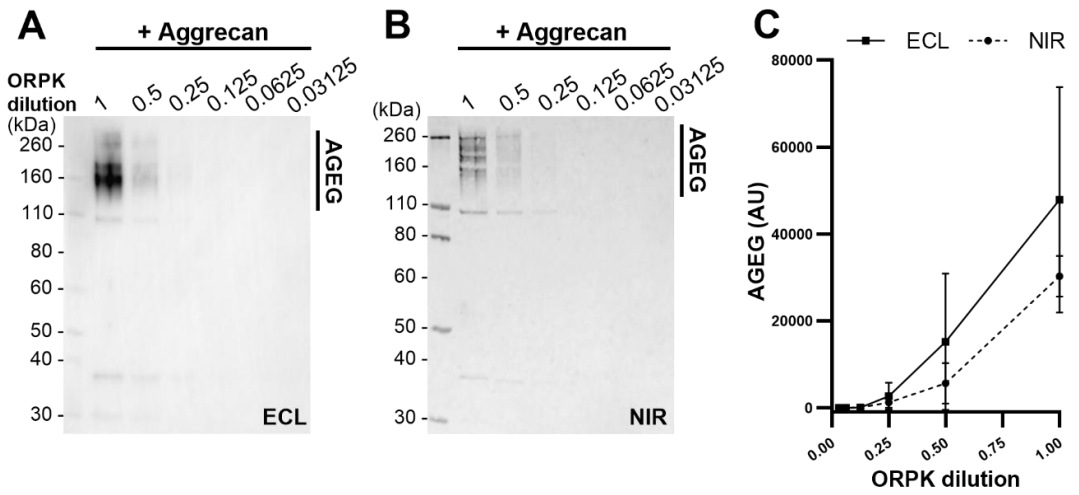

Appendix figure 1 Comparison of electrochemiluminescence and near-infrared fluorescence detection of the AGEG neoepitope by western blot. ***A***) ORPK cells were incubated with 50 µg/ml aggrecan for 24 hours. AGEG neoepitope in ORPK conditioned media serially diluted with serum-free media, was detected by western blot using electrochemiluminescence (ECL) detection or ***B***) near-infrared fluorescence detection. Blots are representative of one experiment conducted in triplicate using one cell subculture (n=3). ***C***) Quantification of AGEG levels in *A*) and *B*). Mean ± SD.

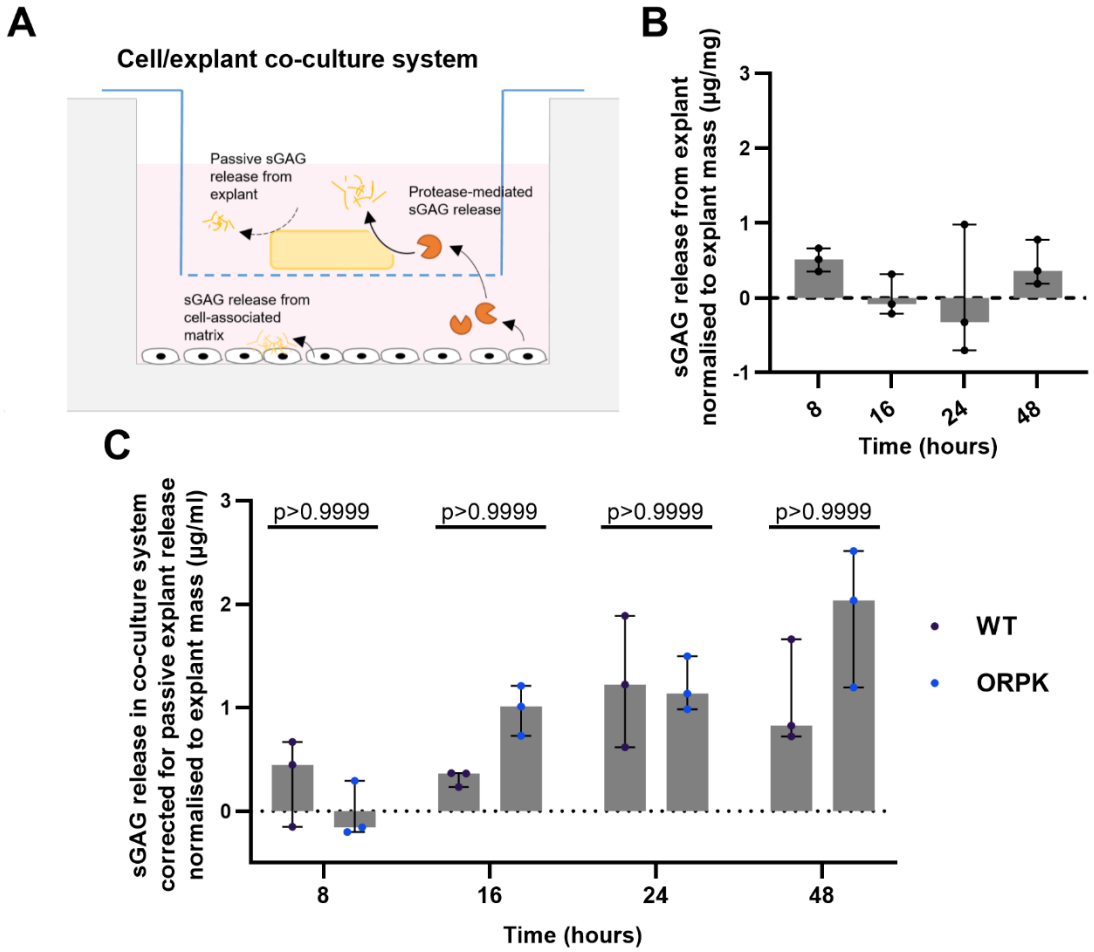

Appendix figure 2 Detection of sulphated glycosaminoglycan release in a cell-porcine explant co-culture system as a method for measuring protease activity. ***A***) WT or ORPK cells were cultured with freeze-thawed porcine cartilage explants in Transwell™ cell culture plates over a 48-hour time course. Levels of sulphated glycosaminoglycan (sGAG) in conditioned media were then measured using the DMMB assay. There were three potential sources of sGAG release: breakdown of the explant cartilage matrix by proteases secreted from WT or ORPK cells, passive release from the explant, and degradation of matrix synthesised by WT or ORPK cells. ***B***) sGAG release from freeze-thawed explants only at 8, 16, 24 or 48 hours, normalised to explant mass. Median ± IQR, one experiment conducted in triplicate using one cell subculture (n=3). ***C***) sGAG release in WT and ORPK cell-explant co-cultures at 8, 16, 24 or 48 hours, normalised to explant mass and corrected for release from explant alone at each time point. Median ± IQR. p values shown on graph, Kruskal-Wallis test with Dunn's multiple comparisons test.

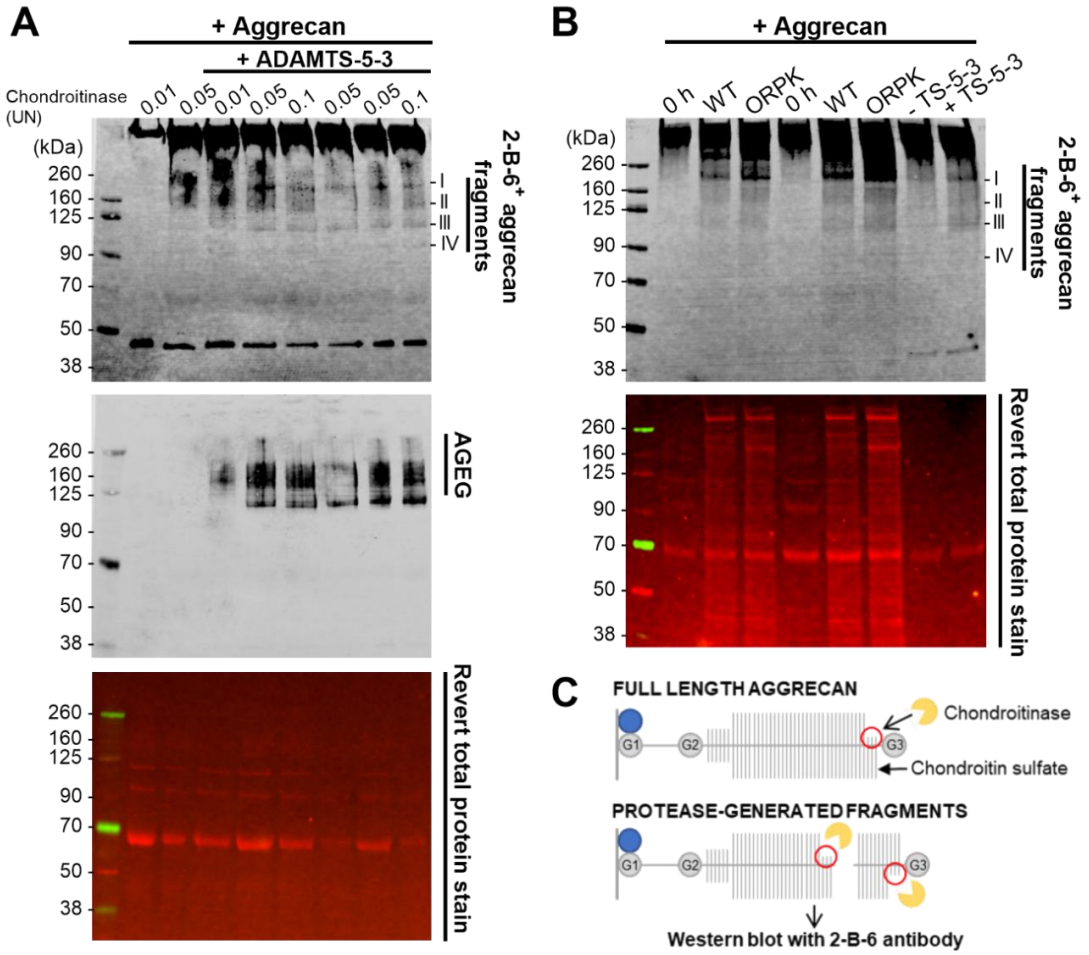

Appendix figure 3 Detection of chondroitinase-resistant chondroitin-4 sulfate stubs on aggrecan fragments with the 2-B-6 antibody as a method for measuring aggrecanolytic activity. ***A***) 1 nM FLAG-tagged human ADAMTS-5-3 was incubated with 50 µg bovine aggrecan for 24 hours. Samples were deglycosylated with 0.01, 0.05 or 0.1 UN of chondroitinase ABC. 2-B-6-positive aggrecan fragments and the AGEG neoepitope were detected in conditioned media by western blot with near-infrared fluorescence detection in the 700 nm and 800 nm channels respectively. Revert total protein stain was imaged in the 700 nm channel before incubation with primary antibodies. Blots representative of one experiment conducted in triplicate (n=3). ***B***) WT or ORPK cells were incubated with 50 µg/ml aggrecan for 24 hours. 2-B-6-positive aggrecan fragments were detected in conditioned media by western blot as above. Blot representative of one experiment conducted in triplicate using one cell subculture (n=3). ***C***) Schematic of chondroitinase-resistant chondroitin sulfate stubs on full-length aggrecan and protease-generated aggrecan fragments detected by the 2-B-6 antibody.

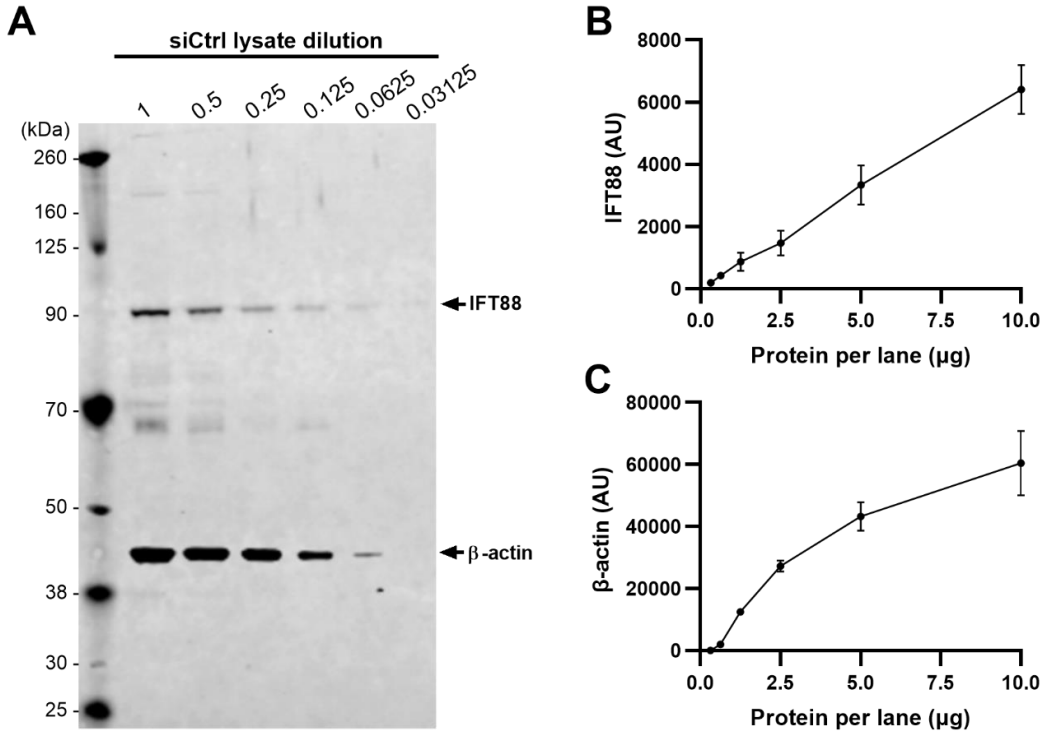

Appendix figure 4 Linear range of IFT88 and β-actin signal in western blots. ***A***) siCtrl cell lysates collected at the end of the aggrecan overlay assay were serially diluted with lysis buffer. Levels of IFT88 and the loading control β-actin were determined by western blot with near-infrared fluorescence detection. Blot representative of one experiment conducted in triplicate using one cell subculture (n=3). ***B***) Quantification of IFT88 or ***C***) β-actin signal in *A*). Mean ± SD.

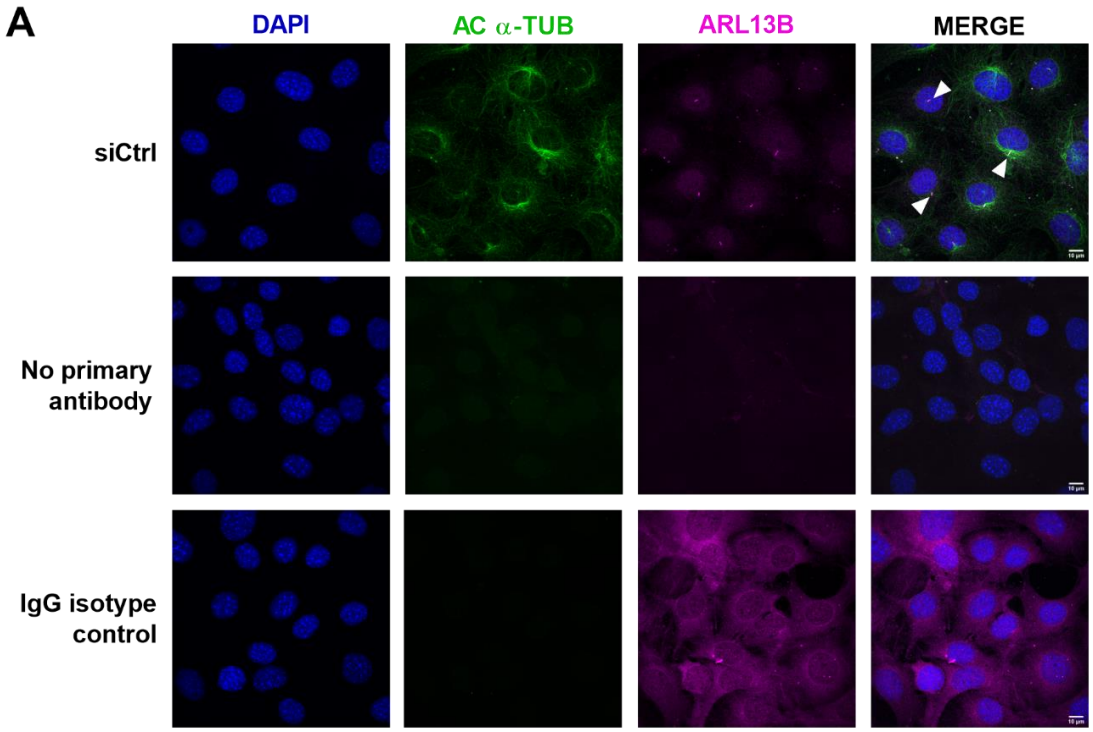

Appendix figure 5 Controls for immunofluorescence microscopy. siCtrl cells were incubated in serum-free media for 24 hours. Cells were fixed and stained with (siCtrl panel, top) or without (No primary antibody panel, middle) antibodies targeting acetylated α-tubulin (green) and ARL13B (magenta), or with a rabbit IgG isotype control (bottom panel). All cells were counterstained with DAPI and imaged using an Olympus FV1200 confocal microscope across three fields of view per coverslip. Images representative of one experiment conducted in triplicate using one cell subculture (n=3). Scale bar 10 µm. White arrowheads indicate cilia.

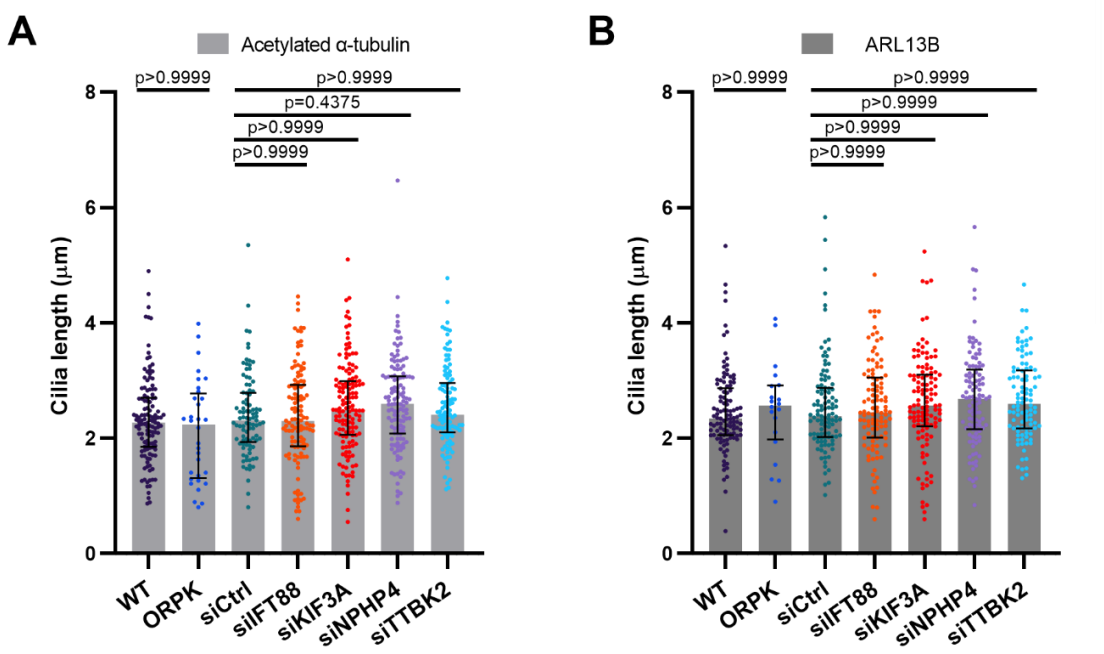

Appendix figure 6 Ciliary protein knockdown did not affect cilia length. ***A***) WT, ORPK or siRNA-treated cells were incubated in serum-free media for 24 hours, fixed and stained for the cilia markers acetylated α-tubulin and ARL13B. Images of cilia were taken using an Olympus FV1200 confocal microscope with 60x objective. Cilia length was measured based on acetylated α-tubulin signal or ***B***) ARL13B signal across 5 fields of view in each replicate for each condition. Median ± IQR, one experiment conducted in triplicate using one cell subculture (n=3). p values >0.05 shown on graph, Kruskal-Wallis test with Dunn's multiple comparisons test.

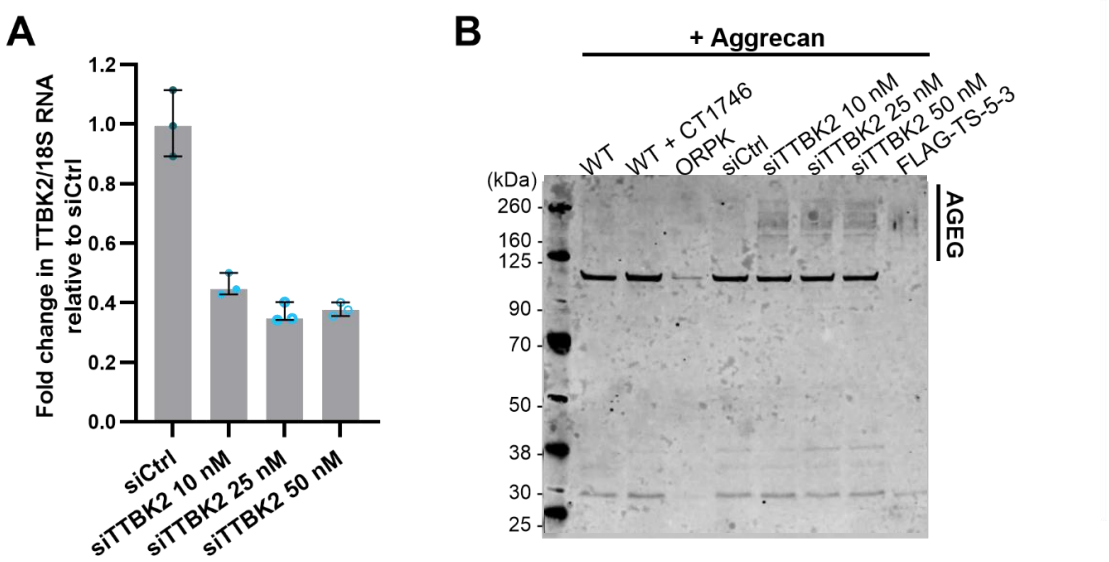

Appendix figure 7 AGEG generation in upon *Ttbk2* knockdown was not affected by siRNA concentration. ***A***) WT cells were transfected with 10 nM non-targeting siRNA, or 10, 25 or 50 nM TTBK2-targeting siRNA. RNA was isolated after cells were incubated with 50 µg/ml aggrecan for 24 hours. Expression of *Ttbk2* was measured by qPCR, then normalised to *18s* expression and presented as a fold change relative to siCtrl. Median ± IQR, one experiment conducted in triplicate using one cell subculture (n=3). ***B***) AGEG neoepitope in conditioned media was detected by western blot with ECL detection. Blot representative of triplicate experiment (n=3).

APPENDIX FIGURES 2 - Investigation of endocytosis-independent mechanisms of ADAMTS-5 regulation upon *Ttbk2* knockdown

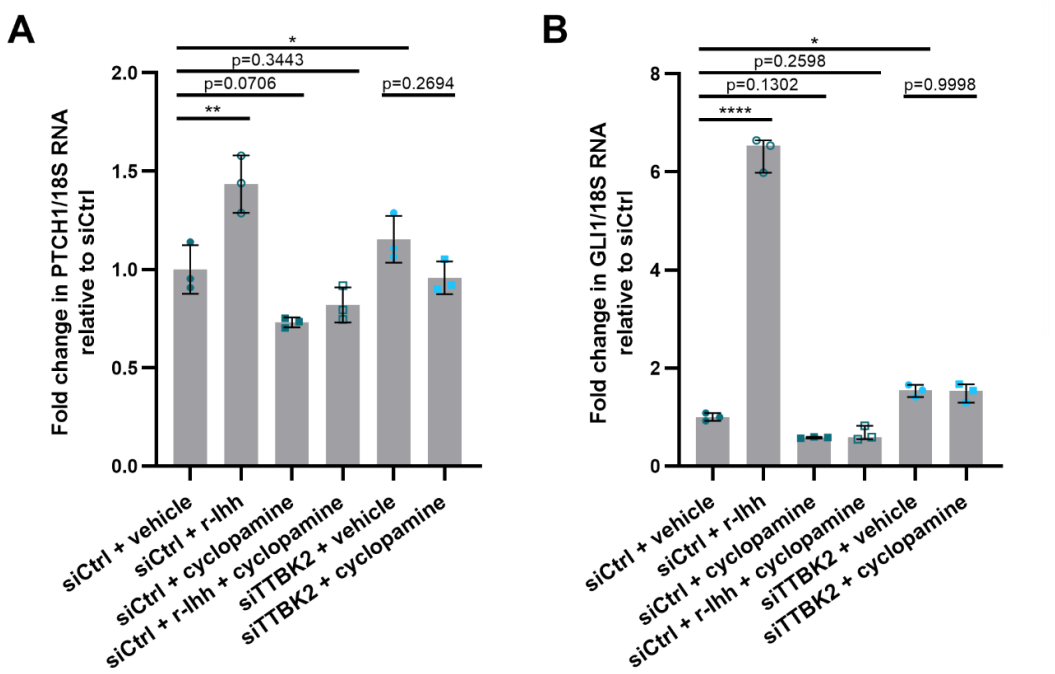

Appendix figure 8 Expression of hedgehog pathway target genes expression upon *Ttbk2* knockdown was not affected by the hedgehog pathway inhibitor cyclopamine. ***A***) RNA was isolated from siRNA-treated cells after incubation with 50 µg/ml aggrecan with or without DMSO, 1 µg/ml recombinant Indian hedgehog (r-Ihh) and 10 µM cyclopamine, for 24 hours. Expression of *Ptch1* or ***B***) *Gli1* RNA was measured by qPCR, then normalised to *18s* expression and presented as a fold change relative to siCtrl. Mean ± SD, one experiment conducted in triplicate using one cell subculture (n=3). * p<0.05, ** p<0.01, **** p<0.0001, p values >0.05 shown on graph, one-way ANOVA with Tukey's multiple comparisons test.

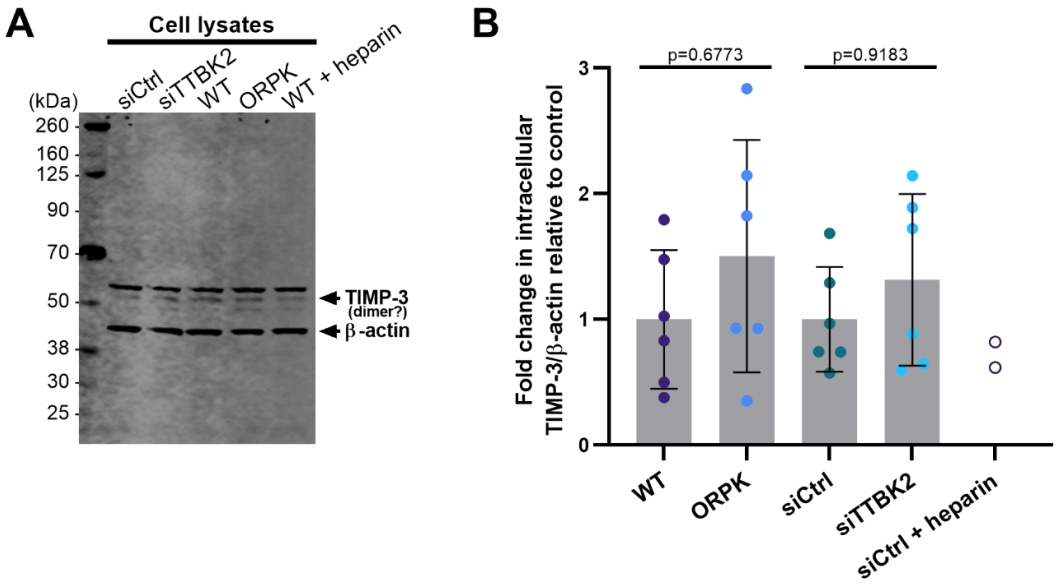

Appendix figure 9 Detection of intracellular TIMP-3 by western blot. *A*) WT, ORPK or siRNA-treated cells were incubated with or without 200 mg/ml heparin in serum-free media for 24 hours. TIMP-3 in cell lysates was detected by western blot, with β-actin used as a loading control. Blot representative of two independent experiments conducted in triplicate using separate cell subcultures (n=6). ***B*)** Quantification of 50 kDa band (possible TIMP-3 dimer form) in *A*), normalised to β-actin. Mean ± SD, n=6 for all conditions except siCtrl + heparin (one experiment conducted in duplicate, n=2). p values >0.05 shown on graph, one-way ANOVA with Tukey's multiple comparisons test.

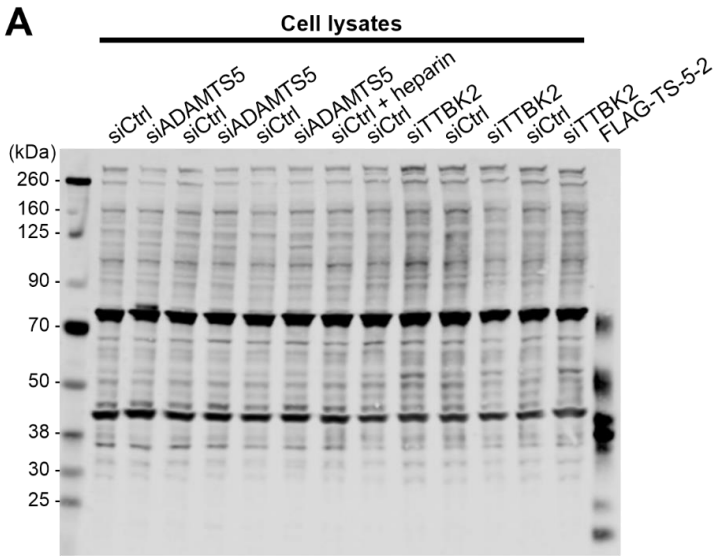

Appendix figure 10 Detection of intracellular ADAMTS-5 by western blot. *A*) siRNA-treated cells were incubated with or without 200 mg/ml heparin in serum-free media for 24 hours. Intracellular ADAMTS-5 in cell lysates was detected by western blot, with β-actin used as a loading control. FLAG-tagged ADAMTS-5-2 was used as a positive control for ADAMTS-5 signal. Blot representative of one experiment conducted in triplicate using one cell subculture (n=3).

APPENDIX FIGURES 3 – Investigation of endocytosis-dependent mechanisms of ADAMTS-5 regulation upon *Ttbk2* knockdown

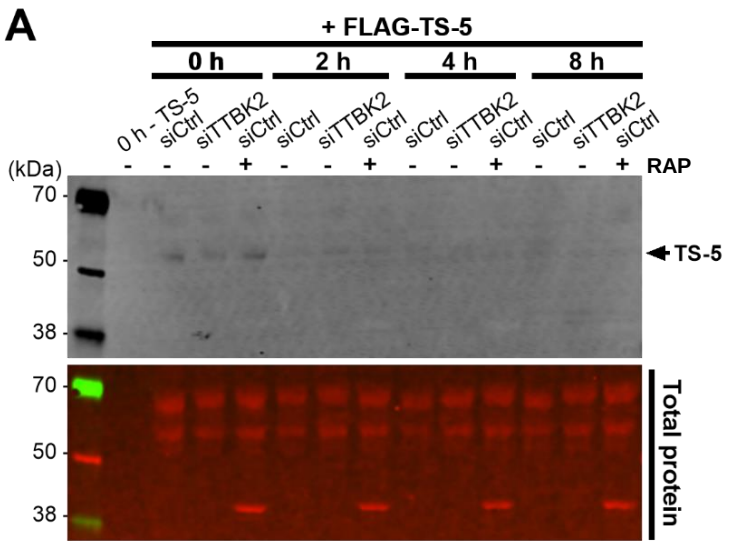

Appendix figure 11 Detection of extracellular FLAG-ADAMTS-5 in the ADAMTS-5 uptake assay by western blot with an antibody targeting the catalytic domain of ADAMTS-5. ***A***) siCtrl and siTTBK2 cells were incubated with or without 10 nM FLAG-tagged ADAMTS-5-3 and 0.5 µM RAP in serum-free media for 0, 2, 4 or 8 hours. Extracellular levels of FLAG-ADAMTS-5 in conditioned media were detected by western blot using an anti-ADAMTS-5 catalytic domain antibody. Blot representative of one experiment conducted in triplicate using one cell subculture (n=3).

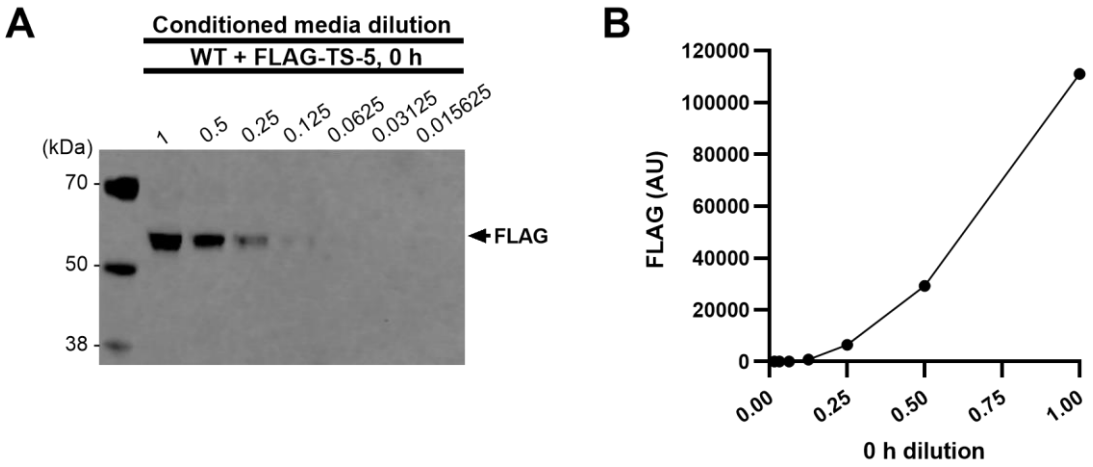

Appendix figure 12 Linear range of FLAG-ADAMTS-5 signal in western blots. ***A***) Conditioned media from WT cells at the 0-hour time point of the ADAMTS-5 endocytosis assay was serially diluted with serum-free media. Levels of FLAG-ADAMTS-5 were determined by western blot with near-infrared fluorescence detection. Blot representative of one experiment conducted in triplicate (n=3). ***B***) Quantification of FLAG signal in *A*).

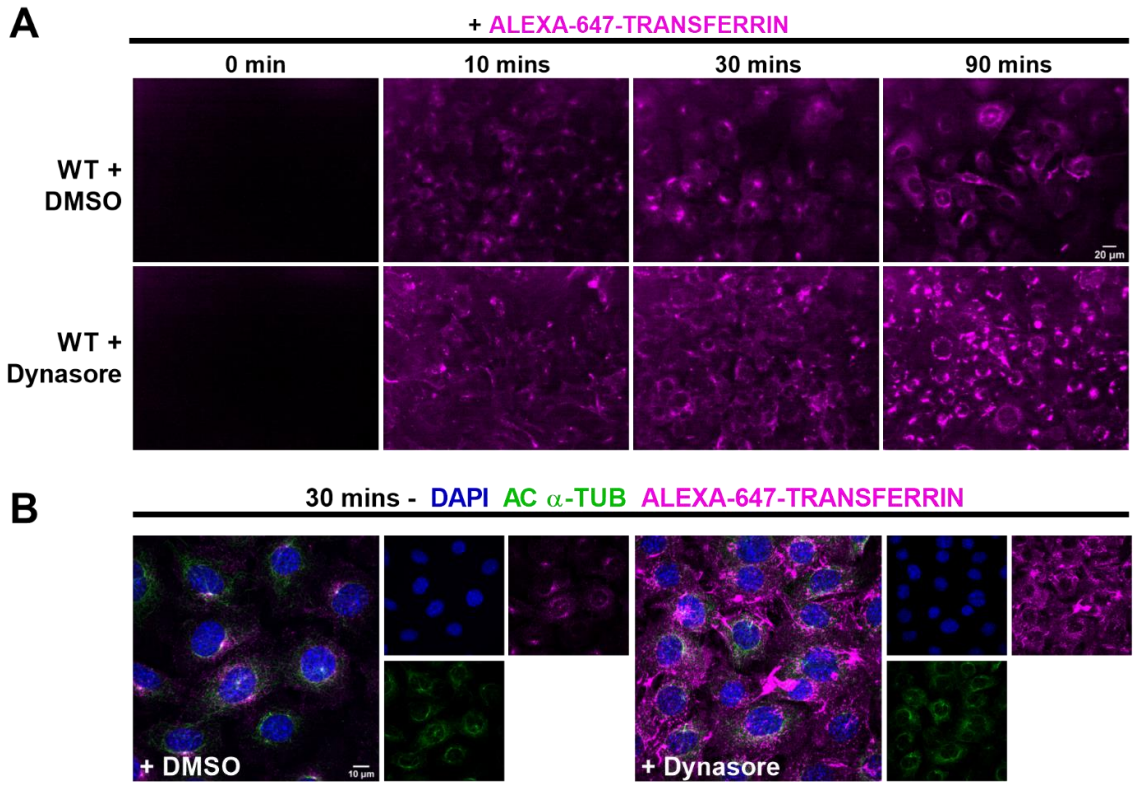

Appendix figure 13 The endocytosis inhibitor dynasore did not affect transferrin uptake in the WT mouse chondrocyte cell line. ***A***) WT cells were incubated with or without 10 ng/ml Alexa-647-conjugated transferrin, 80 µM dynasore and DMSO vehicle control, in serum-free media for 0, 10, 30 or 90 minutes before fixation. Cells were imaged by epifluorescence microscopy across three fields of view per coverslip. Scale bar 20 µm. ***B***) Cells were stained with antibodies targeting acetylated α-tubulin (green), and counterstained with DAPI (blue) to visualise cell nuclei. Cells were imaged using an Olympus FV1200 confocal microscope. Maximum projection images were created in ImageJ. All images shown are representative of one experiment conducted in triplicate using one cell subculture (n=3). Scale bar 10 µm.

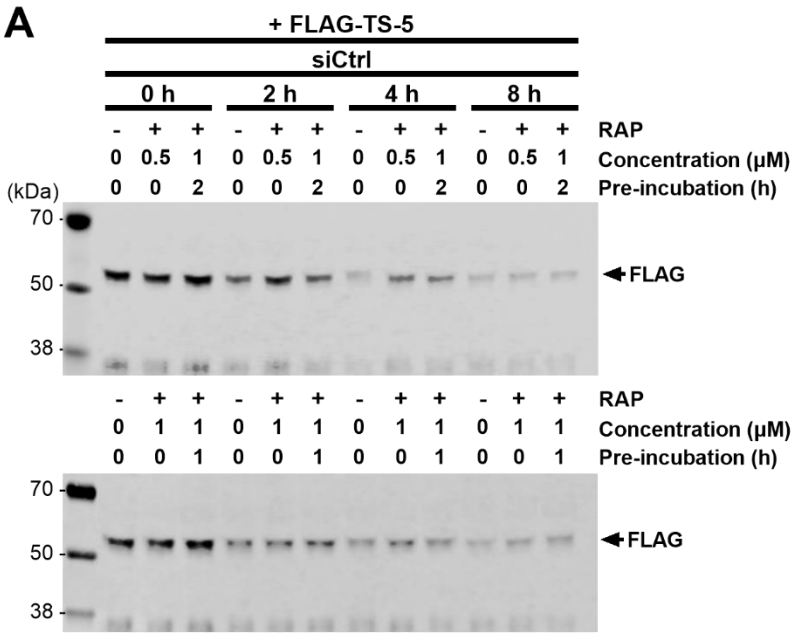

Appendix figure 14 Increasing RAP concentration or pre-incubating cells with RAP did not affect extracellular levels of FLAG-ADAMTS-5 in the ADAMTS-5 uptake assay. ***A***) siCtrl cells were incubated with or without 10 nM FLAG-tagged ADAMTS-5-3, and 0.5 or 1 μM RAP, in serum-free media for 0, 2, 4 or 8 hours. RAP was added directly to cells with FLAG-ADAMTS-5 at 0 hours, or pre-incubated with cells for 1 or 2 hours. Extracellular levels of FLAG-ADAMTS-5 were detected in conditioned media by western blot using an anti-FLAG antibody. Blots representative of one experiment conducted in duplicate using one cell subculture (n=2).

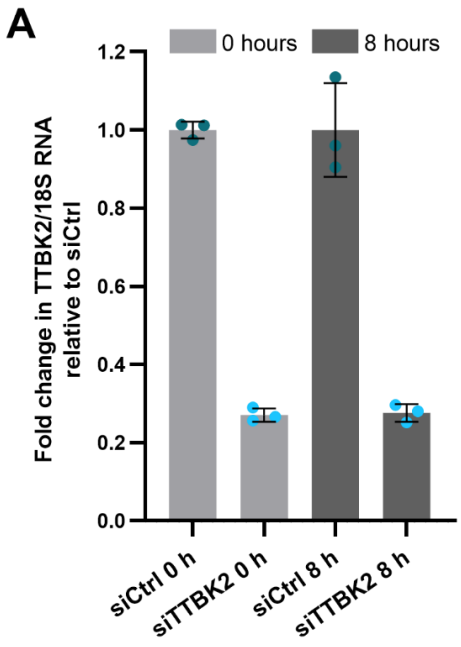

Appendix figure 15 ***Ttbk2*** **knockdown efficiency during the ADAMTS-5 uptake assay time course.** ***A***) RNA was isolated from siRNA-treated cells at the start (0 hours) and end (8 hours) of the ADAMTS-5 endocytosis assay. Expression of *Ttbk2* RNA was measured by qPCR, then normalised to *18s* expression and presented as a fold change relative to siCtrl. Mean ± SD, one experiment conducted in triplicate using one cell subculture (n=3).

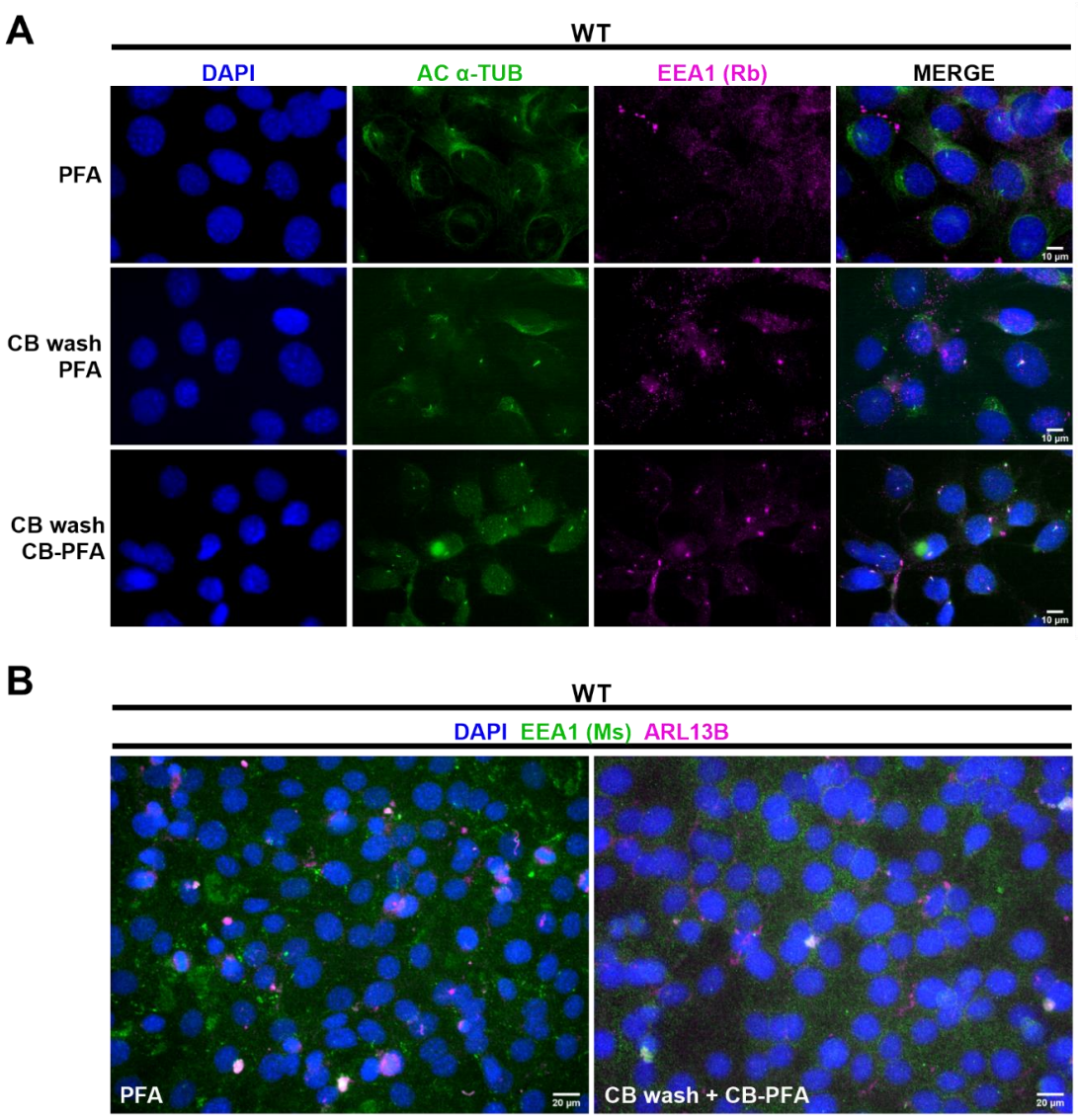

Appendix figure 16 Optimisation of early endosome marker EEA1 staining. ***A***) WT cells were incubated in serum-free media for 24 hours. Cells were immediately fixed with PFA, or washed with cytoskeletal buffer and fixed with PFA or PFA made up in cytoskeletal buffer. Cells were stained with antibodies targeting acetylated α-tubulin (green) or EEA1 (magenta, rabbit antibody), and counterstained with DAPI (blue). Cells were imaged by epifluorescence microscopy (100x objective) across three fields of view per coverslip. Scale bar 10 µm. ***B***) Cells were also stained with antibodies targeting EEA1 (green, mouse antibody) and ARL13B (magenta) and imaged as above (40x objective). Scale bar 20 µm. Images shown are representative of one experiment conducted in triplicate using one cell subculture (n=3).